

IN-SITU AND NUMERICAL ASSESSMENTS TO EVALUATE SITE
EFFECTS IN ORTA-ÇANKIRI PROVINCE BY COMPARATIVE
GEOPHYSICAL AND GEOTECHNICAL INVESTIGATIONS

A THESIS SUBMITTED TO
THE GRADUATE SCHOOL OF NATURAL AND APPLIED SCIENCES
OF
MIDDLE EAST TECHNICAL UNIVERSITY

BY

ARİF MERT EKER

IN PARTIAL FULFILLMENT OF THE REQUIREMENTS
FOR
THE DEGREE OF DOCTOR OF PHILOSOPHY
IN
GEOLOGICAL ENGINEERING

MARCH 2016

Approval of the thesis:

**IN-SITU AND NUMERICAL ASSESSMENTS TO EVALUATE SITE
EFFECTS IN ORTA-ÇANKIRI PROVINCE BY COMPARATIVE
GEOPHYSICAL AND GEOTECHNICAL INVESTIGATIONS**

submitted by **ARİF MERT EKER** in partial fulfillment of the requirements for
the degree of **Doctor of Philosophy in Geological Engineering Department,**
Middle East Technical University by,

Prof. Dr. Gülbin Dural Ünver
Dean, Graduate School of **Natural and Applied Sciences**

Prof. Dr. Erdin Bozkurt
Head of Department, **Geological Engineering**

Prof. Dr. Haluk Akgün
Supervisor, **Geological Engineering Dept., METU**

Examining Committee Members:

Prof. Dr. Candan Gökçeoğlu
Geological Engineering Dept., Hacettepe University

Prof. Dr. Haluk Akgün
Geological Engineering Dept., METU

Prof. Dr. Mehmet Cemal Göncüoğlu
Geological Engineering Dept., METU

Prof. Dr. Kemal Önder Çetin
Civil Engineering Dept., METU

Assoc. Prof. Dr. Ünal Dikmen
Geophysical Engineering Dept., Ankara University

Date: 11 / 03 / 2016

I hereby declare that all information in this document has been obtained and presented in accordance with academic rules and ethical conduct. I also declare that, as required by these rules and conduct, I have fully cited and referenced all material and results that are not original to this work.

Name, Last name : ARİF MERT EKER

Signature :

ABSTRACT

IN-SITU AND NUMERICAL ASSESSMENTS TO EVALUATE SITE EFFECTS IN ORTA-ÇANKIRI PROVINCE BY COMPARATIVE GEOPHYSICAL AND GEOTECHNICAL INVESTIGATIONS

Eker, Arif Mert
Ph.D., Department of Geological Engineering
Supervisor : Prof. Dr. Haluk Akgün

March 2016, 232 pages

Local site conditions of Orta district in Çankırı were deduced from in-situ measurements of dynamic and geotechnical properties of the soils in the context of evaluation of the site effects under a possible earthquake. The study area is under the control of active faults in the form of a strike slip basin and is almost entirely located within this basin. Plio-Quaternary and especially Quaternary alluvial sediment conditions were determined through the development of a geo-engineering database for the study area. The database was constructed by the results obtained by destructive geotechnical and non-destructive geophysical field methods along with geotechnical laboratory tests. In order to identify the dynamic soil behavior within the Orta pull apart basin under a possible ground motion, 1D and 2D numerical analyses utilizing equivalent linear approach were performed. Additionally, an experimental site effect study was carried out by using a single mobile velocimeter in the study area. The results of the microtremor method and the numerical analyses were compared with each other and the performances of the utilized methods were evaluated to determine the site effects at the study area. As a result, the seismic responses of the young and soft sedimentary units within the Orta pull apart basin have been proposed.

Keywords: Geotechnical and seismic characterization, microtremor, site effect estimation, 1D and 2D site response, Orta, Çankırı.

ÖZ

KARŞILAŞTIRMALI JEOFİZİK VE JEOTEKNİK ARAŞTIRMALAR İLE ÇANKIRI-ORTA İLÇESİNDEKİ YER ETKİSİNİN YERİNDE VE SAYISAL DEĞERLENDİRMELER İLE BELİRLENMESİ

Eker, Arif Mert
Doktora, Jeoloji Mühendisliği Bölümü
Tez Yöneticisi : Prof. Dr. Haluk Akgün

Mart 2016, 232 sayfa

Olası bir deprem sırasındaki yer etkilerinin değerlendirilmesi kapsamında Çankırı Orta İlçe'sindeki yerel saha koşulları, zeminlerin dinamik ve jeoteknik özelliklerinin yerinde ölçümlerinden elde edilmiştir. Çalışma alanı aktif fayların kontrolü altında olup, bir doğrultu atımlı havza şeklindedir. Neredeyse tüm çalışma alanı bu havza içerisinde yer almaktadır. Bu neden ile Pliyo-Kuvaterner ve özellikle Kuvaterner alüvyal sediman özellikleri arazi için geliştirilen bir jeomühendislik veri tabanı ile belirlenmiştir. Bu veri tabanı tahrip edici jeoteknik ve tahribatsız jeofizik arazi yöntemleriyle jeoteknik laboratuvar deneylerinin sonuçlarına göre oluşturulmuştur. Orta çek-ayır havzasındaki zeminlerin potansiyel bir yer hareketi sırasındaki dinamik tepkilerini belirlemek için eş değer doğrusal yaklaşımını kullanan 1B ve 2B nümerik analizler gerçekleştirilmiştir. Ek olarak, çalışma sahasında taşınabilir bir hız ölçer ile deneysel bir yer etkisi çalışması da uygulanmıştır. Mikrotremör yönteminin ve nümerik analizlerin sonuçları birbirleriyle karşılaştırılmış, çalışma alanındaki yer etkilerinin belirlenmesinde kullanılan yöntemlerin performansları değerlendirilmiştir. Sonuç olarak, Orta çek-ayır havzasındaki genç ve yumuşak sedimanter birimlerin yer tepkileri ortaya konulmuştur.

Anahtar Kelimeler: Jeoteknik ve sismik karakterizasyon, mikrotremör, yer etkisinin tahmini, 1B ve 2B yer tepkisi, Orta, Çankırı.

To my grandfather, ARİF EKER. I miss you...

ACKNOWLEDGMENTS

There are so many people who gave their kind contributions either morally or scientifically throughout this work. Here I would like to acknowledge my gratitude to them.

I must acknowledge and express my deepest gratitude to my supervisor Prof. Dr. Haluk Akgün for his understanding, guidance, patience and continuous support during my academic career. Beside these, I thank him for his kind attitude towards me in every step of my career. I appreciate the value of the technical discussions with him. I am indebted to him for giving me the chance to study on this project and for his trust in me.

I would like to express my respectful gratitude to the members of the thesis monitoring committee namely Prof. Dr. Kemal Önder Çetin and Prof. Dr. Cemal M. Göncüoğlu for their guidance and support during this study.

I would like to thank The Scientific and Technological Research Council of Turkey (TUBİTAK) for financial support throughout either my Masters or Ph.D. programs. I am very grateful for this support.

I would like to thank Mr. Selim Cambazoğlu, Mr. Karim Yousefi-Bavil, Ms. Arzu Arslan, Mrs. Gözde Pınar Yal, Mr. Mehmet Abdullah Kelam, Mr. Gökalp Öner, Mr. Aydın Çiçek, Dr. Evrim Sopacı, for their contribution and support during this study. I am very thankful for their support.

I would like to especially thank Mr. Selim Cambazoğlu (to be Dr.). He has always been with me on the way. I appreciate his continuous and endless moral and technical support during my last 12 years. I am so very glad to have met him.

I would like to express my respectful gratitude to Dr. Mustafa Kerem Koçkar for his guidance, motivation and support not only during this study but also during my entire academic career. Thank you for everything which you have tried to do for me.

I would like to thank Dr. Osman Şen, Mr. İrfan Acar, Mr. Hüseyin Dünya and the technical personel of SDS Energy for their understanding and for their kind attitude towards me not only during this study but also during my professional life in SDS Energy. I would like to especially thank Dr. Osman Şen for his unbelievable support in every aspect which I could never forget.

I would like to especially thank Kaya Engineering, Consulting, and Trading Co. Ltd., Mr. Mete Mirzaoğlu, Felek Group Engineering and Consulting Co. Ltd. and Demirkapılar Trading Co. Ltd. who provided assistance and conducted all of the field tests that have been performed in this study.

I would like also to thank several governmental organizations, especially General Directorate of Mineral Research and Exploration (MTA), General Directorate of Highways (TCK), Orta Municipality, General Directorate of Provincial Bank (İlbank) and General Directorate of Railways, Harbors and Airports Construction Railroad (DLH) for their documentation supports.

The last but not the least I would like to thank my wife Fatma Eker. Without her, the my life would have been miserable. You are my love and happiness, I am very glad to have you and my son who is due to be born. Also, I would like to thank my family, Menşure Eker, Özge Eker, Berk Eker and İlker Eker for their endless support and encouragement during my life.

TABLE OF CONTENTS

ABSTRACT	v
ÖZ	vi
ACKNOWLEDGMENTS	viii
TABLE OF CONTENTS	x
LIST OF TABLES	xii
LIST OF FIGURES	xiv
CHAPTERS	
INTRODUCTION	1
1.1. Purpose and scope.....	1
1.2. Motivation of the study.....	4
1.3. Study Area	6
1.4. Procedure.....	9
REGIONAL GEOLOGY AND SEISMOTECTONICS	13
2.1. Introduction	13
2.2 Sedimentary Geological Units	17
2.2.1. Miocene Sediments.....	17
2.2.2. Pliocene Sediments	19
2.2.3. Quaternary Sediments.....	21
2.3. Tectonic setting and seismicity of the area.....	23
2.3.1. The Orta earthquake.....	31
METHODOLOGIES FOR CHARACTERIZATION STUDIES.....	33
3.1. Introduction	33
3.2. Geotechnical characterization studies	36
3.2.1. Introduction.....	36
3.2.2. Geotechnical field and laboratory studies	37
3.2.2.1. Standard penetration test	38
3.2.2.2. Trial pits and geotechnical laboratory tests	40
3.2.3. Results of the geotechnical characterization studies.....	42

3.3. Seismic characterization studies.....	48
3.3.1. Introduction.....	48
3.3.2. Fundamental background of the utilized method.....	51
3.3.3. Data acquisition and field configuration of the SWMs.....	54
3.3.4. Field procedure of seismic survey utilized in this study	57
3.3.5. Construction of dispersion curves	63
3.3.6. Results of the surface wave velocity measurements.....	70
3.4. Generalization and comparison of the characterization studies.....	82
METHODOLOGIES PERFORMED IN ESTIMATION OF SITE EFFECT	93
4.1. Introduction	93
4.2. Nakamura (H/V) method	96
4.2.1. Recording microtremor measurements.....	98
4.2.2. Processing of microtremor records.....	102
4.3. 1D and 2D numerical methods.....	107
4.3.1. Introduction.....	107
4.3.2. The methodology utilized in this study	110
4.3.2.1. Construction of the target spectrum.....	112
4.3.2.2. Selecting and scaling of the input motions	122
4.3.2.3. Construction of 1D and 2D soil profile geometries	126
4.3.2.4. Characterization of non-linear soil behavior.....	137
RESULTS OF THE SITE EFFECT STUDIES.....	147
5.1. Results of the microtremor survey	147
5.2. Results of 1D and 2D numerical analyses.....	157
5.3. Comparison of the results of the site effect studies	170
DISCUSSION AND CONCLUSION.....	181
REFERENCES	199
CURRICULUM VITAE.....	229

LIST OF TABLES

TABLES

Table 1. The list of the major earthquakes that occurred within the study area and its close vicinity (compiled from EERC - ERD, 2009; DDA, 2015; KOERI, 2015)	30
Table 2. Soil classification according to IBC 2012 (ICC, 2012).	35
Table 3. The list of selected field configuration and data acquisition parameters in Phase 1 and Phase 2. Please note that the numbers given in parenthesis show the selected parameters in Phase 1. The numbers without parentheses show the utilized parameters during Phase 2.	62
Table 4. The summary of the surface ruptures of four major earthquakes located in the close vicinity of the study area. The closest segments of the fault zones to the study area are indicated by bold format (SRL: Surface rupture length, FS: fault segment, FSL: Fault segment length, Mech: Mechanism, FW: Fault width).	115
Table 5. The calculated moment magnitudes (mean and mean + standard deviation) according to the different fault mechanisms by using the relationship proposed by Wells and Coppersmith (1994).	117
Table 6. PGA values of the 2000 Orta Earthquake records at six different strong motion stations and distance between the study area and these stations along with their V_{S30} values.	118
Table 7. A summary of the applicability of the GMPEs utilized in this study. ...	119
Table 8. Assignment of weights regarding the results of the GMPEs. The weight sum up to 1.	120
Table 9. Summary of the selected ground motion records.	123
Table 10. Summary of the seven earthquake records utilized to form the suit matching the target spectrum the best.	126
Table 11. The lateral and vertical variations of layer thickness at the sites located along the A-A' section. "C" is the abbreviation of Comb.	128

Table 12. The lateral and vertical variations of layer thickness at the sites located along the B-B' section. "C" is the abbreviation of Comb.	128
Table 13. Variations of unit weights of the layers along the A-A' section. "C" is the abbreviation of Comb.	128
Table 14. Variations of unit weights of the layers along the B-B' section. "C" is the abbreviation of Comb. "BH" is the closest borehole at the V_S measurement sites.	129
Table 15. Shear wave velocity variation of the layers in lateral and vertical directions along the A-A' section. "C" is the abbreviation of Comb and "BH" is the closest borehole at the V_S measurement sites.....	129
Table 16. Shear wave velocity variation of the layers in the lateral and vertical directions along the B-B' section. "C" is the abbreviation of Comb.....	129
Table 17. Plasticity index values of the layers along the A-A' section. "C" is the abbreviation of Comb.	130
Table 18. Plasticity index values of the layers along the B-B' section. "C" is the abbreviation of Comb.	130
Table 19. The maximum height (m) for 1D soil response analysis along the A-A' section. "C" is the abbreviation of Comb.	133
Table 20. The maximum height (m) for 1D soil response analysis along the B-B' section. "C" is the abbreviation of Comb.	133
Table 21. A summary of the geometric model and mesh properties.	135

LIST OF FIGURES

FIGURES

Figure 1. The classification and distribution of the damages with respect to the villages after the Orta earthquake (Modified from Taşkın et al., 2003).	5
Figure 2. A regional map showing the study area.....	7
Figure 3. The study area where the investigations have concentrated.....	8
Figure 4. A flow chart of the study.	10
Figure 5. Regional geological map of the study area along with the neotectonic features. The geological map was reproduced from the MTA digital records (MTA, 2008). The red rectangular area shows the area that is concentrated in this study.	15
Figure 6. The simplified geological map of the study area [compiled and modified from Tokan and Özgen (1976); Türkecan et al., (1991); Türkmenoğlu et al. (1991); Emre et al., (2000); Koçyiğit et al. (2001) and MTA digital records (2008)] along with the distribution of the deep borings over the area.	17
Figure 7. A view from sandstone-marl-tuff intercalation in the Miocene sediments located at the northern side of the Orta basin.....	18
Figure 8. A view from the upper lignite seam located at the southeast of the study area.....	20
Figure 9. A close view of the Pliocene sediments including the tuff particles.	21
Figure 10. A view of the Quaternary terraces from the WNW of the study area...	23
Figure 11. Major paleotectonic and neotectonic features of Turkey (compiled and modified from Okay and Tüysüz, 1999; Bozkurt, 2001; Kaymakçı et al., 2003; Şengör et al., 2005; Moix et al., 2008; Kuşçu et al., 2009)	25
Figure 12. Simplified seismotectonic map of the study area overlying the hillshade of the area (Modified from Emre et al., 2000; Koçyiğit et al., 2001; Akyüz et al., 2002; Kaplan, 2004).	27
Figure 13. The record of the 2000 Orta Earthquake at the Çerkeş station.....	32

Figure 14. An illustration of the split barrel sampler (tube) for standard penetration test (Murthy, 2002) (not to scale).....	38
Figure 15. Spatial distribution of the compiled geotechnical borings and the excavated trial pits in the study area.	40
Figure 16. A view during the excavation of the trial pit in the Orta area.	41
Figure 17. The SPT-N value variations with respect to depth for the Quaternary, Pliocene and entire data.	43
Figure 18. The variation of natural water content (w_n) with depth for the Quaternary, Pliocene and entire data.....	43
Figure 19. The variations of the percent of the samples retained on the No. 4 sieve with respect to depth for the Quaternary, Pliocene and entire data.	44
Figure 20. The variations of the percent of the samples passing through No. 200 sieve with respect to depth for the Quaternary, Pliocene and entire data.	45
Figure 21. Distribution of the soil class for the entire dataset according to the USCS (ASTM, 2006).....	45
Figure 22. The distribution of the general soil groups for the entire dataset based on the USCS (ASTM, 2006).....	46
Figure 23. The variations of the LL (a), PL (b) and PI (c) values with depth for the Quaternary, Pliocene and entire data.....	47
Figure 24. The distribution of ML, MH, CL and CH soil classes regarding the PI and LL values on the Casagrande chart for the entire data.....	48
Figure 25. Principle of geometric dispersion (Geovision, 2009).....	52
Figure 26. The flowchart of the main steps followed in the analysis of the SWMs (reproduced from Foti, 2005).....	53
Figure 27. The spatial distribution of the first and second phase surface wave measurements along with the selected sections.....	59
Figure 28. Distribution of the Surface Wave Measurements with respect to the geological units.....	59
Figure 29. The configurations of the linear arrays utilized in the active surface wave survey. The numbers given in parentheses show the selected field	

configuration parameters in Phase 1. The numbers without parentheses show the utilized parameters during Phase 2. 60

Figure 30. The configurations of the linear arrays utilized in the passive surface wave survey. The numbers given in the parentheses show the selected field configuration parameters in Phase 1. The numbers without parentheses show the utilized parameters during Phase 2. 63

Figure 31. Configurations of the geometrical arrays utilized in the surface wave investigations in the second phase of the study a) triangular and b) L-shape array geometries configured in the passive surface wave survey. 63

Figure 32. a) A contaminated MASW measurement [Comb02 (2)] by the interference of higher mode of Rayleigh wave observed at the higher frequency component of the record, an example of the constructed experimental dispersion curve of b) the L-shape and c) linear MAM records at Comb 12 (2). 66

Figure 33. An example combined dispersion curve after the inversion process was performed at Comb07 (1). The red dashed line at the top of the figure shows the signal to noise ratio at each frequency of the phase velocity..... 68

Figure 34. An example combined dispersion curve after the inversion process was performed at Comb12 (2). The red dashed line at the top of the figure shows the signal to noise ratio at each frequency of the phase velocity..... 69

Figure 35. The final shear wave velocity profile obtained from the MASW method at Comb 14(1). The small green circles shows the dispersion curve which this V_S profile was derived from. The dark shaded area indicates the reliable parts of the shear wave velocity profiles. 72

Figure 36. The final shear wave velocity profile obtained from the MAM method at Comb13 (2). The small green circles shows the dispersion curve which this V_S profile was derived from. The dark shaded area demonstrates the reliable parts of the shear wave velocity profiles..... 72

Figure 37. Some examples of the representative V_S profiles from the a) Quaternary, b, c) Pliocene and d) Miocene sites..... 76

Figure 38. The general distribution of the calculated V_{S30} results with respect to different geologic deposits and corresponding to the site classes based on IBC 2012.....	78
Figure 39. Spatial distribution of the V_{S30} value over the study area based on IBC 2012.....	79
Figure 40. a) 3D V_S model with digital elevation, b) vertical and lateral variation of the V_S values along the x-y direction and c) iso-surface map with a V_S value of 600m/s.....	81
Figure 41. The distribution of the geotechnical borings and shear wave velocity measurements along with the trend of two sections. The orange circles show the used pairs for the comparison of the results.	83
Figure 42. The selected pairs for the comparison a) BH-7 & Comb01 (2), b) BH-15 & Comb07 (1) and c) BH-17 & Comb02 (2).	85
Figure 43. Comparison of the new inverted layers with the results of the blind way technique at the sites of a) [Comb03 (2)], b) [Comb04 (2)] and c) [Comb13 (2)].	87
Figure 44. The two constructed sections a) A-A' section and b) B-B' section to determine lateral and vertical V_S variations. The red line shows the possible direction of the faults given in Figures 27 and 39.....	90
Figure 45. Simple model assumed by Nakamura (1989) to interpret microtremor measurements. SH/V is the horizontal to vertical spectral ratio, ST is the spectral ratio of transfer functions of the horizontal component of microtremor spectrum (SHS) at the surface to the horizontal component of microtremor spectrum (SHB) on the basement rock, ES is the ratio of vertical spectrum at the surface (SVS) to that spectrum at the base ground (SVB).....	96
Figure 46. The spatial distribution of the first and second phase microtremor measurements.	99
Figure 47. Statistical distribution of the measurement sites with respect to the geological units.....	99
Figure 48. a) A close-up view of the UP-255s velocimeter, b) a view of the inside of the velocimeter, c) the amplifier and the notebook PC utilized during the recordings.....	100

Figure 49. a) A view from the microtremor measurements at the Ort01 (2) site, b) a close-up view of the CMG-40TD velocimeter, c) A view from setting up the seismograph before the recording	102
Figure 50. An example of the waveform from the unprocessed 5 min microtremor data recorded at the Ort07 (1) site. The hatched twelve rectangular areas are the selected 20 s windows for further analysis.....	103
Figure 51. The FFT and H/V spectra of the selected 20 s windows to the left and right of the figure, respectively at the Ort07 (1) site. The thick lines show the average values of the spectra of selected windows which are demonstrated by the thin lines.....	104
Figure 52. The selected windows from the filtered 30 minute microtremor data recorded at the Ort02 (2) site. The colored 14 rectangular areas are the selected 25 s windows for further analysis.....	106
Figure 53. Geometrically averaged H/V spectra of 14 windows of 25 s length at the Ort02 (2) site. The solid black lines show the average values of the spectra of selected windows and the dashed lines represent the variation of the mean by considering \pm one standard deviation.....	106
Figure 54. The cross sections and the measurement sites for 1D and 2D site response analysis performed in this study. This figure is intentionally re-given for the readers' convenience.....	112
Figure 55. The surface ruptures of the four major earthquakes (Gerede, Kurşunlu, Ilgaz and Orta Earthquakes) and the distance between these surface ruptures and the Orta District along with the distributions of the strong motion stations and major earthquake epicenters ($M_w > 5.5$).....	114
Figure 56. Comparison of PGA values of the Orta Earthquake records at six strong motion stations with the estimation of four GMPEs.	120
Figure 57. Constructed target spectrum by using a logic-tree approach.....	121
Figure 58. The mean match spectrum formed by averaging seven earthquake records and the target spectrum.	125
Figure 59. Original accelerograms of the seven earthquakes and the target spectrum. Please see Table 7 for the abbreviations of the records.	125

Figure 60. Matched accelerograms of the seven earthquakes according to the target spectrum. Please see Table 7 for the abbreviation of the records.	126
Figure 61. a) and c) Soil model of sections A-A' and B-B', respectively. b) and d) a close view of these sections to show the lateral and vertical variations of the layers. Colors are assigned to the layers for illustration purposes only. The dimension of the squares in a) and c) is 100m x 100m.	134
Figure 62. a) The Generated mesh of A-A' and b) a close view of the generated mesh along with the defined layers.	136
Figure 63. A comparison of using vertical and confining effective stresses for the overconsolidated cohesive layers at the Comb01 (2) site.	139
Figure 64. A comparison of using vertical and confining effective stresses for the overconsolidated cohesive layers at the Comb01 (2) site.	140
Figure 65. A comparison of using vertical and confining effective stresses for the unconsolidated cohesive layers at the Comb06 (1) site.	140
Figure 66. A comparison of using vertical and confining effective stresses for the unconsolidated granular layers at the Comb06 (1) site.	140
Figure 67. Normalized modulus curves of the first layer utilized in the 1D soil response analysis.	142
Figure 68. Material damping curves of the first layer utilized in the 1D soil response analysis.	142
Figure 69. Normalized modulus curves of the second layer utilized in the 1D soil response analysis.	142
Figure 70. Material damping curves of the second layer utilized in the 1D soil response analysis.	143
Figure 71. Normalized modulus curves of the third layer utilized in the 1D soil response analysis.	143
Figure 72. Material damping curves of the third layer utilized in the 1D soil response analysis.	143
Figure 73. Normalized modulus curves of the fourth layer utilized in the 1D soil response analysis.	144

Figure 74. Material damping curves of the fourth layer utilized in the 1D soil response analysis. 144

Figure 75. Normalized modulus curves of the fifth layer utilized in the 1D soil response analysis. 144

Figure 76. Material damping curves of the fifth layer utilized in the 1D soil response analysis. 145

Figure 77. Normalized modulus curves of all layers utilized in the 2D soil response analysis. "c" is the abbreviation of the layer having lateral continuity and the others are the individual ones. 145

Figure 78. Material damping curves of all layers utilized in the 1D soil response analysis. "c" is the abbreviation of the layer having lateral continuity and the others are the individual ones. 145

Figure 79. Normalized modulus curves of all layers utilized in 2D soil response analysis. "c" is the abbreviation of the layer having lateral continuity and the others are the individual ones. 146

Figure 80. Material damping curves of all layers utilized in 1D soil response analysis. "c" is the abbreviation of the layer having lateral continuity and the others are the individual ones. 146

Figure 81. The observed maximum and minimum fundamental periods with respect to the geological units after the first phase of the microtremor survey.... 149

Figure 82. The observed maximum and minimum fundamental periods with respect to the geological units after the second phase of the microtremor survey. 150

Figure 83. The comparisons of the H/V spectra obtained after implementing both phases. Please note that the numbers in the parentheses show the Phase number. .. 152

Figure 84. An interpolation map of the fundamental period along with the graduated symbols of amplification values observed at these periods overlying the geological units and the structural geological elements for a) Phase1 and b) Phase2. 154

Figure 85. The individual spectral curves of vertical (z), N-S and E-W components of a) Ort-07 (2), b) Ort19 (2). 156

Figure 86. The comparison of the stability of the soil responses by investigating the variations of the acceleration spectra after running 1D and 2D analyses for seven earthquakes.	159
Figure 87. The comparison of the stability of the soil responses by investigating the variations of the amplification ratio spectra after running 1D and 2D analyses for seven earthquakes.	160
Figure 88. The obtained spectral acceleration curves for one representative site of the geological groups after performing 1D and 2D numerical analyses.	163
Figure 89. 1D and 2D S_a responses of the sites a) Comb12 (2), b) Comb04 (2) and c) Comb01 (2) where 2D effect phenomenon is observed.	166
Figure 90. Comparison of the results of the a) 1D and b) 2D numerical analyses in terms of the peak spectral acceleration values and their corresponding periods.	169
Figure 91. Comparison of the maximum horizontal accelerations obtained by the 1D and 2D numerical analysis.	170
Figure 92. a) The 2D soil model of N-S (A-A') section along with distribution of the b) 1D and 2D A_{MHA} values.	174
Figure 93. a) The 2D soil model of E-W (B-B') section along with distribution of the b) 1D and 2D A_{MHA} values.	175
Figure 94. The acquired amplification ratio curves obtained by the site effect studies.	180

CHAPTER 1

INTRODUCTION

1.1. Purpose and scope

The purpose of the study is to construct an elaborative database including the results of the geotechnical field and laboratory tests, geophysical in-situ tests based on surface wave testing methods, experimental and numerical ground response analyses; in order to characterize the dynamic soil properties, to identify the non-linear behavior of the local site effects and to integrate the geological characteristics of the area with the field test results within soft and unconsolidated Upper Pliocene to Pleistocene fluvial clastics and especially Quaternary alluvial sediments (henceforth named as Plio-Quaternary sediments in their entirety) deposited towards the north of the Orta pull-apart basin due west of the Çankırı Province. The study area is close to the North Anatolian Fault System (NAFS), one of the most important earthquake regions in Turkey with its high seismicity potential.

One of the main aims of this study is to present validations for the results of each methodology by utilizing the in-situ characterization and site effect estimation techniques, depending on different fundamentals. The database was constructed by destructive (geotechnical boring log with standard penetration test N-value measurements and trial pits) and non-destructive (active and passive surface wave measurements) field and geotechnical laboratory tests at the study area. By comparison and correlation of the results of the geological survey, field and laboratory tests, this study aims at quantifying the vertical and lateral variations of

the Plio-Quaternary sediments. Even in a stratigraphic succession, this study indicates the possibility to differentiate between Upper Pliocene to Pleistocene fluvial clastics and Quaternary alluvial sediments, which are geologically difficult units to be distinguished distinctly in an area. Also, apart from the quantitative characterization of the depositional setting, effects of the presence of faults and thickness of their deformation zones to stiffness of the sediments as well as their contributions to the vertical and horizontal heterogeneity were identified. The spatial variations of the results were investigated within a GIS environment.

Local soil conditions were seismically characterized by non-destructive active (Multi-Spectral Analysis of Surface Wave) and passive (Microtremor Array Method) surface wave techniques in the content of this study. A combined usage of these surface wave methods was performed to enhance the resolution throughout the shear velocity profile. Various field configurations and data acquisition parameters for both methods, especially passive surface method (Linear, L-shape and triangular), were performed at the area by utilizing different types of seismographs to investigate the variability of the records with respect to the array geometry and the recording parameters. In addition, the seismic survey was conducted at the area at two different time intervals to especially investigate the consistency of the passive surface wave records with respect to time.

In-situ ambient noise measurements were performed by using different types of single mobile velocimeter. Within the delineated area, in order to obtain soil predominant periods and spectral ratio amplitudes of the soft soils, these measurements were taken in two phases conducted at different time intervals. Two sets of microtremor data were collected by using a systematic grid including shorter and longer records. By analyzing and comparing these two data sets, this study has a purpose to present an examination of at what degree data sets acquired at different time intervals are compatible with each other. These results were compared and correlated with the deep borehole data at different locations that are

in close proximity to the study area which were performed for assessment of the coal potential of the region in 1970.

In the context of this study, geological, geotechnical and geophysical data were integrated, the relationships among the geologic units, possible subsurface geometry of the bedrock, vertical or lateral variations in standard penetration test N-value, shear wave velocity data, the fundamental periods and spectral ratio amplitudes were investigated. A comparison was performed to correlate the results of the destructive and non-destructive field tests performed in the area. The result of this correlation study gives an idea regarding the degree of ability of the quantification analysis to characterize the soil stiffness present at relatively shallower parts of the study area (< 15 m depth). The results of this analysis back up the study related with idealization of the soil columns which is one of the stages in the numerical analyses.

Another main purpose of this study was to investigate the site effect phenomenon by performing 1D and 2D numerical analyses and comparing their results. Numerical analyses were performed with strong ground motion records as related to the seismotectonic characteristics of the study area. Based on the acquired results, a simplified scaling for the results of the 1D analysis have been proposed based on amplification ratios due to 2D topographic and basin effect. Also, this study included a comparison between the microtremor results and the numerical results. The final assessments of the results were performed within a Geographical Information Systems (GIS) environment by constructing a database in a manner to cover the region in its entirety. Therefore, the possible non-linear behavior of the ground response under a potential excitation was proposed for the determined sites.

1.2. Motivation of the study

On a regional scale, the study area is located at the base of a triangular area structurally outlined by the Ezine-Sungurlu Fault Zone at the southeast, the İnönü-Eskişehir Fault Zone at the southwest, and the North Anatolian Fault System at the north. Also, the area is very close to the Dodurga Fault Zone (DFZ) where the 06.06.2000 Orta earthquake ($M_W = 6.0$) has occurred. However, no active fault in the region between Çerkeş and Orta Districts was reported neither by governmental nor academic authorities. After the occurrence of the Orta earthquake, of which the epicenter was located to the south of the NAFS, it was noticed that there was a N-S trending active fault.

When the station records were examined, even though the moment magnitude of the earthquake was 6.0, it was observed that the peak ground acceleration (PGA) value of the earthquake was relatively lower than anticipated. However, the field studies performed shortly after the earthquake indicated that the quality of the superstructures in the villages was poor and these structures were those that were most affected from the earthquakes. In general, this earthquake caused heavy, moderate and light damage to more than 800 superstructures located within the border of the Orta District (Figure 1). Also, the Orta Earthquake caused the loss of 3 lives with more than 200 injuries within the District and its close vicinity. When Figures 1 and 2 are compared, it could be observed that the degree of the damage severity increased at some villages located at the western parts of the Orta District which are on the way of the DFZ. The destruction level of the earthquake was low especially in the center of the Orta district, due to the low PGA value and common usage of reinforced concrete in the structures.

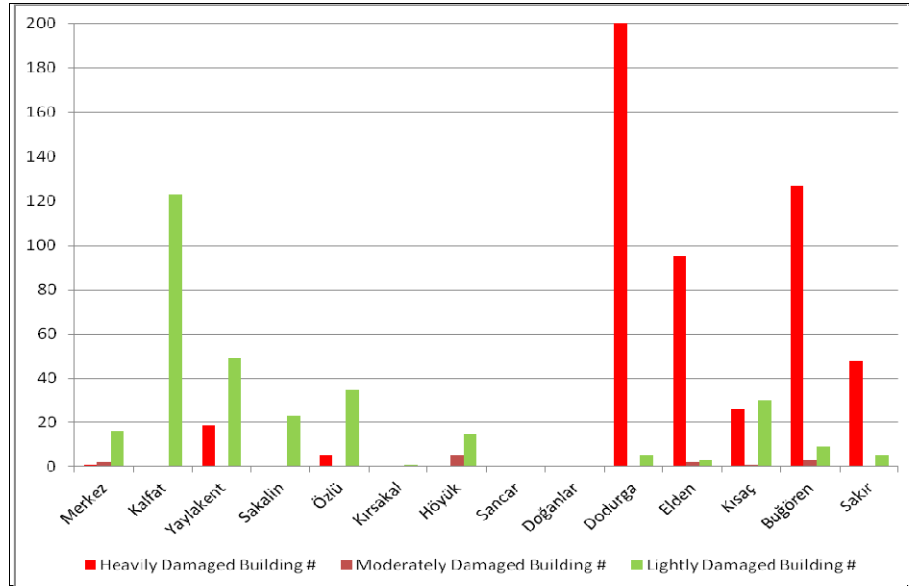


Figure 1. The classification and distribution of the damages with respect to the villages after the Orta earthquake (Modified from Taşkın et al., 2003).

The 06.06.2000 Orta Earthquake, its foreshocks and aftershocks are the only instrumentally recorded events since 1900 between the Ankara and Çankırı Provinces. These events have provided valuable data regarding the seismicity of the NW Central Anatolia. The other studies conducted after this earthquake propose that the DFZ is a sub-fault belt of the NAFS and it can continue towards the SSW direction towards the Çubuk District as a buried fault. This means that the seismic hazard potential of the area increases under a possible excitation along the fault zone since the possible surface rupture length can be greater than the observed case. Rather than the hazard potential regarding the activity of the DFZ, the study area is also close to the NAFS. Therefore, this state increases the possibility of an earthquake having a magnitude greater than 7.

Furthermore, in the study area, there are many local faults having a strike slip mechanism with considerable normal component. These faults result in the Orta pull-apart basin. The basin was formed under the control of the margin faults and the depth of depression increases due to the center line. This implies that a non-linear spatial variation of a ground motion can manifest itself due to the local soil

conditions, edge to basin and basin effects. Because of the reasons given above, the north of the Orta basin, covering Orta District and Kanlıca Village, was selected as the study area, in order to conduct geotechnical and geophysical characterization studies along with the experimental and numerical site effect analyses. These studies focused on the Plio-Quaternary sediments deposited near or within the basin under the control of the faults.

1.3. Study Area

The study area is located within the Orta District of the Çankırı Province that is situated approximately 80 km north of capital city, Ankara as an air distance and it is situated nearly 42 km west of the Çankırı Province center at the Şabanözü-Çerkeş motorway. The transportation network is highly developed in the area and connects Orta District to the Black Sea region, Çankırı Province and capital city Ankara (Figure 2). There are a number of villages close to this district such as Kanlıca, Dodurga, Yuva, Buğdüz, Sakarcören and Salur (Figure 2). The study area mainly encompasses the Orta District center and Kanlıca Village, and has approximately 30 km² areal coverage. The area is included in some portions of 1/25.000-scaled topographic quadrangles of G30-d1, G30-d2, G30-d3 and G30-d4 and, 1/100.000 scaled geological map of Çankırı G30.

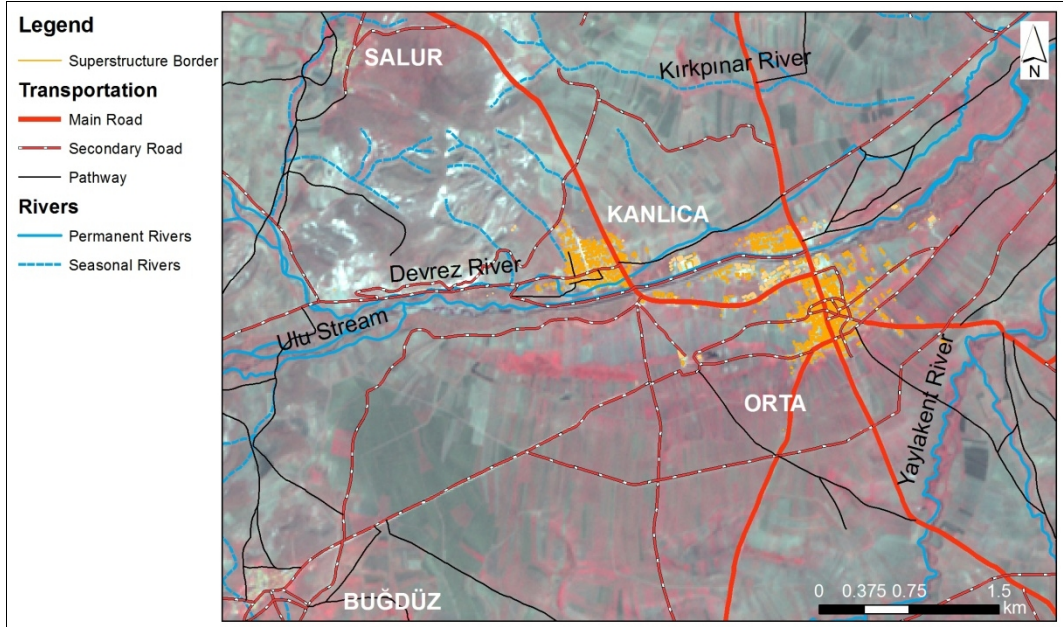


Figure 3. The study area where the investigations have concentrated.

The significant rises in the vicinity of the study area are Akbayır (1445 m), Tokluca (1405 m), Çal (1418 m), Güleyşen (1367 m) Hills in N and NW directions, Yazıpınar (1338 m), Belen (1391 m), Değirmen (1445 m) Hills in S and SW direction. The elevation of the study area from the sea level is considerable as stated above. The average elevation of the area surrounded by barren hills formed by volcanic units is approximately 1290 m. Despite this elevation, the topography of the Orta Plain where deltoid shaped Plio-Quaternary deposits are abundant is almost flat. Both side of the plain where Plio-Quaternary deposits are present are controlled by faults. The general trend of the long diagonal of the deltoid is along SW-NE direction which is parallel with the trend of the Devrez River. The topography of the study area is very gentle and the majority of the area has a slope less than 1 degree. Slope aspects of the central settlement area presents considerable variation and are generally in N, NW, S and SE direction which are perpendicular to the path of the Devrez River.

1.4. Procedure

The procedure followed in the content of this study can be mainly grouped in 5 stages: i) compiling a detailed database consisting of geological field survey data, deep and geotechnical borings along with standard penetration test N-value, geotechnical laboratory tests and the results of geophysical surveys carried out prior to this investigation, ii) expanding the database by excavating trial pits, performing geotechnical laboratory tests, implementing active and passive surface wave methods, recording microtremor measurements, iii) geological, geotechnical and geophysical characterizations of the area and identifying the lateral and vertical variations of local soil conditions within the area, iv) performing 1D and 2D soil response analyses and determination of the site response period and spectral amplitudes, and v) comparison of the site response studies. A flow chart of the study is given in Figure 4.

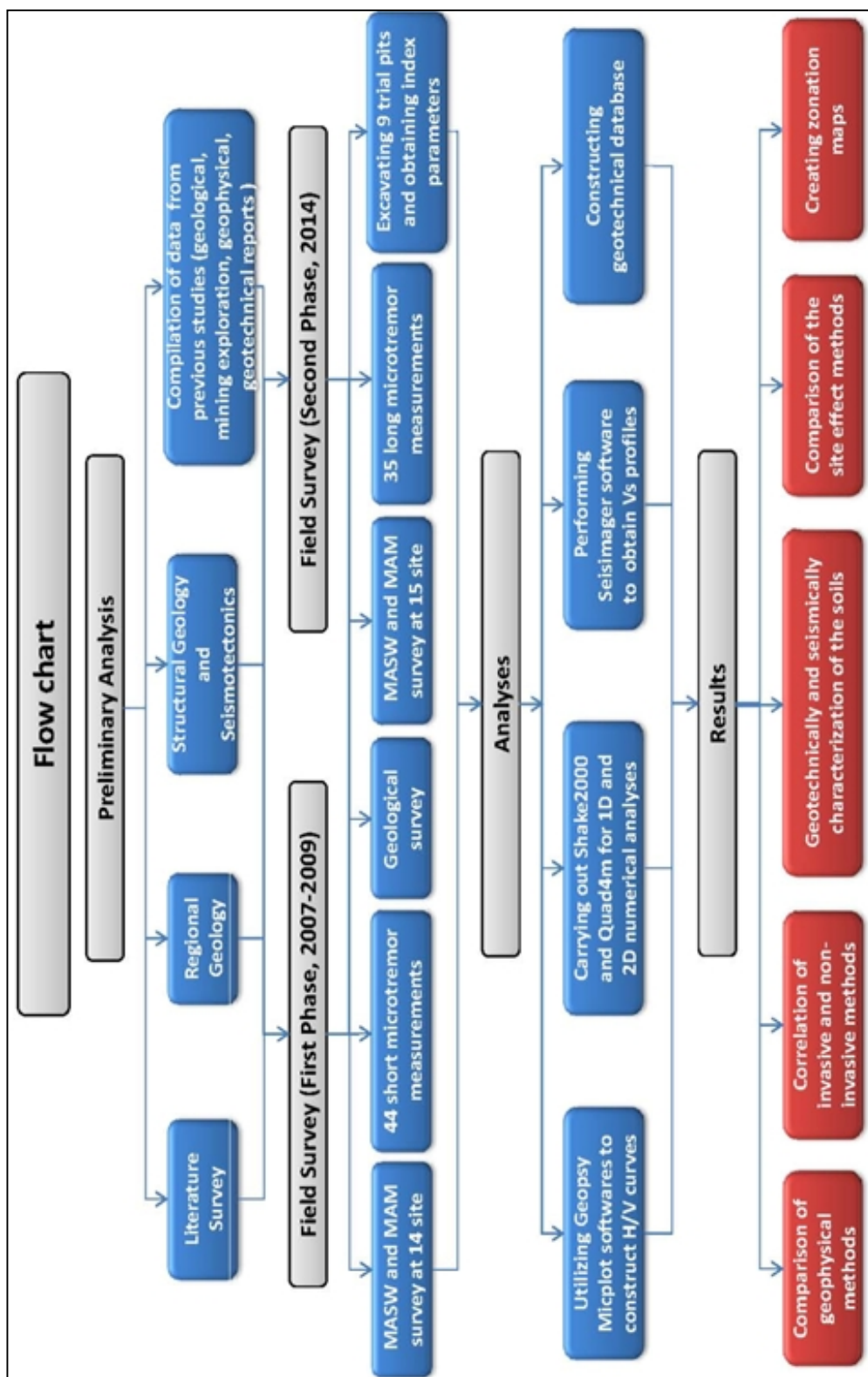


Figure 4. A flow chart of the study.

This dissertation consists of 6 chapters. The first chapter includes information regarding the outline of this study in the purpose and scope sections. Also, the reasons of the motivation to commence this study are explained in the second section. Description of the study area and reporting the thesis organization are given in the following sections in this chapter.

In Chapter 2, regional geology and seismotectonics of the study area from both regional and local scale are given. Also, the geological properties and characteristics of Plio-Quaternary sediments are given in the second section of this chapter. Along with these, tectonic setting of the region and dominant fault mechanism are presented. This chapter is concluded with the characteristics of the study area in terms of seismicity.

Theoretical background of the methodologies utilized in characterization studies are briefly given in Chapter 3 along with information regarding their advantages, disadvantages and the field application procedure. In the same chapter, the results of the destructive and non-destructive techniques along with their comparisons are discussed.

Chapter 4 includes the methodologies regarding estimation of site effect. 1D and 2D numerical ground response analyses along with the experimental field survey such as microtremor method are introduced in this chapter. The selection and the construction of 2D V_S sections and the sites where the 1D the analyses were performed are explained. In the following chapter, the results and comparison of the site effect studies are given. The last chapter encompasses a discussion part including the utilized methodologies in this study and their results, and a summary of this dissertation.

CHAPTER 2

REGIONAL GEOLOGY AND SEISMOTECTONICS

2.1. Introduction

Units from Lower Triassic to Quaternary outcrops are present in the Orta district and around its vicinity. The oldest rock unit is the formation named as Ankara Group or Karakaya formation (Bingöl et al., 1973) containing metadetrritic material and volcanic rock units metamorphosed at low degree green schist facies (Kasapoğlu et al., 2000). The formation also includes Upper Carboniferous-Permian limestone blocks, Lower Triassic in age (Sevin and Uğuz, 2011). The Triassic age metamorphic rock units are composed of metasandstone, metaconglomerate and metapelites in the region (Kasapoğlu et al., 2000). As can be seen in the regional geological map given in Figure 5, the oldest unit exposed over the area is located at the south and southeast of the study area. Terrestrial sedimentary rock units, deposited in Paleocene time, are conglomerate, sandstone and mudstone (Duru and Aksay, 2002). This geological unit can be observed at the west of the study area. According to Figure 5 prepared based on the digital record of the General Directorate of Mineral Research and Exploration (MTA, 2008), the above mentioned units are present outside the delineated region where this study has focused on. Therefore, they are have not been included in the further sections in this chapter.

Also, in a large scale, the area of focus is surrounded by Miocene sediments and the products of the volcanisms occurred in different Miocene age periods. Miocene sediment outcrops can be observed at the northern side of the investigated area. This unit has a significant lateral extend (Figures 5 and 6) when the scale of the

detailed investigation area is considered. This unit is composed of sandstone, siltstone, marl, argillaceous limestone, tuff intercalation and includes bituminous shale, coal and gypsum from place to place. These lacustrine environment sediments are interfingering with volcanics and pyroclastics. The volcanic rocks exposed especially at the southeast and east of the delineated area is composed mostly of andesite, basalt, dacite, tuff, and agglomerate in some places. These Lower, Middle and Upper Miocene volcanics cover a large area as can be seen in Figure 5. The Lower-Middle Miocene volcanics fall within the boundary of study area. This Lower Miocene unit is named as Tekke Volcanics by Akyürek et al. (1982) and it can be seen at the southeast and the east of the area (Figure 5). The last volcanic product in the region is Özlü Basalt (Türkecan et al., 1991) which has spread over the Miocene and Pliocene deposits. Lower Pliocene Özlü Basalt is exposed as a strip in approximately NW-SE direction at the east of the study area and this unit shows large outcrops at the northwest of the area. At the end of the Pliocene, the volcanic activity stopped and the sedimentation has been initiated by fluvial depositional system in the Orta basin (Akyürek, 1984). The detailed description of the units exposed to the surface within the Orta basin can be found in the following sections of this dissertation.

The study area has been exposed to a new tectonic period by the continental collision during the Neogene. In the literature, there are different geological models proposed by Koçyiğit (1991a, 1991b, 1992) and Koçyiğit et al. (1995); Seyitoğlu et al. (1997 and 2000); Kaymakçı (2000) and Kaymakçı et al. (2001) regarding the Neogene evolution of the area. However, assessment of the validity of these models for the entire region located at the NW central Anatolia is not the subject of this study. By considering the purpose of the study, the results of the proposed studies was summarized in this chapter.

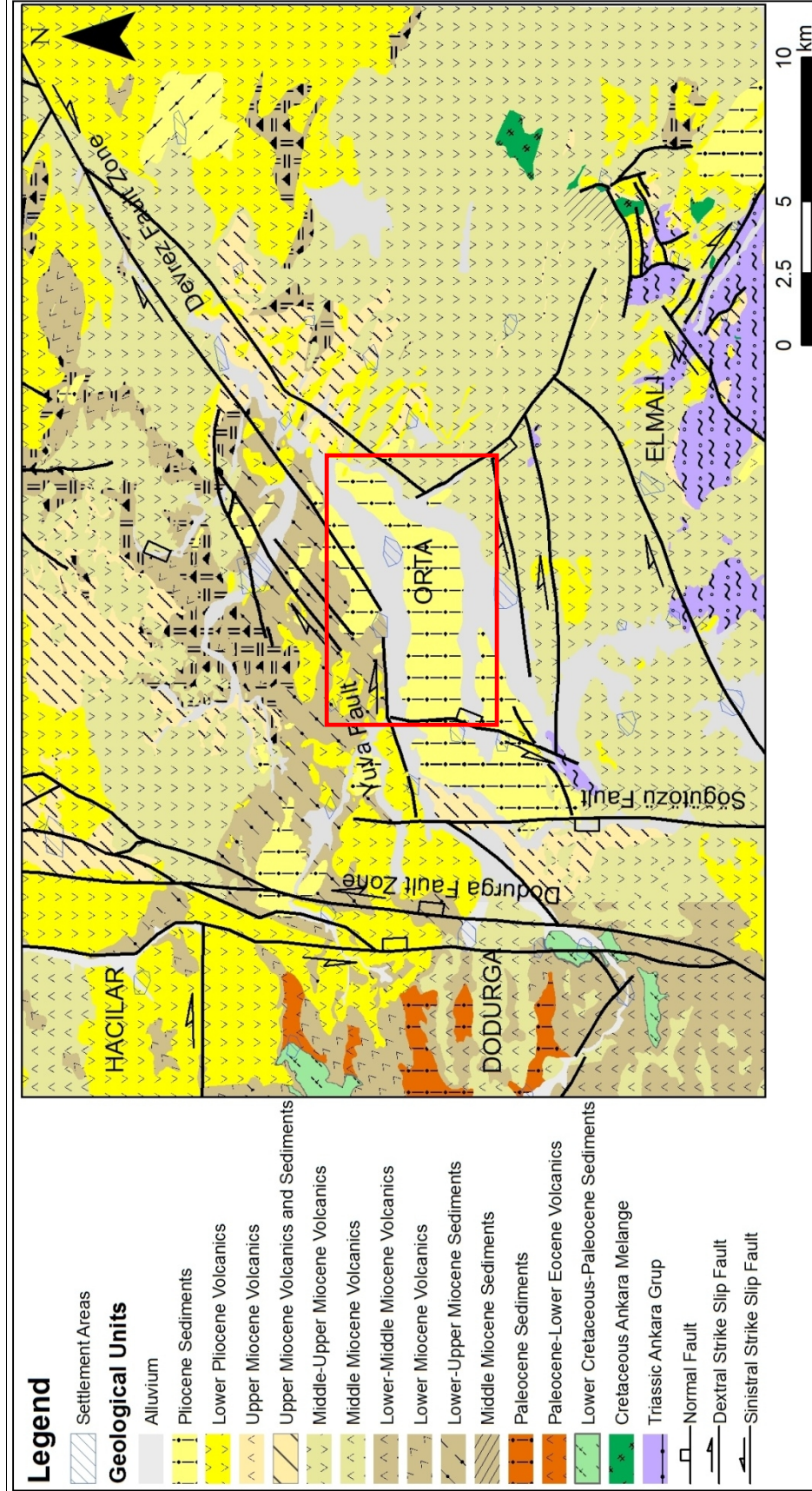


Figure 5. Regional geological map of the study area along with the neotectonic features. The geological map was reproduced from the MTA digital records (MTA, 2008). The red rectangular area shows the area that is concentrated in this study.

The main scope of this study is to determine the site effects regarding soft and unconsolidated local soil conditions and topographical effect. In the context of this purpose, local soil conditions were characterized quantitatively by using geological, geotechnical and geophysical studies in the Orta basin. Site effects analyses were performed by either 1D or 2D ground soil response analyses based on the results of the field work or the experimental field surveys. Therefore, based on this scope, the soft and unconsolidated deposits, and their geological characteristics were determined and described in this chapter. In this respect, the neotectonic period of the area indicates that the soft lithologies were deposited under the control of the new tectonic regime. It implies that these young sediments have not been settled long enough to manifest any considerable indications of soil formation or lithification.

In the dissertation, the classification of the geological units based on the paleotectonic and neotectonic periods was not performed since all measurements were conducted in Quaternary, Pliocene and Miocene sediments in order to show the lateral variation of the seismic characteristics of the layers within the delineated area given in Figure 5. The study area is one of the strike slip (pull-apart) basins in NW central Anatolia. Based on the deep boring studies (Tokan and Özgen, 1976) to investigate the coal/lignite reserve of the Orta area (Figure 6), it is known that the sediment thickness within the basin is more than 145 m. According to the deep boring logs, volcanic products, especially basalts are interfingering with the sedimentary deposits at the western edge of the basin. This synsedimentary intrusion may show a considerable lateral extent at the base of the Orta area. Based on the tectonic setting, it should be stated that the Upper Pliocene -Quaternary sediments are the most susceptible deposits in terms of the scope of this study.

In the following section, a detailed geological description of these sediments are given. A local geological map of the area was prepared by compilation and modification of the studies proposed by Tokan and Özgen (1976); Türkecan et al.,

(1991); Türkmenoğlu et al. (1991); Emre et al., (2000); Koçyiğit et al. (2001) and MTA digital records (2008). This compiled and modified geological map of the delineated area is given in Figure 6.

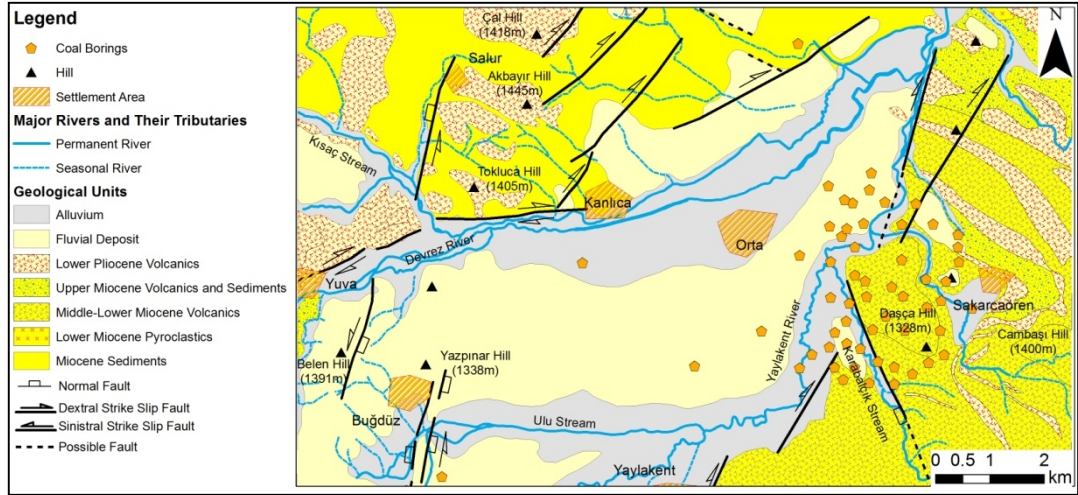


Figure 6. The simplified geological map of the study area [compiled and modified from Tokan and Özgen (1976); Türkecan et al., (1991); Türkmenoğlu et al. (1991); Emre et al., (2000); Koçyiğit et al. (2001) and MTA digital records (2008)] along with the distribution of the deep borings over the area.

2.2 Sedimentary Geological Units

2.2.1. Miocene Sediments

This sedimentary unit was deposited in a lacustrine environment. It has a large areal coverage at the study area, especially at the northern section (Figure 6). The unit is composed of intercalations of sandstone, siltstone, marl, argillaceous limestone and tuff (Figure 7). It also includes bituminous shale, coal and gypsum from place to place (Siyako, 1987; Akyürek et al., 1980). The unit is cemented epiclastic rocks with a high clay content (Türkmenoğlu et al., 1991).



Figure 7. A view from sandstone-marl-tuff intercalation in the Miocene sediments located at the northern side of the Orta basin.

In this unit, the argillaceous limestone and the marl deposits are white, yellowish white colored and thin to moderately bedded. The siltstones are grey colored, loosely packed, thin bedded and laminated. Claystone, siltstone and marl levels generally form the upper layers of this unit. Also, these sediments can be observed as interlayers at other levels of the Miocene unit. These are white, grey, greenish white colored and are thin bedded (Açıkgöz, 2004). The sandstones and conglomerates are yellowish grey colored, loosely packed and their beddings are unclear. The sandstone shows well sorted and well rounded deposition. They are polygenetic in composition and cemented by carbonate, silica and clay. This formation is also composed of laminated and white colored bituminous shales. It contains leaf fossils, silicified wood fragments and gastropod fossils (Türkecan et al., 1991). Furthermore, it is possible to observe coal and gypsum bearing levels within the Miocene sediments. This indicates that the depositional environment was shallower from time to time (Sevin and Uğuz, 2011). An exact thickness of the unit cannot be determined in the literature since the base of the formation could

not be observed within the study area, but the regional studies reported that the thickness of this unit can be up to 500 m (Akyürek et al., 1980).

2.2.2. Pliocene Sediments

Özlü Volcanics are the last volcanic product within the study area and their distribution within the area is in the shapes of the islands, lenses and strips. The Özlü Volcanics is composed of basaltic volcanics, which commenced the activity in the region during Late Pliocene; and cut the underlying volcanics. It is the last product of the volcanic activity in the region spread over the Upper Miocene and Pliocene deposits (Akyürek et al., 1984). At the uppermost part of the sequence, Pliocene terrestrial-lacustrine deposits cover unconformably all of the older units (Figure 6).

The study area is located in an area where the Pliocene lacustrine and fluvial sediments were deposited (Figure 6). The products of the Pliocene volcanic activity can be observed as interlayers within these sediments from place to place. In general, it is possible to observe this formation in two facies, as lacustrine and terrestrial deposits. Lacustrine Pliocene deposits are composed of transported gravel and tuff of lava origin mixed mainly with marl and clay. It is possible to observe limestone lenses within the deposits. Furthermore, these limestones can be mapped as a separate member of this formation at the west of the study area (Bilginer et al., 2002). The thick clay layer forming the lower section of the formation was deposited in the lacustrine environment. In this Pliocene unit, some lignite levels are present with a varying thickness (Tokan and Özgen, 1976; Türkmenoğlu et al., 1991). The upper level of the lignite seam can be seen in Figure 8. Macro plant fossils are present at the clay abundant section of this formation (Türkmenoğlu et al., 1991).



Figure 8. A view from the upper lignite seam located at the southeast of the study area.

Channel fill and flood basin deposits transported by the rivers overlie the clay layers in the Orta basin. This deposition took place when the intensity of the tectonic activity was high (Koçyiğit et al., 2001). The grain size distribution of these deposits decreases towards the deposition center. The distinct outcrops are very limited to observe the geological characteristics of this unit in the area. The unit is composed of grey, greenish grey, white colored, sub-horizontal bedded conglomerates, sandstone and siltstone intercalation. The unit includes light grey colored tuff particles as well (Figure 9). Conglomerates are composed of cross-bedded, loosely packed, grain supported gravels of different origin and grain sizes. Sandstone and siltstone layers are thin bedded and are present in the form of lenses. The sandstones are cross-bedded or parallel laminated. The siltstone interlayers are present within these sandstones and can be observed as relatively thick beds (Sevin and Uğuz, 2011). This formation has a large areal coverage throughout the study area and is among the units where field tests have been performed extensively (Figure 6). A high groundwater level was observed at some

localities in this unit. This unit unconformably overlies the basement rock and is overlain unconformably by Quaternary alluvial deposits of Devrez river (Figure 6). The approximate thickness of the unit varies between 50 m and 150 m according to Bilginer et al. (2002).



Figure 9. A close view of the Pliocene sediments including the tuff particles.

2.2.3. Quaternary Sediments

Quaternary alluvium and terrace sediments deposited along the courses of the Devrez and Yaylakent rivers are the important components of the recent fluvial system of the area (Figure 6). These deposits can also be observed along Gindek, Kısaç, İçin and Köçet streams in the area (Figure 6). The width of the unconsolidated deposits reaches their maximum extent of 1.5 km near the Orta district center. The thickness of the unit increases especially towards the center of the flood plain and decreases to 1 m – 2 m towards the north and south edges of the basin. The groundwater level is located at the shallower parts of this unit. The

level has a range between 0.6 m and 2 m in this unit (according to this study). The Quaternary alluvial fill forms a relatively thick layer (>20m) that disconformably covers the older units within the Orta basin.

A significant part of the study area is covered with the alluvial materials (Figure 6). Young alluvium deposits are observed along the course of Devrez river and its flood plains while the other areas are covered with older alluvium deposits. Due to their similar geological and geotechnical properties, however, no discrimination could be made between these two alluvium sediments. For this reason, young and old alluvium deposits were considered together as Quaternary alluvial deposits. The Quaternary terraces were formed by the shifting of the river courses due to the uplifting in the area. These deposits have an undulated topography because of the erosions caused by the rivers (Figure 10). The upper levels of the alluvium material within the study area are mostly composed of sandy and gravelly soil of 10 m thickness at the center of the basin. Conglomerates are polygenetic in composition and they are well rounded, poorly spherical and well graded. Grayish brown colored clay and silty layers are generally present underlying this coarse grain bearing level. This fine grained level has a considerable thickness that exceeds 20 m. Also it should be noted that these coarse grained layers can be observed as interlayers within the clayey soils.



Figure 10. A view of the Quaternary terraces from the WNW of the study area.

2.3. Tectonic setting and seismicity of the area

According to the structural geological studies proposed by Koçyiğit (1991), post-collision compressional regime is dominant in NW Central Anatolia until Late Miocene and a new compressional tectonic period due to strike slip faulting has initiated after Late Miocene. During this new tectonic period, intracontinental continuous deformation direction indicating compression has changed from NW-SE to N-S in Late Pliocene and current dominant compression direction is in N-S direction (Koçyiğit, 1991b and 1992). Consequently, according to the study, a continuous compressional regime is dominant at the NW Central Anatolia from the Neogene to recent. According to Koçyiğit (1992), the termination age of the compressional regime following collision through the Ankara-Erzincan suture zone is Pontian (Late Miocene) and then Plio-Quaternary neotectonic period was initiated due to strike slip faulting.

Koçyiğit et al. (1995) state that the termination age of the compressional regime following the collision which is defined as “Ankara Orogenic Phase” is Late-Early Pliocene. According to Koçyiğit et al. (1995), the intracontinental convergence

between Sakarya Continent, Menderes-Taurides and Kırşehir Blocks continued up to Late-Early Pliocene and old basement rocks (arc massif), active edge deposits of Sakarya Continent and ophiolitic melange material were thrust to the south as slices onto the Menderes-Taurides Platform and the Kırşehir Block (Figure 11). Along with this southward trending tectonic transportation, the continental molasses and the post-collision volcanic activity at the Oligocene-Early Pliocene Galatia Volcanic Complex have occurred within a piggyback basin. During this tectonic transportation and movement period, deformations such as folding and thrusting have occurred at all these rock units and the cover units of the Oligocene-Lower Pliocene molasses (Koçyiğit et al., 1995). The rock units that have undergone deformation prior to Late-Early Pliocene have overlain by Plio-Quaternary fluvial sediments and deposition of this sequence has been accompanied by steeply angled normal faults with dominant strike-slip components (Koçyiğit et al., 1995). Consequently, according to Koçyiğit et al. (1995) a new tectonic regime as a result of gravity subsidence has become dominant in the region starting from Late-Early Pliocene.

Seyitoğlu et al. (1997) suggest a new opinion on Late Cenozoic tectonic evolution of NW Central Anatolia. Seyitoğlu et al. (1997) have re-investigated the four key regions in the vicinity of Ankara where the study was conducted by Koçyiğit (1991) before. According to Seyitoğlu et al. (1997), the thrusting boundaries between the older basement rock and the Neogene units identified by Koçyiğit (1991b) are bounded by a normal fault. Based on this observation as well as previous geochemical studies (Keller et al., 1992, Seyitoğlu and Scott, 1992) Seyitoğlu et al. (1997) state that the post-collision compressional tectonic regime has ceased in Early Miocene and an extensional tectonic regime has developed due to the orogenic collapse during the Early Miocene-Pliocene period, and a transpressional or transtensional tectonic regime due to the strike slip movement of the North Anatolian Fault System (NAFS) has been dominant in the region from Pliocene to recent.

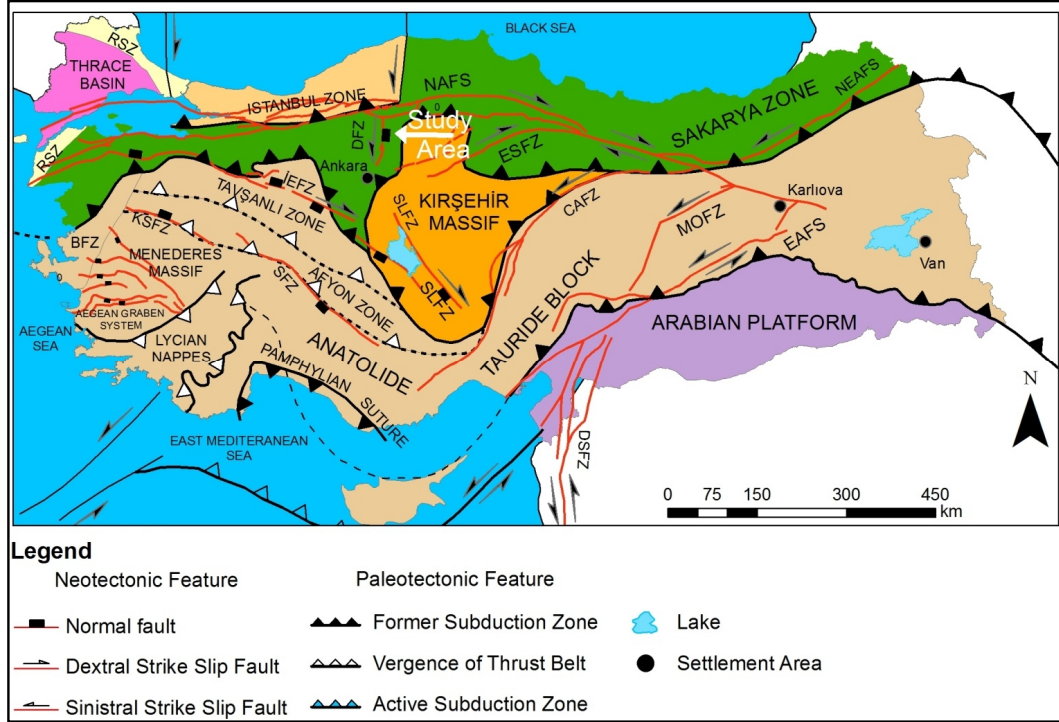


Figure 11. Major paleotectonic and neotectonic features of Turkey (compiled and modified from Okay and Tüysüz, 1999; Bozkurt, 2001; Kaymakçı et al., 2003; Şengör et al., 2005; Moix et al., 2008; Kuşçu et al., 2009)

According to the study performed by Seyitoğlu et al. (2000), in which they performed at the western side of the Çankırı Basin and investigated the relationship between the Neotethys suture zone units and the Neogene rock units, the eastern flank of the Neotethys suture zone is bounded by a thrust fault (Figure 11). They also state that the western flank is controlled by a normal fault. Seyitoğlu et al. (2000) indicate that during the Pliocene, the Neotethys suture zone rock units are embedded as a tectonic wedge (Burchfiel et al., 1992; Fossen, 2000) to the Çankırı Basin located between the NAFS and the Kırıkkale-Erbaa Fault as a result of the compressional effect of these two faults, thus dividing the basin as normal faulted at western flank and thrust at eastern flank. These observations are different from the results of the other studies (Akyürek et al., 1980, Hakyemez et al., 1986, Koçyiğit 1992, Koçyiğit et al., 1995, Kaymakçı 2000, Kaymakçı et al., 2001) in the literature.

According to Kaymakçı (2000) and Kaymakçı et al. (2001), the extensional tectonic regime was active during Burdigalian (Early Miocene) and Tortonian (Late Miocene) period after the termination of pre-Neogene compressional regime and a transpressional tectonic regime was active from Tortonian to recent with the influence of the NAFS (Figure 11). According to the tectonic model proposed by Kaymakçı (2000) and Kaymakçı et al. (2001), the Kırşehir Block has compressed the Sakarya Continent due to collision of the plates before Burdigalian. According to these studies, the extensional regime is dominant in the region as a result of orogenic collapse in the Burdigalian-Serravalian period and the pre-Neogene units (Neotethys suture zone rock units) divides the Çankırı and Hançili Basins with a normal faulted paleo-rise at the edges of the basin. The units deposited in these two basins are different from each other even though they have been deposited during the same tectonic period (Kaymakçı 2000, Kaymakçı et al., 2001). The planes acting as normal faults during the extension period have transformed to a new compressional regime characterized by the strike slip faults from Late Miocene to present (Kaymakçı 2000, Kaymakçı et al., 2001).

As stated above, although there are major differences in the models for the area as given above, all models state that the region has been controlled by a new tectonic regime after the continental collision at the Neogene. Most of these models agree that the new tectonic regime is characterized mainly by strike slip faulting (Figure 11). Therefore, the neotectonic regime has caused the development of NS and NNE trending faults, fault sets and strike slip basins (Koçyiğit, 1991; Koçyiğit et al., 1995 and 2001; Kaymakçı, 2000; Kaymakçı, et al., 2000). The Orta basin is one of these strike slip (pull-apart) basins in NW Central Anatolia. Based on the type and nature of active tectonic regimes and related structures such as faults and basins, an intracontinental tensional neotectonic regime and oblique slip normal faulting characterize the study area, as stated by Koçyiğit et al. (2001) and Koçyiğit (2003). These structures can be seen in the simplified tectonic map of the region given in Figure 12.

The area is surrounded by fault zones and fault systems where moderate and large magnitude earthquakes can occur. From a general view, the study area is located at the base of a triangular area structurally outlined by the Ezine-Sungurlu Fault Zone at the southeast, the İnönü-Eskişehir Fault Zone at the southwest, and the NAFS at the north (Figure 12). The most important of these faults which have a potential to generate earthquakes with magnitudes 6 and higher are located at the İsmetpaşa-Kargı section of the NAFS. This section can also be seen in Figure 12.

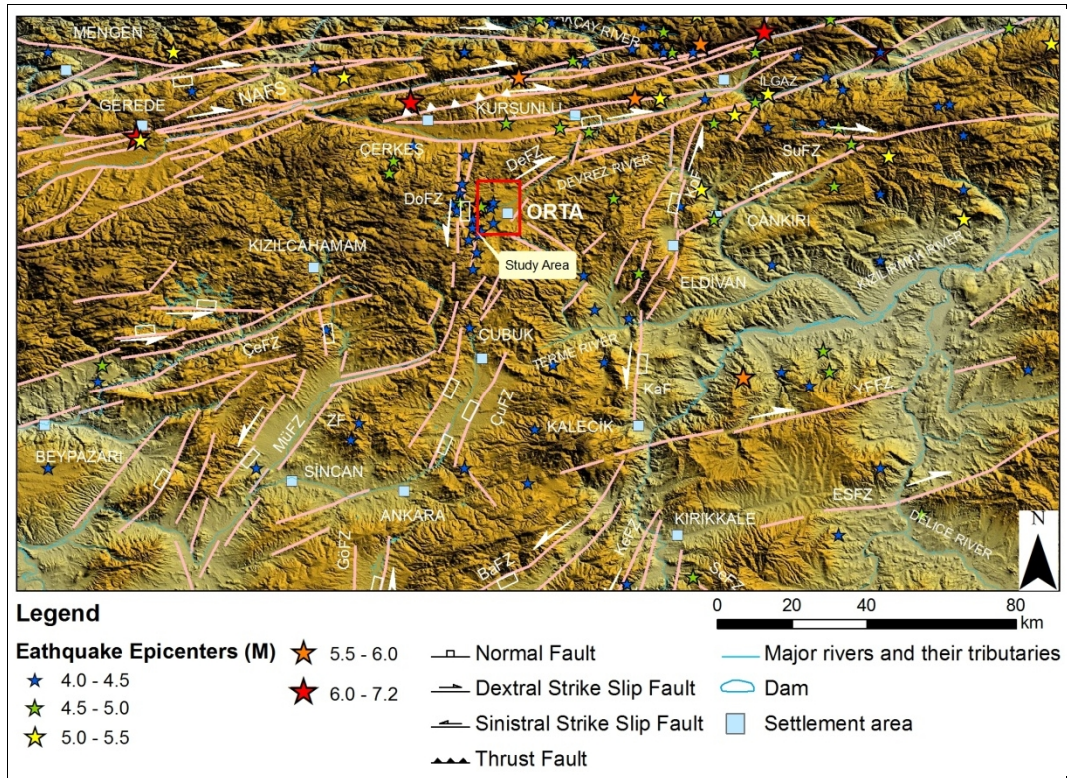


Figure 12. Simplified seismotectonic map of the study area overlying the hillshade of the area (Modified from Emre et al., 2000; Koçyiğit et al., 2001; Akyüz et al., 2002; Kaplan, 2004).

The İsmetpaşa-Kargı section of the NAFS is formed by 6 different sub-fault zones, which are; Eskipazar, Ulusu, Tosya, Çerkeş-Kurşunlu, Devrez and Dodurga Fault Zones. While the Ulusu Fault Zone is a main section of NAFS, the Dodurga and Devrez Fault Zones are faults splaying from NAFS. The remaining three fault

zones (Eskipazar, Tosya and Çerkeş-Kurşunlu) have anastomosing pattern. In general, these fault zones have lengths ranging between 35 km and 320 km (Blumental, 1945; Ambraseys, 1970; Barka and Kadinsky-Cade, 1988; Koçyiğit et al., 2001), and have deformation zone widths ranging from 1 km to 7 km (Koçyiğit et al., 2001). As can be seen in Figure 12, apart from the Dodurga Fault Zone (DFZ), the remaining faults are right lateral strike slip faults. The DFZ, on the other hand has a considerable normal component and is a left lateral strike slip fault. The Dodurga Fault Zone is 4 km to 7 km in width at the surface and has a length of 36 km (Koçyiğit et al., 2001).

If seismic activity of the İsmetpaşa-Kargı section is to be examined from 1900 to recent, the earthquakes that have occurred on the above mentioned fault zones are the 09.03.1902 Korgun (Io=IX), the 26.11.1943 Tosya-Ladik (M= 7.6), the 01.02.1944 Bolu-Çerkeş (M= 7.6), the 13.08.1951 Kurşunlu (M= 6.5), the 07.09.1953 Çerkeş-Kurşunlu (M= 6.4), the 05.10.1977 Ilgaz (Ms= 5.8) and the 06.06.2000 Orta (M=6) in a chronological order (Ergin et al. 1967; Ambraseys, 1970; Alsan et al., 1975; Ambraseys and Finkel 1987). The list of the earthquakes recorded during the instrumental period is listed in Table 1.

These earthquakes which occurred between 1902 and 2000 have resulted in the rupture of most of the sections of Ulusu, Çerkeş-Kurşunlu, Tosya and Dodurga fault zones. Apart from the Orta earthquake, the other earthquakes have manifested distinct surface ruptures (Taşman, 1944; Blumental, 1945; Pınar, 1953; Öztürk, 1968; Ketin, 1969; Tokay et al., 1973, Demirtaş, 2000 and Emre et al., 2000). When the earthquakes listed in Table 1 are to be observed, it can be seen that a total of five large earthquakes ($M \geq 6$) have occurred within the study area since 1900. Their spatial distribution is given in Figure 12. This indicates that the study area has gone through high activity in terms of seismicity. The moment magnitudes of these five earthquakes range between 6 and 6.8. This indicates that the study area and its close proximity may be subjected to destructive earthquakes. In the further chapters of this study, a study was performed in regards to

determining which of these faults have potential to generate large magnitude earthquakes based on the investigations regarding the distance to the area and which one can generate events with larger magnitude.

On a local scale (Figure 6), the western side of the basin is bounded by NNE trending left lateral strike slip faults having considerable normal components. The northern part of the basin is under the control of a NE trending right lateral strike slip fault with a significant normal component. The southern side of the depression is constrained by ENE trending right lateral strike slip faults with normal components. The East and East-Southeast margin of the basin is controlled by a NW striking normal fault with strike slip component. These faults form the Orta pull-apart basin.

Table 1. The list of the major earthquakes that occurred within the study area and its close vicinity (compiled from EERC-ERD, 2009; DDA, 2015; KOERI, 2015)

Date	Time	Lat.	Long.	Depth (km)	Magnitude Type	Magnitude	District	City
09.03.1902	-	40.67	33.57	-	Ms (Mw)	5.5 (-)	Merkez	Çankırı
09.08.1918	00:39:10	40.89	33.41	10	Ms (Mw)	5.8 (5.8)	Ilgaz	Çankırı
09.06.1919	15:47:17	40.68	33.89	10	Ms (Mw)	5.0 (5.3)	Yapraklı	Çankırı
09.06.1919	07:13:50	41.16	33.20	10	Ms (Mw)	5.7 (5.8)	Araç	Kastamonu
16.08.1923	03:52:00	41.02	34.41	40	Ms (Mw)	5.2 (5.4)	Kargı	Çorum
03.10.1928	00:57:08	40.47	33.42	70	Ms (Mw)	5.0 (5.3)	Şabanözü	Çankırı
04.10.1928	11:14:08	40.22	33.67	10	Ms (Mw)	5.7 (5.8)	Sulakyurt	Kırıkkale
21.09.1936	11:41:25	41.21	33.53	20	Ms (Mw)	5.1 (5.3)	İhsangazi	Kastamonu
18.11.1936	15:50:14	41.25	33.33	10	Ms (Mw)	5.4 (5.5)	Araç	Kastamonu
31.05.1938	17:55:22	40.90	33.73	10	Ms (Mw)	5.1 (5.3)	Ilgaz	Çankırı
21.11.1942	14:01:53	40.82	34.44	80	Ms (Mw)	5.5 (5.6)	İskilip	Çorum
26.11.1943	22:20:41	41.05	33.72	10	Ms (Mw)	7.2 (6.8)	Ilgaz	Çankırı
02.01.1944	10:59:00	41.00	33.70	10	Ms (Mw)	5.0 (5.3)	Ilgaz	Çankırı
01.02.1944	03:22:40	40.80	32.22	10	Ms (Mw)	7.2 (6.8)	Gerede	Bolu
10.02.1944	12:05:27	41.00	32.30	10	Ms (Mw)	5.3 (5.5)	Mengen	Bolu
18.10.1944	12:54:05	40.89	33.47	10	Ms (Mw)	5.2 (5.4)	Ilgaz	Çankırı
02.03.1945	10:39:44	41.20	33.40	10	Ms (Mw)	5.6 (5.7)	Araç	Kastamonu
07.06.1945	01:20:41	41.17	33.25	10	Ms (Mw)	5.2 (5.4)	Araç	Kastamonu
21.01.1946	11:25:32	41.05	33.48	60	Ms (Mw)	5.0 (5.3)	Ilgaz	Çankırı
13.05.1949	20:14:07	40.94	32.71	20	Ms (Mw)	5.1 (5.3)	Eskipazar	Karabük
13.08.1951	18:33:34	40.88	32.87	10	Ms (Mw)	6.9 (6.6)	Çerkeş	Çankırı
14.08.1951	18:46:08	41.08	33.18	40	Ms (Mw)	4.9 (5.2)	Kurşunlu	Çankırı
07.09.1953	03:59:04	40.94	33.13	40	Ms (Mw)	6.0 (6.0)	Kurşunlu	Çankırı
21.09.1957	20:16:59	40.75	34.02	40	Ms (Mw)	5.1 (5.3)	Yapraklı	Çankırı
10.12.1966	17:08:33	41.09	33.56	13	Ms (Mw)	5.2 (5.1)	İhsangazi	Kastamonu
23.06.1967	10:06:55	40.85	33.65	20	Mb (Mw)	5.1 (5.4)	Ilgaz	Çankırı
22.12.1969	-	40.60	34.20	-	Mb (Mw)	5.1 (-)	Bayat	Çorum
05.10.1977	05:34:43	41.02	33.57	10	Ms (Mw)	5.8 (5.6)	Ilgaz	Çankırı
14.02.2000	06:56:35	40.94	31.70	10	Md (Mw)	5 (5.1)	Yığılca	Düzce
06.06.2000	02:41:50	40.63	33.03	10	Md (Mw)	5.9 (6.0)	Orta	Çankırı
06.06.2000	05:59:39	40.64	33.07	8	Ms (Mw)	4.0 (4.4)	Orta	Çankırı
08.06.2000	21:27:58	40.64	32.99	-	Ms (Mw)	4.2 (4.4)	Orta	Çankırı
09.06.2000	03:14:19	40.52	33.03	-	Ms (Mw)	4.4 (4.7)	Orta	Çankırı

2.3.1. The Orta earthquake

The 06.06.2000 Orta Earthquake, its foreshocks and aftershocks are the only instrumentally recorded events since 1900 between Ankara and Çankırı. The Orta Earthquake has a moment magnitude of 6.0 and it provides valuable data regarding the neotectonics of the NW Central Anatolia. This event was felt from the capital, Ankara (70 km to the south), where the earthquake caused minor property damage in the town of Orta and some villages to the west, and caused 3 casualties with more than 200 injuries (Demirtaş, 2000 and Taşkın et al., 2003).

The Orta earthquake was somewhat an unexpected event for the area since its epicenter is located in a region nearly 30 km away from the NAFS, where no active faults were previously reported (Şaroğlu et al., 1992). The Orta Earthquake record at the Çerkeş Station located nearly 12 km away from the DFZ is given in Figure 13. Moreover, the fault plane solutions show that the event is associated with an oblique-normal-slip fault trending at a high angle to the strike-slip NAFS (Figures 11 and 12). Most of the focal mechanism solutions proposed by Taymaz et al. (2007) and different earthquake research institutes (Harvard and ERI) are in good agreement and show an oblique normal displacement on east dipping and N-S trending left-lateral strike-slip fault. This supports the structural geological observations of Emre et al. (2000) and Koçyiğit et al (2001).

The main event was recorded by strong motion stations located at Çerkeş, Karabük, Kastamonu, Bolu and Düzce (in the order proximity to the DFZ). The record at the Düzce station shows that the peak ground acceleration (PGA) has occurred in a E-W direction and had a low magnitude of 63.2 cm/s^2 (Figure 13). The peak ground acceleration recorded in the other stations were also in the E-W direction with a PGA value lower than 63.2 cm/s^2 due to the greater distances between the DFZ and the stations. Along with this, the records in the E-W direction for all five stations were similar to those in the N-S direction.

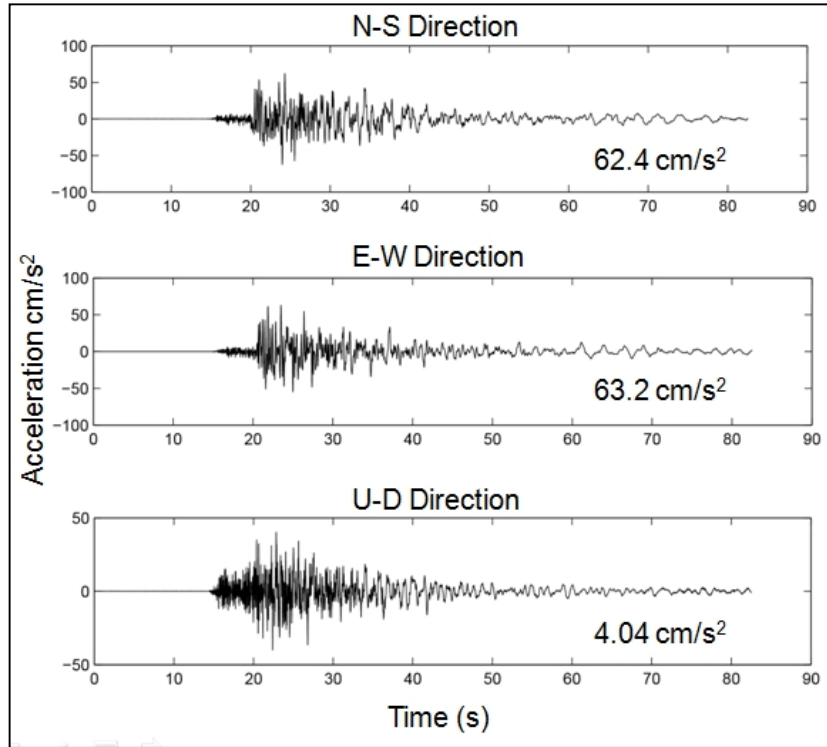


Figure 13. The record of the 2000 Orta Earthquake at the Çerkeş station.

Although having a low PGA value, this earthquake caused heavy, moderate and light damage to more than 800 superstructures located within the Orta District. Structural damage observed at the reinforced concrete structures in the region was smaller than those of masonry, etc., structures. As stated above, there are many fault zones located in close proximity to the area which have capability to generate potential destructive earthquakes with a higher PGA value than that of the Orta Earthquake. Also, according to Koçyiğit (2008), the DFZ continues to the south and it is also stated that the Çubuk Fault Zone in the Ankara Province might be a continuation of the DFZ. This suggestion also increases the intensity level of a possible earthquake when compared with the Orta Earthquake. Therefore, when the characteristics of the area in terms of the seismicity and the vulnerability of the buildings in the area to the low PGA Orta Earthquake are taken into consideration, the significance of this study increases.

CHAPTER 3

METHODOLOGIES FOR CHARACTERIZATION STUDIES

3.1. Introduction

The process of identifying the layers that underlie a site and their physical characteristics is the main purpose of the in-situ testing. Generally, the in-situ field techniques are categorized based on the necessity of a boring to acquire information. Based on their nature, these tests are classified as destructive and non-destructive field tests. The most preferred data for soil characterization studies are mainly dependent on the Standard Penetration Test (SPT) and shear wave velocity surveys either in engineering practice or in scientific researches. These two techniques provide the important parameters required to establish a seismic design criterion for an engineering site. The results of these techniques substitute each other for any engineering practice. In the literature, there are many investigations demonstrating how these two parameters can be derived from each other (e.g. Kanai, 1966; Ohto and Goto, 1978; Fumal and Tinsley, 1985; Pitilakis et al., 1992; Kayabalı, 1996; Koçkar and Akgün, 2008; Dikmen, 2009; Koçkar et al., 2011).

The SPT is a destructive test since a geotechnical borehole should be drilled in order to implement the test. Although the requirements of this in-situ geotechnical test makes it more costly when compared with the surface geophysical methods, it reveals the concrete findings regarding the identification of the soil layers, determination of the stiffness parameters of these layers, designation of the ground

water level and acquisition of samples for geotechnical laboratory tests. Also, the disturbed soil samples can be obtained at any desired depth throughout a boring while performing SPT. On the other hand, non-destructive geophysical methods have significant attractive advantages when compared with the SPT. For example, a large area can be covered within a relatively short period of time. Also, much deeper parts can be characterized more cost efficiently. Therefore, these methods are highly feasible in terms of time and money.

Moreover, besides the main usage of SPT and V_s in engineering applications and in correlation studies, these are the main parameters utilized as the fundamental inputs in order to determine soil classes in the site effect studies. Some of the well known building codes such as the International Building code [International Code Council (ICC), 2012] and Eurocode (European Committee for Standardization, 2004, EC8) follows an approach to describe the effect of local soil conditions on the ground responses by minimizing the required data. Based on the acquired shear wave velocity and/or geotechnical data from a site, these codes suggest to classify the site by calculating the harmonic average of shear wave velocity and/or SPT-N values for the uppermost 30 m of the soil profile (Equation 1). The average value of these parameters can be used solely or together to identify the site class (ICC, 2012). The soil classification table suggested by IBC 2012 (ICC, 2012) is given in Table 2.

$$P_{30} = \frac{\sum_{i=1}^n d_i}{\sum_{i=1}^n \frac{d_i}{P_{si}}} \quad \text{Eq. (1)}$$

where P_s is the required parameter where shear wave velocity (m/s) and SPT-N value can be used interchangeably. d_i is the thickness of any layer between 0 and 30 m, and the total thickness of the soil profile should be equal to 30 m. In order to

determine the site class by using this equation, each layer up to a depth of 30 m should be characterized with geophysical and geotechnical field tests.

Table 2. Soil classification according to IBC 2012 (ICC, 2012).

SITE CLASS	SOIL PROFILE NAME	AVERAGE PROPERTIES IN THE TOP 30 m	
		Soil shear wave velocity, V_s (m/s)	Standard penetration resistance, N, blows/30 cm
A	Hard rock	$V_s > 1500$	N/A
B	Rock	$760 < V_s \leq 1500$	N/A
C	Very dense soil and soft rock	$360 < V_s \leq 760$	$N > 50$
D	Stiff soil profile	$180 \leq V_s \leq 360$	$15 \leq N \leq 50$
E	Soft soil profile	$V_s < 180$	$N < 15$

The SPT, geotechnical laboratory tests and boring logs were utilized as the geotechnical data in the context of the characterization techniques used in this study. The Active Multi-Spectral Analysis of Surface Wave (MASW) Method and the Passive Microtremor Array Method (MAM) were the techniques performed for the geophysical characterization surveys in this study. By integrating all of the data obtained from the above mentioned destructive and non-destructive methods, local site conditions and dynamic soil characteristics of the study area were assessed. In this chapter, the theoretical background of the utilized methodologies and details regarding their applications, data processing and results can be found.

The characterized sites and the results were incorporated into a Geographical Information System (GIS) environment. Additionally, the sites were grouped based on the soil classes suggested by IBC 2012 (ICC, 2012). This classification chart can be seen in Table 2. Due to unavailability of the SPT-N data to the depth of 30 m, only shear wave velocity values were utilized to calculate V_{s30} in order to identify the local soils in the Orta pull-apart basin.

3.2. Geotechnical characterization studies

3.2.1. Introduction

Besides for the determination of the ultimate bearing capacity, for the calculation of settlement amount, evaluation of liquefaction phenomenon and so on (Kramer 1996, Bowles, 1996; Murthy, 2002), the SPT is utilized to classify soils according to the seismic codes (e.g., Eurocode8; Turkish Seismic Code 2007; International Building Code 2012) for the design of earthquake resistant structures. Most of these codes utilize the results of the SPT for the uppermost 30 m soil layer. Additionally, besides performing a standard penetration test, the geotechnical boring gives the opportunity to take disturbed and undisturbed samples to conduct laboratory tests in order to determine the index parameters, shear strength, hydraulic and consolidation parameters, etc. of the soils.

The natural water content (w_n), Atterberg limits [liquid limit (LL), plastic limit (PL) and plasticity index (PI)], grain size distribution, unit weight are the main index properties of soil (Murthy, 2002). These parameters are determined for the classification and correlation purposes of the geotechnical properties (Kramer, 1996). In a site response study, these properties are used especially as fundamental input parameters in order to define non-linear behavior of soil under cyclic loading in terms of soil degradation and damping ratio curves (Vucetic and Dobry, 1991; Darendeli, 2001).

The standard penetration test results were used along with the geotechnical boring logs to figure out the stiffness of the soils and vertical variation of the layers throughout the boring, to check the validity of the shear wave velocity results and to observe whether or not lateral variation exists. In addition to these, to generate an input database for 1D and 2D soil response analyses, these index parameters were utilized in order to correlate the geotechnical data with the geophysical results and to construct the geometry of the substrata by identifying the vertical

and lateral variation of the soils deposited, especially for the shallower parts of the Orta basin.

3.2.2. Geotechnical field and laboratory studies

The majority of the data were compiled from the previous studies conducted within the Orta basin. All geotechnical works were performed after the 2000 Orta Earthquake. Therefore, there is no abundant geotechnical data regarding the area. However, in 2007, a geological and geotechnical study was conducted within the area in order to prepare a development plan for the Orta Municipality. This study was a project of the General Directorate of Provincial Bank (ILBANK) and its results were compiled, reprocessed and re-evaluated in the context of this study (hereafter named as the Ilbank study). This data encompasses 20 geotechnical boreholes having a total of 308 m depth drilled at the sites falling within Quaternary and Pliocene geological units. Almost all geotechnical borings have a depth of 15 m except BH04 and BH08. The depth of the deepest borehole (BH04) is 20 m. The SPT was performed at every 1.5m of the boreholes at each of the 20 sites. Along with this data, a total of 122 soil samples including either disturbed or undisturbed specimens were taken from the borings for geotechnical laboratory testing to determine the soil index properties.

In order to expand the database, to take samples where the previously conducted study did not cover, to observe the soil conditions and to check the results of the compiled database, 9 trial pits were excavated. The undisturbed samples were taken by the help of an equipment developed from an ordinary Shelby tube. In the context of this study, the index properties of the samples were determined by laboratory tests.

All the data regarding the results of SPTs, the information of geotechnical borings and the outputs of the laboratory tests compiled from the previous studies were merged with the results of geotechnical laboratory tests conducted in this study

leading to the creation of a geotechnical database for the study area. The database was evaluated in a GIS environment.

3.2.2.1. Standard penetration test

The standard penetration test (SPT) is an in-situ dynamic penetration field test. The principle of this test is the determination of the resistance of soil against ramming of a special steel sampling tube called split-barrel by using a standard driving energy (Schmertmann, 1978). The sketch of the sampler can be seen in Figure 14. A standard split tube of 50.8 mm outer diameter and 34.93 mm inner diameter is penetrated to soil via the free fall of a 63.5 kg weight from the height of 76.2 cm, and the number of blows are counted for 3 sets of 15 cm penetration (a total of 45 cm). The total of number of blows for the last two 15cm section is defined as N_{30} or SPT-N value of that soil layer (Murthy, 2002).

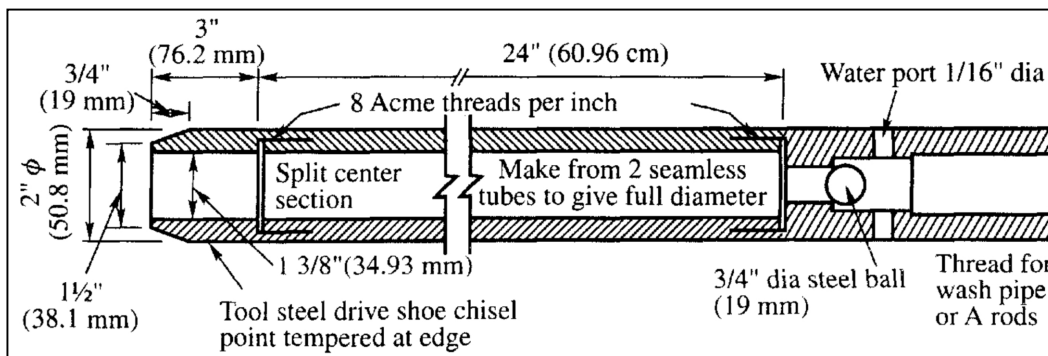


Figure 14. An illustration of the split barrel sampler (tube) for standard penetration test (Murthy, 2002) (not to scale).

Based on some codes of practice, the implementation of the SPT is ceased if any of the three items given below are observed during the measurement where the measurement is termed as refusal (Bowles, 1998):

- Any 15 cm increment is obtained by 50 or more blows,

- The required 30 cm is driven by 100 or more blows,
- No advance is observed after 10 successive blows.

The validity and usability of the SPT results can be affected by many factors such as drilling method, drill pipe type, borehole diameter and dimensions, borehole stabilization, sampler type, blow frequency, ram type and the energy exerted by its drop, and test procedure (Sağlamer, 1979; Nixon, 1982; Coduto, 1994). Based on these variables, the measured in-situ penetration resistance ($SPT-N_{field}$) can be high or low when compared with the actual conditions. In order to acquire more reliable and comparable results, many corrections can be applied to the obtained $SPT-N_{field}$ value. The main commonly utilized corrections are with regard to effective overburden pressure, hammer energy, diameter of borehole, length and diameter of rod and sampler (Schmertmann, 1978; Seed et al., 1985; Liao and Whitman, 1986; Riggs, 1986; Skempton, 1986). It is crucial to know the reason of using these corrections and determine the soil type prior to obtaining the corrected SPT-N value.

Utilization of the SPT-N corrections are not suggested in the soil characterization studies based on the well established seismic codes such as TSC 1998 (Turkish Seismic Code; Ministry of Public Works and Settlement of Turkey, 1998), IBC, 2012 [International Building Code, International Code Council (ICC), 2012]. Also, rather than avoiding underestimated and/or overestimated design parameters for any type of building (Kramer, 1996; Bowles, 1996) or for the determination of liquefaction hazard (Çetin and Seed, 2002; Çetin et al., 2004), one of the main aim is to validate the shallow portion of the shear wave velocity (V_s) profiles based on the variations of the SPT-N value with depth. Therefore, in this study no SPT-N corrections were used due to the reasons given above. It should be noted that in the Ilbank study, the standard penetration test was performed with an automated ram drop assembly, thus the weight was dropped exactly from 76.2 cm as per standard. The distribution of the geotechnical boring where the SPTs were performed is given in Figure 15.

As stated above, the geotechnical borings were drilled in 20 different sites in the study area. These measurements were performed at sedimentary deposits which are Quaternary, Pliocene and Miocene in age. The majority of the borings are within the boundary of the Quaternary deposits since almost all settlement areas of the Orta District are located at these deposits. Also, the candidate areas in the development plan of the Orta Municipality regarding the new construction for the near future falls within these deposits. A total of 14 and 5 borings were located at the Quaternary alluvium deposits and the Pliocene sediments in the basin, respectively (Figure 15). As can be seen in Figure 15, the remaining borings were drilled in the Miocene sediments.

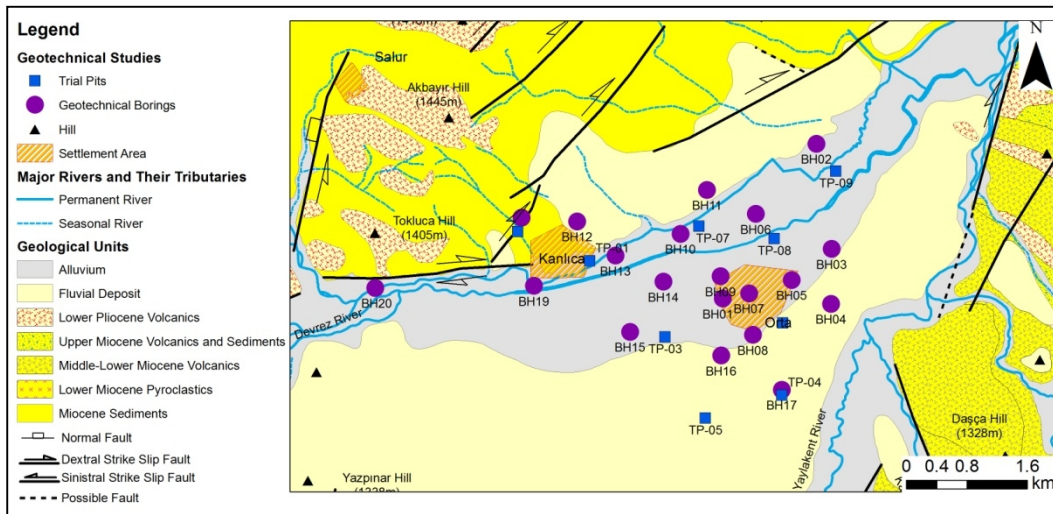


Figure 15. Spatial distribution of the compiled geotechnical borings and the excavated trial pits in the study area.

3.2.2.2. Trial pits and geotechnical laboratory tests

In order to conduct a detailed geotechnical characterization study, apart from the drilled boreholes in the context of the Ilbank study, nine trial pits were excavated by using an excavator in order to conduct a geological inspection of the shallow soil deposits and to take samples to determine the index parameters of the soil

(Figure 15). The trial pits were excavated until the organic soil was removed from the site and good conditions allowing proper visual examination were achieved (Figure 16). In order to be sure about the stabilization, the depth of the pits was constrained to 2 meters. The pits were excavated until the minimum base area was greater than 1.5 m^2 as suggested by the Site Investigation Steering Group (1993).



Figure 16. A view during the excavation of the trial pit in the Orta area.

A total of 5 and 3 trial pits were excavated at the site falling within the Quaternary alluvium deposits and the Pliocene sediments, respectively, and the remaining pit was excavated within the Miocene sediments (Figure 15). Nine disturbed and four undisturbed samples were acquired from these trial pits in order to perform the laboratory tests. In the context of this study, only undisturbed samples were utilized to obtain the index properties of the samples. The natural water content, PL, LL and PI values and grain size distribution along with the natural unit weight of the soil samples were determined based on TS 1900-1 standards (TS1900-1, 2006). The acquired results were integrated with the compiled database in order to

geotechnically characterize the Quaternary and Pliocene sediments deposited in the Orta pull-apart basin.

3.2.3. Results of the geotechnical characterization studies

Since the vertical boundary between the Quaternary and Pliocene sediments are unknown, to evaluate the SPT results, the geotechnical borings were classified based on the geological units where they were located. According to this classification, a total of 83 SPT-N data from 1.5 m to 18 m was obtained for the Quaternary sites and 30 SPT-N data from 1.5 m to 20 m was obtained for the Pliocene sites. Since there was only one boring in the Miocene geological unit, the SPT-N value distribution was not examined individually, however, its effect on the variation of the data was considered in the entire dataset (Figure 17). Additionally, due to the insufficient amount of data at depths between 15 m and 20 m, this portion was excluded from further discussions. Moreover, a total of 23 SPT-N measurements were omitted during the construction of this database due to the refusal values. Most of these refusal values are present at the Quaternary sites due the gravel content of layers as the SPT-N count values were unrealistically high as stated by Eker et al. (2012) and WSDOT (2013).

As can be seen in Figure 17, the variation of the SPT-N values with depth shows a similar trend after a depth of 12 m when compared with the Quaternary and Pliocene data. However, these two datasets show significant variations at the shallower parts of the 12 m soil column as it is expected due to the presence of the coarse cohesionless soil bearing layers. Also, as the variation of the mean SPT-N values of the entire data with respect to depth was examined in Figure 17, it is clearly seen that the average SPT-N values increase almost gradually with depth. Additionally, the entire dataset shows that the deviation of the data with respect to the mean starts to decrease after 6 m.

During evaluation of the variations of the SPT-N value with respect to the geological units, the ground water level (GWL) fluctuations among the borings also needs to be considered. When the GWL between the Quaternary and Pliocene units are compared, higher variations are observed within the Quaternary dataset. The GWL ranges between 0.9 m and 5.4 m, and the data shows clustering around 2 m. Interestingly, the GWL level is located at the shallower parts of the soil within the Pliocene unit. The GWL has a range between 0.6 m and 2 m in this unit. This situation was also observed during the excavation of the trail pits in the study area. The state of the GWL reflects itself in the variation of the natural water content (w_n) with depth in the Pliocene data (Figure 18). Also, the higher GWL in the Pliocene sites also manifests itself in the diversion of the average of SPT-N values at the shallow soil layers (Figure 17).

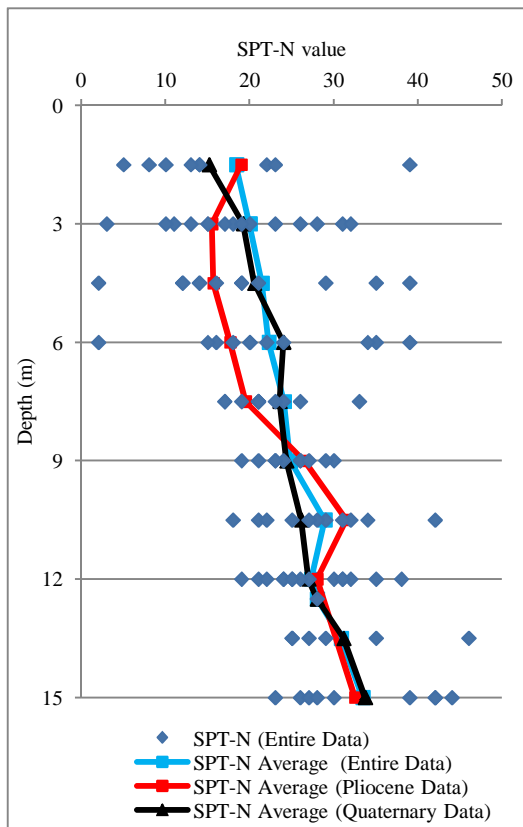


Figure 17. The SPT-N value variations with respect to depth for the Quaternary, Pliocene and entire data.

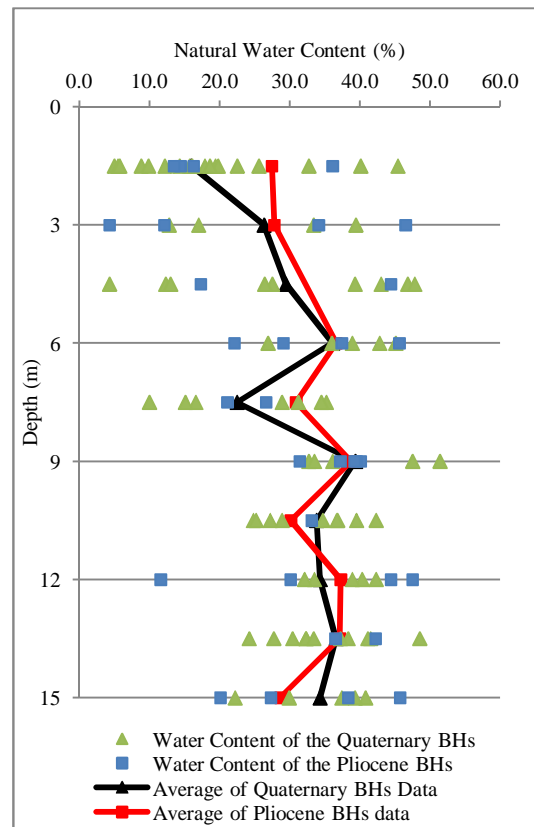


Figure 18. The variation of natural water content (w_n) with depth for the Quaternary, Pliocene and entire data.

Based on the results of the geotechnical laboratory tests, the soils were classified according to the Unified Soil Classification System [(USCS), ASTM, 2006]. Coarse grained soils are present at the uppermost depth of 8.5 m within the Quaternary alluvium deposits (Figures 19 and 20). As can be seen in Figures 21 and 22, coarse grained soils within this unit are generally classified within occasionally blocky sediments containing coarse gravel GW-GP-GM-GC-SC, SM, SW and SP soil group (ASTM, 2006). The fine grained content within the GW, GM, GP, SM, SW and SP soil classes (ASTM, 2006) is below the value of 22%. On the other hand, clayey gravel (GC) and clayey sand (SC) soil classes contain fine grained material. The fine grained content within the clayey sand is between 21% and 45% (Figures 19 and 20). The clayey gravel (GC) soil class, on the other hand, contains fine grained material that is in the range of 14.2% to 20% (Figures 19 and 20). Coarse grained soils within the Quaternary unit are generally coarse sand and gravelly soils having occasional block content.

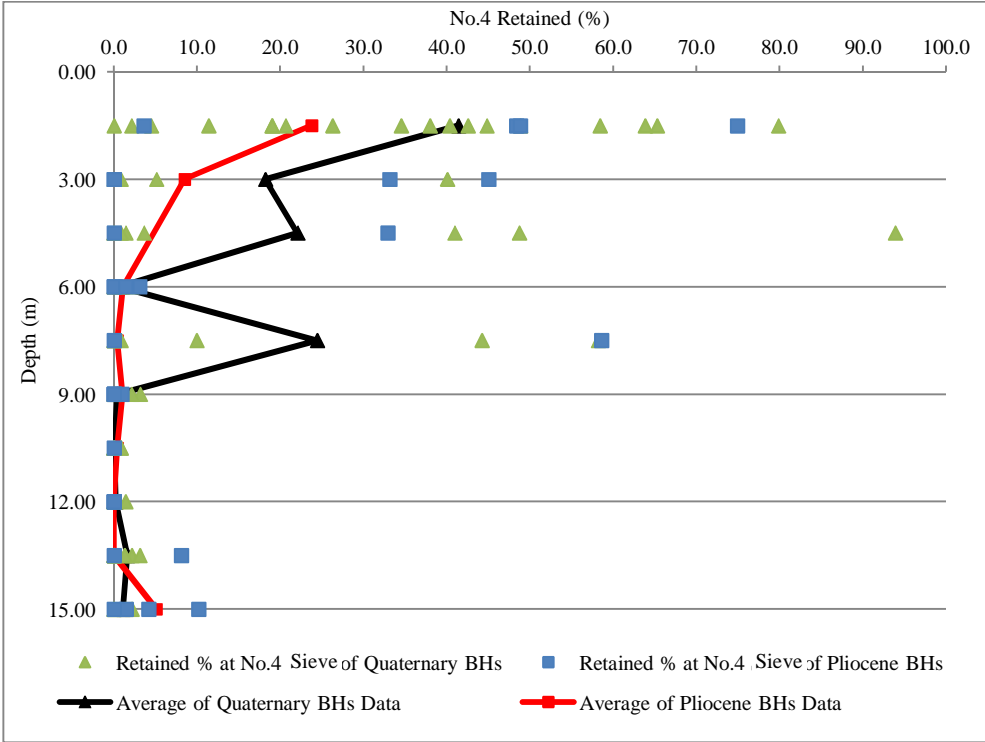


Figure 19. The variations of the percent of the samples retained on the No. 4 sieve with respect to depth for the Quaternary, Pliocene and entire data.

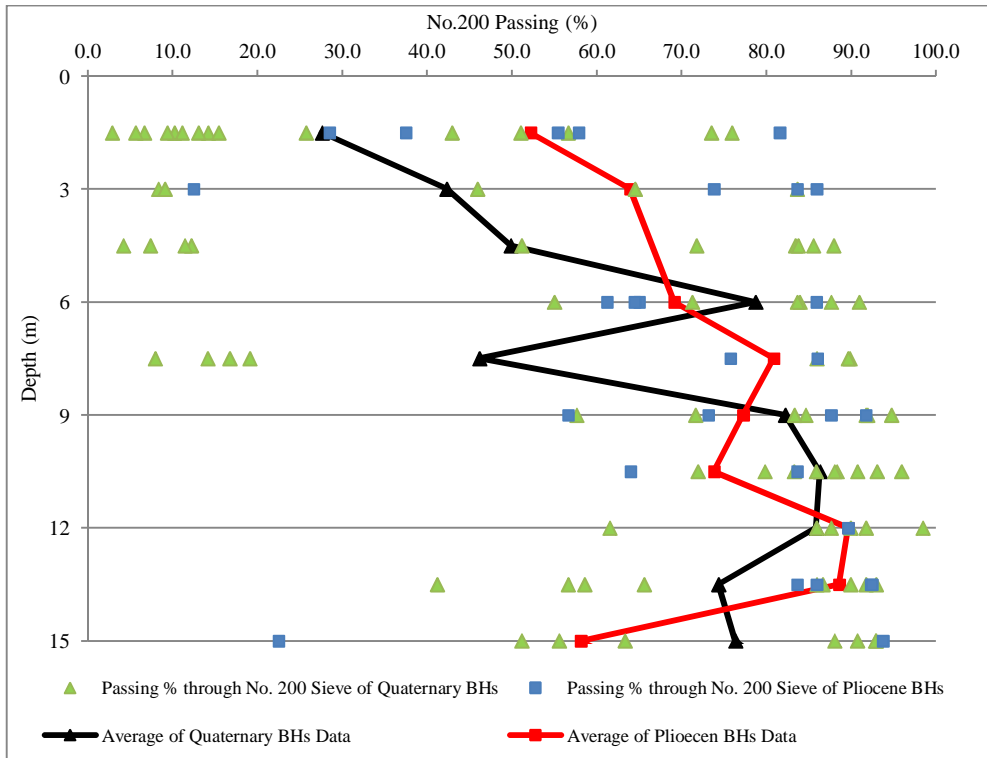


Figure 20. The variations of the percent of the samples passing through No. 200 sieve with respect to depth for the Quaternary, Pliocene and entire data.

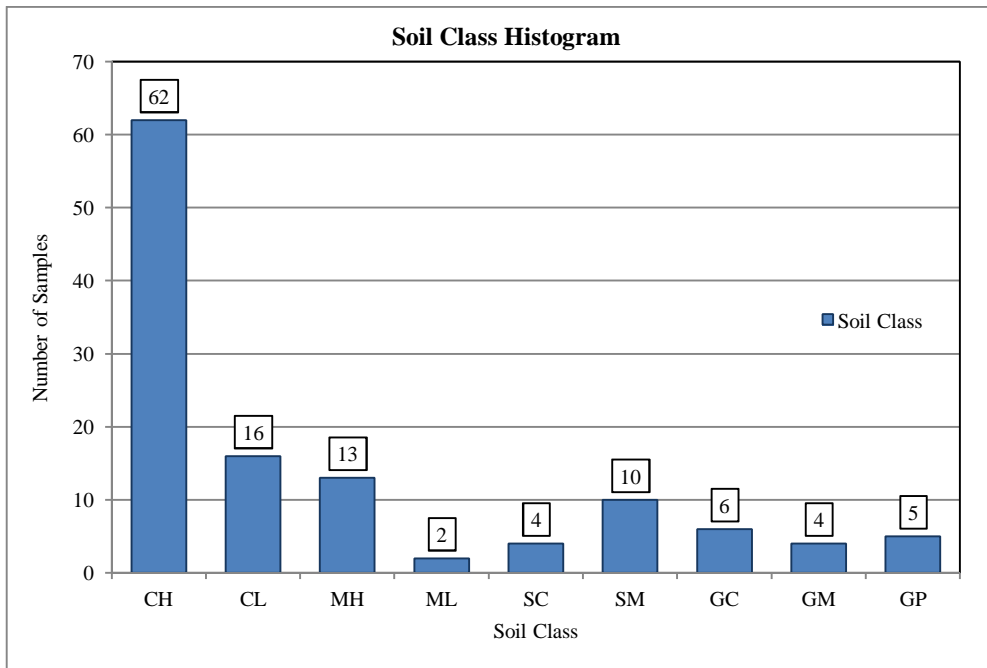


Figure 21. Distribution of the soil class for the entire dataset according to the USCS (ASTM, 2006).

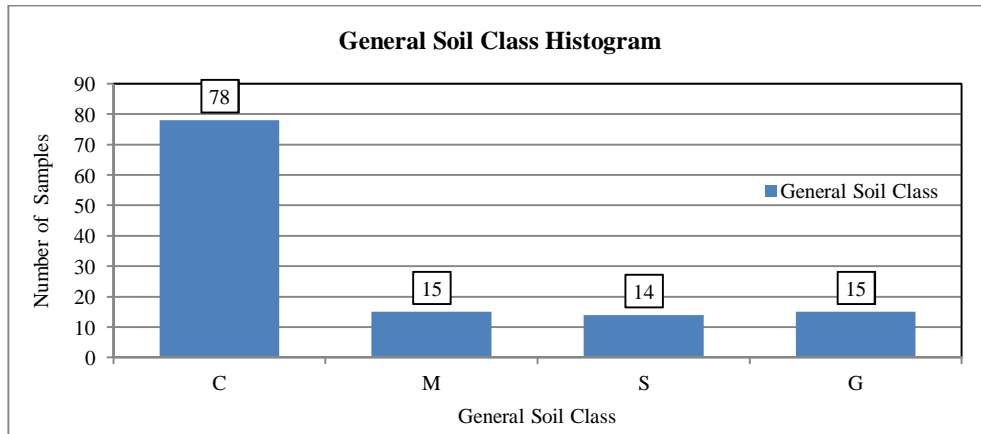


Figure 22. The distribution of the general soil groups for the entire dataset based on the USCS (ASTM, 2006).

The deeper parts of the Quaternary units (>8.5m) and the entire Pliocene data are mostly comprised of fine grained particles. This can be observed for the Pliocene unit particularly at depths greater than 2 m as given in Figures 19 and 20. The natural unit weight of the clay type soil class changes between the values of 1.8 g/cm³ and 2.1 g/cm³. This range is mainly clustered between the values of 1.84 g/cm³ and 1.88 g/cm³. The distribution of the soil class can be seen in Figures 21 and 22. The soil layers are dominantly formed by low plastic clayey silt (ML), silty soils (MH), low plastic clay (CL) and high plastic clay (CH) soils based on the USCS (ASTM, 2006). The major population of the constructed dataset is formed by these clay soil groups (Figure 22).

The LL, PL and PI (LL-PL) variations of these two units with depth are given in Figures 23a, b and c, respectively. As can be seen in these figures, even though there is a difference in their magnitude, variations have the same trend after the depth of 8.5 m. In addition to these, MH and ML soil groups are in the close vicinity of the A-line of the Casagrande chart (Figure 24). The CH soil class is clustered far from the LL value of 50% along the upper side of the A-line and this clustering is parallel to this line. As can be observed from the figure, parallel clustering to the A-line indicates that the PI values are approximately half of the LL values.

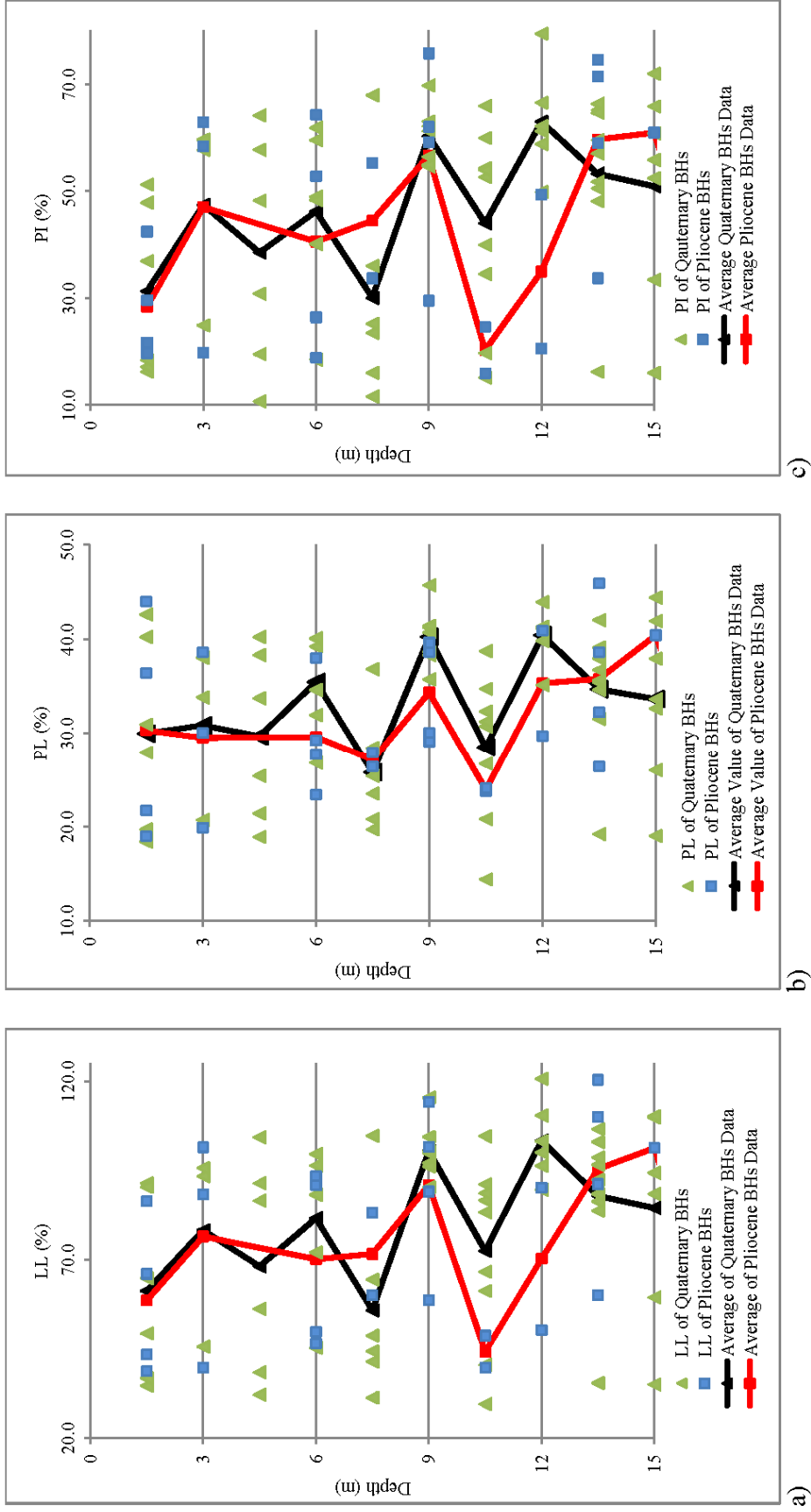


Figure 23. The variations of the LL (a), PL (b) and PI (c) values with depth for the Quaternary, Pliocene and entire data.

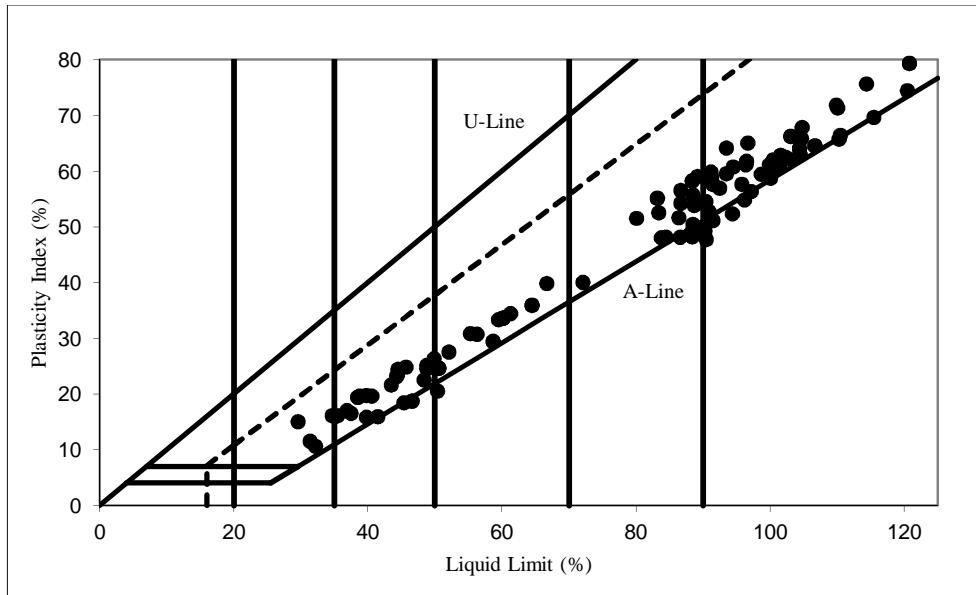


Figure 24. The distribution of ML, MH, CL and CH soil classes regarding the PI and LL values on the Casagrande chart for the entire data.

3.3. Seismic characterization studies

3.3.1. Introduction

Today, the harmonic average of the first 30 meters of shear-wave velocity profile, (i.e., V_{S30}) is considered to be standard for soil characterization studies in general (Boore et al., 1993; Borchardt, 1994; ICC, 2006). Many studies (Bodin et al., 2001; Nguyen et al., 2004; Andrus et al., 2006; Chapman et al., 2006; Parolai et al., 2006) regarding evaluation of the site effect of the deep basins indicate that it is necessary to consider the deeper sections of the sedimentary profile in order to acquire a suitable ground motion prediction. Recognition of the influence of deeper geology on the seismic ground motion behavior at the surface presents a major challenge. Therefore, it is necessary to accurately determine the seismic profile as deep as possible and correspondingly 2-D basin topography for accurate and sufficient results to be acquired from seismic characterization studies to be performed for rigorous interpretation of dynamic behavior generated by ground

motion at the surface. Thus, it is necessary to develop and/or apply geophysical approaches that are suitable for this type of a study.

There are various seismic methods available for the determination of shear wave velocity (V_s) profiles in the literature. Some of these methods (down-hole, cross-hole, PS log, etc.) give more accurate results, but they are costly and time consuming methods due to the requirement of a boring (Gosar et al., 2008). Among other non-destructive methods, seismic refraction, performed for many decades, considers soil profile characterization process with linear relation to depth and may not present accurate results due to complex geology (Xia et al., 2004). Furthermore, active and passive surface wave methods (SWMs) are mainly based on the dispersive nature of Rayleigh waves. When compared with body waves, Rayleigh waves have relatively higher amplitude, allowing surface wave measurements to be undoubtedly used for determination of shear wave velocity profiles as these are not highly susceptible to environmental (ambient) noises and have flexibility in data acquisitions at locations where other geophysical methods are limited (Miller et al., 1999).

Surface waves are generated by utilizing active and passive sources. In the implementation of the active SWMs such as MASW (Park et al., 1999) and Spectral Analysis of Surface Wave (SASW) (Nazarian, 1984; Stokoe et al., 1994), seismic energy is intentionally generated at a specific location relative to the geophone spread and the recording begins when the source energy is imparted into the ground. However, in passive SWMs such as MAM (Okada, 2003; Hayashi, 2008) or Refraction Microtremor (ReMi; Louie, 2001) methods, there is no time break and motion from ambient energy generated by a range of natural phenomena (i.e., wind, wave motion) and artificial sources (cultural noise, i.e., traffic, machinery and so on) at various and usually unknown locations relative to the geophone spread is recorded (Hayashi, 2008).

The important assumption regarding passive SWMs is that the recorded microtremors are the surface waves which are the fundamental mode of the Rayleigh waves (Aki, 1957; Asten and Boore, 2005; Park et al., 2007). It should be noted that the passive surface wave methods are named based on the utilized inversion method. The MAM is one of these methods based on spatial auto-correlation (SPAC) inversion (Okada, 2003). Passive SWMs are used with different configurations to identify the shear wave velocities characterizing deeper layers (Asten and Boore, 2005). Resolution of these methods, however, may be low at near surface locations and they are not appropriate at quiet locations and the locations where local data quality variations are dependent on proximity to ambient noise, as these conditions cause insufficient passive energy (Tokimatsu, 1997; Rix, 2005).

Within the context of geophysical characterization surveys in this study, Multi-Spectral Analysis of Surface Wave [(MASW), Park et al., 1999] Method and Microtremor Array Method [(MAM), Okada, 2003] were performed as active and passive surface wave measurements, respectively. The MAM allows gathering more accurate mechanical information of the geological units lying at deeper sections of a soil profile while the MASW allows more rigorous solution of shear wave velocity profiles at shallower depths.

Moreover, the methodology where mechanical information obtained from the active and passive surface waves were utilized together before the inversion process is termed as Combined Surface Wave Method (CSWM) (e.g., Eker et al. (2010, 2012 and 2013). It allows to create a shear wave velocity profile by preserving high resolution at shallow depths and extending the V_s measurements to greater depths. Therefore, this approach was utilized in the context of this study in order to characterize the deeper parts of the geological units as much as possible. Moreover, the determination of the shear wave velocity can present different possibilities in classification of soils as a result of co-characterization of shallow and deep sections of layers at the same profile to generate a representative

shear-wave velocity profile reflecting local site conditions (e.g., validation of lateral heterogeneity assumption, determination and cleaning of higher mode saturation, determination of near and far field saturation, identification of environmental dominant noise, etc.). Due to these reasons, the V_S acquired from utilization of surface wave profiles constructed by using this method was more effectively used in the determination of ground responses of the soil deposits in the Orta pull-apart basin.

3.3.2. Fundamental background of the utilized method

Surface wave methods are based on the dispersive nature of the Rayleigh waves at layered media for acquisition of subsurface shear wave velocity profiles. The Rayleigh wave, one of the surface wave types, travels along a free surface such as the earth-water or the earth-air interface. The characteristics of the Rayleigh wave are relatively low velocity, low frequency and high amplitude. The Rayleigh wave is generated by the interfering SV and P-waves which are the radial and vertical components of the surface waves, respectively. In a homogeneous medium, the particle motion of the Rayleigh wave is elliptical in a counterclockwise (retrograde) direction along the free surface when it moves from the left side to the right. The amplitude of this wave motion decreases exponentially with depth. Surface waves become planar towards sufficient depth. The motion is constrained to a vertical plane consistent with the wave propagation direction (Xia et al., 2004). Also, the depth is a function of the wavelength (Park et al., 1999).

The phase velocity of the surface waves depends on frequency. By assuming vertical velocity variation, each unique frequency component of a surface wave has a different propagation velocity or phase velocity. This, resulting in a different wave length at each propagated frequency, is called dispersion (Park et al., 1999). Shear wave velocities of the subsurface layers are characterized by inversion (back calculation) process utilizing the constructed dispersive curve. Unlike the conventional methods, SWMs are based on elastic wave equation and the analyses

are performed completely in a frequency domain due to this property (Hayashi, 2008).

In spite of having different scales, the SWMs are mainly based on the same principles. They are established on the geometrical dispersion (Figure 25). It makes the propagation velocity of the Rayleigh wave dependent on frequency in vertically heterogeneous media. As can be seen in the figure, high wavelength (low frequency) Rayleigh waves have information regarding deep seated layers as they can penetrate to deeper layers and their velocity is affected from material properties present at the deeper parts (Louie, 2000; Okada, 2003; Hayashi, 2008). On the other hand, short wavelength (high frequency) Rayleigh waves disperse at layers closer to the surface and includes information related with mechanical properties of shallow layers (Park et al., 1999). Combining these low and high wavelengths, Rayleigh waves provide a possibility for the characterization of materials at a considerably large scale range (Foti, 2005).

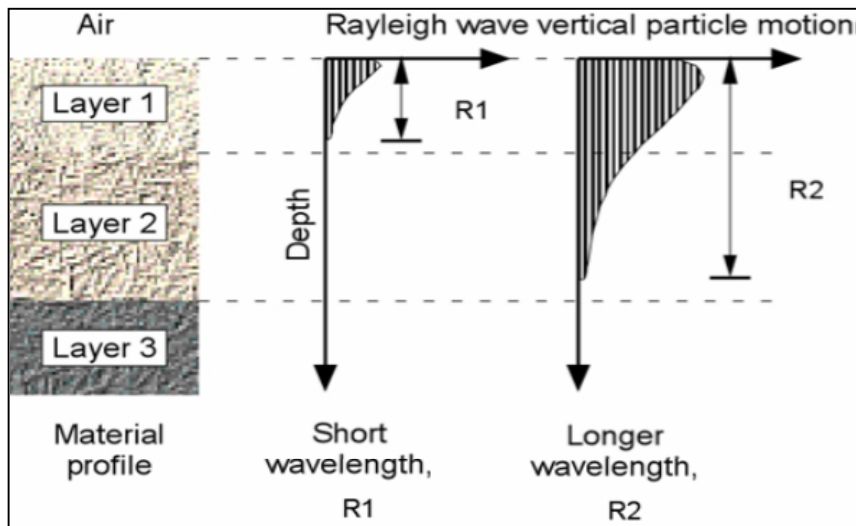


Figure 25. Principle of geometric dispersion (Geovision, 2009).

The scale of the interested frequency range and the field configuration differences during the data acquisition are the main differences between the SWMs. Despite

these discrepancies, the same main three steps are utilized to perform the SWMs as these methods rely on the dispersive nature of the Rayleigh waves in layered media (Foti, 2005). These main steps are:

- 1) Acquisition of the field data (i.e., seismic waves are generated or detected and recorded by sensors),
- 2) Signal processing in order to obtain the dispersion curve,
- 3) Inversion of the field dispersion curve in order to construct a shear wave velocity profile. The schematic drawing of this procedure is given in Figure 26.

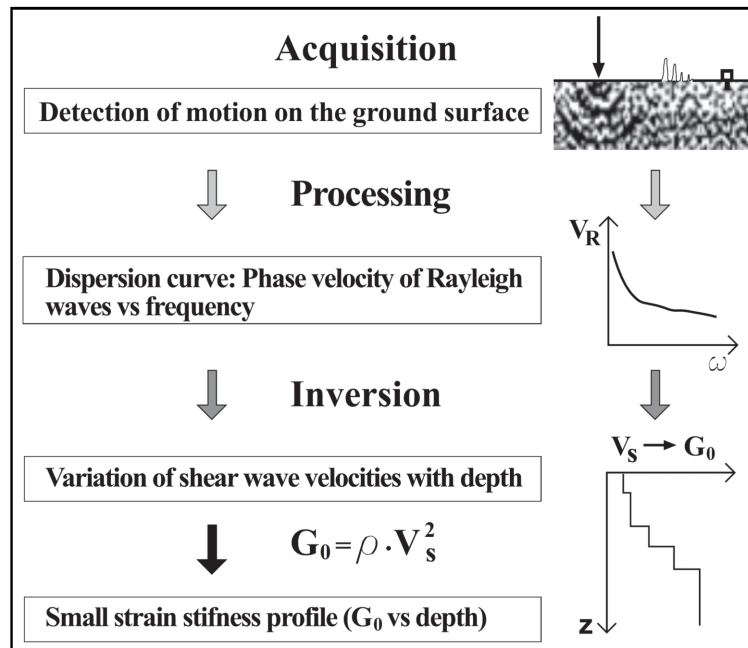


Figure 26. The flowchart of the main steps followed in the analysis of the SWMs (reproduced from Foti, 2005).

3.3.3. Data acquisition and field configuration of the SWMs

Although there is a general consensus on recording length, sampling interval, source and geophone type for surface wave methods in the literature, there are discussions regarding optimum field configurations such as near offset (distance between source and first receiver geophone), geophone (receiver) spacing and spread length (distance between first and last geophone). These parameters should be selected properly in order to avoid data contamination and loss in the record due to near and far field effects (Stokoe et al., 1994; Park et al., 1999, 2001, 2002; Xia et al., 2004).

The maximum investigation depth of the MASW and the MAM survey is generally equal to half of the spread length even though it also depends on several parameters regarding the field geometry and data acquisition as explained in detail in the further parts of this section. However, the array length can be almost equal to the investigation depth in a SPAC analysis (Geometrics, 2006; Hayashi, 2008). Also, this depth is related to the seismic velocities of the subsoil as well (Natale et al., 2004). Moreover, the geophone spacing is associated with the resolution of the measurement. If the spacing increases, the detectable minimum thickness decreases (Xia et al., 2004). In this study, the field configuration and data acquisition parameters were selected by considering all the discussions given below in order to penetrate the deeper parts of the geological units as much as possible along with the accurate characterization of the shallower layers.

In the MASW method, selection of a sufficient energy source and natural period of geophones depends on investigation depth during the analysis. It is known that 4.5 Hz geophones can detect minimum 5 Hz frequency during MASW measurements (Park et al., 2002). It is mentioned in the literature that 4.5 kg and 9 kg hammer can generate sufficient energy to obtain depth information down to 50 m during these types of studies (Park et al., 2002). This depth shows variations based on the

number of geophones, natural frequency of geophones, weight and type of the energy source, array length and number of channels.

Besides the construction of the field geometry based on the target depth required in a study, these configuration parameters given above should also be selected in order to prevent the records from the near and far field effects leading to spatial aliasing. When aliasing problems arise during recording of the signals, the original signal cannot be reformed uniquely from the sampled signal. Information on the deeper layers cannot be obtained accurately due to the near field effect because in order to become planar, surface wave is supposed to travel a certain distance from the source to the seismic array, where this distance is known to be a function of the wavelength as explained in the previous section in this chapter. As suggested by Xu et al (2006), this effect can be minimized or removed by using different near offset distances with respect to the stiffness of the surficial soil at the measurement site. However, this near field effect is not observed especially on the combined analysis as stated by Yoon and Rix (2005) due to the integration of the MAM data. Rather than the near field effect, if the MASW method is performed with a long offset range, certain problems may arise as related with the far field effects due to rapid attenuation of the high frequency component of the Rayleigh wave (Park et al., 1999; 2001 and 2002). This effect was minimized by a stacking procedure, by utilizing shorter offset range and by comparing results of reverse shot measurements and the MAM measurements in this study.

Moreover, rather than the spatial aliasing and loss of information of the shallow layer problems, other problems related to the lateral heterogeneity can be introduced when utilizing long spread length to take surface wave measurements. In the SWMs, one of the main assumptions is that there is no lateral variation in the elastic properties of the materials underlying a seismic array. In order to confirm the validity of this assumption, the existence of the lateral heterogeneity can be checked by the comparison of the experimental dispersion curves constructed by forward and reverse shots for the same seismic array without

changing any other data acquisition parameters in a MASW survey (Foti, 2005). This application also provides possibility to validate the measurement results of forward array. Therefore, by confirming the validation of this assumption, the spread length can be kept longer by considering the far field effects.

As stated in the previous section, the Microtremor Array Method (MAM) uses passive or ambient energy generated by man-made noise, traffic, factories, wind, wave motion, etc. As these microtremor sources are randomly distributed in space, they do not have a distinct propagation direction. Therefore, 2D arrays are generally required to calculate phase velocities of microtremors. Isotropic arrays such as circular or triangular are theoretically the best array types for passive analysis (Hayashi, 2008). However, finding the appropriate area for these types of arrays are hard, especially for urban areas where it is mostly impossible. The anisotropic array types such as L-type or linear array are more suitable for urban surveys and allow selection of suitable areal coverage. Results in the literature indicate that irregular arrays can be used for small scale passive surface wave method where relatively high frequency microtremors are used. Recently, various theoretical and experimental studies were conducted for the applicability of irregular arrays (e.g., Louie, 2001; Louie et al., 2002; Pullammanappallil et al., 2003; Rucker, 2003; Jin et al., 2006; Chavez Garcia et al., 2006 and 2007; Chavez Garcia, 2007; Panca et al., 2007; Yokoi and Margaryan, 2007; Hayashi, 2008; Eker et al., 2012 and this study). These studies show that different passive methods (MAM, ReMi) with anisotropic geometry present good conformity with each other and furthermore, the results of some of these passive methods present good correlations when compared with the active surface wave method.

In linear configuration of the MAM method, a common seismic refraction recording equipment just like in that the MASW is utilized. 12 or more geophones are required in order to effectively record the surface waves (Hayashi, 2008). Long array size (spread length) and longer period geophones are significant to acquire the data from deeper sections (Asten and Boore, 2005). The natural frequency of

the 4.5 Hz geophones is a more appropriate choice due to its cost effectiveness and durability. Furthermore, experimental dispersion curves acquired from 4.5 Hz geophones are practically same with 2 Hz geophones at passive method down to a 2 Hz frequency (Hayashi, 2008).

The array length can be modified based on the target depth. As passive surveys are performed with a larger geophone spacing than those used during active surveys (generally 5 m or more), the processed dispersion curve generally gives limited information for shallow depths or high frequencies. Shorter geophone spacing and higher frequency geophones can be used in order to interpret shallower structures in more detail. Although these uncertainties can be reduced by performing multiple surveys with decreasing lengths, higher frequencies of passive surface waves may not be effectively recorded due to their rapidly attenuating character (Park et al., 2007). Therefore, the best practice may be to perform an active survey with the same array (e.g., Park et al., 2007; Gosar et al., 2008; Eker et al., 2012).

3.3.4. Field procedure of seismic survey utilized in this study

In the scope of this study, two campaigns were organized to take active and passive surface wave measurements in order to characterize seismically soft and unconsolidated Quaternary alluvium deposits and Pliocene sediments in the Orta pull-apart basin. The first survey was performed in September of 2009 and the second was carried out in June of 2014. All measurements were taken at the sites where microtremor data (explained in detail in next chapter) was recorded in order to investigate the degree of the relation of the position of the H/V curves with the depth dependent variation of the shear wave velocity values.

The SWMs were performed by adopting a grid system by considering the distribution of the sites at Phase 1 (2009 campaign). This distribution decided during Phase 1 was based on the conditions of the deposition environment and the spatial variation of the geological units in the study area. Prior to conducting the

second phase (2014 campaign), the grid system was created with the consideration of the distance between the seismic measurement points ranging between 500 m and 1000 m in order to properly characterize the local soil conditions and to determine their contributions to the seismic hazard distribution. However, during the application of the SWMs in the field, this grid system had to be revised because of dense vegetation and planted agricultural areas, environmental noise, man-made structures, especially infrastructures and electrical lines as well as accessibility problems.

In the first phase of the survey, 14 sites were characterized by both active (MASW) and passive (MAM) surface wave measurements. In other words, 28 surface wave measurements were taken by carrying out these two SWMs (Figure 27). As can be seen in the figure, these surface wave measurements were recorded to determine the local soil characterization of different sedimentary deposits which are Quaternary, Pliocene and Miocene in age within the Orta pull-apart basin. A total of 8 and 5 measured sites fell within the boundaries of Quaternary alluvium deposits and Pliocene sediments, respectively. The remaining 1 site was measured within the Miocene sediments. This distribution is given in Figure 28.

In the second phase of this geophysical survey, 48 shear wave velocity measurements were taken at 15 different sites by using both active (MASW) and passive (MAM) surface wave methods (Figure 27). The MASW and MAM with linear configuration were performed at all 15 sites. In order to check the reliability of the experimental dispersion curves constructed by the MAM survey linear array, different geometric array configurations were used at some of these sites. The MAM survey was performed by using Triangular and L-shape array geometries at a total of 6 and 12 sites, respectively.

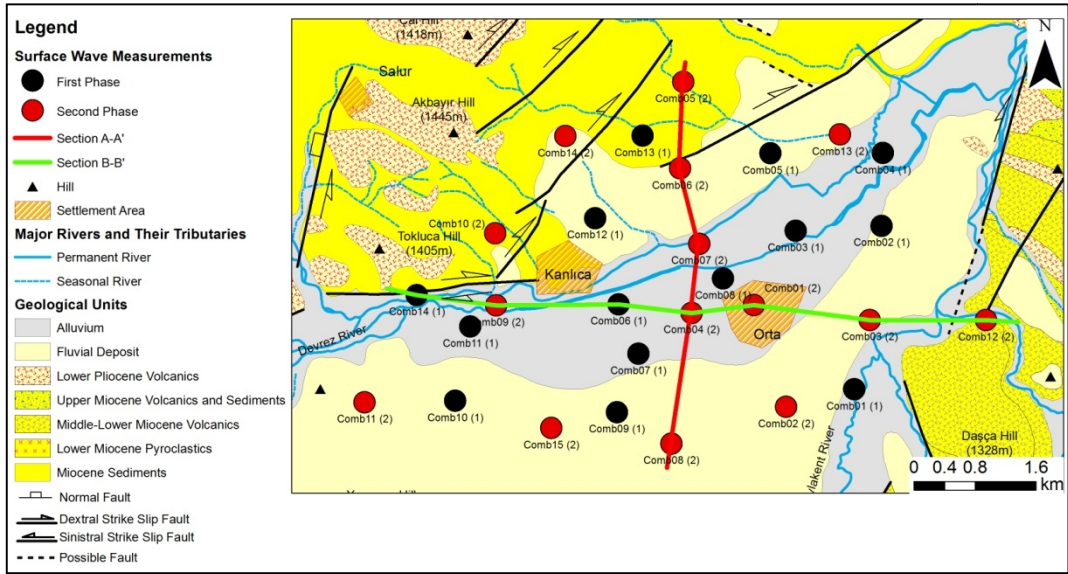


Figure 27. The spatial distribution of the first and second phase surface wave measurements along with the selected sections.

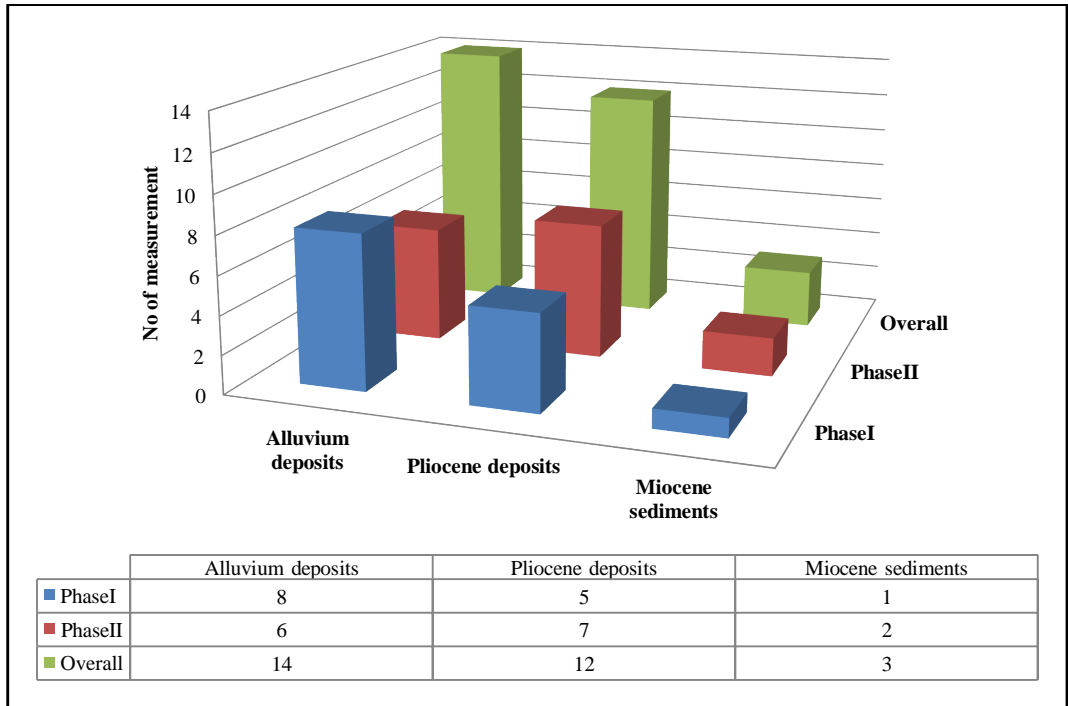


Figure 28. Distribution of the Surface Wave Measurements with respect to the geological units.

When the spatial distribution of the measurements are to be examined, it is observed that all measurements fall within the boundaries of Quaternary, Pliocene and Miocene sediments in the context of the seismic characterization studies of this dissertation. As can be seen in Figure 28, a total of 6 and 7 measured sites fall within the boundaries of the Quaternary alluvium deposits and Pliocene sediments, respectively. The other 2 sites were measured within the Miocene sediments.

In the first phase, the MASW measurements were taken by using a linear array configuration with twelve (12) 4.5 Hz natural frequency vertical geophones with a 2.5 m spacing. Geophones with spikes were connected to the seismograph through a spread cable and active surface wave measurements were acquired by an ABEM-RAS 24 seismograph having 12 channels. Figure 29 illustrates the utilized array geometry in Phase 1. Also, the parameters regarding both field configurations and data acquisition utilized at two phases are summarized in Table 3. In the second phase, the same array configuration was utilized in the MASW survey. Also, the number and type of the geophones in this phase was similar with those used in Phase 1. However, the measurements were recorded by a GEODE seismograph having 12 channels. Different from the field configuration constructed in Phase 1, the geophone spacing was selected as 1.5 m in Phase 2 (Figure 29 and Table 3).

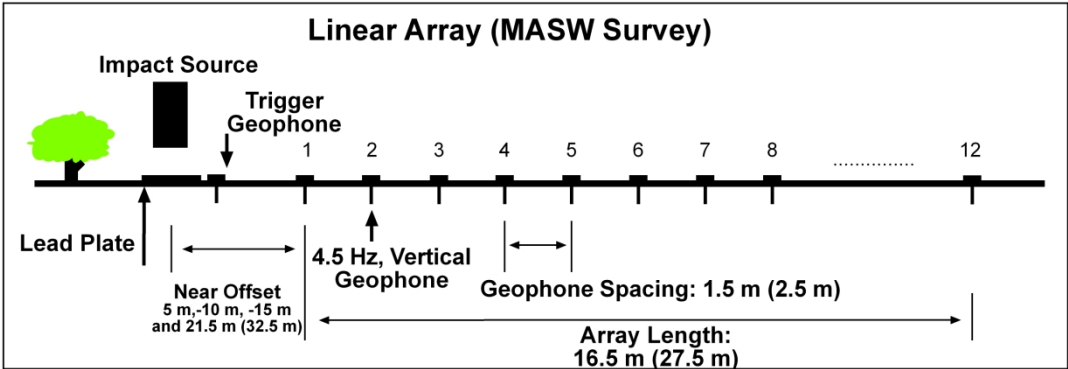


Figure 29. The configurations of the linear arrays utilized in the active surface wave survey. The numbers given in parentheses show the selected field configuration parameters in Phase 1. The numbers without parentheses show the utilized parameters during Phase 2.

The qualities of all MASW measurements in both phases were preliminarily checked in the field via a notebook computer after recording the signals. In all MASW measurements, the source was generated by hitting a 6 kgf (13.2 lbf) sledge hammer on a 0.35 m x 0.35 m striker plate. In both phases, forward and reverse measurements were taken by generating a source at both ends of the array to confirm continuity of the lateral homogeneity in the processing stage. Moreover, in both phases, the forward shots were repeated for three near offset distances (5 m, 10 m and 15 m) at the array. Therefore, problems regarding the proper generation of a Rayleigh wave for the relatively deeper parts of the soil profiles and the degree of the contamination level at the measurements were minimized at the records. In order to eliminate the environmental background noise, vertical stacking was implemented 3 or 5 times at each shot point of each array to improve the quality of data (i.e., to increase the signal to noise ratio) during the first and second phases. The recording length for the measurements of the generated surface waves was selected as 2 s with 1 ms sampling interval. The utilized data acquisition methods and selected parameters in each phase are listed in Table 3.

The MAM measurements in the first phase were taken by using twelve 4.5 Hz natural frequency vertical geophones in a linear array configuration with a geophone spacing of 5 m. Geophones with spikes were connected to the seismograph through a spread cable and passive surface wave measurements were acquired by a 12 channel ABEM-RAS 24 seismograph. Figure 30 illustrates the utilized array geometry for the passive SWM in Phase 1 and the parameters regarding field configuration and utilized data acquisition method at both phases are summarized in Table 3. In the second phase, the same array configuration was utilized in the MAM survey along with the isotropic geometries such as triangular and L-shape. For the linear array configuration, the number and type of the geophones in this phase was similar with those used in Phase 1. Different from the linear array configuration constructed in Phase 1, the geophone spacing was selected as 10 m in Phase 2 (Figure 30 and Table 3). Additionally, 7 and 11 geophones were utilized for the measurement of the ambient noise by using the

triangular and L-shape geometries, respectively (Figure 31). All passive measurements were recorded by a GEODE seismograph with 12 channels in Phase 2. In the MAM survey during the first and second phase, the sampling time interval was selected as 2 ms as given in Table 3. Ambient noise records were taken for approximately 5 minute and 10 minute durations in the former and latter phases, respectively.

Table 3. The list of selected field configuration and data acquisition parameters in Phase 1 and Phase 2. Please note that the numbers given in parenthesis show the selected parameters in Phase 1. The numbers without parentheses show the utilized parameters during Phase 2.

Survey type	MASW	MAM
Source	6 kg sledge hammer	Ambient noise
Seismograph	GEODE (ABEM RAS 24)	GEODE (ABEM RAS 24)
Geophones	4.5 Hz (Spike coupling)	4.5 Hz (Spike coupling)
Receiver array	12 channel linear	11 Channel L, 7 Channel Triangular and 12 channel Linear (12 channel Linear)
Array dimension	16.5 m (27.5 m)	50 m in L, 34 m in Triangular 110 m in Linear (55 m in Linear)
Receiver Spacing	1.5 m (2.5m)	10 m in L, 17 m in Triangular 10 m in Linear (5 m in Linear)
Source offset	5 m, 10 m, 15 m for forward shot and 21.5 m (37.5 m) for reverse shot	-
Sampling Frequency	1 ms	2 ms
Recording Time	2 s	32 s for each record
No of stack / records	3 or 5 stacking	20 (11) records

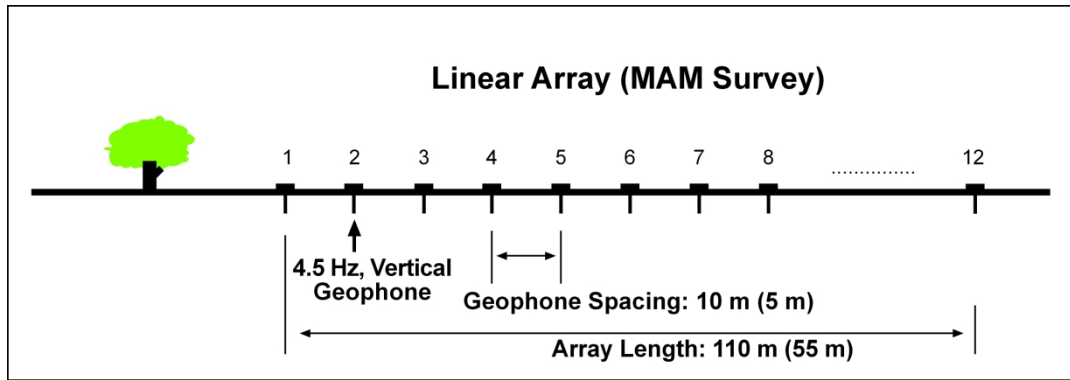


Figure 30. The configurations of the linear arrays utilized in the passive surface wave survey. The numbers given in the parentheses show the selected field configuration parameters in Phase 1. The numbers without parentheses show the utilized parameters during Phase 2.

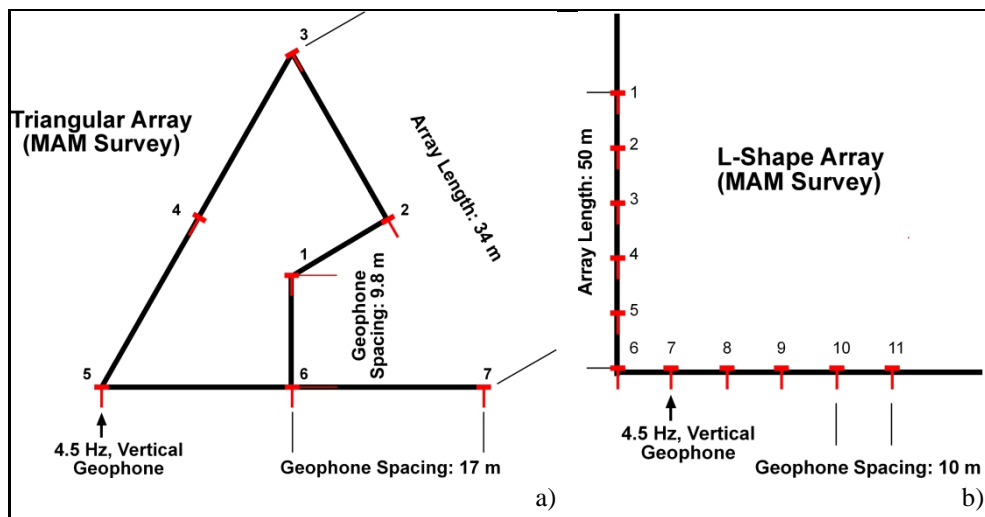


Figure 31. Configurations of the geometrical arrays utilized in the surface wave investigations in the second phase of the study a) triangular and b) L-shape array geometries configured in the passive surface wave survey.

3.3.5. Construction of dispersion curves

The initial model assumption for surface wave measurements is generally that linear elastic half-space layers used for interpretation of surface wave survey are homogeneously stacked. Rayleigh wave phase velocity of layered soil/rock model is a function of four components; i) frequency, ii) P-wave velocity, iii) density and

iv) thickness of each layer. The number of unknowns for a model with n number of layers including the half-space is $4n-1$ (excluding the half-space with undefined depth). As can be clearly observed, it is not possible to directly solve the inversion of surface waves. Therefore, it is necessary to apply an optimization method to decrease the number of unknowns and it is required to introduce possible limiting conditions in order to acquire more reliable results (Foti, 2005). For this purpose, a preliminary assumption is made for density and Poisson ratio in order to decrease the sensitivity of the experimental dispersion curve based on the values of the density and P-wave velocity soil parameters. Xia et al. (1999) defined the relative effect of each soil parameter on a dispersion curve by analyzing the Jacobian matrix. Based on the results of the study performed herein and the study proposed by Xia et al. (2004), the shear wave velocity for the fundamental mode of dispersion curve of high frequency Rayleigh wave (>2 Hz) is the most dominant parameter among the other soil parameters that effects the phase velocity variations of the Rayleigh wave. Therefore, inversion of the shear wave velocity from the phase velocity of the Rayleigh wave is the basis of this process.

Moreover, in order to decrease the effect of the layer thickness on the dispersion curve, it is necessary to select thinner layers. This effect can be reduced by selecting a subsurface model of 10 or 15 layers as proposed by Hayashi (2008). This approach is termed as the “blind-way technique” (Hayashi, 2008). In the literature, many researchers have proposed to show the applicability of blind-way method (the Subcommittee for Geotechnical Survey of the Ashigara Valley Blind Prediction Test, 1992; Boore and Brown, 1998; Louie, 2001; Brown et al., 2002; Hunter et al., 2002; Rix et al., 2002; Xia et al., 2002; Martin and Diehl, 2004; Asten and Boore, 2005; Stephenson et al., 2005; Comina et al., 2006; Moss, 2008). During the inversion process of data acquired throughout this study, the blind-way technique was utilized to obtain the surface wave profiles. The validity of this technique was checked by the available geotechnical boreholes down to a depth of 15 m.

The processing and analysis of all MASW and MAM records acquired during the first and the second phase were performed by using a SeisImager/SW™ V. 2.2 Surface Wave Analysis software. The same software was also used for the combined analysis of active and passive SWMs at the same location. The phase shift (Park et al., 1999) and spatial auto-correlation (SPAC) inversion (Okada, 2003) methods were utilized to obtain dispersion curves in the phase velocity-frequency (v - f) domain for the MASW and MAM records, respectively. Figure 32 shows the examples of the exponentially constructed dispersion curves v - f domain for the MASW and MAM records.

At first, all of the necessary editing (e.g., excluding low quality data and higher mode contamination) was applied at the processing stage of the field records by using the raw data prior to building the initial model of the soil profile for both active and passive surfaces in order to obtain a reliable shear wave velocity model. The reason for this approach is that purity, specificity and accuracy of the dispersion curves are the prominent properties influencing the accuracy of the inverted shear wave velocity profile as stated by Jin et al. (2006). By editing, the low quality data (i.e., low signal to noise ratio) was removed from the dispersion curves. The low quality data was observed especially at the lower frequency levels of the MAM records and at the higher frequency components of the MASW data. In some MASW records acquired in the first phase, it was observed that the higher frequency components of the data were highly contaminated due to interference of the higher modes of the Rayleigh wave. One of the MASW records taken during the second phase is given as an example in Figure 32 to show this contamination clearly. For some measurement points like the site given in Figure 32a, it was not possible to catch high frequency components (greater than 15 Hz) of the fundamental mode Rayleigh wave. However, this inconvenience was tolerated as much as possible by using the other measurements having different near offset distances.

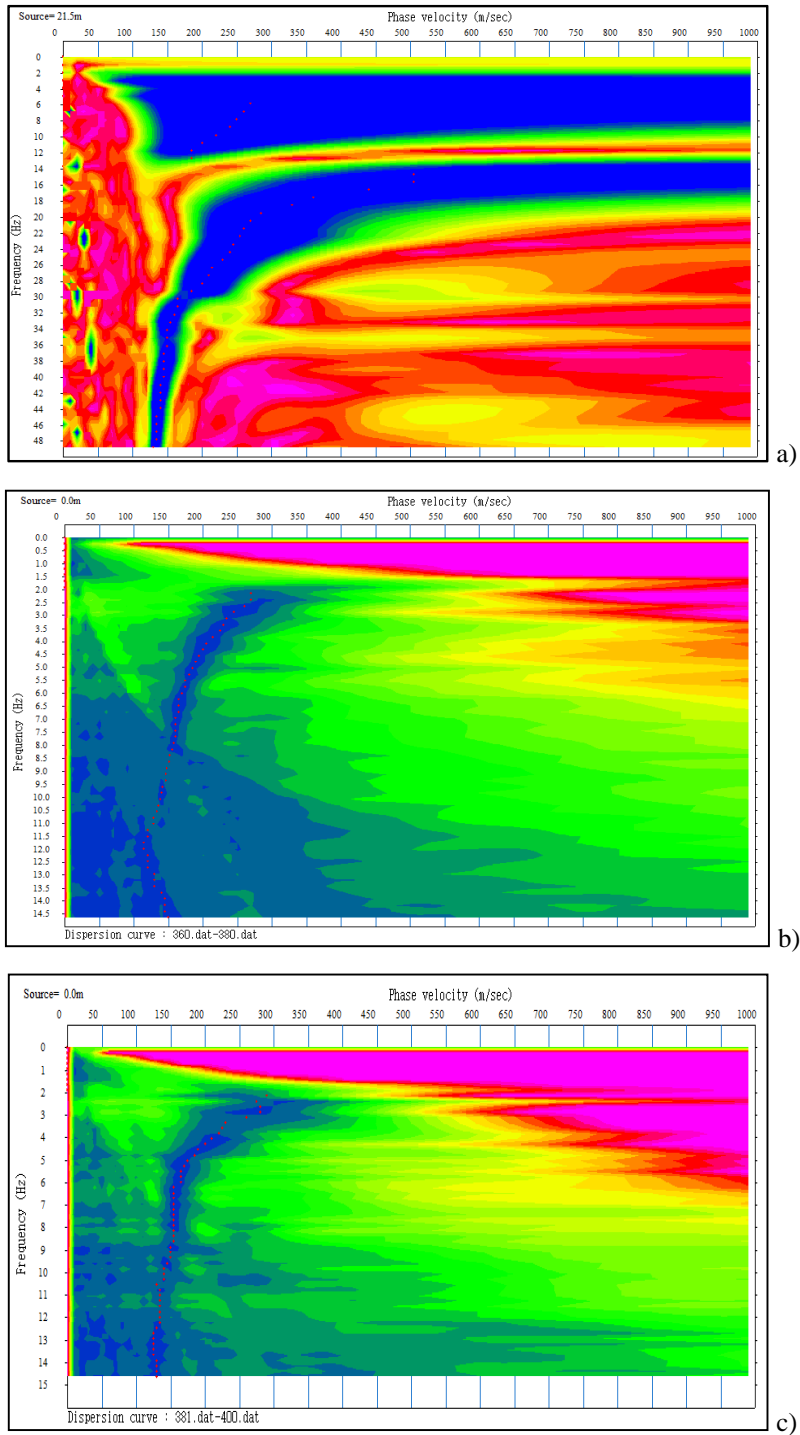


Figure 32. a) A contaminated MASW measurement [Comb02 (2)] by the interference of higher mode of Rayleigh wave observed at the higher frequency component of the record, an example of the constructed experimental dispersion curve of b) the L-shape and c) linear MAM records at Comb 12 (2).

After the editing process, the assumption regarding the continuation of the lateral homogeneity was checked by comparing the records obtained by forward and reverse shots for the MASW survey. In the MAM survey, 6 and 10 records were selected randomly and processed in order to confirm the validity of this assumption. As a result, the lateral heterogeneity effect was not observed at any signal recorded during the first and the second phase. Additional considerations taken in the selection of the trend of the array geometries during field work has made a significant contribution to the acquisition of well representative data.

After performing the stages given above, the dispersion curves of all of the surface wave measurements were generated and the initial soil models were constructed by a simple wavelength-depth conversion. This conversion utilized a multiplication factor (1.1) to the acquired phase velocity and one third wavelength approximation in the estimations of the shear wave velocity and depth, respectively. In the context of this study, the initial soil models were created by using 15 layers based on the blind way technique, and only the shear wave velocity values were changed throughout the inversion process. The depth of the initial models was assigned based on the effective penetrated depth of the phase velocity. The inversion process was performed by utilizing a non-linear least square method. After a number of iterations determined based on the amount of the root mean square error (<5%), the final calculated dispersion curve and the final shear wave velocity model were obtained.

As stated before, this study aims to characterize shallow layers at a higher resolution by using a relatively shorter array with the active method. Therefore, the depth information acquired from the MASW method is insufficient in general for deep basin analysis. Thus, MAM measurements were taken at MASW locations and dispersion curves of these two methods were combined and thus a larger frequency range was characterized while results identifying both shallow soils and also deeper sections were acquired (e.g., Asten and Boore, 2005; Gosar et al., 2008; Eker et al., 2012 and 2015). In the analysis of the CSWM, after merging the

dispersion curves of both methods conducted at the same site, the initial soil models were re-constructed with a similar procedure given above and the models were inverted by using a non-linear least square method with the same error margin consideration given above. No smoothing was applied during the combination procedure of the methods (Figures 33 and 34).

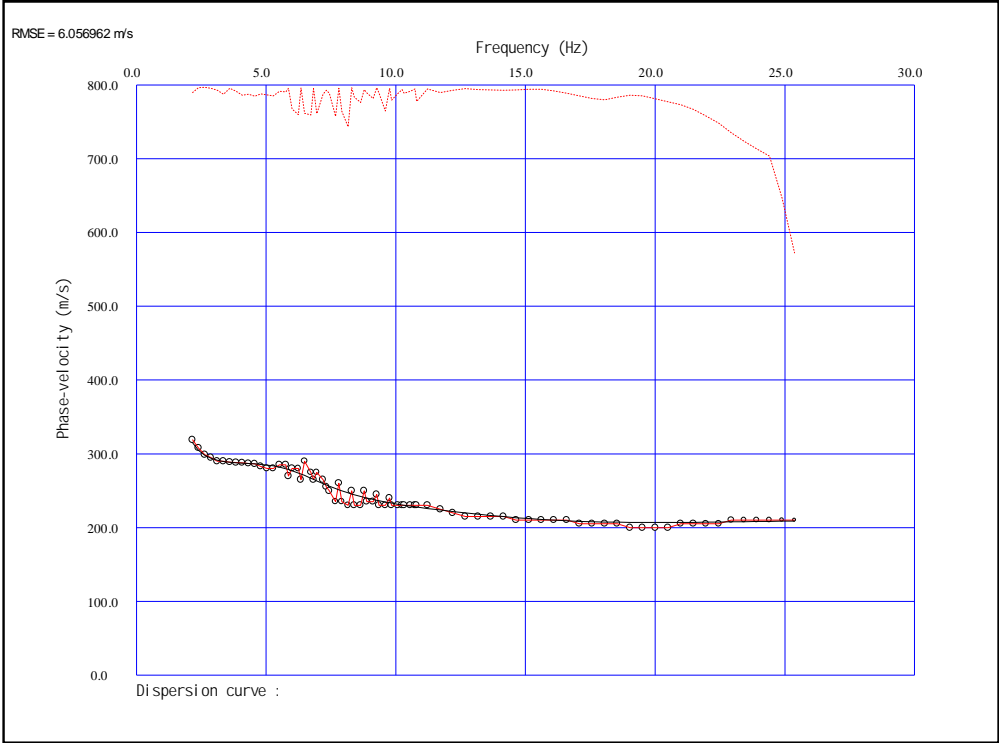


Figure 33. An example combined dispersion curve after the inversion process was performed at Comb07 (1). The red dashed line at the top of the figure shows the signal to noise ratio at each frequency of the phase velocity.

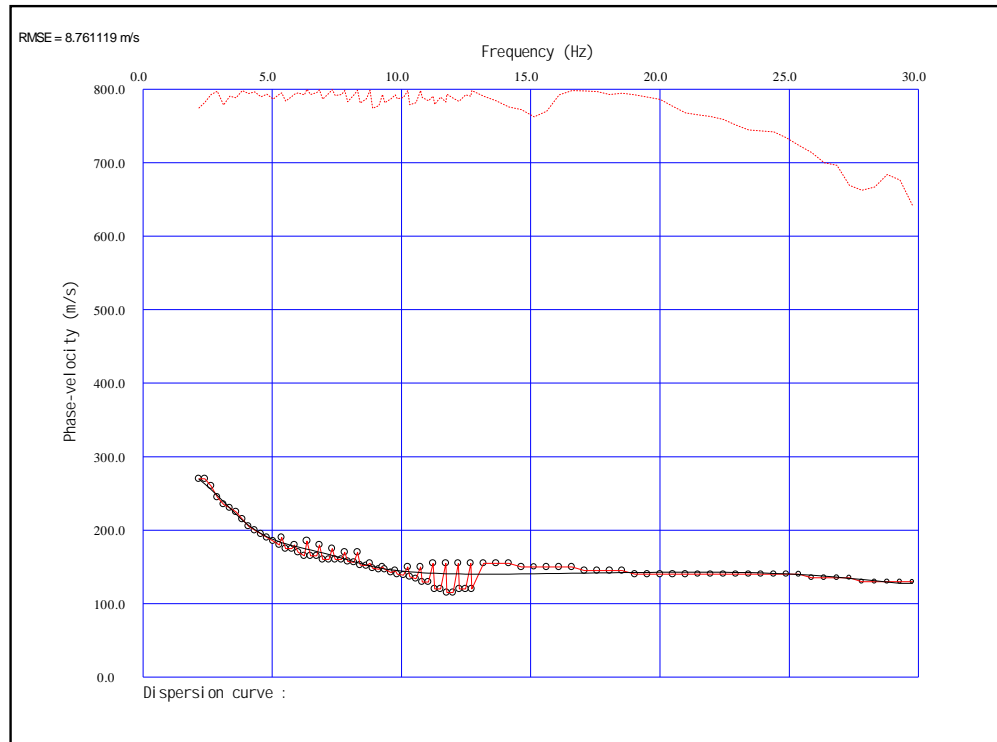


Figure 34. An example combined dispersion curve after the inversion process was performed at Comb12 (2). The red dashed line at the top of the figure shows the signal to noise ratio at each frequency of the phase velocity.

The resolutions of the dispersion curves were very high due to the utilization of the long and short array sizes together (Figures 33 and 34). Therefore, the high frequency components (greater than 15 Hz) of the fundamental mode Rayleigh wave were successfully detected in the MASW record. Also, as can be seen from Figures 33 and 34, nearly the entire frequency range (between 2 Hz and 15 Hz) was characterized by the MAM survey. This statement was valid for almost all measurements taken in both phases. Moreover, the same procedure was applied to the records taken by geometric arrays. When the dispersion curves of the MAM results recorded by the linear array configuration with the dispersion curves of the geometrical arrays were compared, it was observed that especially the lower frequency component of dispersion curves of geometrical array were slightly lower. When the results of the 12 sites are taken into account, the difference between the curves have a range of 2% to 7%. This difference is negligible when

the error margin of the utilized inversion technique in this study is to be considered. This margin is reported as $\pm 15\%$ according to Xia et al. (2002). Therefore, this confidently shows that a linear array is applicable for the passive MAM measurement. In order to make comparison, the experimentally constructed dispersion curves obtained from the geometric and the unisotropic arrays conducted at Comb 12(2) are given in Figure 32b and 32c, respectively. Additionally, as explained before, the maximum penetration distance can be as deep as the amount of the spread length. As given in Table 3, the array lengths are 34 m and 50 m in the triangular and L-shaped field configurations of the passive SWM, respectively. Therefore, the results of the MAM with the linear configuration were taken into consideration due to the capability of reliably characterizing the deeper parts of the sedimentary sites.

3.3.6. Results of the surface wave velocity measurements

The main aim of this study is to rigorously penetrate the deeper parts of the sediments as much as possible along with the accurate characterization of the shallower layers in terms of shear wave velocity values. As stated in the previous section, characterization of the target depth depends on several field acquisition parameters and their combinations along with the geological conditions. Also, it is related to the seismic velocities of the subsoil (Natale et al., 2004). This means that the same field acquisition parameters present different sampling depths at different locations. However as explained before, the general expectation is the maximum investigation of the MASW and the MAM survey to be generally equal to half of the spread length. At some cases, the maximum characterization depth can be increased up to the array length in the passive surface measurements.

In accordance with the purpose of this study, the local soil conditions of the Quaternary alluvial deposits and Pliocene sediments (hereafter termed as Plio-Quaternary sediments) were characterized in terms of shear wave velocity (V_s) values by utilizing a combination of the MASW and MAM surface wave

measurement results. As explained before, in order to implement this characterization study, these measurements were taken at different time periods. Mainly, the vertical and lateral variations of V_S data, and the harmonic average of the V_S values at the uppermost 30 m part at 29 sites were determined after analyzing the inverted V_S profiles. It should be noted that the phase number is given in parenthesis when the characterized sites are mentioned in this section.

The maximum reliable depth of investigation is between 11 m and 18.1 m for the MASW survey in the first phase. This range is varying between 13.2 m and 15 m after the implementation of the active SWM in the second phase. Figure 35 shows the final V_S soil profile that was obtained by the MASW survey at Comb14 (1). On the other hand, the MAM method was also performed at the same locations where the MASW method was implemented to increase the characterization depth. In the first phase, the maximum reliable depth that could be penetrated by the MAM survey was in the range of 35 m and 55 m. As a result of utilizing greater array length, the accurately characterized depth increased the range from 50 m to 85 m. The constructed V_S profile after implementation of the MAM survey can be seen at Comb13 (2) in Figure 36. It should be noted that the dark shaded area in Figures 35 and 36 shows the reliable parts of the V_S profiles.

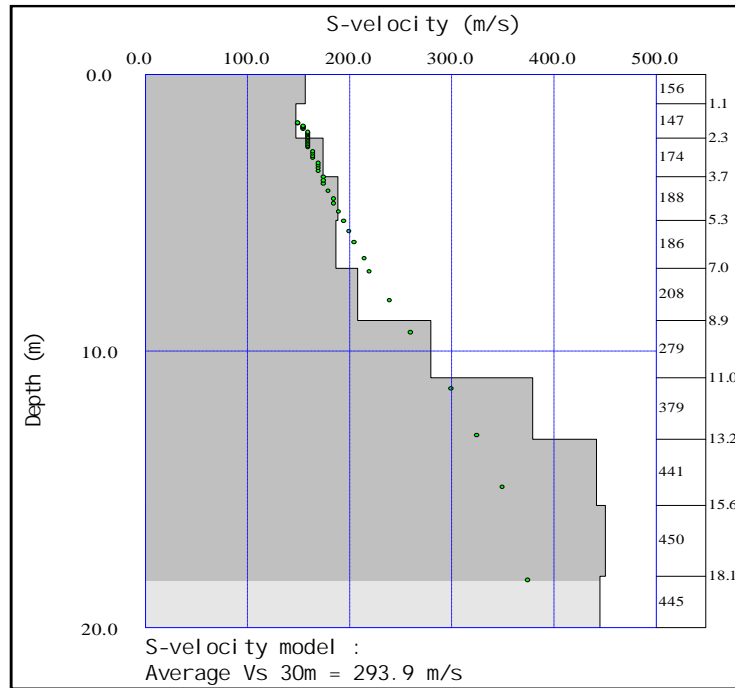


Figure 35. The final shear wave velocity profile obtained from the MASW method at Comb 14(1). The small green circles shows the dispersion curve which this V_S profile was derived from. The dark shaded area indicates the reliable parts of the shear wave velocity profiles.

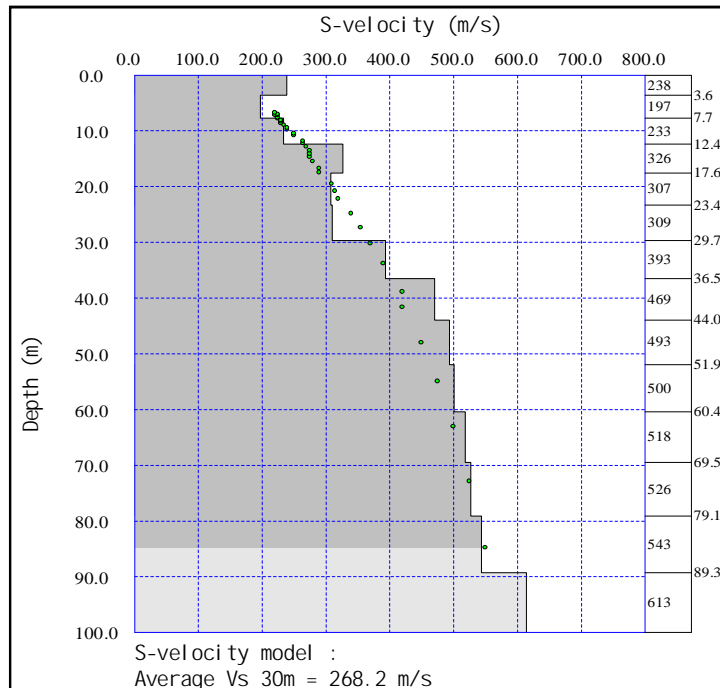


Figure 36. The final shear wave velocity profile obtained from the MAM method at Comb13 (2). The small green circles shows the dispersion curve which this V_S profile was derived from. The dark shaded area demonstrates the reliable parts of the shear wave velocity profiles.

As explained in the previous section of this dissertation, the passive SWM results were integrated with the 1D active ones to obtain more reliable information on the deeper sites. By combining active and passive source dispersion curves, high resolution V_s soil profiles were constructed for the 29 sites in this study. This can be clearly seen in Figures 33 and 34. As explained above in detail, these methods were performed based on the extent permitted by the properties of the utilized field equipment and approaches such as geophone, length of the spread cable, amount of energy exerted to the ground along with the degree of environmental noise, the proximity to the source of the noise and seismic properties of the geological units. The utilized equipment were not changed during the survey phase. Therefore, the variation of the maximum investigation depth in the same phase was controlled by the second set of the factors regarding the properties of the geological units and environmental noise. By performing the combined methodology, the maximum investigation depths were obtained as 55 m and 85 m according to results of the surveys conducted at Phase 1 and 2, respectively.

In the areas where an active river system dominates the depositional setting, the recent sediments may be deposited under the influence of both marginal and axial depositional systems. Mostly coarse grained soils are deposited due to the marginal depositional setting and these soils are composed mainly of terrace and alluvial fan conglomerates. This setting is controlled by debris flow and braided rivers. On the other hand, the axial depositional system includes fine grained alluvial plain sediments such as clay, silt and sand. The variations of the grain size in the soil layers causes the variation of the shear wave velocity values as stated by many studies by Ohta and Goto (1978), Inazaki (2006), Wills and Clahan, 2006 and Eker et al. (2012). However, these depositional characteristics were not observed at the study area together since the topography of the study area is very gentle and the majority of the area has a slope less than 1 degree. All results show that the area is dominantly under the axial depositional setting. The reason of the lateral and vertical variations of the cohesionless soils is the severity degree of the flooding and this is dependent on the intensity of the rainy seasons in the area.

As stated before, the Orta pull-apart basin has a diamond shape and it is elongated in the ENE-WSW direction. Three sites [i.e., Comb04 (1), Comb14 (1) and Comb13 (2)] are located at the places where the width of the alluvium deposit starts to narrow down as can be seen in Figure 27. The V_S variation of these sites show that softer sediments have V_S values ranging between 100 m/s and 270 m/s; the thickness decreases and the relatively stiffer geological layer that underlies this unit has an average V_S greater than 350 m/s. This difference provides an opportunity to determine the thickness of the soft and unconsolidated sediments for the area. Based on this threshold value, the thickness of these soft sediments are determined as 10.5 m and 9 m at the eastern and the western sides of the basin, respectively. This small difference can be related with the depositional and erosional effect of the river due to its flow direction. According to the sites located at the center of the basin [i.e., Comb03 (1), Comb08 (1), Comb01 (2) and Comb04 (2)] (Figure 27), despite the slight variation, the thickness of the soft sediment was determined by using this cut off value (i.e., 270 m/s) that is between 15 m and 20 m. The V_S profile of Comb01 (2) can be seen in Figure 37a.

When the variations of the Pliocene V_S values with respect to depth are examined, it can be stated that the thickness of this soft layer shows some variations at the measured sites [i.e., Comb09 (1), Comb06 (2) and Comb08 (2)]. As can be seen in Figure 27, these sites fall within the boundaries of the Pliocene sediments at the longitudinal axis of the basin center. While one of these sites [Comb06 (2) site] is situated at the northern part of the axis, the others are located at its southern side (Figure 27). While Comb06 (2) shows that the soft Pliocene sediment thickness is around 20 m, the thickness of this sediment layer at Comb08 (2) is determined as approximately 25 m. The V_S profiles constructed at the two sites can be seen in Figures 37b and 37c. Based on the variation of the topography and the spatial distribution of the geological units, normally, the V_S values at Comb06 (2) should have increased radically after a certain depth. When Figure 37b is examined, it is observed that the V_S variations become uniform at the value of 300 m/s. This unexpected behavior causing this non-linearity may be explained by the existence

of the geological elements. As can be seen in Figure 27, Comb06 (2) is located very close to a fault which controls the shape and depositional system of the valley. These results might be due to the presence of this fault and its deformation zone.

The cut off value is utilized as 270 m/s to distinguish the vertical variation of the soft overlying sediment from those of the stiffer underlying layers. When the lateral variation of the V_S values are examined, it is interestingly observed that the shallower parts of the shear wave velocity values at the Pliocene sites (Figures 37b and 37c) are lower than the Quaternary deposits (Figure 37a). This means that the older Pliocene deposits have lower V_S values at shallower depths. However, it was expected to be stiffer (Koçkar and Akgün, 2008). This phenomenon may be related with the grain size distribution, density, consolidation and degree of cementation in the deposits (Ohta and Goto, 1978; Wills et al., 2000; Inazaki; 2006; Wills and Clahan, 2006; Koçkar et al., 2011; Eker et al., 2012). Besides these, the degree of the weathering, the presence of faults and their deformation zones might have had a significant influence on the variation of the V_S values either in the vertical or lateral direction (Eker, 2009; Koçkar et al., 2011, Eker et al., 2012) while the other parameters are slightly changed for the deposits having different geological ages.

As stated above, this study mostly focuses on the characteristics of the Plio-Quaternary sediments. However, to properly describe the lateral variation of the sediments in terms of V_S values, the SWMs were taken at three Miocene sites [i.e., Comb13 (1), Comb05 (2) and Com10 (2)] which are present at the northern part of the Orta basin (Figure 27). The V_S profile of Comb05 (2) is given in Figure 37d. Based on these measurements, the thickness of the relatively softer layers having a V_S value of lower than 200 m/s is determined to be around 10 m. According to Figure 37d, it can be seen that this thickness is approximately 9 m. This finding regarding the soft Miocene sediments is highly related with the degree of the weathering and the proximity to the fault and its deformation zones as illustrated in Figure 27.

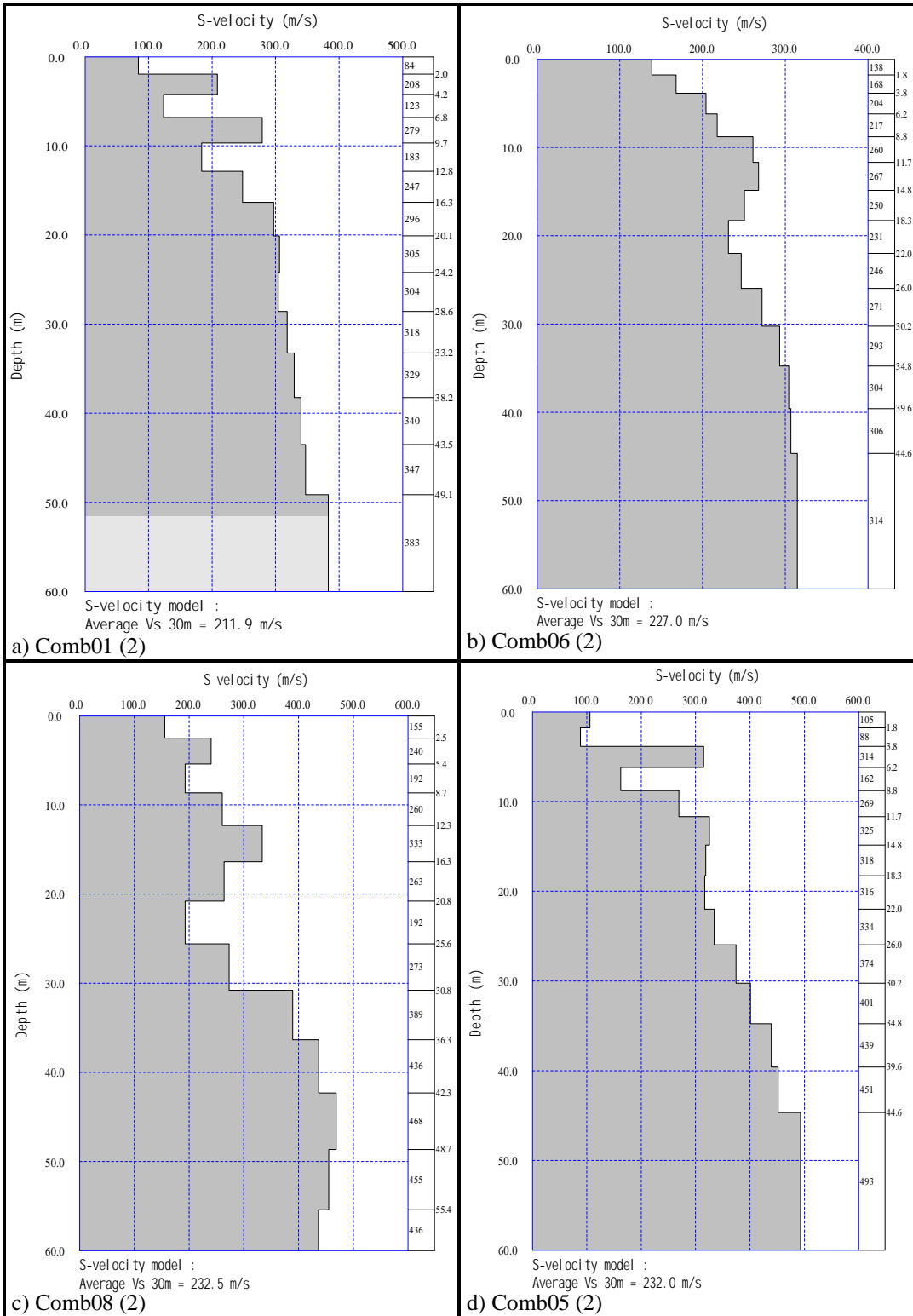


Figure 37. Some examples of the representative V_s profiles from the a) Quaternary, b, c) Pliocene and d) Miocene sites.

By integrating all of the information given above, it can be concluded that the shallower layers of the deposits which are divided into three groups based on geological age show similar variations with each other when the clay content of the soil layer is high. The presence of the coarse grained materials such as gravel and sand create the deviations especially at the alluvium deposits. Therefore, it can be concluded that the characteristics of the Quaternary sediments and shallower parts of the Pliocene and Miocene sediments are almost identical (Figure 37).

Due to the insufficiency of comparison of the seismic characteristics of the layers of different geological units, it was required to use another methodology in order to distinguish especially the shallower parts from each other. In this methodology, as given at the beginning of this chapter, the harmonic average of the shear wave velocity values for top 30 m of the soil profile were determined at 29 sites. The calculated V_{S30} values were grouped based on the age of the geological units and compared with each other (Figure 38). As can be seen in Figure 38, the Quaternary alluvial deposits, Pliocene and Miocene sediments fell within the boundary of site class D (between 180 m/s and 360 m/s) according to the design code of IBC 2012. Figure 38 shows that the V_{S30} values of the Quaternary sites change between 186.9 m/s and 289.3 m/s. However, the upper and lower bounds of the V_{S30} values (225.9 m/s and 300.6 m/s) at the Pliocene sites shifts to the stiffer parts of the charts (Figure 38). When the V_{S30} value distribution of the limited number of Miocene sites is examined in the same figure, it can be observed that three sites characterize this unit in a wider range. Also, these sites are at the same soil class with the others. This means that besides the correlation studies of the V_s profiles at the different geological units, the V_{S30} value does not give distinctive bounds for these units in order to quantitatively differentiate them.

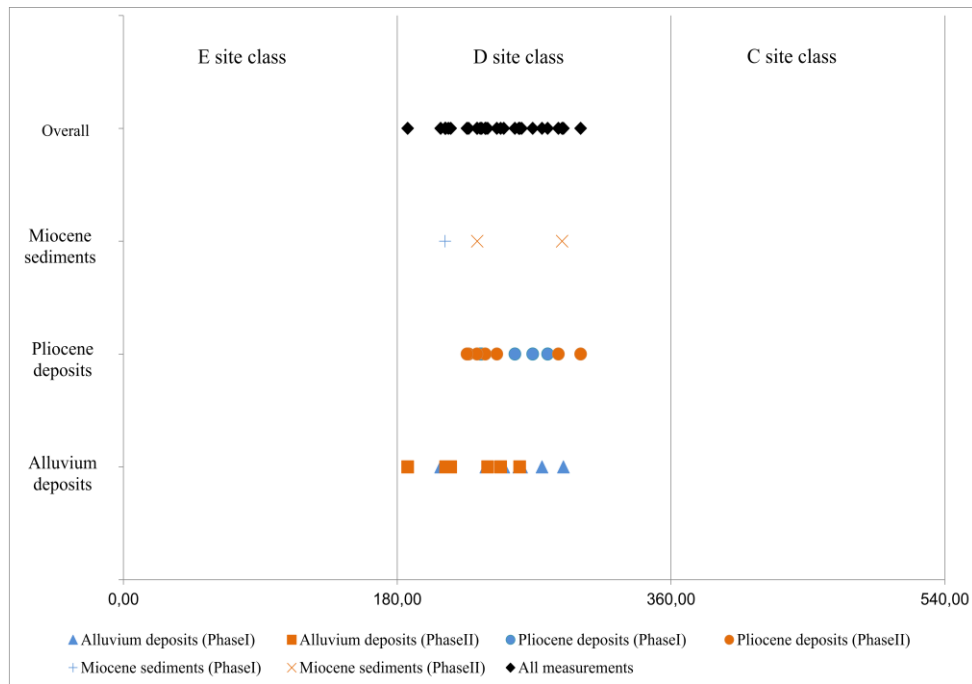


Figure 38. The general distribution of the calculated V_{S30} results with respect to different geologic deposits and corresponding to the site classes based on IBC 2012.

Depending on the results of the CSWMs performed, the regional seismic zonation map of V_{S30} was prepared in order to investigate the spatial variation of this value over the area (Figure 39). In order to quantify the spatial structure of the V_{S30} data, an ordinary kriging method with exponential semi-variogram model type was utilized by using the ArcGIS V9.3 software. In the creation of the V_{S30} prediction (interpolation) map, the anisotropy in the spatial distribution of the data was considered as well. In this technique, no transformation was applied since a normal distribution is statistically more representative when the distribution of the data is taken into consideration (Figure 39). By performing the trend analysis, the presence of the second order trend was determined and removed from the data. The local polynomial interpolation was utilized in the de-trending stage. It should be noted that although some parts of the study area were not covered by the performed SWMs, these sites were included in the regional seismic map in order to avoid distorting the shape of the map (Figure 39).

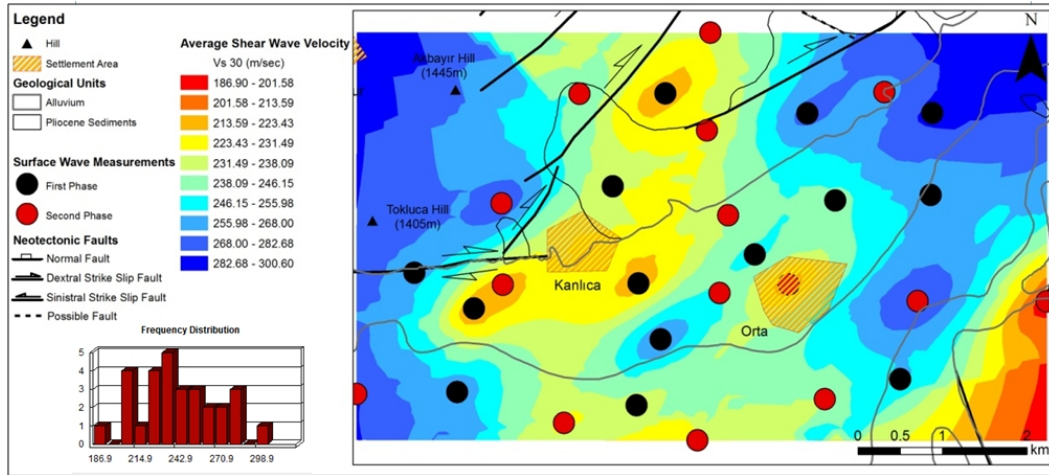


Figure 39. Spatial distribution of the V_{S30} value over the study area based on IBC 2012.

As can be seen in Figure 39, the general trend shows that the V_{S30} values tend to increase towards the northeastern and western parts of the basin. Towards these parts, the Quaternary alluvium thickness is gradually decreasing since the basin starts to narrow down. By comparing the V_{S30} values of the sites at the western boundary of the delineated area [i.e., Com04 (1), Com13 (2)] and the locations at the northeastern part of the area [Com14 (1) Com11 (2)], it can be stated that the recent alluvium is thinner at the NE of the study area. Additionally, it can be observed that there are some packages having lower V_{S30} values within the basin based on the measured sites. These sites [from west to east Comb11 (1), Comb 09(2); Comb06 (1) and Comb07 (2)] are clustered at the northern part of the Quaternary deposits where the course of the major river is present. This observation may show that these lower value data are related with the domination of the axial depositional system in the basin.

When Figure 39 is to be examined in detail, it can be observed that rather than the age of the geological units, spatial distribution of the geological elements such as faults play a significant role in the distribution of the V_{S30} values. None of the faults shown in the figure are pure strike slip faults. These have strike slip mechanism with a considerable normal component. This means that the dip

amounts of these faults are not so high and their planes have an inclination towards beneath the basin. The faults located at the northern side of the basin dip towards south. The others located at the south of the Orta basin have a north dip direction. The southern part of the basin cannot be observed in Figure 39 due to the extent of the figure, where Chapter 2 includes a detailed explanation of the subject. This state increases the deformation zone of the faults especially for the Quaternary and Pliocene sites. When the measurement sites located at NW of the study area [Com12 (1), Com13 (1), Comb5 (2), Comb10 (2) and Comb14 (2)] are to be taken into account, the variation of the V_{S30} values may indicate the spatial significance of the sites where downthrown and/or upthrown sides of the faults are present. In Figure 39, the lowest V_{S30} value (186.9 m/s) was observed at the site of Comb12 (2) located to the east of the study area and this location determines the extent of the eastern border of the survey. When Figures 27 and 39 are examined, it is clearly seen that this site is situated very closely to the NE-SW trending oblique slip fault controlling the basin. This is also another example for the effect of the presence of the faults and their deformation zones at the measurement locations.

In order to clarify the discussion given above and to understand the subsurface geometry of the basin, a 3D model was created by using V_S values. In creating the 3D V_S model given in Figure 40, a digital elevation map of the study area produced from 1:25.000 topographic maps of the General Command of Mapping was utilized to create the topography. The upper surface limit of the models was truncated with respect to the topography. The topography and the model itself was exaggerated 8 times in the vertical direction. Furthermore, the lower surface of the models was adjusted based on the maximum depth of the V_S profiles among the measurements. The model was constructed by using the anisotropic inverse distance technique with high fidelity and smoothing (filter size was selected as 1 for both horizontal and vertical directions) options. In the preparation of the interpolated model, the combined results of the MAM and MASW measurements were used. The model consists of voxels (3D pixels) having 25m x 25m x 2m resolution in the X, Y and Z axes, respectively.

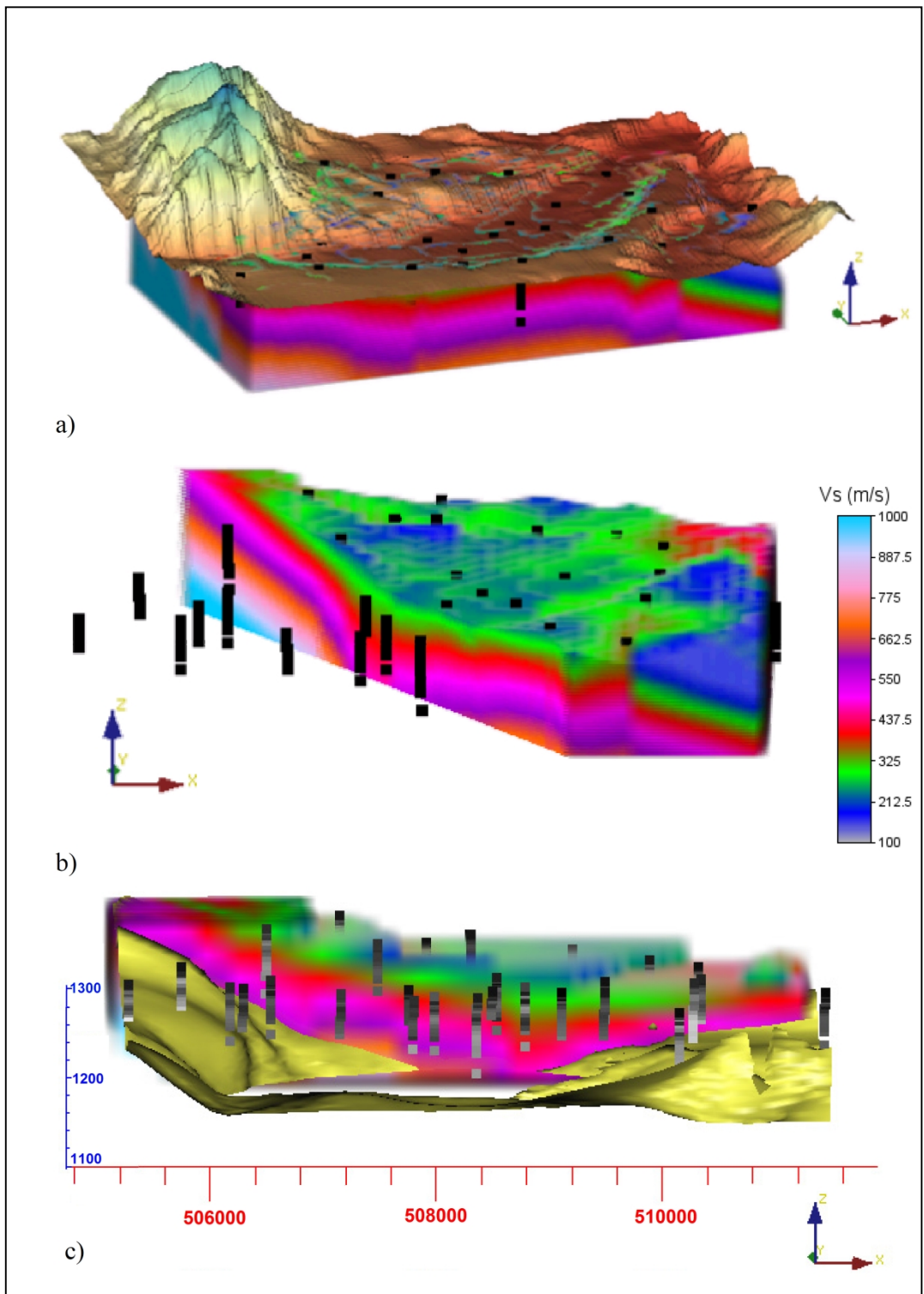


Figure 40. a) 3D V_s model with digital elevation, b) vertical and lateral variation of the V_s values along the x-y direction and c) iso-surface map with a V_s value of 600m/s.

The 3D V_S model with a digital elevation model of the area, vertical and lateral variation of the V_S values along the x-y direction are given by Figures 40a and 40b, respectively. As can be seen in the model, the extent of the area that was investigated by the surface wave methods was constrained at the southeastern part of the study region because this region has a hilly topography (Figure 40a). Also, this area is out of the scope of this investigation due to the type of the lithological unit present. Therefore, the geophysical survey was not implemented over the area intentionally. As stated before, the layers having a V_S value of greater than 600 m/s (illustrated as pinkish color in Figure 40) has an inclination towards the basin and it continues either from the west to the east or from the north to the south beneath the basin. The iso-surface of this layer can also be clearly seen in Figure 40c as well.

3.4. Generalization and comparison of the characterization studies

At the construction stage of the V_S profiles, the inversions of the measured phase velocities were performed by utilizing a blind way technique as explained above. In order to determine the performance of this methodology, the characterized V_S profiles were compared with concrete findings acquired from geotechnical borings. For this purpose, the SWM sites and borings were coupled and selected based on the distance between the pairs. The comparison was made for the layers down to a depth of 20 m due to the unavailability of the geotechnical data for the greater depths. This means that only the portion of the V_S data mostly acquired from the MASW survey was utilized at this step. Unfortunately, there is no way to validate the MAM results, except checking the compatibility of the dispersion curves from both methods. As discussed above the obtained curves agree fairly well with each other.

This comparison study shows that the lithological boundaries determined for each of the units at the boring log can be characterized by using the shear wave velocity results. Apart from the minor differences, it can be said that the results correlated

well and were generally consistent with each other. To show the reliability of this observation for each case, three pairs were selected from the Quaternary [BH-7 & Comb01 (2) and BH-15 & Comb07 (1)] and Pliocene sites [BH-17 & Comb02 (2)]. It should be mentioned that the Quaternary sites are closely located at the boundary of this unit. All the pairs are illustrated by an orange circle in Figure 41. The distance between the geotechnical and seismic sites is around 75 m for each pair. It should be noted that, if the distance between the compared data increase, the correlation of the data may not be descriptive based on the degree of the lateral heterogeneity.

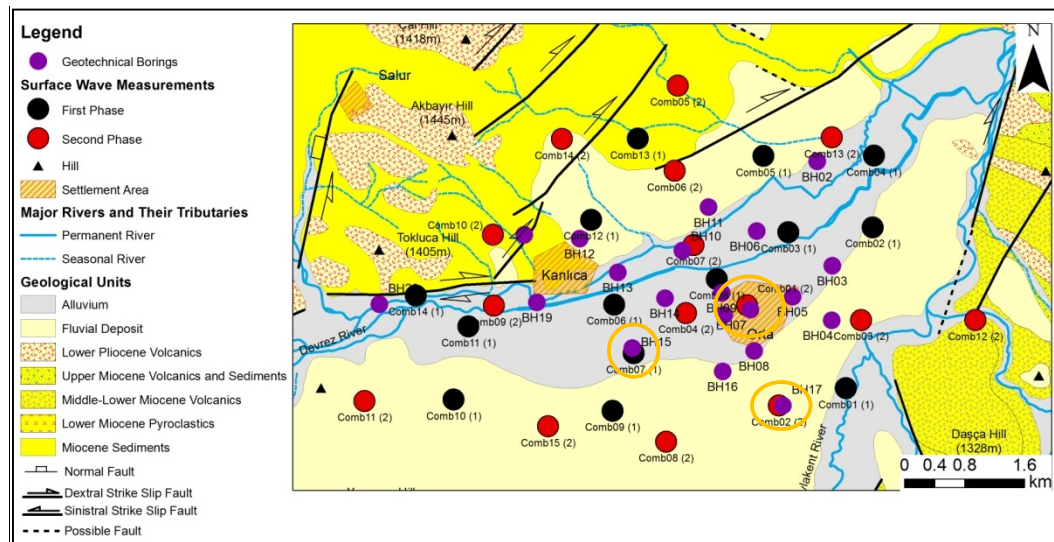


Figure 41. The distribution of the geotechnical borings and shear wave velocity measurements along with the trend of two sections. The orange circles show the used pairs for the comparison of the results.

Although there are minor differences between variations of the V_s , and SPT-N values and the soil types (Figure 42), based on the variations of the characterized soft alluvial and Pliocene sediments with high water table ($V_s < 200$ m/s) and medium dense sand and gravel (200 m/s $< V_s < 360$ m/s), these pairs are highly descriptive. This confirms that utilization of V_s values obtained by blind way technique can be used for the seismic characterization purposes. In Figures 42a

and 42b, the deficiency of the SPT to characterize a clayey gravel layer can be observed. As stated before, artificially high results can be obtained during performance of the SPT due to the presence of coarse grained bearing layers. However, the stiffness of the gravel layers can be characterized by the V_S value without facing any technical difficulties (Figures 42a and 42b). Apart from the slight differences, the variations between the V_S and geotechnical data (SPT-N value and geotechnical boring) are in good agreement with each other up to a depth of 15 m. Also, it should be noted that the V_S values start to increase after a depth of 16 m like the SPT-N value behavior which can be observed between depths of 12 m and 15 m for the pairs given in Figure 31b.

In general, it can be concluded that if the proximity between the compared data is close (<100m), trend of the V_S variation can be quietly compatible with the geotechnical data. Depending on the degree of the lateral heterogeneity, it can be stated that the variations of the V_S value can be compatible with the geotechnical data for the other pairs spatially separated with a large distance (>200 m) in this study if the elevation difference effect is corrected.

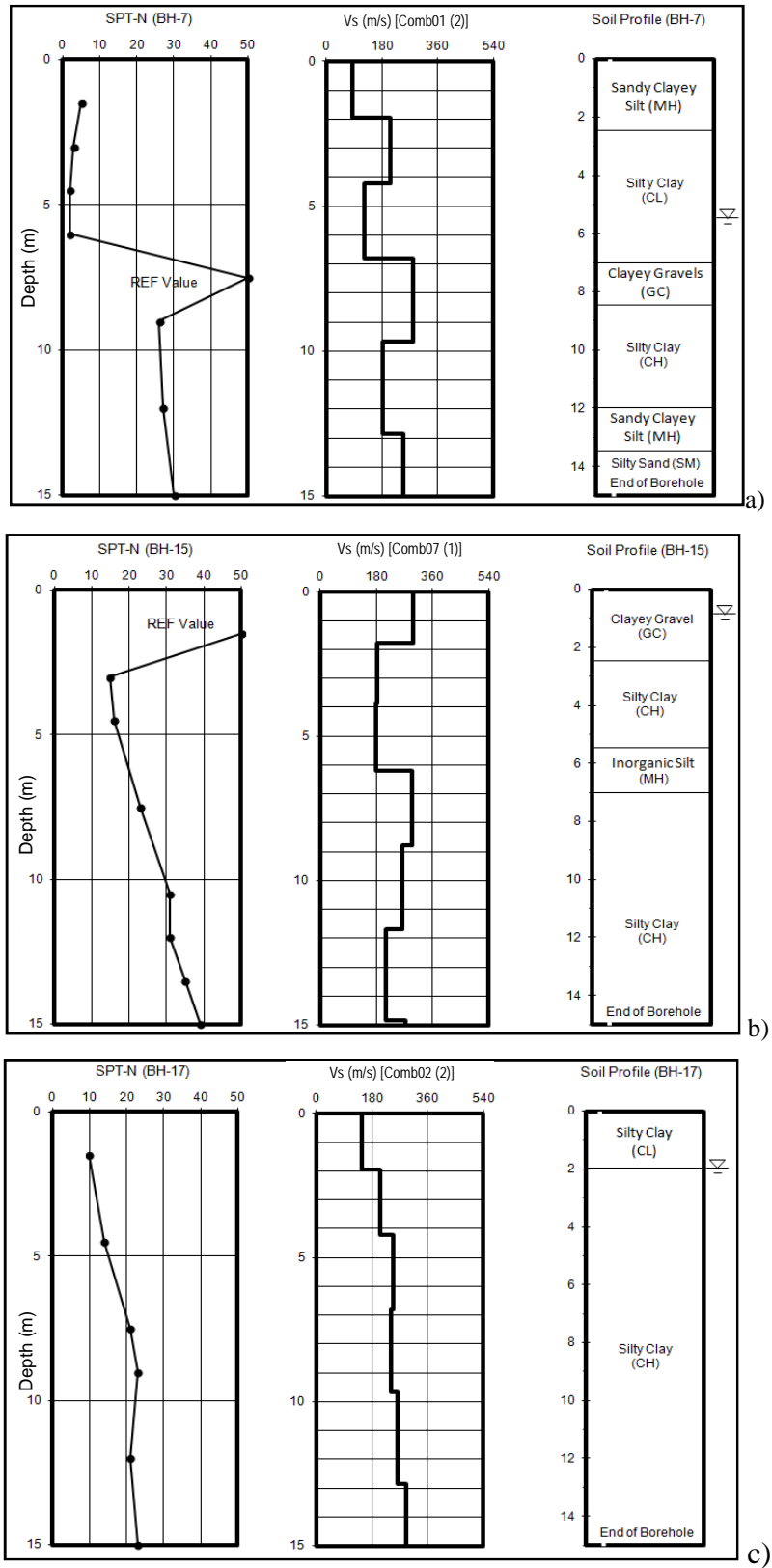


Figure 42. The selected pairs for the comparison a) BH-7 & Comb01 (2), b) BH-15 & Comb07 (1) and c) BH-17 & Comb02 (2).

After correlation of the results of the seismic survey with that of the geotechnical data, it was observed that the shallower parts of the soil sites (<20m) has two layers in a general sense. The first layer is composed of softer sediments and it shows variance in the grain size. Mostly, the cohesionless soil and cohesive clay form this layer in the Quaternary and the Pliocene sites, respectively. The thickness of this layer shows a variation depending on the location with respect to the course of the river. However, as can be seen in Figures 43a and 43b, the thickness was determined as about 10 m for the Quaternary sites, respectively. For the Pliocene site (Figure 43c), the soft first layer has a thickness around 15 m.

Therefore, a new inversion process was performed by using the constructed dispersion curves via the combination of the SWMs. In this process, the initial model was created by using 4 layers. A non-linear least square method was utilized to obtain the inverted V_S profiles for all sites in this study. The new inverted layers were compared with the results of the blind way technique in Figure 43. The comparison shows that the new ones also roughly characterize the layer and the variations of the values are concordant with each other. In the new constructed profiles, the V_S values increases with the depth rather than showing variations especially for the shallower layer as discussed before. This means that the new V_S structure follows the rule of thumb which is that the layers become stiffer towards the deeper parts due to the overburden thickness. This is true for most of the cases with a few exceptions. In order to generalize the V_S profiles at the sites, the new constructed profiles were utilized. This was an important approach performed in this study to simplify the layers in order to construct 2D V_S sections in a more acceptable manner.

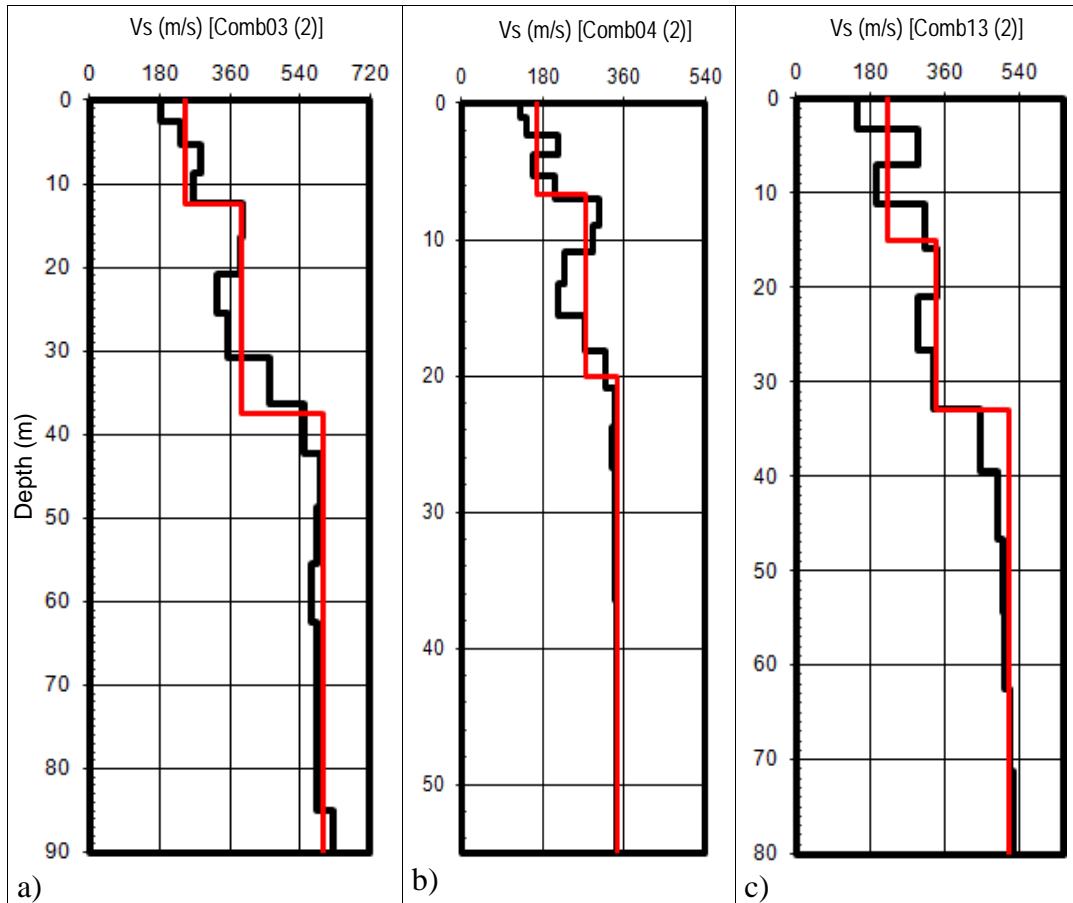


Figure 43. Comparison of the new inverted layers with the results of the blind way technique at the sites of a) [Comb03 (2)], b) [Comb04 (2)] and c) [Comb13 (2)].

As stated before, construction of the shear wave velocity profile up to the engineering or seismic bedrock is an important point in the ground response analyses. As stated in the previous section, a methodology, termed as CSWM, was adopted in this study to characterize the deeper parts of the soil profiles while preserving the high resolution throughout these profiles. The performances of the CSWM at the 29 sites show that sites could be described in terms of the V_S values up to a depth of 85 m. At that depth, the sites have the V_S values ranging from 500 m/s to 600 m/s. Based on the some studies (e.g., Borchardt, 1994; Pitilakis, 2004; Boore, 2006; Havenith et. al, 2007; Sitharam and Anbazhagan, 2008), this value is sufficient in order to make an extrapolation to the V_S value of 760m/s or it can be directly used in order to characterize the bedrock. However, it is a fact that more of

the sediment column should be considered to obtain an appropriate ground motion projection (Bodin et al., 2001; Nguyen et al., 2004; Parolai et al., 2006; Boaga et al., 2012). Andrus, et al. (2006) and Chapman et al. (2006) suggest extrapolation of the shear wave velocity up to 3500m/s in the ground response analyses. However, the characterization of the deeper geological units is a major challenge.

Based on the deep borings drilled for the purpose of calculating the coal reserve of this Orta area (Tokan and Özgen, 1976), it is known that the sediment thickness within the basin is more than 145 m and also the most probable unit underlying the sediments is the basalt and/or the andesite layer, a product of the volcanic activity in the Miocene. But this volcanic unit may not show lateral continuation throughout the basin either from the south to the north or from the east to the west. Additionally, based on these deep drilling logs, it can be stated that these volcanic intrusions are intercalated with sediments at the western edge of the Orta basin. Despite these facts, the presence of the volcanics within the basin and its thickness are not known after all the surveys are performed in this study. Therefore, some assumptions had to be made in order to locate the depth of the bedrock depending on the findings from the geological and geophysical data.

The main assumption is that the volcanic layer has a consistent lateral extent beneath the Orta basin and its shear wave velocity value is greater than 1500 m/s. Another important assumption during generation of these sections was that this layer possessed homogeneous engineering and seismic properties at every point within the area. Based on the information acquired from the deep drillings, a basalt unit was geologically assigned to the engineering bedrock. As stated above, if this unit intruded to the lake environment during the sedimentation, the boundary between the basalt and sedimentary deposits should have been sharp. Under these assumptions, the sections were constructed and the vertical and lateral variations of the layers were characterized by using extrapolated V_S values. At the extrapolation stage, the results of the microtremor surveys performed in the scope

of this study were also taken into consideration since this method can be used to determine the bedrock depth, as discussed in the next chapter.

In order to perform 1D and 2D analyses, initially representative data and sections were selected by examining all of the V_S profiles in detail. As can be seen in Figure 41, two sections covering a total of 11 different measurement sites with one common site [i.e., Comb04 (2)] were selected. One of the sections is almost in the N-S direction and the other one is nearly in the E-W direction. In the generation of these two sections, the digital elevation map of the study area produced for the creation of the 3D model was utilized to create the topography. The upper surface limit of the models was truncated according to this topography. The lower surface of the models was adjusted according to the depth of the V_S profile which was extrapolated up to layer having a V_S value of 1500 m/s. Both sections were modeled by using the anisotropic inverse distance weighting (IDW) technique with high fidelity option. It should be noted that the N-S (A-A') and E-W (B-B') sections were exaggerated 5 and 10 times in the vertical direction, respectively (Figure 44).

The B-B' section is a transversal cross section and it covers all sites under the dominant axial depositional setting. It is observed that surficial soils at the B-B' cross section comprises softer sediments based on the shear wave velocity values (Figure 44a). However, the A-A' section is a longitudinal cross section and it starts from the Miocene site and passes through the recent alluvial deposit terminating at the Pliocene sediments (Figure 44b). As can be observed in Figure 44, this section consists of stiffer layers at its both ends. The subsurface geometry of the bedrock was determined in both of the sections. When the geometries in Figure 44 are to be compared, some variations in the bedrock depth can be easily observed. This situation meets the expectations in terms of geology as discussed above. Both of these sections strongly reflect the depositional setting of the area and the influence of the faulting as discussed above.

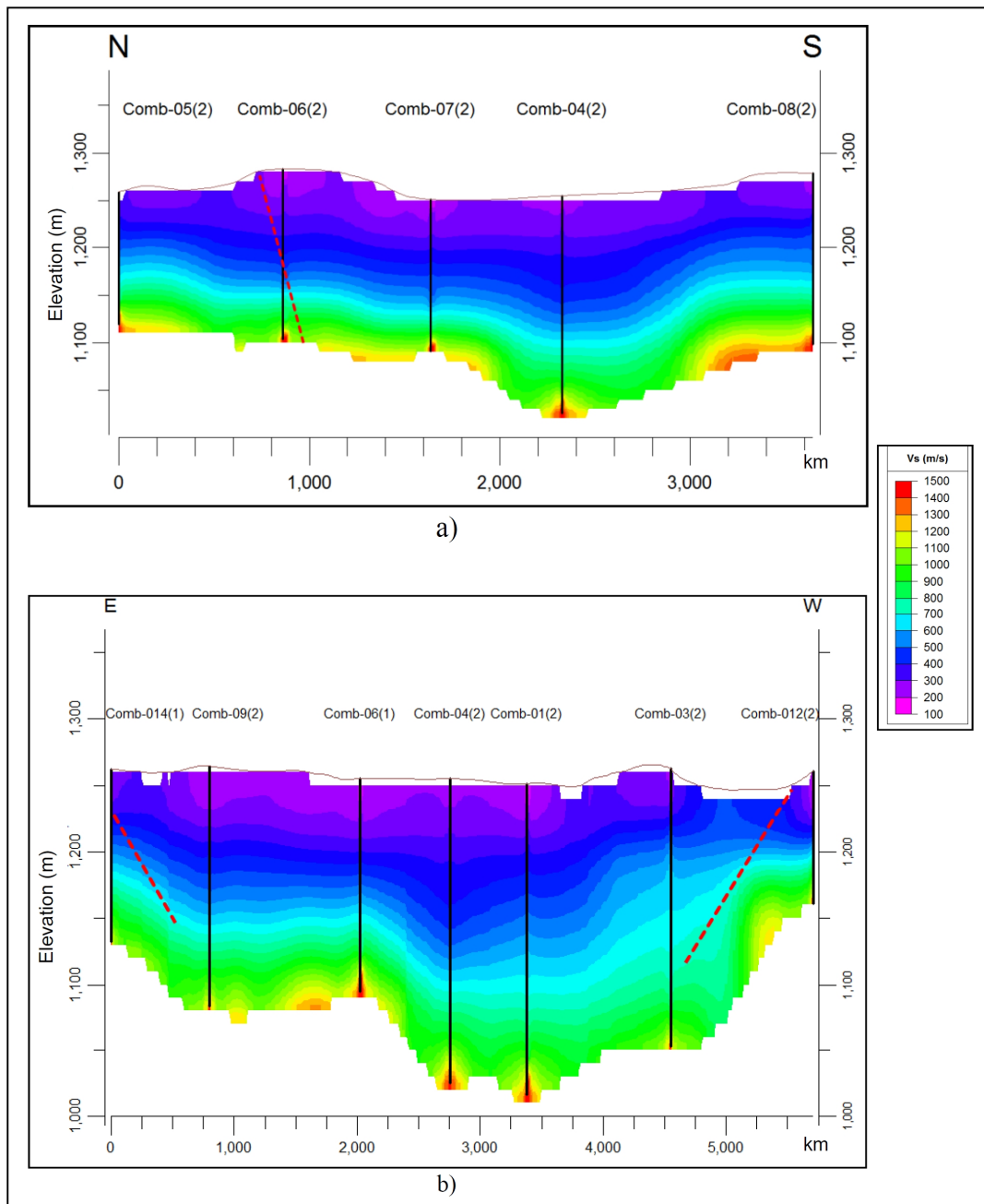


Figure 44. The two constructed sections a) A-A' section and b) B-B' section to determine lateral and vertical V_s variations. The red line shows the possible direction of the faults given in Figures 27 and 39.

Based on the correlation studies between the geotechnical and V_S data, geological principles, the extrapolated V_S profiles and the results of the microtremor surveys, the sites are divided stratigraphically into 6 layers. The first layer of the soil models can consist of either the cohesionless or cohesive soils. The soil types were assigned to this layer based on the geotechnical data. The layers between 2 and 4 were differentiated as clay deposits. The fifth layer was considered as the weathered upper part of the basalt layers based on the total core recovery taken from the deep borings (Tokan and Özgen, 1976). In the classification stage the contribution of the seismic behavior of the sediments is very high. It means that the layers were grouped based on the distribution of the V_S data especially for the deeper layer (>15m-20m) since the depth of the boundary between the Pliocene and the Miocene units as well as the Quaternary and the Pliocene sediments are not precisely known. Although the age of the geological layer is not a required knowledge in the further analyses, generally the first layer was assigned to Quaternary deposits if the sites are located within boundary of this unit. The deposits The second layer was classified as Pliocene clay and the third and fourth underlying layers were assumed as Miocene clay based on the vertical and lateral V_S variations. This classification varies based on the location of the sites with respect to the geological units. The performed procedure and results regarding the determination the V_S values and mechanical properties of the layers (i.e., unit weight, plasticity index and mean effective confining pressure, etc) is given in the next Chapter where implementation of 1D and 2D seismic response analyses is elaborated.

CHAPTER 4

METHODOLOGIES PERFORMED IN ESTIMATION OF SITE EFFECT

4.1. Introduction

The proximity to water sources and fertilized agricultural areas always offer convenient areas for people to live from the ancient times to recent. Most of these areas have wide topographically flat regions hosting a large population. However, these wetlands in Turkey are generally under the control of tectonic activity and they were chosen as the settlement areas. The increasing rate of the population growth have resulted in increasing the necessity of constructing buildings for residential, industrial, educational, religious and governmental purposes in Turkey. Meeting these requirements urgently can cause urban sprawl and sometimes leads to a decreased quality of construction. Therefore, in Turkey all of these concerns have already raised an issue related to the vulnerability of these structures located at these regions to a possible earthquake. All of the recent destructive earthquakes, namely, the 1999 Kocaeli Earthquake (M_w : 7.4) and the 2011 Van Earthquake (M_w : 7.2) in Turkey, the 2008 Sichuan Earthquake (M_w : 7.9) in China, the 2010 Christchurch Earthquake (M_w : 7.1) in New Zealand have clearly showed that local soil conditions have a prominent effect on ground motion and on the damage pattern.

Seismic waves generated during an earthquake propagate through different geological units until they reach the ground surface. The travel path of these waves through the geological units, especially which are present closest to the surface considerably influences the character of the waves and causes different effects on

the motion of the earthquake at the surface. Soft and unconsolidated deposits with considerable thickness have a tendency to amplify certain wave frequencies and to change the frequency content of the ground motion. This complex phenomenon is known as local soil effect. Along with this, local topography can also change the character of the earthquake waves. Depression (valley) or elevated (hills) surface features can lead to this effect. Local soil and topographic effects are classified within site effects (Oliveira, 2004). Pace of the studies on local site effects have increased in the last two decades. Although studies related to the influence of local site conditions on ground motion is more common (Fäh et al., 1997; Bour et al., 1998; Rodriguez-Marek et al., 2001; Tevez-Costa et al., 2001; Cara et al., 2008; Koçkar and Akgün, 2012) and the studies on investigation of the influence of topographic effect have considerably increased in the recent years (Hestholm, 1999; Komatitsch and Vilotte, 1998; Helstholm et al., 2006; Lee et al, 2008; Lee et al, 2009; Anggraeni, 2010).

Soft and unconsolidated sediments have a tendency to amplify selectively different wave frequencies since the seismic waves are trapped between the bedrock and overlying sediment layers due to the high impedance contrast between them. The effect of the local soil can manifest itself at low or high frequency regarding the sediment thickness (Lacave et al., 1999; Pitilakis, 2004 and Chavez-Garcia, 2007). Additionally, as stated before, the ground motion characteristics (the amplitude and frequency content) can be affected by surface topography (Jibson, 1987; Geli et al., 1988; Finn, 1991; Lebrun et al., 1999). The studies (Jibson, 1987; Geli et al., 1988; Hestholm, 1999; Komatitsch and Vilotte, 1998; Helstholm et al., 2006; Lee et al, 2008; Lee et al, 2009; Anggraeni, 2010) show that the ground motion is amplified at elevated topographies while de-amplification of the peak ground motion acceleration is observed over depressions.

When 2-D or 3-D geometries such as an area where fault controlled valley basins or topographical rise field conditions are present, lateral variation of these types of structures as well as the morphology of soil-bedrock boundary cause ground

motions to vary considerably when compared with 1-D conditions (Silva, 1991; Kramer, 1996). The main principal factors causing these changes are focusing or de-focusing of seismic waves, generation of surface waves at fault controlled edge structures and possible 2-D resonance. Effects related with these phenomena generally increase ground movement and lead to amplification at longer periods and continuation of movement. Furthermore, even though there are little or no changes in local site conditions, spatial variation of surface ground motion can be considerable even at neighboring locations. These are named as basin effect in general. Another factor contributing to ground amplification or de-amplification is the non-linear behavior of soils. This is highly dependent on the magnitude of movement generated by the earthquake (Idriss, 1991). Therefore, 1-D modeling at high strain levels at valley basins with sediment fill may not sufficiently represent the ground amplification levels observed in the field (Kramer, 1996, Rathje and Bray, 2001, Cılız et al., 2007).

The study encompasses a comparison of the results by performing 1D analysis based on amplifications due to 2-D influences by considering factors such as spatially non-linear variations in amplification and determination of soil response based on earthquake magnitude simulated by using 1-D and 2-D softwares. Seismic response analyses were performed via the 2D QUAD4M (Hudson et al., 1994) and 1D Shake2000 (Ordonez, 2000) softwares which use equivalent linear assumptions and consider non-linear stress-strain behavior of soils during estimation of effects of ground motion on basin/edge topography. Furthermore, differences and similarities between small unit deformation measurements acquired by the field surveys and the soil responses at high strain levels acquired from numerical simulation were determined by comparing H/V curves obtained from microtremor records and numerical analyses results.

4.2. Nakamura (H/V) method

There are many techniques in the determination of a soil response other than the numerical analyses. Among these, the Nakamura method, which is utilized for the determination of the main characteristics of site response of soft soils (i.e., fundamental periods and spectral ratio) have prominent applications in the site effect analysis since it is easy to use, low cost and time efficient. The signals are the records of natural noise of the ground, therefore no local or regional seismic activity and a reference point is required in the implementation of this technique. This experimental method (Lacave et al., 1999 and Pitilakis, 2004) is probably one of the most common methods preferred all over the world. This method is called as the Nakamura technique or H/V method (Nakamura, 1989). The pioneer study was proposed by Nogoshi and Igarashi (1971) to introduce this method based on the initial findings of Kanai and Tanaka (1961). The Nakamura method mainly depends on deriving the ratio of the Fourier amplitude spectra of the horizontal components to the vertical components of the records at the surface (Figure 45).

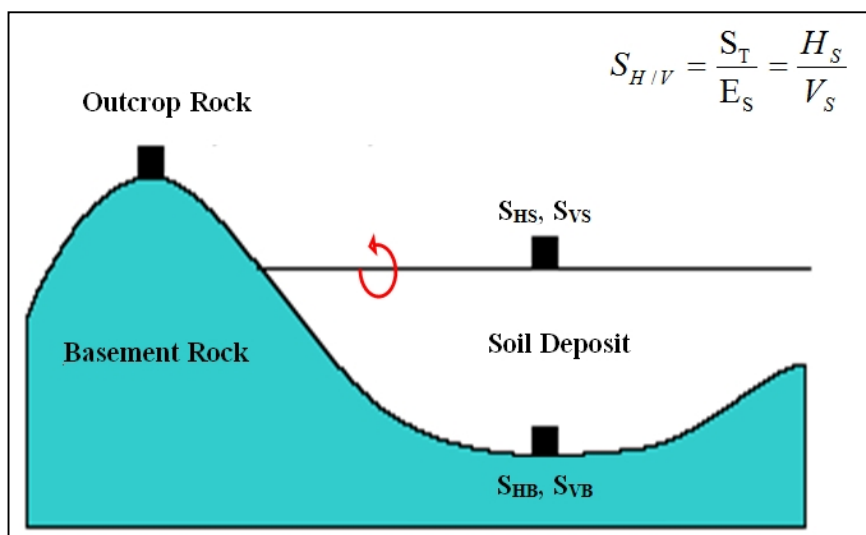


Figure 45. Simple model assumed by Nakamura (1989) to interpret microtremor measurements. SH/V is the horizontal to vertical spectral ratio, ST is the spectral ratio of transfer functions of the horizontal component of microtremor spectrum (SHS) at the surface to the horizontal component of microtremor spectrum (SHB) on the basement rock, ES is the ratio of vertical spectrum at the surface (SVS) to that spectrum at the base ground (SVB).

Many studies utilizing spectral ratios of horizontal and vertical components (H/V) method proposed by Nakamura have shown that all the information required for the accurate estimation of the dominant period of the site can be acquired with this method (e.g., Fäh et al., 1997; Duval et al., 1998; Guegen et al., 1998; Bodin et al., 2001; Cid et al., 2001; Satoh et al., 2001; Tevez-Costa, 2001; Delgado et al., 2002; Rodriguez and Midorikiwa, 2002; Nguyen et al., 2004; D'Amico et al., 2008; Haghshenas, et al., 2008; Özalaybey et al., 2011; Koçkar and Akgün, 2012; Eker et al., 2015). These observations have also been supported by various theoretical investigations (e.g., Field and Jacob, 1993; Lachet and Bard, 1994; Lermo and Chavez-Garcia, 1994). The accuracy of the amplification ratios acquired by this method, however, is still in debate. Certain theoretical (e.g., Lachet and Bard, 1994) and experimental (e.g., Teves-Costa et al., 1996; Bour et al., 1998 and Nguyen et al., 2004) studies show that the spectral ratio acquired from the Nakamura method does not supply all the information required for a reliable estimation of amplification of surface ground motion. Other studies (Lermo and Chavez-Garcia, 1993; Nakamura, 1989 and 2000), on the other hand, show that there is a good association between amplification ratios acquired from the H/V method and the standard spectral ratios along with the actual earthquake records.

This method has been implemented to figure out bedrock geometry (Bodin et al., 2001; Di Giulio et al., 2008; Walling et al., 2009 and Del Monaco et al., 2013), dynamic characteristics of the lithological units (Kudo et al., 2002; Fäh et al., 2003; Mirzaoğlu and Dikmen, 2003; Tokimatsu et al., 2004; Asten et al. 2004; Nunziata, 2007; Panzera et al., 2014), the zones prone to liquefaction hazard (Beroya et al., 2009), dynamic slope response (Del Gaudio et al., 2014) as well as soil-structure interaction (Gosar, 2007; Panzera et al., 2013), along with the fact that this method has been preferred all around the world for the last two decades by many scientists in order to investigate site effects (i.e., Guegen et al., 1998; Bodin et al., 2001; D'Amico et al., 2008; Koçkar and Akgün, 2012; Eker et al., 2015).

4.2.1. Recording microtremor measurements

Two campaigns were organized to take microtremor records for the purpose of investigating the site effect phenomenon experimentally. The first one was conducted in November, 2007 and the second was carried out in June, 2014. Two different velocimeters as suggested by Guillier et al. (2008) were utilized to record the microtremors along with the different data acquisition parameters during the field surveys performed at these two phases. The microtremor measurements were conducted at both phases, because of the reasons given above, and additional attention were given to determine the local site effect on the ground motion. Therefore, a grid system was adopted with changing spacing from 500 to 750 m because of the environmental noise, planted agricultural areas, man-made structures (especially electrical lines and infrastructures), accessibility problems, etc. at both phases in order to properly describe the site effect.

The main purpose of implementing two surveys was to investigate the effect of the acquisition parameters and different time periods, to compare the results of the H/V curves derived from the measurements of different seismographs and to increase the data in the study area in order to determine the site effects (if compatibility were to be observed between the two datasets). After completing both phases, Quaternary and Pliocene sediments constituted the majority of the measured sites in this study (Figures 46 and 47) and Miocene sediments observed at the northern part of the area in Figure 46 consisted of the minority of the measurements (Figure 47).

During the first phase of the survey, a total of 44 ambient noise measurements were taken to estimate the site effects of different lithologies within the Orta pull-apart basin. All these measurements were recorded at sedimentary deposits which are Quaternary, Pliocene and Miocene in age. A total of 23 and 19 measured sites fell within the boundaries of Quaternary alluvium deposits and Pliocene sediments, respectively, and the remaining 2 sites were measured within the Miocene

sediments. The spatial distribution of the first phase microtremor measurements is given in Figure 46 and Figure 47 shows the distribution of these measurements with respect to the geological units.

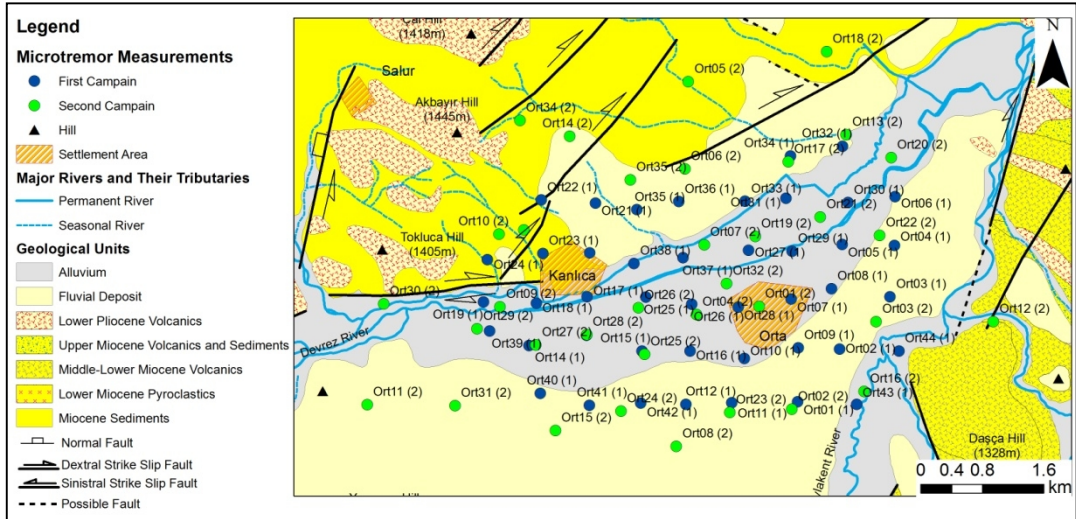


Figure 46. The spatial distribution of the first and second phase microtremor measurements.

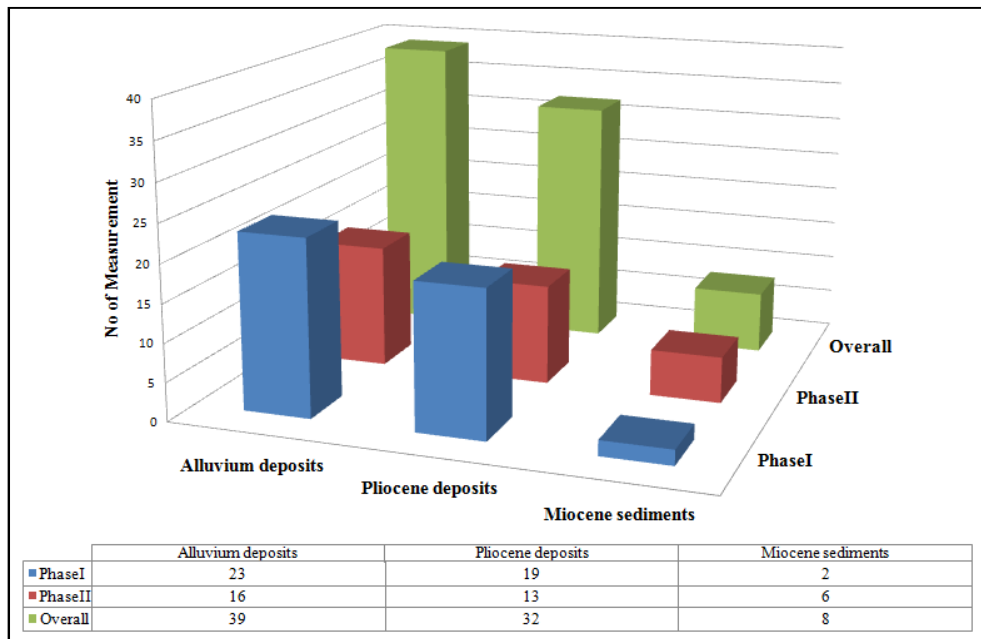


Figure 47. Statistical distribution of the measurement sites with respect to the geological units.

In the first phase, microtremor measurements were recorded by a NS/A model PC connected to a three component (two horizontal, one vertical) velocimeter (VCT Corp. model UP-255s seismograph) with a natural period of 1.0 s (Figure 48a and 48b). All the measurements have been taken through an A/D converter with a resolution of 12 bits via utilizing an amplifier (Figure 48c). The short-period noises were recorded with a duration of 5 minutes at each site with a frequency sampling range of 100 Hz. The quality of the data (measurements) taken was simultaneously checked by means of a notebook computer during the recording process.

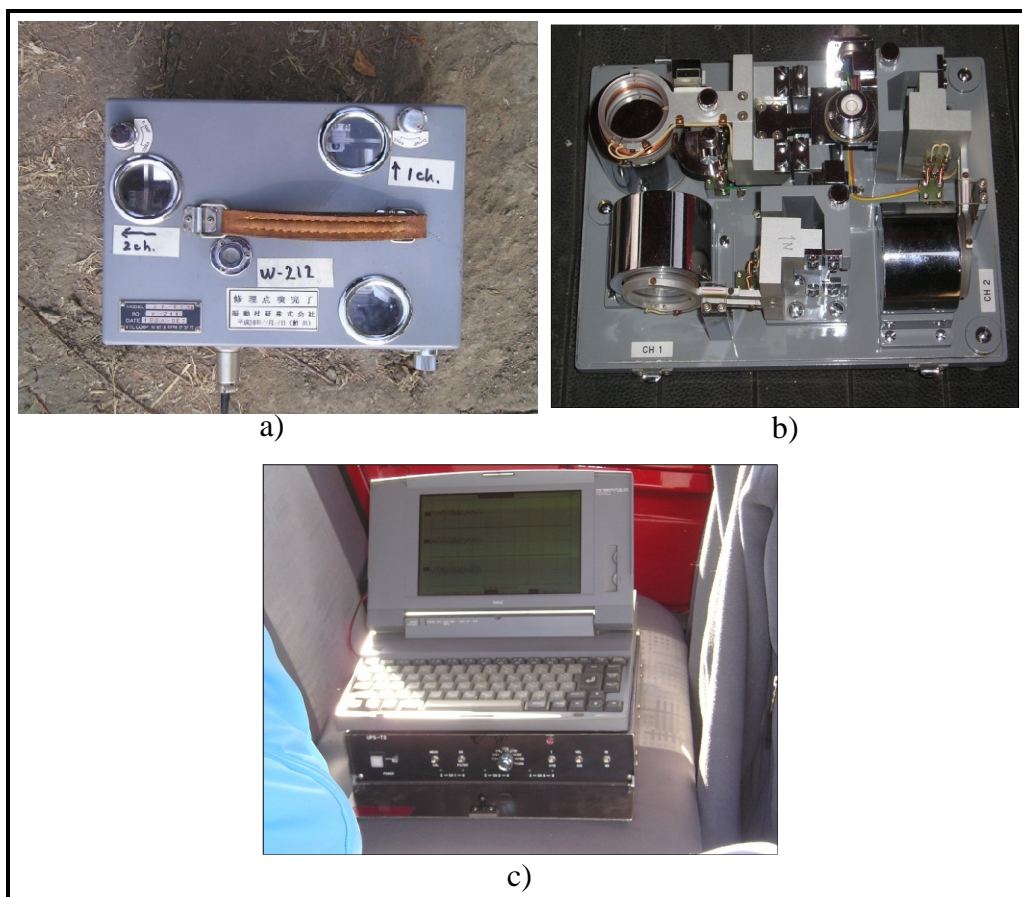


Figure 48. a) A close-up view of the UP-255s velocimeter, b) a view of the inside of the velocimeter, c) the amplifier and the notebook PC utilized during the recordings.

In the second phase of the survey, total of 35 ambient noise measurements were recorded to evaluate the site effects of the sedimentary unit deposits within the Orta pull-apart basin. A total of 16 and 13 measured sites fell within the boundaries of Quaternary alluvium deposits and Pliocene sediments, respectively. The remaining 6 sites were measured within the Miocene sediments. The spatial distribution of the second phase microtremor measurements is given in Figure 46. Additionally, Figure 47 shows the distribution of these measurements with respect to the geological units

In the second phase microtremor survey, the measurements were recorded with a Güralp model PC connected CMG-40TD velocimeter seismograph having a frequency band ranging between 0.033 Hz and 50 Hz with two horizontal and one vertical, three component “servo type” velocity sensor (Figures 49a, 49b and 49c). The sensor has a 24 bit digital output. In this survey, the data acquisition was performed by considering internationally accepted SESAME procedures (SESAME, 2004). Although the duration of the microtremor records were changed depending on the natural noise of the ground, measurements were generally taken with 30 minutes of unprocessed wave form records and 100 Hz sampling interval. The seismograph was warmed up for 5 minutes at each locations before recording microtremors during 30 minutes. Similar to the first phase, the quality of the data (measurements) taken was simultaneously checked by means of a notebook PC during the recording process (Figure 49c).



Figure 49. a) A view from the microtremor measurements at the Ort01 (2) site, b) a close-up view of the CMG-40TD velocimeter, c) A view from setting up the seismograph before the recording.

4.2.2. Processing of microtremor records

Before the processing of the records taken at the first phase, a noise filtering process was applied to the raw microtremor data in order to eliminate the noisy portion of the records. In this respect, an average envelope of waveform was calculated in the time domain for each record based on the noise level at the site. A higher noise level indicates that the record is intensely contaminated by the environmental noise. Although it depends on the waveform of the record, the

application of the high level noise can cause omitting an important portion of the record from the further analysis. In this study, 3.5, 4 and 4.5 noise levels were applied as a threshold value for the elimination of the contaminated parts of the records at 44 sites based on the influence level of environmental factors.

The stationary parts of each record were selected by at least 5 windows of 20 second length (Figure 50). A Fast Fourier Transform (FTT) procedure was applied to the selected windows following the noise analysis. Then, the Fourier spectrum of the window was smoothed by utilizing appropriate bandwidth (0.3 Hz) for parzen window to catch all possible peaks in the velocity spectrum (Figure 51). After these processes, during construction of the H/V spectra, in order to smooth the calculated Fourier spectra, filtering was not applied so that the H/V curves constructed at this phase with the others obtained from the second phase could be compared.

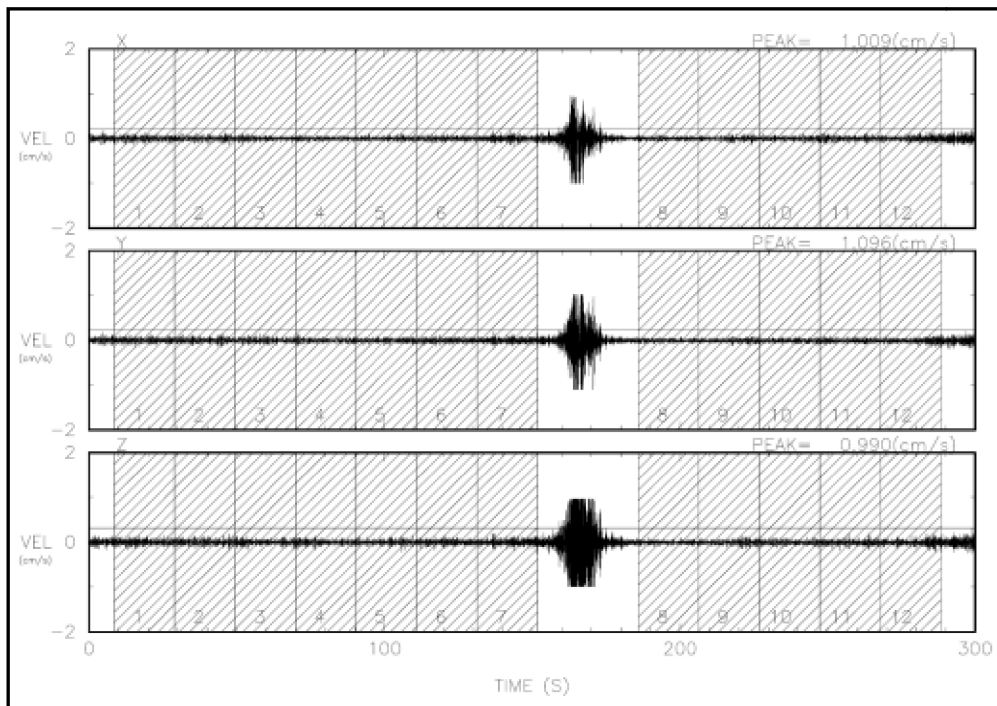


Figure 50. An example of the waveform from the unprocessed 5 min microtremor data recorded at the Ort07 (1) site. The hatched twelve rectangular areas are the selected 20 s windows for further analysis.

After performing this procedure, the spectral ratio of the horizontal to vertical noise components ($S_{H/V}$) was derived by dividing the resultant spectra of the horizontal components of the sediment site (NS and EW) by the spectrum of the vertical component (UD) of the measurement site (Equation 2). After acquiring the spectral ratios of all the selected windows, their arithmetic average was calculated to obtain the H/V spectrum of the site (Figure 51). During the data processing, the recorded signals were processed and analyzed by Micplot Version 1.1 for UNIX developed by Motoki (2002). The constructed average H/V curve after this procedure was demonstrated as a dark black colored in the figure and the thin lines represented the spectra of the selected windows.

$$S_{H/V} = \frac{\sqrt{(NS^2 + EW^2)}}{UD} \quad \text{Eq. (2)}$$

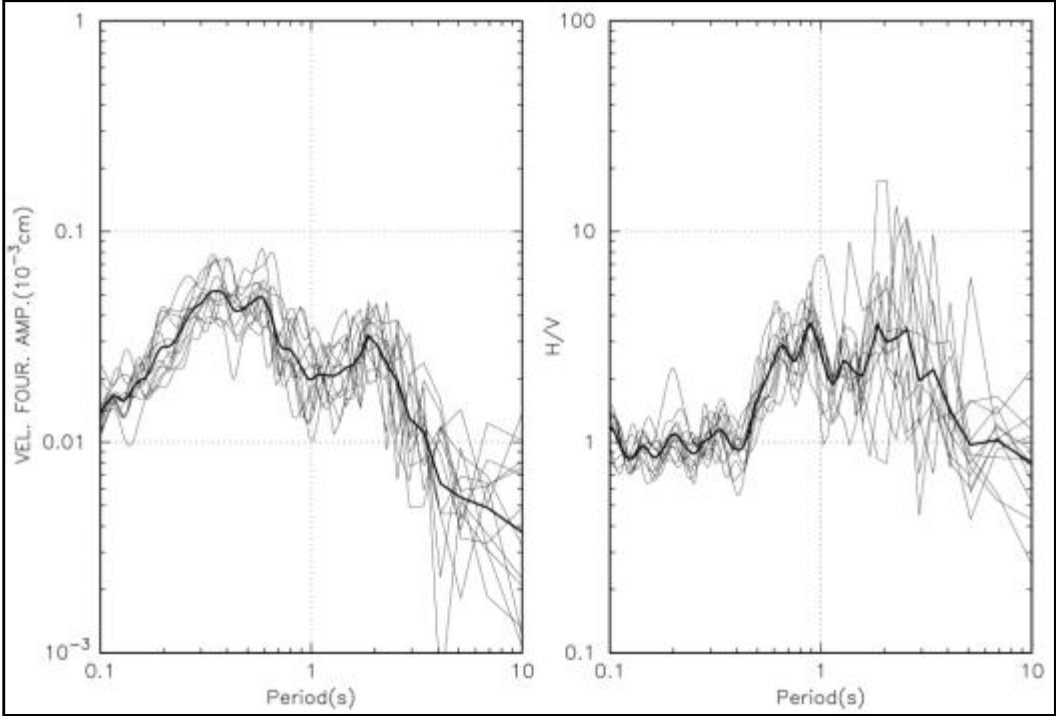


Figure 51. The FFT and H/V spectra of the selected 20 s windows to the left and right of the figure, respectively at the Ort07 (1) site. The thick lines show the average values of the spectra of selected windows which are demonstrated by the thin lines.

For the microtremor measurements recorded at the second stage, processing and analysis of raw data of the recorded natural noise was performed with GEOPSY V. 2.6.3 software. Prior to the data processing stage, a noise filtering process was applied to the raw microtremor data in order to eliminate the noisy portion of the records. First of all, baseline correction was applied to the raw records. Then, band pass filtering was utilized to keep the frequencies between 0.5 Hz and 20 Hz. After filtering of the raw signals, at least 10 windows of 25 second length were selected automatically (Figure 52) based on the ratio of short term amplitude to average long term amplitude (STA/LTA). Each window was tapered with a 5% cosine function in order to minimize the boundary effects regarding the extraction of selected windows. Fourier spectra of the selected windows were calculated for each noise component and smoothed using the algorithm proposed by Konno and Omachi (1998) having a smoothing constant b -value of 40. By using Equation 2 given above, $S_{H/V}$ for each selected window was obtained. At final stage, geometrically averaged $S_{H/V}$ was obtained in order to determine fundamental periods and spectral ratio amplitudes of the sites (Figure 53). The averaged H/V curve was demonstrated as a solid black color and mean \pm one standard deviation curves are given as dashed black lines in the figure. The H/V spectrum of all selected windows in Figure 52 is also given in Figure 53 with the same colors.

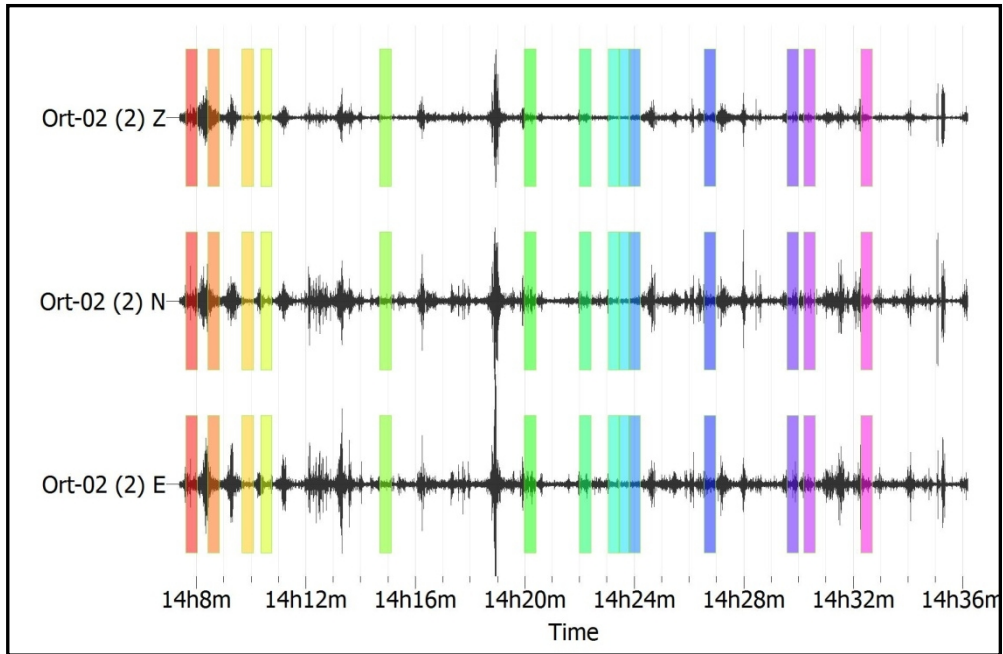


Figure 52. The selected windows from the filtered 30 minute microtremor data recorded at the Ort02 (2) site. The colored 14 rectangular areas are the selected 25 s windows for further analysis.

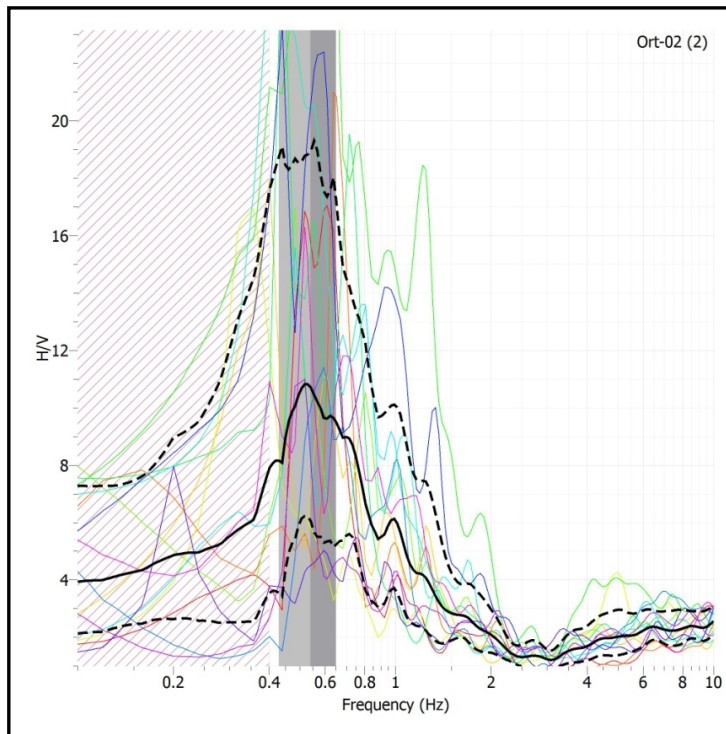


Figure 53. Geometrically averaged H/V spectra of 14 windows of 25 s length at the Ort02 (2) site. The solid black lines show the average values of the spectra of selected windows and the dashed lines represent the variation of the mean by considering \pm one standard deviation.

4.3. 1D and 2D numerical methods

4.3.1. Introduction

Soil response analyses include identification of non-linear soil properties along with identification of shear wave velocity profiles in context of the characterization of the site effects studies. There are various methods that can be used for simulation of seismic response analysis. These methods include different stress strain constitutive models. These methods can be performed to simulate the soil response under a possible excitation in 1D, 2D and 3D. Dynamic soil responses can be obtained by utilizing linear (e.g., Boore, 1972; EPRI, 1988), equivalent linear (e.g., Idriss and Seed, 1967; Wallace and Rollins, 1996; Rathje and Bray, 2001; Ordonez, 2009; Barani, et al., 2013) and non-linear (e.g., EPRI, 1988; Dawson et al. 2001; Andrade and Borja, 2006; Gelagoti et al., 2010) techniques.

In general, it is assumed that 1D analysis can identify key response properties regarding the actual 3D problem. One dimensional analysis of vertical propagation of horizontal shear waves along with modeling of non-linear soil responses with equivalent linear approach is extensively performed both in scientific and also in engineering applications for many decades to figure out soil response under a possible excitation (Rathje and Bray, 2001; Chouinard et al., 2004; Cavallaro et al., 2008 ve 2012; Lanzo et al., 2011; Pagliaroli et al., 2011; Boaga et al., 2012). However, reliability of 1D soil seismic response analysis results is a debatable subject regarding estimation of actual soil response at ground surface (Kramer, 1996). Since the lateral and vertical irregularities of subsurface layers and topography can be integrated into a 2D/3D soil response analysis, the strata is assumed as horizontal in the vertical direction in the 1D analysis due to the nature of this analysis.

The other reason is that the mechanical properties of near surface soils which can produce significant amplifications during an earthquake plays an important role in the spatial variability of the seismic ground motions. Because of these reasons, 2D/3D (Wallace and Rollins, 1996; Rathje and Bray, 2001; Ordonez, 2009; Gelagoti et al, 2010; Barani, et al., 2013) or 3D (Pitarka, 1999; Delavaud et al., 2006; Anggraeni, 2010) dynamic response analyses are proposed as a more reliable way during scientific and engineering applications. However, due to the requirement of a relatively uncomplicated database, cost and computational efficiency, 2D analysis are commonly preferred rather than 3D either in engineering practice or scientific researches (Chavez-Garcia, 2007). Additionally, their common usage allows to compare the 2D results with the other analyses in the literature (i.e., parametric studies).

To implement soil response analysis including a 1D, 2D and/or 3D environment, many techniques have been developed. These are Finite Difference Method [(FDM), e.g., Dawson et al., 2001; Moczo et al., 2002; Bohlen and Saenger., 2006], Finite Element Method [(FEM), e.g., Rathje and Bray, 2001; Gelagoti et al., 2010], Spectral Element Method [(SEM), e.g., Faccioli et al., 1996; Delavaud., 2006], Boundary Element Method [(BEM), e.g., Chaillat et al., 2009] and so on. In the scope of this study, seismic response analysis was performed by using 2D QUAD4M (Hudson et al., 1994) and 1D Shake2000 (Ordonez, 2000) softwares which use equivalent linear assumptions and consider non-linear stress-strain behavior of soils during studies on effect of ground motions on basin/edge topography. However, it should be noted that seismic response analyses performed via equivalent linear approach causes over-attenuation especially at high frequencies and over-amplification at soil response spectrum during large magnitude earthquakes due to the nature of the method (Kramer, 1996).

In the soil response analyses, independent from the dimensionality, the characterization of soils to the depth of bedrock is one of the critical subjects. According to a seismological and geotechnical point of view, there are two

bedrock concepts based on the shear wave velocity value. One of them is seismic bedrock and the other is engineering bedrock. It is accepted that the seismic one has a considerable lateral extent and is of relatively more homogeneous and of uniform composition when compared with the overlying layers. The lower bound of the shear wave velocity value of seismic bedrock is taken as 3500 m/s according to Andrus, et al. (2006) and Chapman et al. (2006). There are different descriptions for the engineering bedrock in terms of the shear wave velocity value. The lower bound of the shear wave velocity value ranges from 500 m/s to 760 m/s (e.g., Ptilakis, 2004; Boore, 2006; Havenith et. al, 2007; Sitharam and Anbazhagan, 2008) for the engineering bedrock utilized in the geotechnical foundation designs and characterization studies.

In some places of the region, the depth of bedrock was estimated to be more than 200 m in this study. However, the geophysical studies conducted in this study were not capable of characterizing the layers up to this depth. Therefore, an extrapolation methodology had to be performed in order to assign V_s data to the deeper layers and then to the characterization depth. In order not to increase the uncertainty in the extrapolation stage due to the high lateral geological heterogeneities as explained in Chapter 2, the 1750 m/s was accepted as a cut-off value and assigned to the bedrock.

The purpose of this study is to determine suitable rock-earthquake records for the study area, scaling these records in time domain, local soil characterization and determination of non-linear soil properties with the most accurate manner, and to perform 1D and 2D soil response analyses and compare the acquired findings. Based on the results, a simplified scaling for the results of the 1D analysis was proposed based on amplifications due to 2D non-linear effects (topographic, basin edge, basin). The analyses were performed by considering the active tectonic structure of the region based on the relatively high ($M > 7$) magnitude earthquake potential evaluated by a deterministic seismic hazard assessment approach. The selection of the required acceleration records were performed based on different

groups to be acquired from rock records of different earthquakes in the Pacific Earthquake Engineering Research (PEER) Center NGA West-2 ground motion database. Therefore, the performances of the equivalent linear 1D and 2D analyses at the same sites were compared.

4.3.2. The methodology utilized in this study

QUAD4M operates in a time domain and uses the finite element method to solve a dynamic equilibrium equation by using unconditionally stable direct time integration of Newmark. It uses a direct integration scheme in time domain and is based on quadrilateral elements. QUAD4M has a transmitting base to model half-space under the mesh and removal of a rigid base assumption. This base property allows escape of part of the energy to the basement rock. By utilization of this base, a ground motion record is allowed to be a function of material properties of half-space present below the model network. S- and P- wave velocities and unit weights of the material under the mesh can be used as an input to the software and response of the mesh above this half-space can be modeled with high accuracy. In cases where deconvolution process is utilized, use of such a boundary condition at the base of the model is a suitable approach (Hudson et al., 1994, Rathje and Bray, 2001). Also, seismic coefficients useful for performing deformation analysis are also predefined in the software. The seismic coefficient is the ratio of the force of an earthquake on a mesh block to the weight of this block and is calculated for each time step.

Furthermore, soil materials are modeled as uniform linear visco-elastic material (Hudson et al., 1994). As in the Shake2000 software, shear modulus and damping ratio is changed in each layer (Ordonez, 2000). Analyses are re-run until effective shear strains developed at each layer is coherent with the pre-determined constant shear modulus and damping ratios of each layer. Shake2000 calculates dynamic response of a layered system by using closed-form solution of 1D wave equation in a frequency domain and models the damping independent from the frequency

(Ordonez, 2000). QUAD4M, on the other hand, employs Rayleigh damping which formulates viscous damping matrix as a linear combination of mass and stiffness matrices (Hudson et al., 1994).

In order to perform QUAD4M analysis in this study, a graphical interface, Visual-Q^{4M} developed by Magnifesta (2015) was utilized to construct complex geometries regarding lateral and vertical variations of lithologies, bedrock surface and topography in a more precise way. It has the capability of generating complex grids for FEM analysis. Also, the Visual-Q^{4M} provides graphical user interfaces for post-processing of the results of QUAD4M analysis. Also, in the running stage of an analysis, it gives the value of the strain check after each iteration. Therefore, it prevents misleading results to be acquired by the interpretation of an incomplete analysis.

In order to perform 1D and 2D soil response analyses, 2 cross sections adequately representing the basin characteristics were prepared (Figure 54). As can be seen in the figure, one of them is in north-south direction (A-A') the other is almost in the east-west direction (B-B'). There are five sites having shear wave velocity measurements along the A-A' section. The order of these sites from north to south is Comb05(2), Comb06(2), Comb07(2), Comb04(2) and Comb08(2). It should be noted that the numbers in the parentheses show the phase stage (September 2009 or June 2014) implemented in this study during the geophysical characterization of the sites. A total of five measurements were taken during the second phase at this section. On the other hand, seven shear wave velocity sites are present along the B-B' section. Five of these sites were characterized at the second phase and the remaining two sites were measured during the first phase. The sequence of these measurements from west to east is Comb14(1), Comb09(2), Comb06(1), Comb04(2), Comb01(2), Comb03(2) and Comb12(2). As it can be observed from the figures, one of the measurements [Comb04(2)] is the common site for both sections. A 1D seismic site response analyses were performed at these 11 sites and 2D response analyses were carried out by using these two sections.

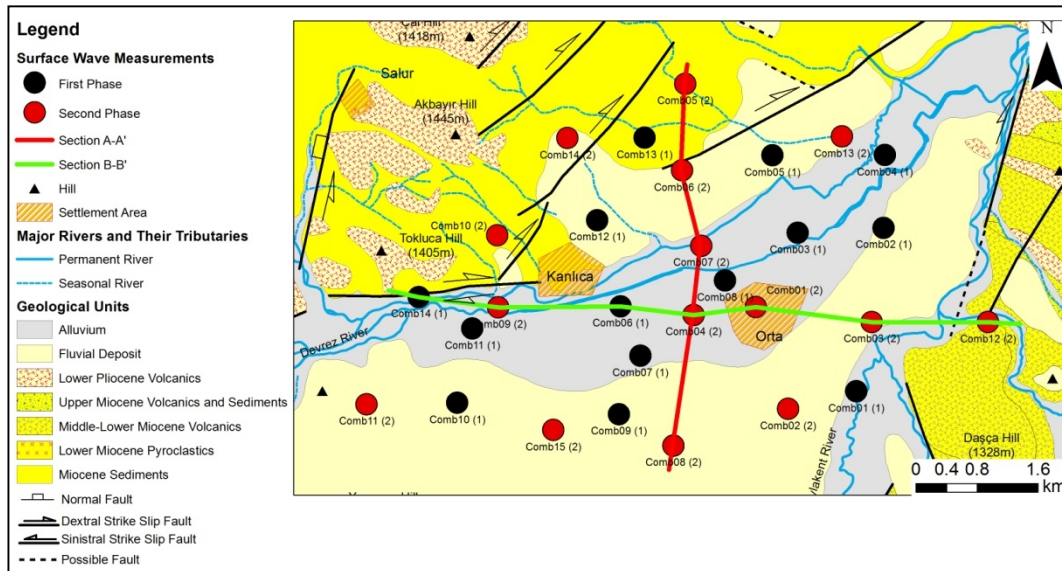


Figure 54. The cross sections and the measurement sites for 1D and 2D site response analysis performed in this study. This figure is intentionally re-given for the readers' convenience.

In order to simulate dynamic soil response behavior by using either the 1D or 2D analyzing techniques stated above, four main tasks should be figured out as given below;

- Construction of a target spectrum for the site,
- selection of and scaling input rock motions,
- characterization of a shear wave velocity profile,
- determination of the non-linear soil characteristics.

Please see the subsequent subsections in this chapter for further information about the methodology regarding each item given above.

4.3.2.1. Construction of the target spectrum

Seismic hazard and risk analyses performed for the design of earthquake resistant structures are based on the principle of quantitative calculation of ground motion hazard at a certain site. For this purpose, there are two types of approaches in the

determination of design ground motion in practice for approximately 40 years, these are: deterministic (Krinitzsky and Chang, 1975) and probabilistic (Cornell, 1968) approaches. In the deterministic approach, individual earthquake scenarios (earthquake magnitude and location) are developed for each seismic source (Wells and Coppersmith, 1994). In the context of this study, rather than the probabilistic approach, the deterministic one is utilized. For this purpose, a characteristic ground motion probability level was selected. In general, this value is generally obtained from the median value (i.e. 50% probability of exceedance) or median plus one standard deviation (i.e. 84% probability of non-exceedance). In this study, a deterministic seismic hazard analysis was performed only for earthquake sources having a destructive potential for the area via utilizing four main steps as stated by Reiter (1990):

The first step is to identify and characterize each earthquake sources that are capable of generating potential destructive earthquakes for the study area. In this step the geometry of each fault was figured out and relocated (please see Section 2.4. of this dissertation for detailed information). The total rupture length of each fault zone having significant potential seismic source for the Orta District was determined based on different studies (Blumental, 1945; Ambraseys, 1970; Barka and Kadinsky-Cade, 1988; Koçyiğit et al., 2001) in the literature and the segmentation of these faults was determined based on the study proposed by Barka and Kadinsky-Cade (1988) and Koçyiğit et al. (2001). Also, a width value was assigned to each fault zone as stated by Cambazoğlu (2012) and Aktuğ et al., 2015.

In the second step, although different distance definitions can be used depending on the standards of the attenuation relations (i.e., Joyner-Boore distance, rupture distance, etc.), the shortest distance between the fault zone and the study area was designated (Figure 55).

When the seismic records of the instrumental period (after 1900) are analyzed for the delineated area in Figure 55, it is observed that the most destructive

earthquakes took place mostly along the Dodurga, Ulusu, Çerkeş-Kurşunlu and Tosya fault zones located in the İsmetpaşa-Kargı section of the North Anatolian Fault System (NAFS). Figure 55 shows the surface ruptures of the major earthquakes such as the Gerede, Kurşunlu, Ilgaz and Orta Earthquakes and the distance between these surface ruptures and the Orta District. The distribution of the earthquake ($M_W > 5.5$) epicenters with their focal mechanisms are also presented in the figure. Moreover, a summary of the surface ruptures of four major earthquakes located at close vicinity of the study area is given in Table 4.

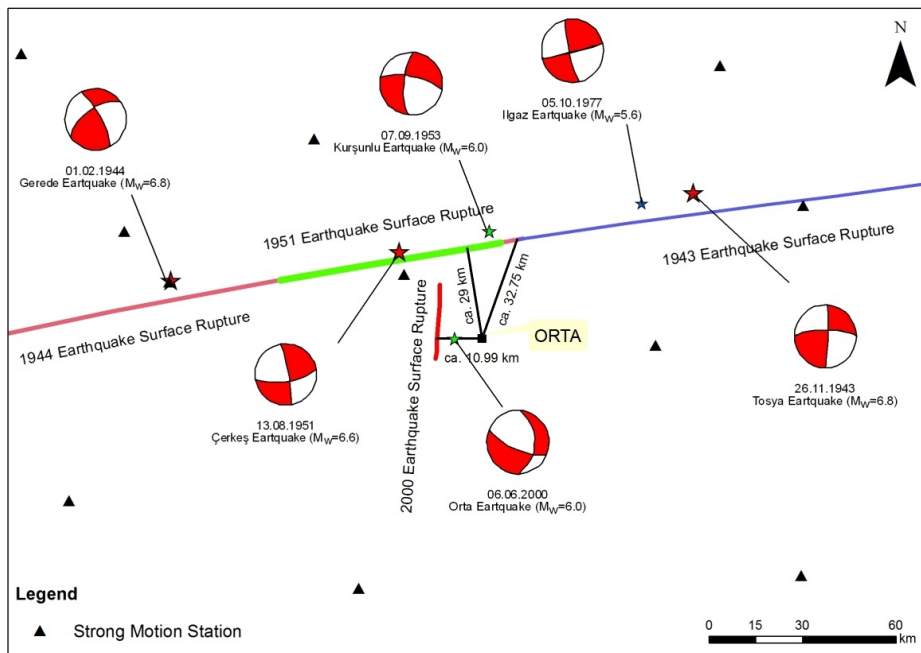


Figure 55. The surface ruptures of the four major earthquakes (Gerede, Kurşunlu, Ilgaz and Orta Earthquakes) and the distance between these surface ruptures and the Orta District along with the distributions of the strong motion stations and major earthquake epicenters ($M_W > 5.5$).

Table 4. The summary of the surface ruptures of four major earthquakes located in the close vicinity of the study area. The closest segments of the fault zones to the study area are indicated by bold format (SRL: Surface rupture length, FS: fault segment, FSL: Fault segment length, Mech: Mechanism, FW: Fault width).

Fault rupture name	SRL (km)	Location of surface ruptures	FS no	FSL (km)	Mech.	FW (km)
1943 Earthquake Fault rupture	265 ^{a,b} - 320 ^c	From ESE of Taşova District at east to NNE of Kurşunlu District at west	Fs 18	45	SS	18 ^{e,f}
			Fs 19	80	SS	
			Fs 20	80	SS	
			Fs 21	50	SS	
			Fs 22	65	SS	
1944 Earthquake Fault rupture	150 ^c - 190 ^{a,b}	From NE of Çerkeş District at east to WSW of Bolu Province at west	Fs 24	40	SS	18 ^{e,f}
			Fs 25	10	SS	
			Fs 26	100	SS	
1951 Earthquake Fault rupture	40 ^{a,b} - 50 ^c	From NE of Kurşunlu District at east to NW of Kurşunlu District at west	Fs 23	50	SS	18 ^{e,f}
2000 Earthquake Fault Rapture	36 ^d	From Saçak village at north to Körselik village at south	Os-1	36	N*	10 ^g

* This fault zone is a normal fault with a considerable amount of left lateral strike slip component (Emre et al., 2000). a) Blumental, 1945; b) Ambraseys, 1970; c) Barka and Kadinsky-Cade, 1988; d) Koçyiğit et al., 2001; e) Aktuğ et al., 2015; f) Cambazoğlu, 2012; g) Taymaz et al., 2007.

In the third step, the characteristic earthquake(s) affecting the region was designated by comparing the ground shaking levels formed by the seismic source identified in the first step at the distance determined in the second step. A characteristic earthquake was defined by its magnitude and its distance to the study area. The closest segments of the fault zones to the study area was selected as the ones with the most destructive potential for the study area. Then, the moment magnitude was calculated based on the equations proposed by Wells and Coppersmith (1994) regarding the segmentation of a portion of the NAFS along the 1943, 1994, 1951 and 2000 fault ruptures according to Barka and Kadinsky-Cade (1988) and Koçyiğit et al. (2001), and widths of the faults stated by Taymaz et al. (2007) and Aktuğ et al. (2015). The equations, proposed by Wells and Coppersmith (1994) in order to estimate the moment magnitude depending on the

surface rupture length and rupture area for normal and strike slip faults are given by Equations 3 to 6.

$$M_W = 4.86 + 1.32 * \log(\text{SRL}) \text{ for normal faults} \quad (\text{Eq. 3})$$

$$M_W = 5.16 + 1.12 * \log(\text{SRL}) \text{ for strike slip faults} \quad (\text{Eq. 4})$$

$$M_W = 3.93 + 1.02 * \log(\text{RA}) \text{ for normal faults} \quad (\text{Eq. 5})$$

$$M_W = 3.98 + 1.02 * \log(\text{RA}) \text{ for strike slip faults} \quad (\text{Eq. 6})$$

where, SRL is surface rupture length in km, RA is the rupture area in km² and M_w is moment magnitude. The rupture area is calculated by multiplication of the surface rupture length by the rupture width.

In order to calculate the characteristic moment magnitudes, the SRL and the RA given in Table 4 were calculated regarding the different fault mechanism by using the relationship proposed by Wells and Coppersmith (1994). It is also possible to utilize the standard deviation value representing the aleatoric variability of the earthquake phenomenon in this empirical relationship. This important uncertainty should be considered in seismic hazard assessments (Kramer, 1996). Therefore, the results are given in Table 4 for both mean and mean plus one standard deviation moment magnitudes. It should be noted that calculation of characteristic magnitudes is made for the closest segments of the fault zones to the study area as indicated in bold face either in Table 4 or Table 5, since these segments give the highest peak ground acceleration values (PGA) for each fault zone by utilizing the ground motion prediction equations. The mean plus one standard deviation results of the calculated characteristic magnitude of the region was preferred to be used based on the rupture area in the further analyses of this study. In this respect, the characteristic moment magnitude of a possible earthquake for the region was selected as 7.2 (Table 5).

Table 5. The calculated moment magnitudes (mean and mean + standard deviation) according to the different fault mechanisms by using the relationship proposed by Wells and Coppersmith (1994).

Fault Segment No*	Calculated Mw (mean) by SRL	Calculated Mw (mean +1σ) by SRL	Calculated Mw (mean) by RA	Calculated Mw (mean+1σ) by RA
Fs 18				
Fs 19				
Fs 20	7.19	7.47	7.13	7.34
Fs 21				
Fs 22				
Fs 24				
Fs 25	6.95	7.23	6.92	7.12
Fs 26				
Fs 23	7.06	7.34	7.02	7.22
Os-1	6.91	7.25	6.53	6.78

* Please see Table 4 for the detailed information on fault segments.

The final step is the identification of seismic hazard based on ground motion to be generated at the study area by characteristic earthquakes affecting the region. The peak ground acceleration and response spectra ordinates were the parameters used during characterization of seismic hazard in this study. A target spectrum was constructed for the sites in order to select a suit of input motions for 1D and 2D soil response analyses. Then the selected motions within the suits were scaled and the suit containing seven input rock motions that best fit the target response spectrum was identified.

The selection of the ground motion prediction equation (GMPE) to be used in a seismic hazard analysis is an important research subject. An important issue to be considered is the selection of the most appropriate GMPE to be used at the area of interest in order to specify a proper spectrum. If a GMPE encompassing the study area has not been developed specifically, then GMPEs developed for areas having similar seismotectonic properties as the study area should be used (Kayabalı, 1995). Utilization of different attenuation relationships (GMPEs) proposed by different researchers is important to model epistemic uncertainties in the PGA and

spectrum. In order to reduce this uncertainty, a logic-tree approach with varying weight factors was utilized in this study as suggested by Çetin et al. (2004) and Yücemem (2008).

Initially, the target spectrum satisfactorily representing the study area was tried to be formed based on assessment of the results of both the next generation ground motion prediction equations [NGAs, Abrahamson et al., 2014 (ASK 2014); Boore et al., 2014 (BSSA 2014); Campbell and Bozorgnia, 2014 (CB 2014); Chiou and Youngs, 2014 (CY 2014)] and also previous attenuation relationship studies (Abrahamson and Silva, 1997; Sadigh et al., 1997, Margaris et al., 2002; Kalkan and Gülkan, 2005) through the logic-tree approach. In order to select the appropriate attenuation relationship and assign reasonable weights to each relations, the Orta Earthquake records at six different strong ground motion stations were utilized and the PGA of this earthquake at these stations was tried to be estimated by the prediction equations (Table 6). It was observed that next generation ground motion prediction equations gave close results to the actual case and the others led to overestimated PGA values at the stations.

Table 6. PGA values of the 2000 Orta Earthquake records at six different strong motion stations and distance between the study area and these stations along with their V_{S30} values.

Strong Motion Stations	Orta Earthquake (Mw=6.0) records		Distance to DFZ (km)	V_{S30} (m/s)
	Recorded PGA (g)	Max. Horizontal Direction		
Çankırı (Çerkeş, Meteorological Station)	0.064	E-W	12.3	347.9
Karabük (City Center, Karabük High School)	0.007	E-W	55.7	702.6
Kastamonu (Tosya, Directorate of Meteorological Station)	0.012	E-W	88	361.8
Bolu (City Center, Directorate of Environment and Urbanization)	0.007	E-W	117	293.6
Düzce (City Center, Directorate of Meteorological Station)	0.004	E-W	156.6	282.0
Kutahya (City Center, Directorate of Civil Defense)	0.005	N-S	276.6	242.5

After investigating suitable attenuation relationships for the study area by comparing the PGA values of the Orta Earthquake records at the stations and estimation of the relationship (Table 6), four different Next Generation Attenuation (NGA) Ground Motion Prediction Equations (GMPEs) were selected to be utilized during deterministic seismic hazard assessment, namely: ASK 2014, BSSA 2014, CB 2014 and CY 2014. A summary of these GMPEs is given in Table 7 to show their applicability and limitations in terms of range of magnitude, distance and VS30 values. Further details on these GMPEs can be found in Abrahamson et al. (2014), Boore et al. (2014), Campbell and Bozorgnia (2014), Chiou and Youngs (2014) and Douglas (2015).

Table 7. A summary of the applicability of the GMPEs utilized in this study.

GMPEs	Applicable to Turkey	M_{min}	M_{max}	M_{scale}	r_{min} (km)	r_{max} (km)	r_{scale}	V_{S30} range(m/s)	Standard Deviation
Abrahamson et al., 2014	YES	3.0	8.5	M_w	0.0	300	r_{rup}	180-1000	Function of M_w, r, V_{S30}
Boore et al., 2014	YES (anelastic attenuation)	3.0	8.5*	M_w	0.0	400	r_{jb}	150-1500	
Campbell and Bozorgnia, 2014	YES	3.3	8.5**	M_w	0.0	300	r_{rup}	150-1500	
Chiou and Youngs, 2014	YES	3.5	8.5***	M_w	0.0	300	r_{rup}	180-1500	

*The maximum moment magnitude decreases to 7.0 for normal faults.

** The maximum moment magnitude is limited to 8.0 and 7.5 for reverse and normal faults, respectively.

*** The maximum moment magnitude is set at 8.0 for either reverse or normal faults, respectively.

A comparison of PGA values of the Orta Earthquake records at the stations in regards to estimation of the selected four different GMPEs (Figure 56), led to an estimation that the median values of all GMPEs overestimate the PGA values for the distance lower than 15 km. Additionally, when the rupture distance increases, the estimation performance of the utilized GMPEs increases. Examination of

Figure 56 reveals that the prediction performance of ASK 2014 and CY 2014 equations are better than the others especially at shorter distances. Therefore, higher weights were assigned to these GMPEs (Table 8).

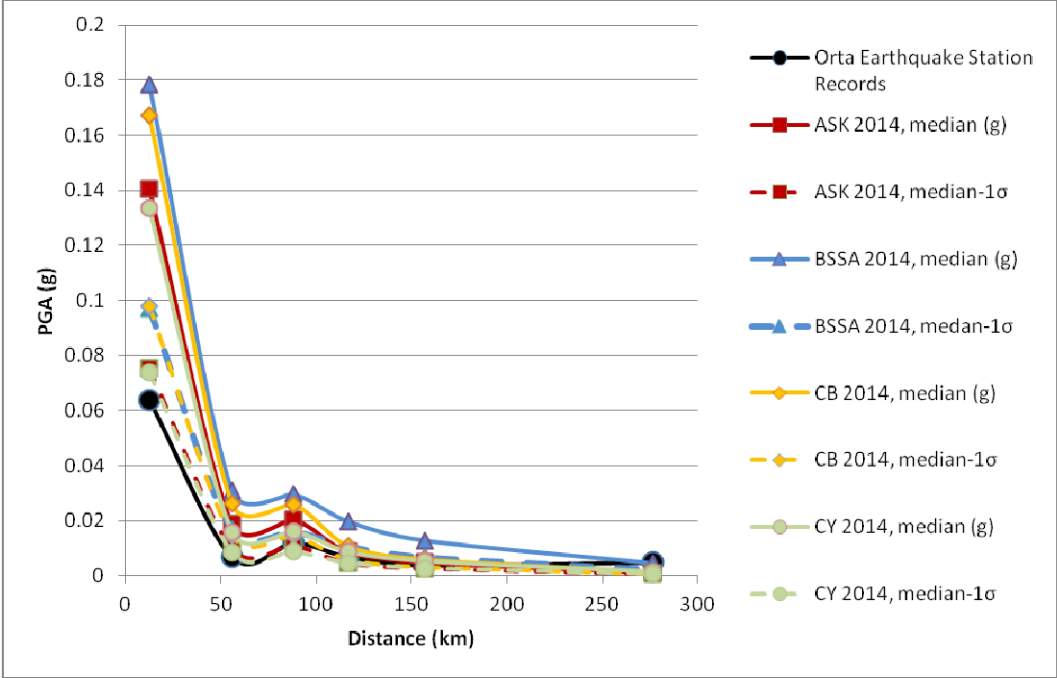


Figure 56. Comparison of PGA values of the Orta Earthquake records at six strong motion stations with the estimation of four GMPEs.

Table 8. Assignment of weights regarding the results of the GMPEs. The weight sum up to 1.

Next Generation of Ground Motion Prediction Equations	Weight
ASK 2014	0.4
BSSA 2014	0.1
CB 2014	0.1
CY 2014	0.4

Target response spectra for the region was obtained by the deterministic method via utilizing the selected ground motion prediction equations (ASK 2014, BSSA 2014, CB 2014 and CY 2014) based on the mechanism of the faults and the

regional tectonic conditions with a logic-tree approach (Table 8). The constructed target spectra is given in Figure 57. In deterministic seismic hazard analysis, integration of uncertainties is possible by considering the standard deviation value of attenuation relationships and should be taken into account (Kramer, 1996). In addition to this, ASCE 7 (2010) suggested that the target response spectrum should be determined by multiplying the response spectrum by 1.5. In Figure 57, the ratio of the spectrum obtained by adding one standard deviation to the median of the spectrum is at least 1.8. Therefore, in order to follow a conservative approach, the former spectrum was utilized in this study. During the specification of the target spectrum given in Figure 57, the distance was taken as 29.8 km based on the average proximity of the sites to the fault segments and the calculations were made by using weighted GMPEs for the possible earthquake ($M_w = 7.2$) along the NAFS and V_{S30} value was taken as 760 m/s to represent the rock site.

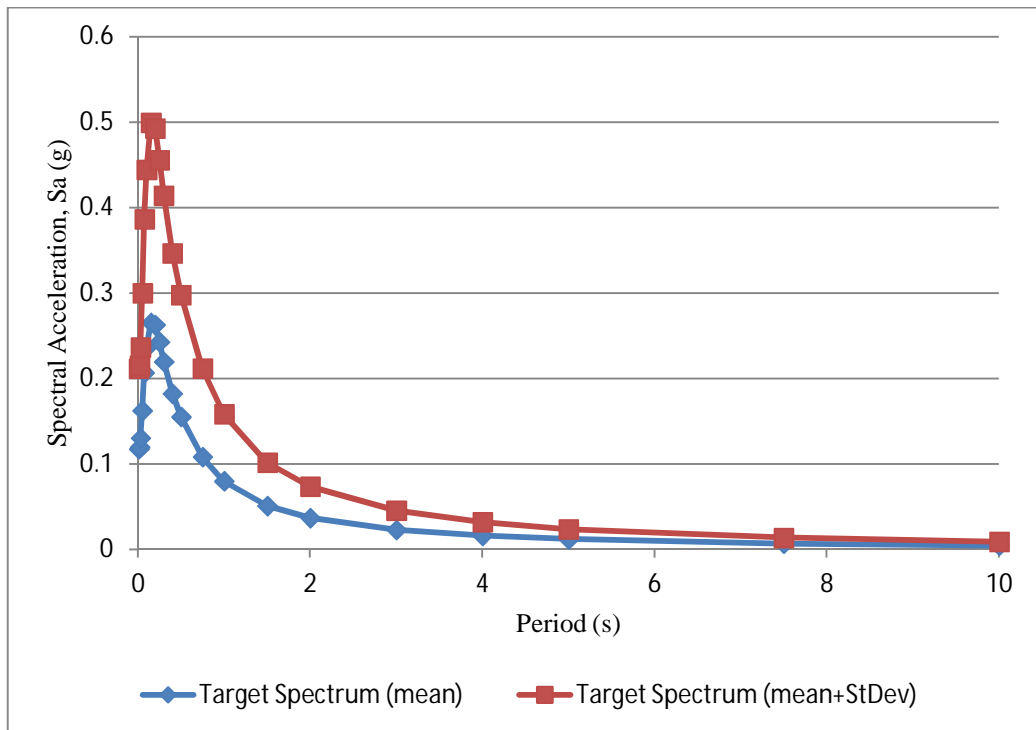


Figure 57. Constructed target spectrum by using a logic-tree approach.

4.3.2.2. Selecting and scaling of the input motions

Earthquake damage pattern is significantly influenced by the non-linear behavior of soil, the ground motion characteristics (intensity, duration and frequency content of ground motion), topography, subsurface geometry, local soil condition when the superstructural information is disregarded. Generating a statistically stable ground motion estimation based on the constructed target rock spectrum is the main purpose of a site response analysis. In other words, the computed response spectra is not highly influenced by the choices of input rock motions (Rathje et al., 2010). As soil behaves non-linearly, the computed seismic site response can be affected by the input rock motion characteristics. This can be handled only by using an adequate number of input rock motions acquired by earthquake records or by creating synthetic records (Bommer and Acevedo 2004; ASCE 7, 2010).

In order to make a proper selection from Pacific Earthquake Engineering Research (PEER) Center NGA West-2 ground motion database and to form proper suits in this study, a set of criteria was followed:

- Suits were formed by searching NGA West-2 database (no aftershocks, etc.),
- Only one record from any single event was selected to form suits,
- Moment magnitude of the earthquake record of interest was limited between 6.5 to 8.0,
- The earthquakes that occurred at a distance ranging from 10 km to 45 km were taken into consideration,
- The minimum and maximum shear wave velocity was selected as 600 m/s and 1500 m/s, respectively,
- An additional criterion used to search appropriate earthquake records was the events maximum horizontal acceleration (MHA) values to be greater than 0.05g.

By using these criteria given above, 15 earthquake records were selected. The summary of these earthquakes are listed in Table 9. To increase the size of the population, these records were scaled according to the PGA value of the target spectrum. A total of 30 earthquakes were scaled and suits were formed from seven of them based on the criterion given above. The maximum horizontal components of each record was used during the scaling process.

Table 9. Summary of the selected ground motion records.

Number of event	Name of the event	Year	Mag.	Mec.	Station Name	R_{rup} (km)	V_{S30} (m/s)	PGA (g)
1	Landers	1992	7.28	Strike Slip	Twentynine Palms	41.4	635.01	0.080
2	Düzce, Turkey	1999	7.14	Strike Slip	Lamont 1060	25.9	782.00	0.053
3	Sitha, Alaska	1972	7.68	Strike Slip	Sitka Observatory	34.61	649.67	0.096
4	Manjil, Iran	1990	7.37	Strike Slip	Abbar	12.55	723.95	0.515
5	Hector Mine	1999	7.13	Strike Slip	Hector	11.66	726.00	0.328
6	Hector Mine	1999	7.13	Strike Slip	Twentynine Palms	42.06	635.01	0.067
7	Tottori, Japan	2000	6.61	Strike Slip	OKYH07	15.23	940.20	0.185
8	Tottori, Japan	2000	6.61	Strike Slip	OKYH08	24.84	694.21	0.241
9	Tottori, Japan	2000	6.61	Strike Slip	OKYH14	26.51	709.86	0.453
10	Tottori, Japan	2000	6.61	Strike Slip	SMNH10	15.59	967.27	0.231
11	Tottori, Japan	2000	6.61	Strike Slip	SMNH11	40.08	670.73	0.059
12	Darfield, New Zealand	2010	7	Strike Slip	CSHS	43.6	638.39	0.116
13	Darfield, New Zealand	2010	7	Strike Slip	LPCC	25.67	649.67	0.357
14	Big Bear-01	1992	6.46	Strike Slip	Slient Valley	35.41	659.09	0.069
15	Kocaeli, Turkey	1999	7.51	Strike Slip	Gebze	10.92	792.00	0.261

As stated above, one of the challenges in the soil response analysis is to scale ground motion properly according to actual tectonic conditions of a site. In spite of the fact that there are no well established procedures in the selecting and scaling of ground motions, many ground motion selection and modification procedures have

been developed to select ground motions for a wide variety of objectives (e.g., Bommer and Acevedo 2004; Kottke and Rathje, 2009; IBC, 2010; ASCE 7, 2010). According to the standards proposed by ASCE 7 (2010), at least five earthquake records should be utilized by considering the active tectonic setting of a site. The study proposed by Rathje et al. (2010) indicates that the average response spectra acquired from 5 different ground motion records has a stable median value when the utilized earthquake records have a good fit to the target spectrum.

In this study, several suits containing seven earthquake records were selected and scaled in the time domain. Selection and linear scaling of ground acceleration records were performed by the SeismoMatch software V. 2.1.2. Rather than using a frequency domain spectral matching (e.g., Gasparini and Vanmarcke, 1976; Silva and Lee, 1987) and linear scaling of ground motions (Kottke and Rathje, 2009) methods, this program utilizes the wavelets algorithm which was proposed by Abrahamson (1992) and Hancock et al (2006), and it is based on the time-domain technique proposed by Lilanand and Tseng (1988). The selection of the suit which fits to target spectrum best was performed by the degree of maximum and average misfits. The mean matched spectrum has an average misfit of 1.7% and maximum misfit of 12.6%. Figure 58 shows the suit matching the target spectrum the best. The details of seven earthquake records in the suit are listed in Table 10. Also, Figures 59 and 60 show the original and matched accelerograms of seven records forming the best fit suit along with the target spectrum.

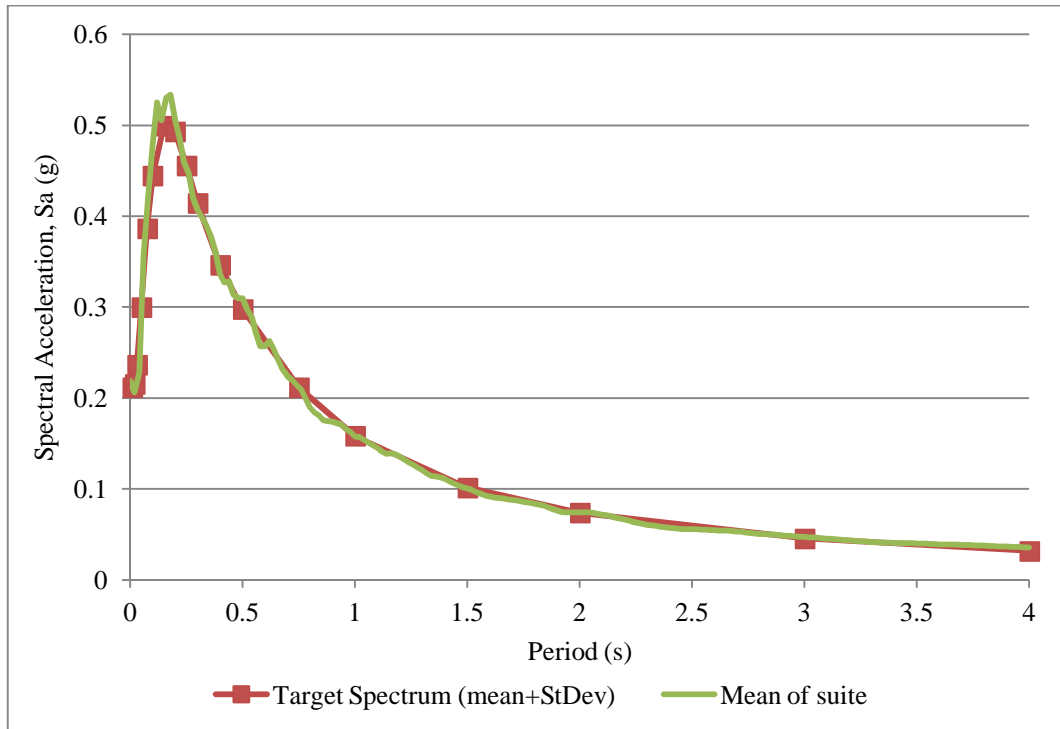


Figure 58. The mean match spectrum formed by averaging seven earthquake records and the target spectrum.

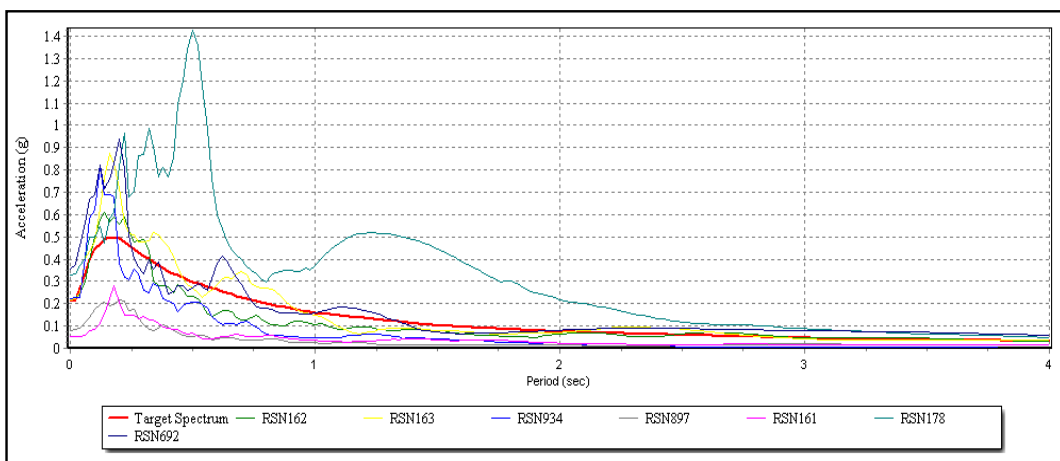


Figure 59. Original accelerograms of the seven earthquakes and the target spectrum. Please see Table 7 for the abbreviations of the records.

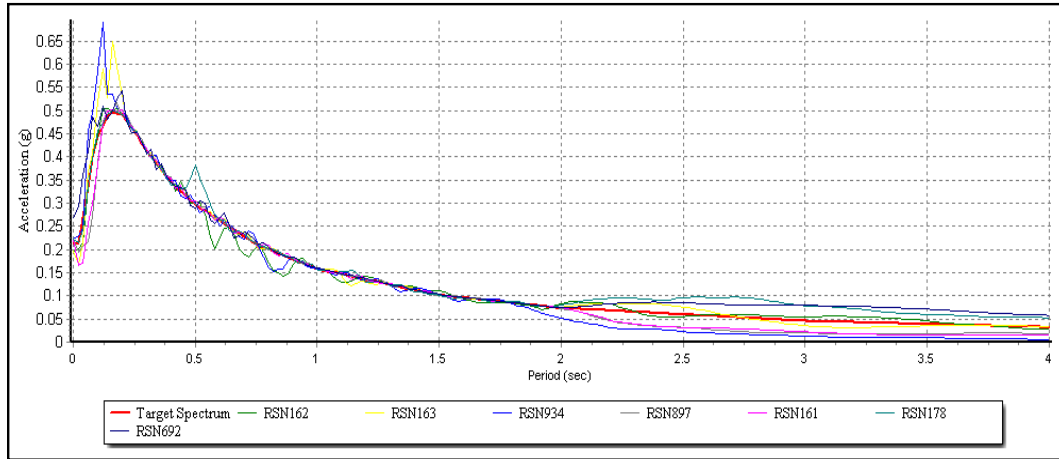


Figure 60. Matched accelerograms of the seven earthquakes according to the target spectrum. Please see Table 7 for the abbreviation of the records.

Table 10. Summary of the seven earthquake records utilized to form the suit matching the target spectrum the best.

Number of event	Name of the event	Abbreviation	R_{rup} (km)	PGA (g)	Scale Factor
1	Landers, USA	RSN897	41.4	0.080	1.0
2	Düzce, Turkey	RSN161	25.9	0.053	1.0
3	Sitha, Alaska	RSN162	34.61	0.096	2.2
4	Manjil, Iran	RSN163	12.55	0.515	0.4
5	Hector Mine, USA	RSN178	11.66	0.328	1.0
6	Darfield, New Zealand	RSN692	25.67	0.357	1.0
7	Big Bear, USA	RSN934	10.92	0.261	0.8

4.3.2.3. Construction of 1D and 2D soil profile geometries

In order to perform 1D and 2D soil response analyses, 2 cross sections adequately representing the basin characteristics were prepared (Figure 54). As can be seen in the figure, one of them is in the north-south direction (A-A') the other is almost in the east-west direction (B-B'). There are five sites having shear wave velocity measurements along the A-A' section. The order of these sites from the north to the south is Comb05(2), Comb06(2), Comb07(2), Comb04(2) and Comb08(2). However, seven shear wave velocity sites are present along the B-B' section. 1D

seismic site response analyses were performed at these 11 sites and 2D response analyses were carried out by using these two sections.

High resolution shear wave velocity curves over the entire tested depth range were successfully constructed by combining active and passive source dispersion curves of all sites. Integration of the passive surface method aids in understanding the subsurface structure down to a depth of 85 m. As stated in the previous chapter, the blind way technique was utilized in order to obtain the shear wave velocity (V_S) profile. After examining the results of these analyses, it was observed that 3 main layers are present in almost all profiles except one. Therefore, an idealization procedure was performed to construct 1D shear wave velocity profiles at 11 sites. The layer having shear wave velocity values greater than approximately 800 m/s in the idealization process is assumed as the bedrock and thus 1750 m/s V_S value is assigned as the shear wave velocity bedrock half-space. Then, all 1D profiles were extrapolated up to this value by considering the adjacent measurement sites, geology and vertical variation of the V_S throughout the profile.

Mainly 6 layers including bedrock was identified at almost each profile except Comb12(2) in 1D profiles (Tables 11-18). As can be seen in the previous chapter, 2D V_S sections were created by using 1D profiles along the A-A' and B-B' sections. Based on the geotechnical and geophysical data, the lateral and vertical variations of the layers were modeled and classified (Tables 11-18). According to the classification, the mean values of the geotechnical and geophysical properties of the layers such as unit weight, thickness, effective vertical stress, effective mean stress, shear wave velocity, plasticity index, etc. were calculated along with their mean and standard deviations (Tables 11-18). These average values were assigned to each layer in 2D sections (Table 11-18). The same properties of the layers in 1D profiles were assigned to the layers that do not have lateral continuation in 2D sections [e.g., the first layers of Comb01(2), Comb03(2), the second layer of Comb14(1) and so on].

Table 11. The lateral and vertical variations of layer thickness at the sites located along the A-A' section. "C" is the abbreviation of Comb.

Thickness of the layers (m)							
Layer No	Site No					Section N-S (A-A')	
	C-04 (2) ^a	C-05 (2) ^a	C-06 (2) ^a	C-07 (2)	C-08 (2)	Mean	St. dev
Layer 1	6.7	7.5	8.3	7.5	8.7	7.9	0.6
Layer 2	13.3	15.0	35.7	35.0	26.3	25.1	10.6
Layer 3	80.0	22.5	36.0	45.5	27.5	42.3	22.8
Layer 4	50.0	20.0	40.0	17.0	37.5	32.9	14.0
Layer 5	55.0	55.0	40.0	35.0	60.0	49.0	10.8
Layer 6	-	-	-	-	-	-	-

^aThe first layer of these sites has a lateral continuation

Table 12. The lateral and vertical variations of layer thickness at the sites located along the B-B' section. "C" is the abbreviation of Comb.

Thickness of the layers (m)									
Layer No	Site No							Section E-W (B-B')	
	C-01(2)	C-03 (2)	C-06 (1) ^a	C-09(2) ^a	C-12(2) ^b	C-14(1) ^{a,c}	C-04 (2) ^a	Mean	St. dev
Layer 1	9.2	6.5	6.7	8.3	7.5	9.2	6.7	7.7	1.2
Layer 2	18.3	6.0	33.3	33.7	34.5	18.3	13.3	23.2	12.3
Layer 3	42.5	25.0	40.0	38.0	none	22.5	80.0	41.3	20.6
Layer 4	70.0	52.5	20.0	40.0	18.0	20.0	50.0	38.6	20.1
Layer 5	70.0	100.0	40.0	40.0	20.0	40.0	55.0	52.1	26.1
Layer 6	-	-	-	-	-	-	-	-	-

^a The first layer of these sites has a lateral continuation. ^bThe third layer was not observed at this site. ^c

The second layer of this site is different than the second layer of the others.

Table 13. Variations of unit weights of the layers along the A-A' section. "C" is the abbreviation of Comb.

Unit Weight (kN/m ³)							
Layer No	Site No					Section N-S (A-A')	
	C-04 (2) ^a	C-05 (2) ^a	C-06 (2) ^a	C-07 (2)	C-08 (2)	Mean	St. dev
Layer 1	19.4	18.4	16.8	18.1	17.9	17.6	1.1
Layer 2	18.5	18.3	18.5	18.5	18.4	18.4	0.1
Layer 3	18.5	18.4	18.7	18.8	18.6	18.6	0.2
Layer 4	19.0	18.5	19.0	19.0	19.0	18.9	0.2
Layer 5	23.5	23.5	23.5	23.5	23.5	23.5	0.0
Layer 6	26.0	26.0	26.0	26.0	26.0	26.0	0.0

*The first layer of these sites has a lateral continuation

Table 14. Variations of unit weights of the layers along the B-B' section. "C" is the abbreviation of Comb. "BH" is the closest borehole at the V_S measurement sites.

Layer No	Unit Weight (kN/m ³)							Section E-W (B-B')	
	Site No							Mean	St. dev
	C-01(2) BH-07	C-03 (2) BH-04	C-06 (1) ^a BH-13	C-09(2) ^a BH-19	C-12(2) ^b	C-14(1) ^{a,c} BH-20	C-04 (2) ^a BH-14		
Layer 1	17.6	18.0	18.3	18.5	18.4	18.2	19.4	18.6	0.6
Layer 2	18.7	18.4	18.3	18.4	18.3	18.2	18.5	18.4	0.2
Layer 3	18.5	18.6	18.5	18.4	none	18.3	18.5	18.5	0.1
Layer 4	19.0	19.0	19.0	18.9	18.9	18.8	19.0	18.9	0.1
Layer 5	23.5	23.5	23.5	23.5	23.5	23.5	23.5	23.5	0.0
Layer 6	26.0	26.0	26.0	26.0	26.0	26.0	26.0	26.0	0.0

^a The first layer of these sites has a lateral continuation. ^b The third layer was not observed at this site.

^c The second layer of this site is different than the second layer of the others.

Table 15. Shear wave velocity variation of the layers in lateral and vertical directions along the A-A' section. "C" is the abbreviation of Comb and "BH" is the closest borehole at the V_S measurement sites.

Layer No	V_S values of the Layers (m/s)					Section N-S (A-A')	
	Site No					Mean	St. dev
	C-04 (2) ^a BH-14	C-05 (2) ^a	C-06 (2) ^a BH-11	C-07 (2) BH-10	C-08 (2)		
Layer 1	167.2	146.8	176.7	174.9	190.0	161.7	21.2
Layer 2	274.2	309.5	276.1	282.3	273.7	283.2	15.1
Layer 3	347.0	414.0	346.9	411.2	449.0	393.6	45.2
Layer 4	506.0	524.6	510.0	510.0	532.2	516.6	11.2
Layer 5	790.0	755.9	805.0	740.0	793.3	776.8	27.5
Layer 6	1750.0	1750.0	1750.0	1750.0	1750.0	1750.0	0.0

^aThe first layer of these sites has a lateral continuation

Table 16. Shear wave velocity variation of the layers in the lateral and vertical directions along the B-B' section. "C" is the abbreviation of Comb.

Layer No	V_S values of the Layers (m/s)							Section E-W (B-B')	
	Site No							Mean	St. dev
	C-01(2)	C-03 (2)	C-06 (1) ^a	C-09(2) ^a	C-12(2) ^b	C-14(1) ^{a,c}	C-04 (2) ^a		
Layer 1	136.9	183.0	171.8	175.1	143.1	178.7	167.2	173.2	4.9
Layer 2	284.9	243.6	246.3	254.6	247.2	367.1	274.2	258.5	17.1
Layer 3	387.1	389.1	385.0	413.1	none	428.6	347.0	391.7	27.9
Layer 4	514.2	604.4	580.0	580.0	610.0	573.0	506.0	566.8	41.1
Layer 5	790.0	734.9	750.0	835.0	900.0	785.0	790.0	797.8	55.3
Layer 6	1750.0	1750.0	1750.0	1750.0	1750.0	1750.0	1750.0	1750.0	0.0

^a The first layer of these sites has a lateral continuation. ^b The third layer was not observed at this site.

^c The second layer of this site is different than the second layer of the others.

Table 17. Plasticity index values of the layers along the A-A' section. "C" is the abbreviation of Comb.

Plasticity index values of the Layers (%)								
Layer No	Site No						Section N-S (A-A')	
	C-04 (2) ^a	C-05 (2) ^a	C-06 (2) ^a	C-07 (2)	C-08 (2)	Mean	St. dev	
Layer 1	none	none	none	50.0	48.0	none	none	
Layer 2	62.0	50.0	45.0	59.0	59.0	55.0	7.2	
Layer 3	62.0	50.0	55.0	61.0	59.0	57.4	4.9	
Layer 4	62.0	50.0	55.0	61.0	59.0	57.4	4.9	
Layer 5	15.0	15.0	15.0	15.0	15.0	15.0	0.0	
Layer 6	BEDROCK						BEDROCK	

^aThe first layer of these sites has a lateral continuation

Table 18. Plasticity index values of the layers along the B-B' section. "C" is the abbreviation of Comb.

Plasticity index values of the Layers (%)									
Layer No	Site No							Section E-W (B-B')	
	C-01(2)	C-03 (2)	C-06 (1) ^a	C-09(2) ^a	C-12(2) ^b	C-14(1) ^{a,c}	C-04 (2) ^a	Mean	St. dev
Layer 1	29.0	40.0	none	none	none	none	none	none	none
Layer 2	37.0	45.0	66.0	50.0	42.0	15.0	62.0	50.3	11.5
Layer 3	50.0	60.0	72.0	56.0	none	40.0	62.0	56.7	10.9
Layer 4	50.0	60.0	72.0	56.0	55.0	50.0	62.0	57.9	7.7
Layer 5	15.0	15.0	15.0	15.0	15.0	15.0	15.0	15.0	0.0
Layer 6	BEDROCK							BEDROCK	

^a The first layer of these sites has a lateral continuation. ^bThe third layer was not observed at this site. ^c The second layer of this site is different than the second layer of the others.

After the determination of the geophysical, geotechnical and geometrical properties of the layers during the idealization procedure of the 11 measurement sites, the geometry of the 1D and 2D profiles were created. As stated by Matasovic and Ordonez (2012), strain dependent properties (e.g., shear modulus and damping values) are the function of the thickness of the layers. These properties significantly vary with depth. Matasovic and Ordonez (2012) suggests that thinner layers can be used to capture this highly non-linear and/or non-uniform variation of shear strain throughout the soil profile. Additionally, layering of a soil column in Shake2000 is required to model vertical V_s variations with depth. However,

when shear wave velocity value is constant with depth and shear strain variation is almost uniform with depth, a relatively thicker layer can be used to model the soil column in Shake 2000 (Ordonez, 2012). In this stage of the study, it is assumed that the shear wave velocity values corresponding to each layer do not significantly vary in the vertical direction and have a uniform behavior. Another assumption taken into account regarding the uniform behavior is the shear strain within each layer.

As can be seen in Tables 11 and 12, the depth of the soil profiles were extended to more than 200 m. The plasticity index values and unit weights were assigned to the extended portion of the soil profiles based on the previous layers where these values were determined by geotechnical laboratory tests (Tables 13-14 and Tables 17-18). But the characterization of the soils based on these tests were constrained up to the depth of 20 m as the maximum depth of the boreholes drilled in the region is 20 m. Therefore, the only parameter that can be used more confidently is the shear wave velocity profile since much deeper parts of the ground subsurface could be characterized by this approach. At some sites [e.g., Comb03 (2) Comb05(2), Comb08 (2)], maximum reliable characterized depth is 85 m. However, this depth can be increased up to 150 m during the inversion process for these sites if it is preferred to utilize the portion of the data where the degree of the reliability is low after a certain depth.

Under these circumstances, these shear wave velocity profiles were extended up to 210 m at some sites (Tables 11 and 12), by considering a linear increase of shear wave velocity values with depth. Additionally, the uncertainty of the modulus reduction and damping curves were taken into consideration as well (Darendeli, 2001). Also, a set of sensitivity analysis was implemented to investigate the effects of the layer thickness and variations of shear wave velocity values at the sublayers of the main layer. It was observed that these two model parameters had no significant effect on the response of the surface soils. As a result, the main layers

were divided into sublayers by using Equations 7 and 8 given below. In addition to this, a uniform behavior of shear strains in the subsets of each layers was assumed.

$$H_{max} \leq V_s / (4 \times f_{max}) \quad \text{Eq. (7)}$$

$$f_{max} = \frac{1}{2 \times DT} \quad \text{Eq. (8)}$$

where, H_{max} is the maximum layer thickness (m), V_s is the shear wave velocity of the layer (m/s), f_{max} is the maximum resolved frequency (Hz) and DT is the sampling interval of the records (s).

In the 1D soil response analysis, a frequency threshold was applied and it was selected as 25 cps. Based on the equations given above, the maximum height of each sublayer was calculated and is given in Tables 19 and 20. According to the H_{max} value, the number of sublayers were figured out for each main layer.

In 2D soil response analyses, initially the 2D geometries of the soil models, given in Figure 61a and 61c, were constructed based on the lateral continuation of the soil layers characterized by 1D shear wave velocity profile at the 11 sites along with the information acquired from the closest geotechnical borings (Tables 14 and 15). The mechanical properties of these soil layers having lateral continuity were assigned by considering the mean values of the data obtained from each site located along the sections (Tables 11 through 18).

Table 19. The maximum height (m) for 1D soil response analysis along the A-A' section. "C" is the abbreviation of Comb.

Maximum height (m) for 1D soil response analysis					
Layer No	Site No				
	C-04 (2)	C-05 (2)	C-06 (2)	C-07 (2)	C-08 (2)
Layer 1	1.7	1.5	1.8	1.7	1.9
Layer 2	2.7	3.1	2.8	2.8	2.7
Layer 3	3.5	4.1	3.5	4.1	4.5
Layer 4	5.1	5.2	5.1	5.1	5.3
Layer 5	7.9	7.6	8.1	7.4	7.9
Layer 6	BEDROCK				

Table 20. The maximum height (m) for 1D soil response analysis along the B-B' section. "C" is the abbreviation of Comb.

Maximum height (m) for 1D soil response analysis							
Layer No	Site No						
	C-01(2)	C-03 (2)	C-06 (1)	C-09(2)	C-12(2)	C-14(1)	C-04 (2)
Layer 1	1.4	1.8	1.7	1.8	1.4	1.8	1.7
Layer 2	2.8	2.4	2.5	2.5	2.5	3.7	2.7
Layer 3	3.9	3.9	3.9	4.1	none	4.3	3.5
Layer 4	5.1	6.0	5.8	5.8	6.1	5.7	5.1
Layer 5	7.9	7.3	7.5	8.4	9.0	7.9	7.9
Layer 6	BEDROCK						

Variations of the data was also taken into consideration especially at the stage of generation of the modulus reduction curve and damping curves as explained in next section of this chapter. The geometry of the individual soil layers (i.e., showing no continuity in the lateral direction) were modeled based on the geological setting of the area (Figures 61b and 61d). This is one of the most critical parts of constructing the geometric model since the study area is a fault controlled basin and numerous rivers control the depositional and/or erosional settings within the area. Therefore, the degree of lateral variability of the surficial deposits is high. Additionally, this variability degree is not negligibly low for soils underlying soft, unconsolidated Quaternary deposits due to the tectonic setting and geological evaluation of the area (see Chapter 2 for detailed explanations).

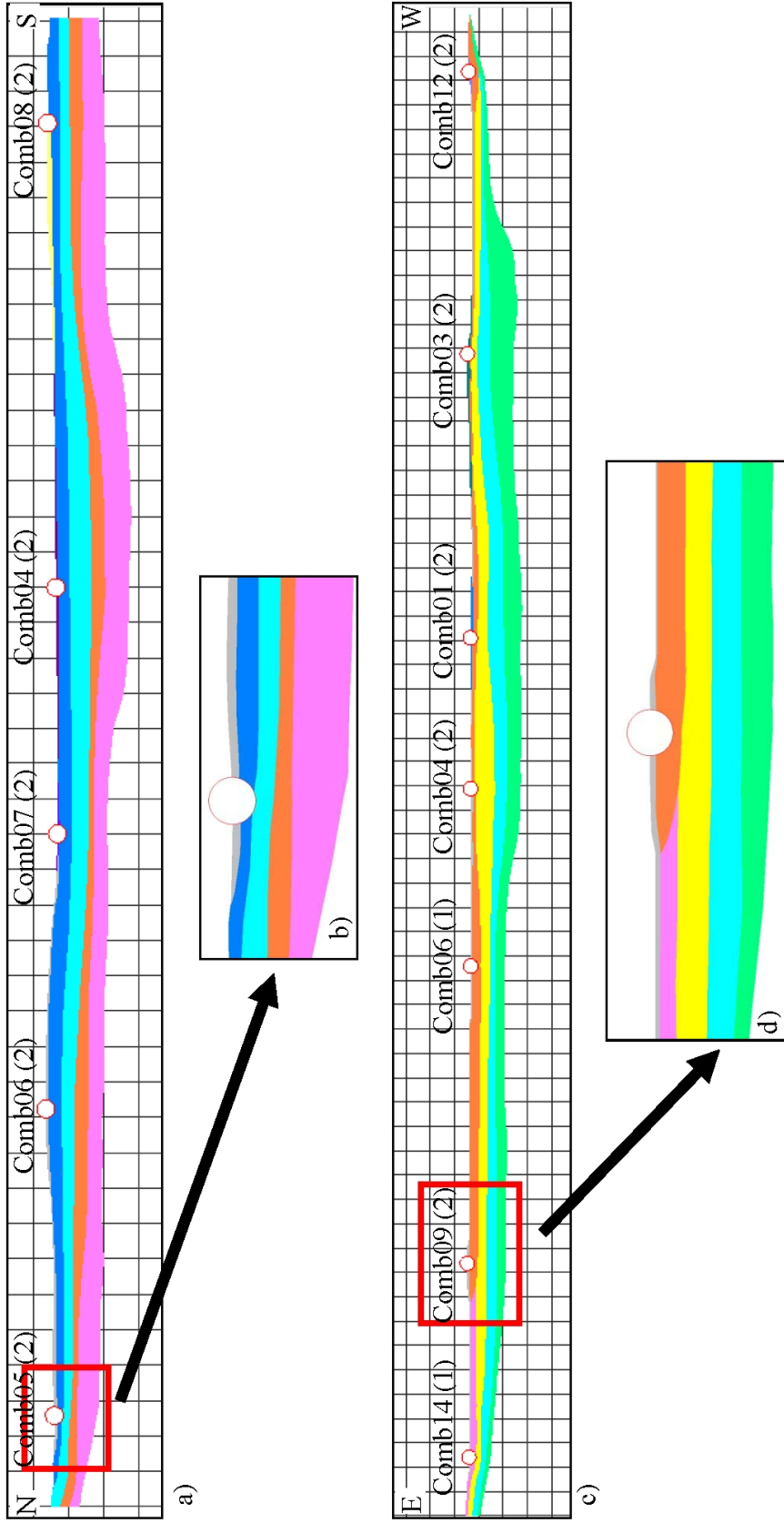


Figure 61. a) and c) Soil model of sections A-A' and B-B', respectively. b) and d) a close view of these sections to show the lateral and vertical variations of the layers. Colors are assigned to the layers for illustration purposes only. The dimension of the squares in a) and c) is 100m x 100m.

In the producing of 2D soil models given in Figure 61, the upper surface of the models were truncated based on the digital elevation map of the study area that was prepared by using 1:25.000 topographic maps of the General Command of Mapping. The lower boundaries of the models were constructed according to the vertical and lateral variation of the bedrock in the study area. After constructing the geometry, in order to perform 2D seismic response analyses by utilizing finite element method (FEM) based QUAD4M, the finite element (FE) meshes were generated for both sections. Due to the complex geometries of the layers forming the sections, quadrilateral and triangular elements were used. The maximum height of the elements was calculated by using Equation 9. The maximum value of the ratio between the horizontal and vertical size of the elements is constrained to be lower than 3 to obtain better accuracy in the results. By using these considerations, FE meshes were created (Figure 62). The geometric model and mesh properties of the sections are given in Table 21.

$$H_{max} \leq C \times \frac{V_s}{f_{max}} \quad \text{Eq. (9)}$$

where, H_{max} is the maximum height of a finite element (m), V_s is the shear wave velocity of the layer (m/s), f_{max} is the maximum resolved frequency (Hz) and C is a constant ranging from 1/5 to 1/10 according to different researches (e.g., Kuhlemeyer and Lysmer, 1973; Lanzo and Silvestri, 1999 and Ordonez, 2009). In this study, the C value is taken as 1/5.

Table 21. A summary of the geometric model and mesh properties.

Sections	Min. Height (m)	Max Height (m)	Min. Length (m)	Max Length (m)	Node No
N-S section	23.1	263.3	0	4207.5	43767
E-W section	21.4	253.8	0	6171.8	43667

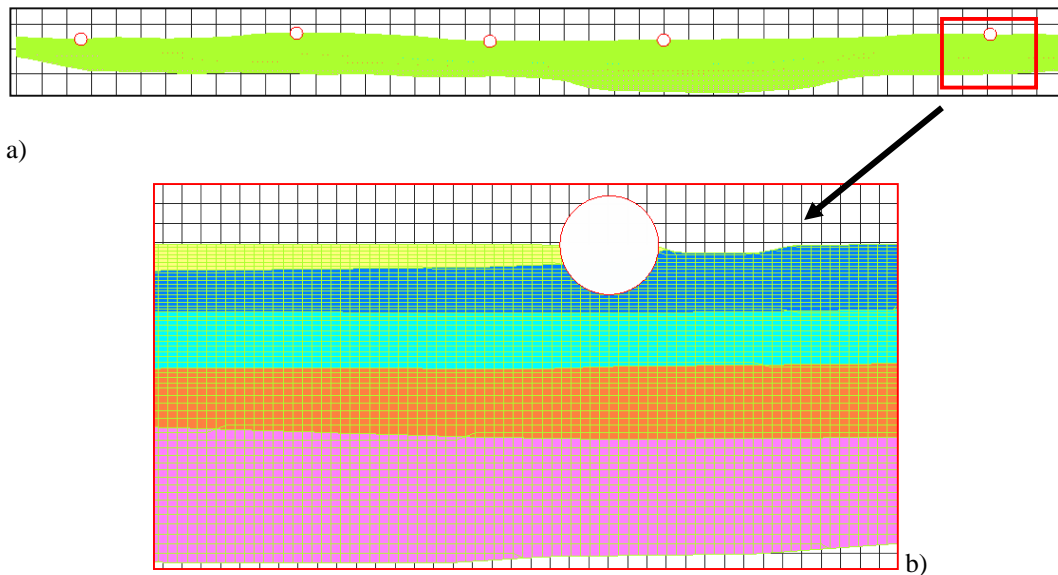


Figure 62. a) The Generated mesh of A-A' and b) a close view of the generated mesh along with the defined layers.

As stated in this section, transmitting boundary conditions was applied to the base of the soil models since deconvolution process was utilized. Also, in order to reduce the effect of the artificially reflected waves, different researchers have reported to have constructed their models by using different lateral extension values ranging from 200 m to 800 m (Augello et al. 1998; Rathje and Bray, 2001; Pagliaroli, 2006). The main reason for this wide range is related with the purpose of the seismic response analysis and the geometries of these models. To overcome this difficulty, Bouckovalas et al. (2006) suggest that the total lateral extension of a model can be used at least 5 times the thickness of soil column. In this study, the side boundaries were extended 250 m in both directions for both models by considering lithological variations and bedrock geometry so that the effect related with the side boundaries which is the interference between the input motion and the artificially reflected waves was tried to be minimized.

4.3.2.4. Characterization of non-linear soil behavior

The variations of normalized modulus reduction and material damping curves depending on the strain level (i.e., G/G_{\max} - γ and D - γ curves) are utilized as fundamental input parameters for any numerical ground motion analysis. A comparison between measured shear moduli and standard degradation curves also requires a value for the small-strain shear modulus (i.e., G_{\max}) against which the shear modulus is usually normalized (Darendeli, 2001; Brennan et al., 2005). Most of the field seismic surveys can be performed to obtain the shear wave velocity at shear strains lower than the percent of 3×10^{-4} . Therefore, in this study, the G_{\max} value was calculated by the results of the surface wave measurements which is the most reliable way to determine the in situ value of G_{\max} for a particular soil deposit (Kramer, 1996), by using Equation 10.

$$G_{\max} = \rho \times V_s^2 \quad \text{Eq. (10)}$$

where, ρ represents the density of material obtained by dividing the total unit weight of the soil by gravity (9.807 m/s^2) and V_s is the shear wave velocity value (m/s).

The most appropriate curves for these soil parameters were determined based on the data acquired by previous geotechnical works and seismic characterization studies performed during this study as well as the results of the experimental studies in the literature. Various parameters have an influence in the variation of these curves for the determination of the proper G/G_{\max} - γ and D - γ curves for the soil layers. These parameters are the mean effective confining stress, soil type and plasticity, frequency of loading, number of loading cycles, degree of saturation, over-consolidation ratio (OCR), void ratio, grain size distribution and characteristics along with the mineralogical properties and so on. Based on the study proposed by Darendeli (2001), not all the parameters control the non-linear

soil behavior with the same degree of effectiveness. Darendeli (2001) states that the mean effective confining pressure, soil type and plasticity are the most prominent parameters that affect the G/G_{\max} - γ and D - γ curves.

The laboratory test results and log data of 20 different geotechnical borings having a total of 308 m depth drilled in the Quaternary and Pliocene units were analyzed and the obtained information was integrated with the results of the geophysical surveys conducted in the area to select predefined experimental curves in the literature (e.g., Seed et al., 1986; Vucetic and Dobry, 1991; Darendeli, 2001). The non-linear properties of the soils were determined by using the soil models proposed by Darendeli (2001) for each layer based on the data regarding soil class, soil plasticity and mean effective confining stress values of the soils.

As stated before, to determine the unit weight, soil type and plasticity values of the soil layers at the 11 sites, the results of the geotechnical laboratory tests were utilized up to 20 m. The properties of the soil layers at the remaining portion of the soil profiles were assigned according to the variation of the shear wave velocity profiles and local geology. In the calculation of the mean effective confining stress, the thickness and unit weights of the soil layers were identified for each site (Tables 11 through 14) and Equation 11 was utilized.

$$\sigma'_m = \sigma'_v \times \left(\frac{1 + 2K'_0}{3} \right) \quad \text{Eq. (11)}$$

where, σ'_m is the mean effective confining stress, σ'_v is the vertical effective stress and K'_0 is the coefficient of effective earth stress at rest.

It is well known that the K'_0 value is a function of the effective angle of internal friction for normally consolidated soils. Additionally the OCR value is integrated to calculate the K'_0 for the over-consolidated ones (e.g., Pruska, 1973; Mayne and Kulhawy, 1982). However, the laboratory tests are not enough to characterize the

entire region in terms of the effective angle of internal friction and the OCR in this study. Therefore, sensitivity analyses were conducted to investigate the variations of the G/G_{max} - γ and D - γ curves and the uncertainties of these curves according to the selected soil model proposed by Darendeli (2001) where the vertical effective stress was utilized instead of the confining stress. In this respect, unconsolidated granular and over-consolidated cohesive layers at Comb01 (2) and Comb06 (1) sites were selected (Figures 63-66). The error margin (\pm one standard deviation) of the curves along with the mean values based on the vertical effective stress was compared with the mean values of the curves drawn by using the confining stress. It can be observed in Figures 63-66 that the upper and lower boundaries of the curves according to the former approach covers the curves constructed by the latter one at almost all shear strain values. Therefore, instead of increasing the uncertainties by assuming OCR and the angle of internal friction values, the effective vertical stress was calculated for the layers at each site and it was used to construct the curves along with the soil type and plasticity in 1D and 2D soil response analyses. As stated above, this approach does not have any effect on the 2D analysis as a result of the selected approach during the determination stage of the geotechnical parameters of the layers.

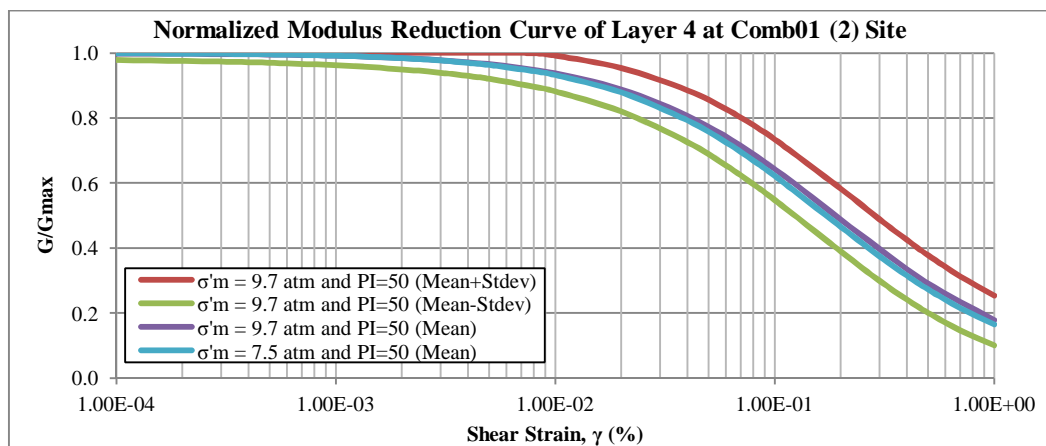


Figure 63. A comparison of using vertical and confining effective stresses for the overconsolidated cohesive layers at the Comb01 (2) site.

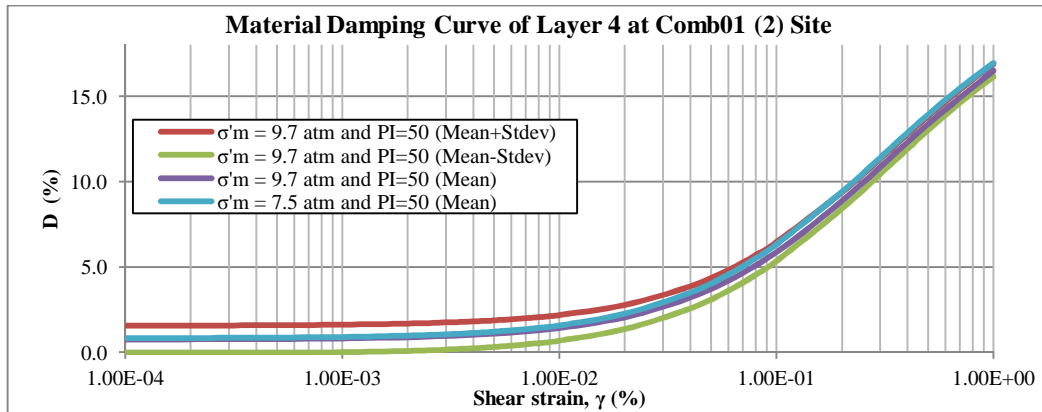


Figure 64. A comparison of using vertical and confining effective stresses for the overconsolidated cohesive layers at the Comb01 (2) site.

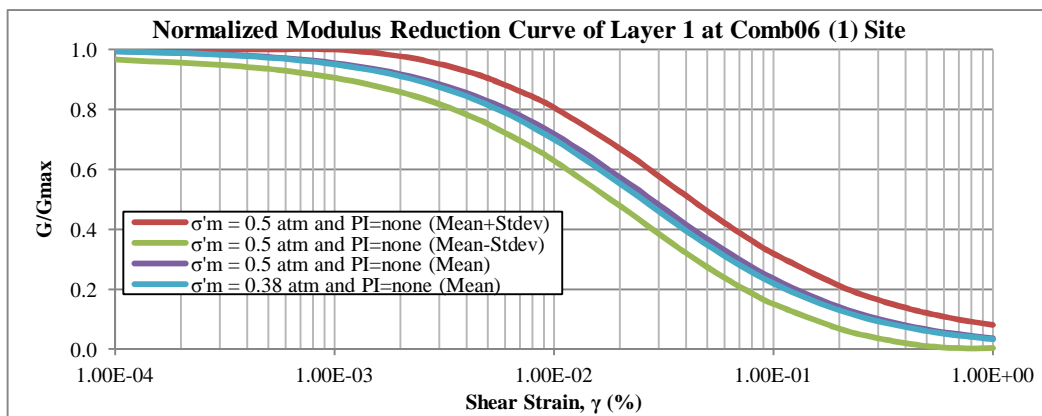


Figure 65. A comparison of using vertical and confining effective stresses for the unconsolidated cohesive layers at the Comb06 (1) site.

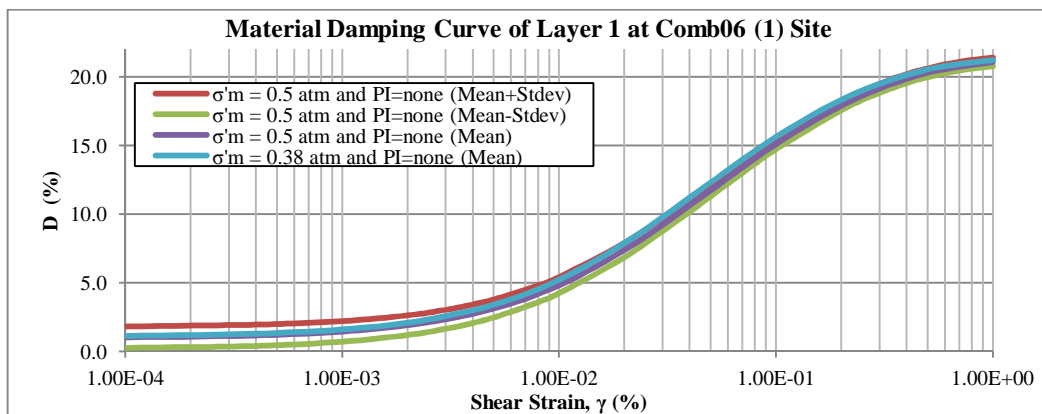


Figure 66. A comparison of using vertical and confining effective stresses for the unconsolidated granular layers at the Comb06 (1) site.

The generated normalized modulus and material damping curves based on the study proposed by Darendeli (2001) are given in Figures 67-77. These curves were used as input parameters for 1D soil response analysis. As can be seen in these figures, these curves were classified according to the layer numbers of each site where Layer 1 represents the shallowest part of the soil profile and Layer 5 is the strata overlying the bedrock.

When the variation of these curves are examined with respect to the layer numbers, it can be easily seen that the trend of the G/G_{\max} ratio increases at higher shear strain levels ($>10^{-3}\%$) from layer 1 to layer 4 due to the rise of the effective vertical stress and plasticity of the soil. However, there is a non-uniform behavior when the curves of layer 5 are reviewed. Although, the vertical stress increases, this behavior is caused by decreasing plasticity value. The same situation is inversely valid for the material damping curves. This implies that the trend of the damping ratio values decreases after a certain shear strain percent ($>10^{-2}\%$) from the shallower portions of the soil column to the deeper parts. But due to the same reason given above, Layer 5 does not behave in the same trend. In 1D response analysis, the bedrock behavior was characterized by using the $G/G_{\max}-\gamma$ and $D-\gamma$ curves proposed by Schnabel (1973). The variation of these curves is not given in a figure, since these curves are not affected by any parameters discussed above. This means that these curves are identical for all sites.

In 2D soil response analysis, based on the mean values of the parameters given in Tables 11 through 18, the normalized modulus and the material damping curves were constructed by using the model proposed by Darendeli (2001). Also, during the generation of the curves, the standard deviation of these properties were taken into account especially for the deeper layers. When the produced curves for each layer constituting two sections were examined (Figures 77-80), the same behavior is observed with the other curves created for the 1D response analysis.

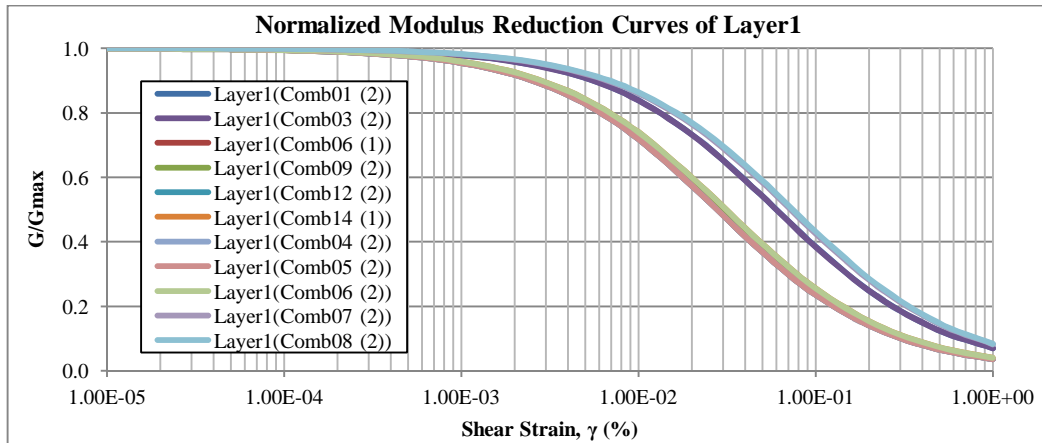


Figure 67. Normalized modulus curves of the first layer utilized in the 1D soil response analysis.

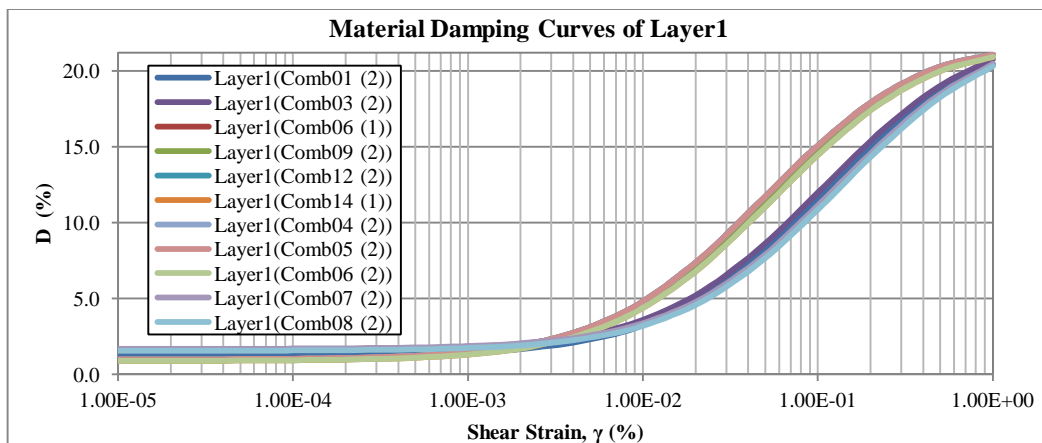


Figure 68. Material damping curves of the first layer utilized in the 1D soil response analysis.

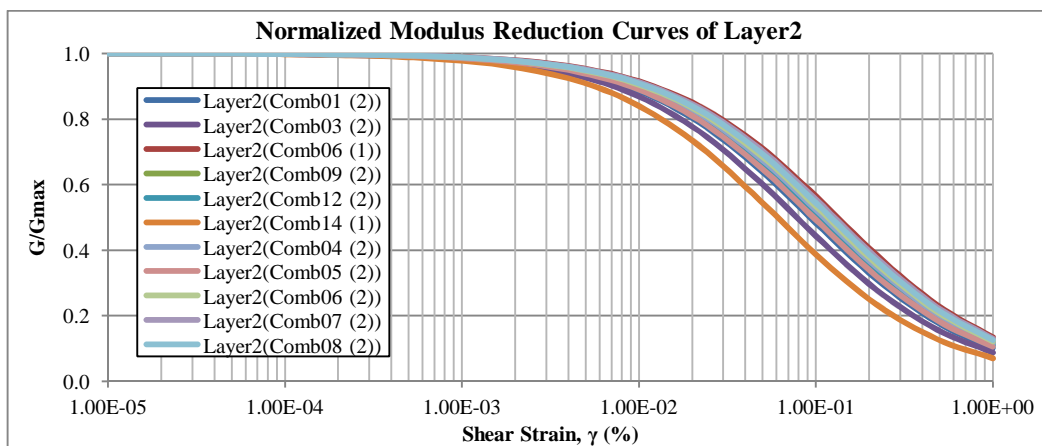


Figure 69. Normalized modulus curves of the second layer utilized in the 1D soil response analysis.

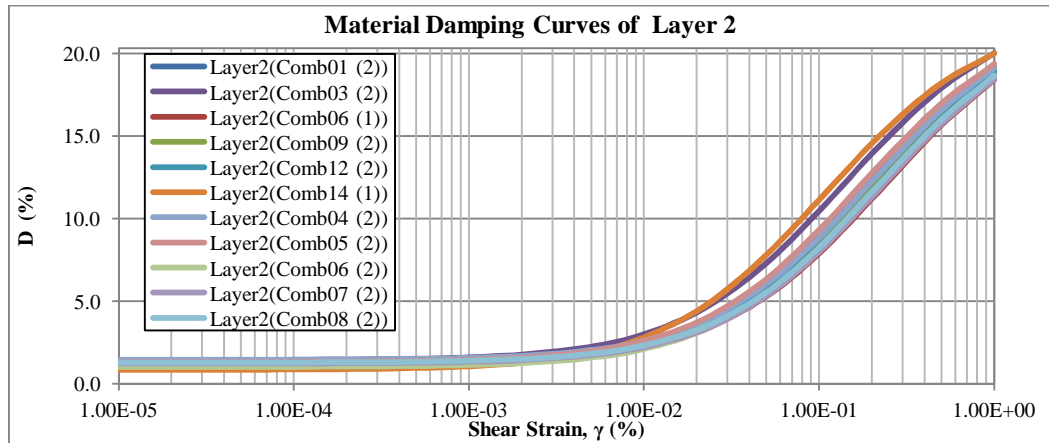


Figure 70. Material damping curves of the second layer utilized in the 1D soil response analysis.

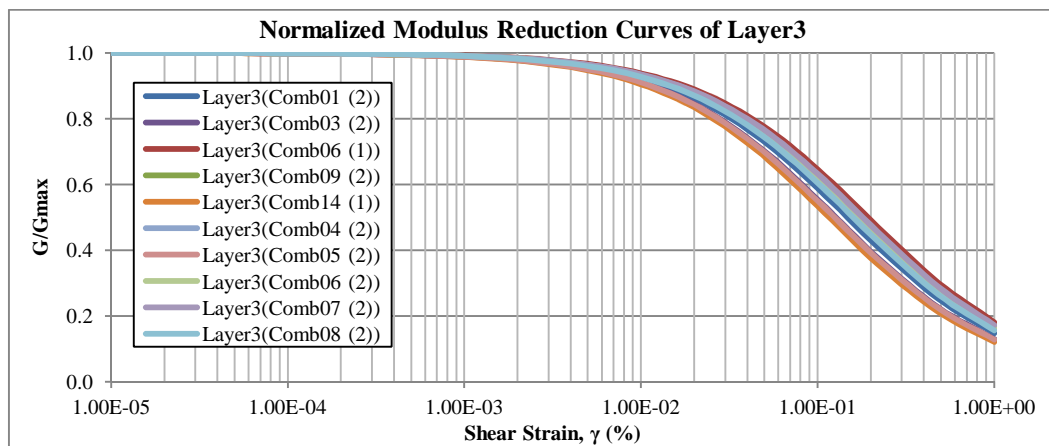


Figure 71. Normalized modulus curves of the third layer utilized in the 1D soil response analysis.

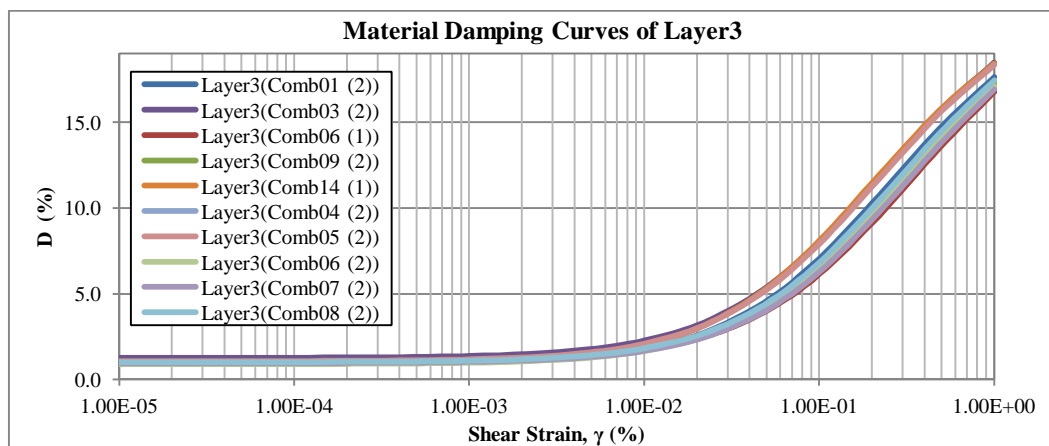


Figure 72. Material damping curves of the third layer utilized in the 1D soil response analysis.

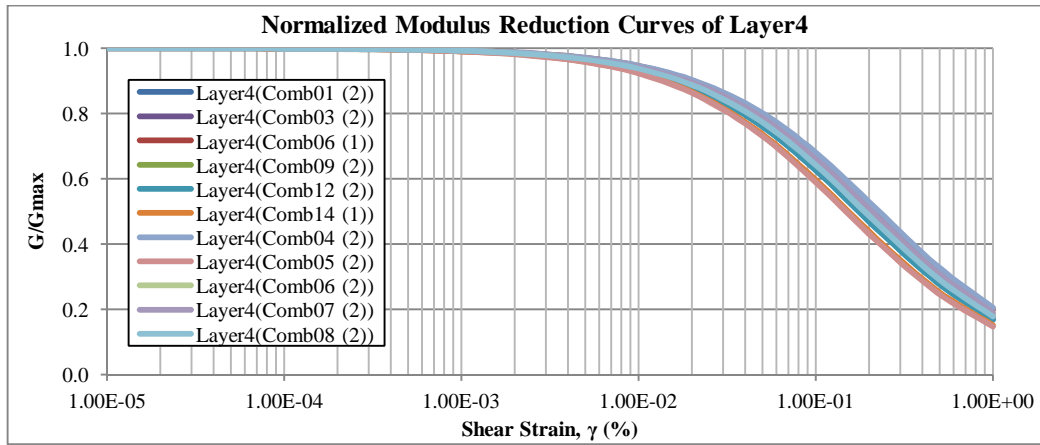


Figure 73. Normalized modulus curves of the forth layer utilized in the 1D soil response analysis.

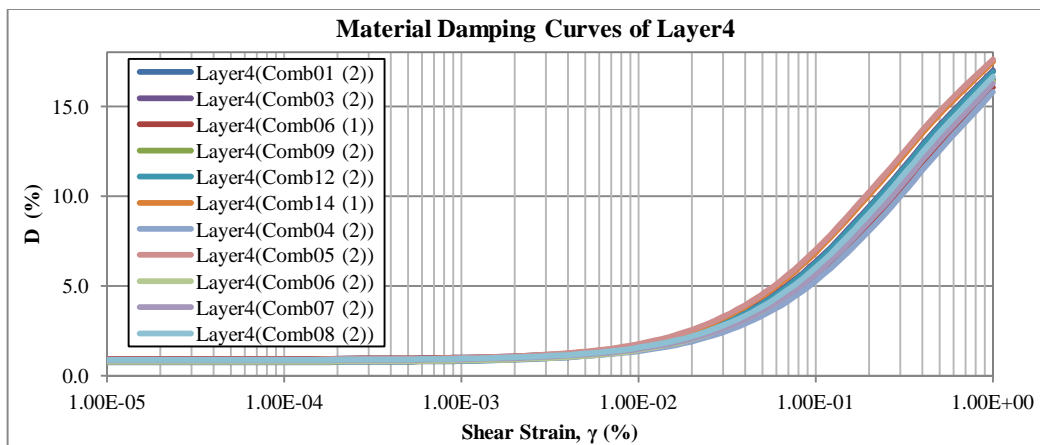


Figure 74. Material damping curves of the forth layer utilized in the 1D soil response analysis.

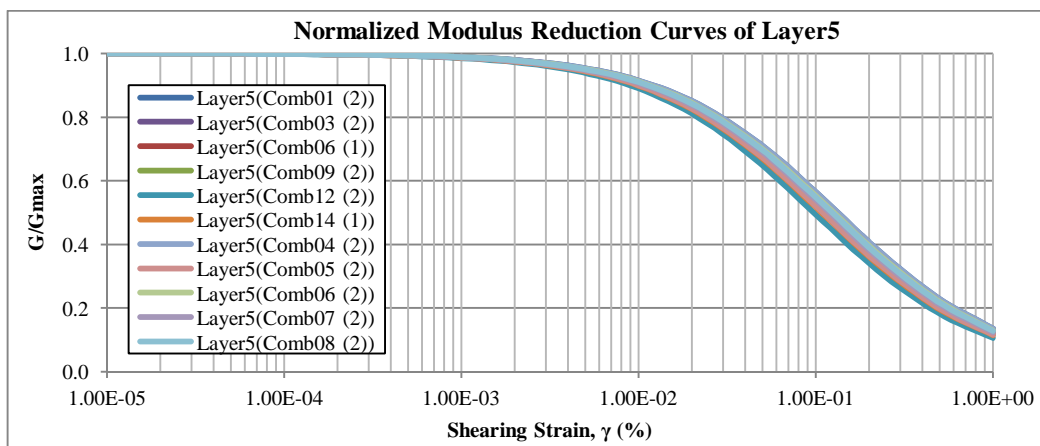


Figure 75. Normalized modulus curves of the fifth layer utilized in the 1D soil response analysis.

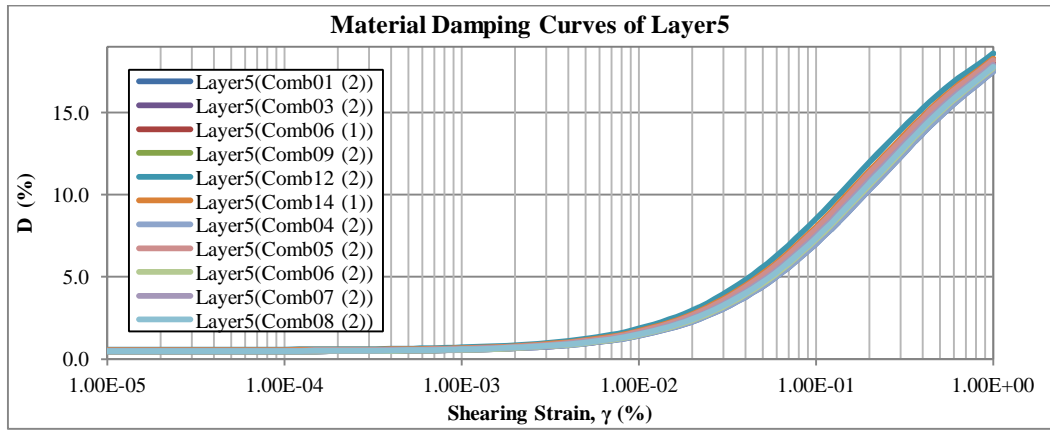


Figure 76. Material damping curves of the fifth layer utilized in the 1D soil response analysis.

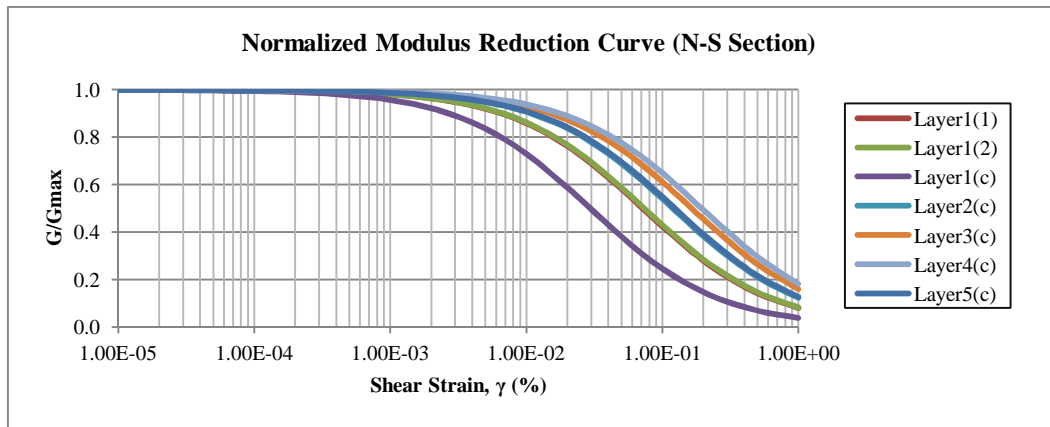


Figure 77. Normalized modulus curves of all layers utilized in the 2D soil response analysis. "c" is the abbreviation of the layer having lateral continuity and the others are the individual ones.

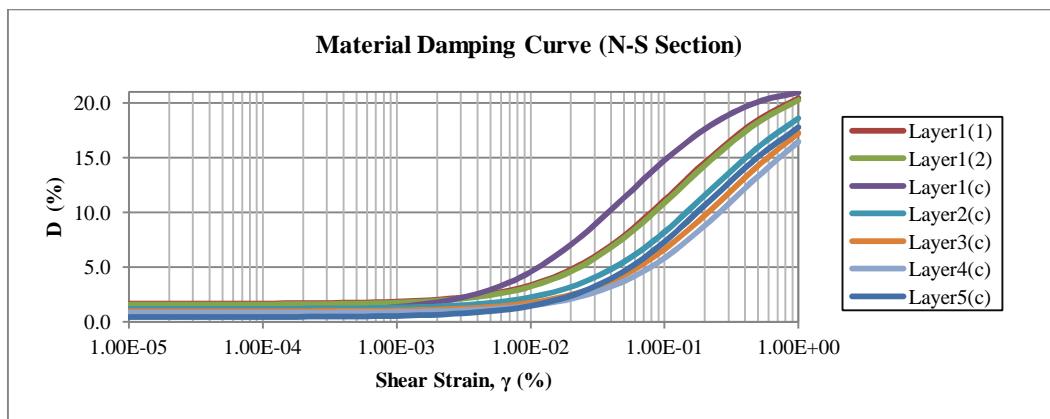


Figure 78. Material damping curves of all layers utilized in the 1D soil response analysis. "c" is the abbreviation of the layer having lateral continuity and the others are the individual ones.

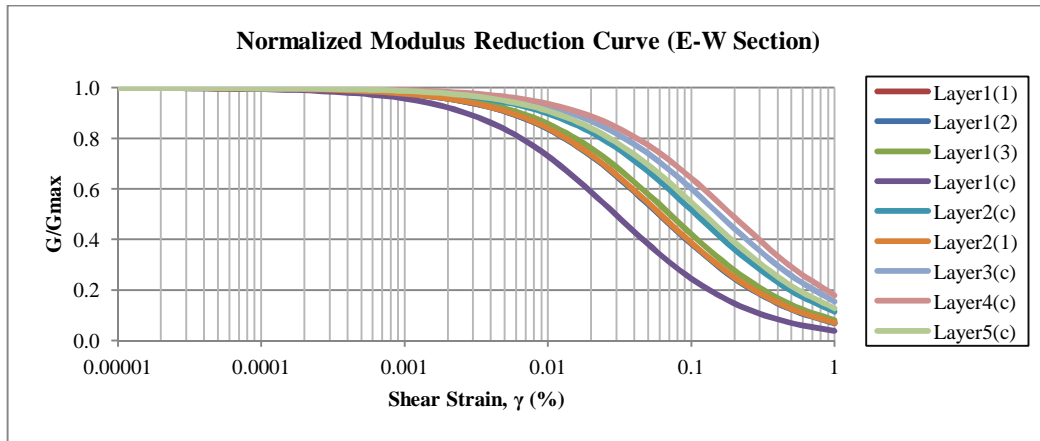


Figure 79. Normalized modulus curves of all layers utilized in 2D soil response analysis. "c" is the abbreviation of the layer having lateral continuity and the others are the individual ones.

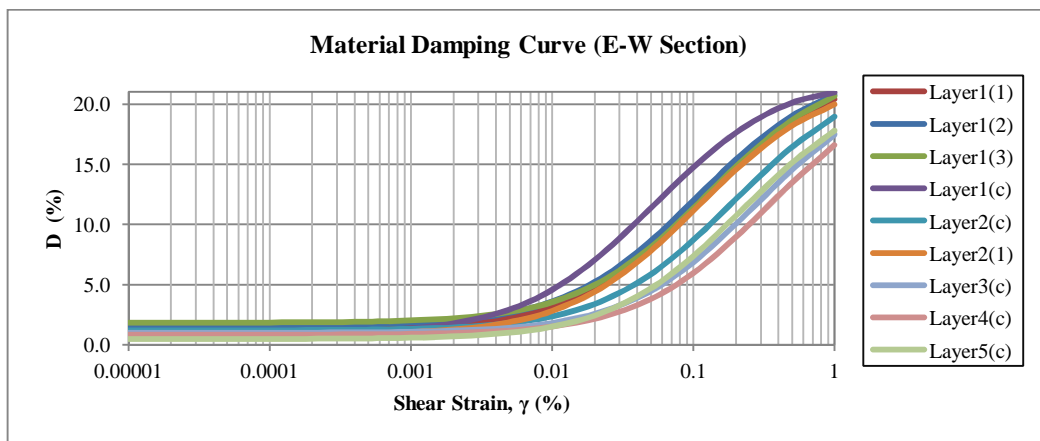


Figure 80. Material damping curves of all layers utilized in 1D soil response analysis. "c" is the abbreviation of the layer having lateral continuity and the others are the individual ones.

CHAPTER 5

RESULTS OF THE SITE EFFECT STUDIES

5.1. Results of the microtremor survey

In the scope of determination of site effects in the Orta pull-apart basin, the performed microtremor survey can be classified as a preliminary evaluation method. In order to correctly investigate the influence of the local site condition and topographical effect on the spatial variation of ground motion, the seismic behavior of shallower deposits, the spectral structure of a possible seismic event, the effects of the small-scale lateral and vertical variations of the soils should be carefully taken into account. However, the H/V spectral ratio (Nakamura Method), one of the experimental technique for the ambient microtremors (vibrations), has been widely used in microzonation studies as it is cost-effective and an easy procedure for application (Bonney-Claudet, 2004).

A fundamental period and a maximum value for the H/V amplitude were estimated from each microtremor measurements conducted at the first and the second phases. As was stated in Chapter 4, the record length, the brand of seismograph and the time period of the conducted surveys are different from each other. Therefore, the results of this study show the degree of the dependency of the microtremor method on the measurement length and the time interval in terms of the stability of the constructed H/V curves.

As mentioned before, the microtremor records were taken at 44 sites in the first phase, however, site effect phenomenon was investigated at 35 sites during the

second phase. Regarding the results obtained from the microtremor study in the Orta basin, different geological units related with their H/V spectral ratio have been identified and surveyed using the short-period noise recordings. According to the range of the fundamental period with respect to the geological units given in Figures 81 and 82, in a general sense, the fundamental periods observed at the sites were higher than the expected periods. When the figures are examined separately, it can be seen that the results show large variability in the H/V spectrum. Although, the results are more stable for the Miocene sediments measured at Phase-1 (Figure 81), this group was not considered within the statement given above due to the low population of the characterized sites.

After conducting the first phase of the survey (Figure 81), the observed maximum H/V amplitudes were at the period range of 0.73 s to 1.37 s with their amplitude changing between 2.7 and 11.5. On the other hand, the second phase showed that the fundamental periods were between 1.01 s and 2.22 s with their corresponding H/V peak amplitudes ranging from 2.9 to 19.0 for the Orta basin (Figure 82). Figures 81 and 82 indicate that the geological sediments do not have typical fundamental periods. In other words, these units cannot be differentiated by utilizing the abscissa value of the H/V curve. These figures individually imply that the relatively higher thickness of the soft soil deposits are present within the Orta pull-apart basin. However, this is an unexpected result, since this basin type has mostly shallower depressions when compared with the graben like basins (Eker et al., 2015). However in the literature, similar types of basins filled by very thick soft deposits are reported by Özalaybey et al. (2011) and Yousefi-Bavil et al. (2015).

There are procedures presented by SESAME (2004) in order to check two fundamental factors on the H/V curve to be generated. These are, conditions regarding reliability of the generated H/V curve and clarity conditions of peak values observed on the H/V curves. Reliability conditions are conditions controlling the parameters such as number of selected windows during processing

and window length based on estimated dominant frequency. Based on this, parameters such as number of windows, window length, recording time vary based on the estimated (predicted) dominant frequency (f_0). In other words, it is necessary to select site specific recording and analysis parameters based on geological and structural conditions. Additionally, the standard deviation values are to be checked after the acquisition of the H/V curves that are calculated for more than one analysis windows via the procedure proposed by SESAME (2004). The reliability of the acquired peaks are to be investigated by considering the amplitude values of the H/V curves, standard deviations of amplitudes, peak frequencies and deviation values on distinct peak conditions.

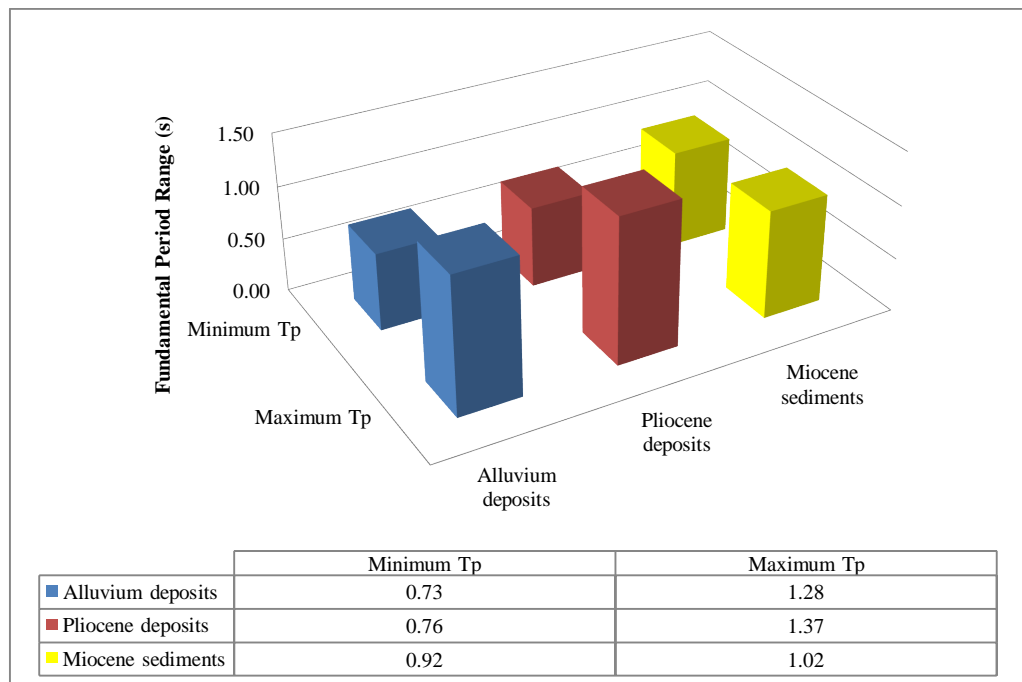


Figure 81. The observed maximum and minimum fundamental periods with respect to the geological units after the first phase of the microtremor survey.

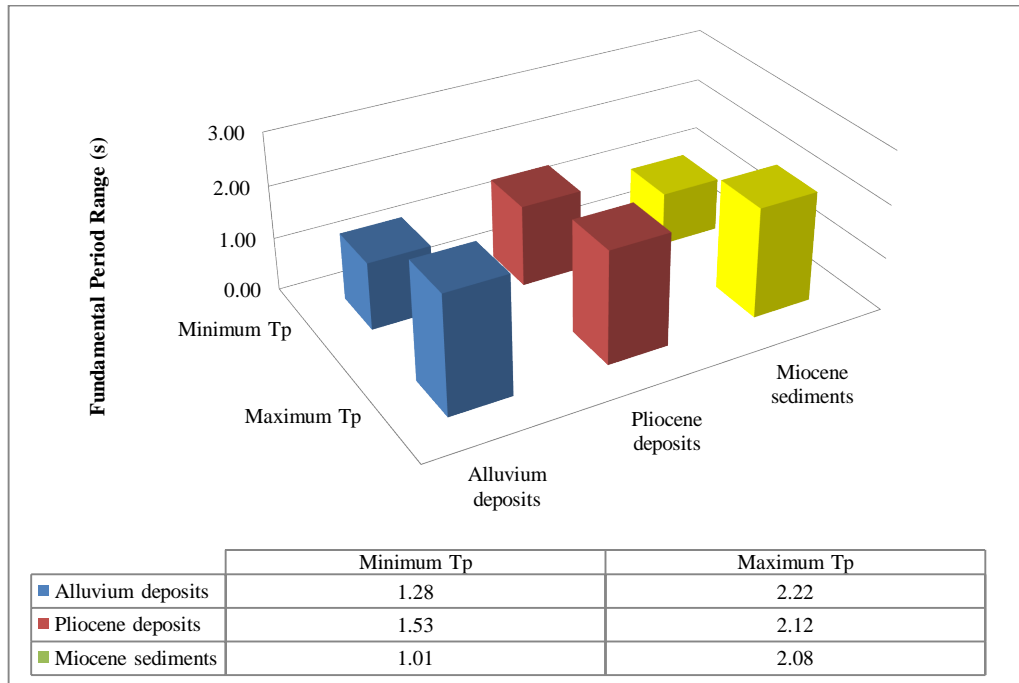


Figure 82. The observed maximum and minimum fundamental periods with respect to the geological units after the second phase of the microtremor survey.

When the H/V curves obtained from the two phases (Figure 83) are inspected, it can be observed that although some of the comparable results given by Figures 83a, 83c and 83e can be obtained, the degree of the correlation is not good for the majority of these pairs as shown in Figures 83b, 83d and 83f. After processing of the other signals recorded in both phases, well defined single, double, multiple and broad peaks are observed in the H/V spectra (Figure 83). These shapes show variations with respect to the subsurface geological conditions and the geometry of the investigated basins (Guegen et al., 1998; SESAME, 2004; D’Amico et al., 2008; Bonnefoy-Claudet et al., 2009). The variations between the results of the phases may be in regards to the smoothness degree of especially the first phase since the smoothness parameter was selected by using smaller bandwidths in order to detect all the possible peaks in the H/V spectrum. The sensitivity analysis of the smoothness step of the generated H/V curves at Phase2 was implemented with the purpose of increasing the correlation degree of the comparisons. This analysis was performed by changing the smoothing constant of the Konno–Omachi algorithm. It

was observed that it is not necessary to adjust the smoothing constant for that purpose since the general trend of the curves are not significantly influenced as illustrated in Figure 83a. In this figure, the H/V curve constructed by processing the signal record at Ort28 (2) was obtained by using no smoothing function.

One of the main reasons of the poor correlation between the pairs can be related with the total record length. Therefore, this difference can be a function of the number of the selected windows and the selected window lengths in the calculation of the average H/V spectra. The longer window length has higher capabilities in order to represent the longer period values of the soils as stressed by SESAME (2004). Due to this effect, although the general trend and shape of the curves were retained, the amplitude amounts of the peaks and their position according to x-axis could change with respect to the soil character (i.e., thickness of the sediments overlying the bedrock). In order to test this statement, the spatial distributions of the fundamental periods were created for both phases.

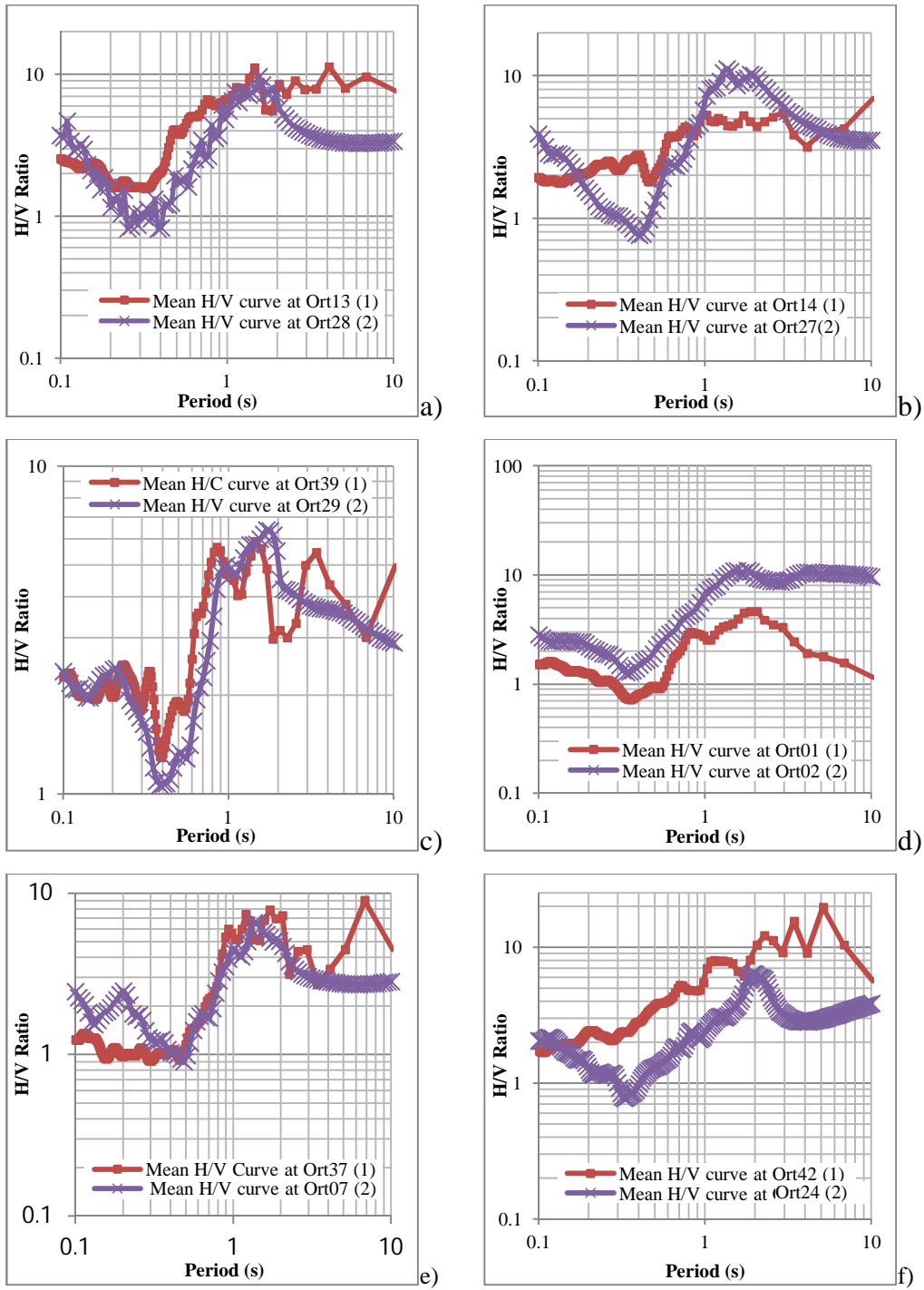


Figure 83. The comparisons of the H/V spectra obtained after implementing both phases. Please note that the numbers the parentheses show the Phase number.

In the generation of the interpolation map of the fundamental period for the conducted phases, the ordinary kriging method with an exponential semi-variogram model type was utilized to quantify the spatial structure of the data by considering the anisotropy. In this method, a logarithmic transformation was selected for the dataset regarding the measurements at Phase1. However, the box-cox transformation (Box-Cox, 1964) was applied with the exponent value of 3 for the dataset of Phase2. By performing the trend analysis, the second order effect was determined at both datasets and the local polynomial interpolation was utilized in the de-trending stage. The generated fundamental period interpolation (prediction) maps for the results of the first and second phases are given in Figures 84a and 84b, respectively.

Even though some parts of the study area were not covered by the microtremor surveys, these were included in the regional seismic map in order not to distort the shape of the maps. It should be mentioned that the qualitative character of the maximum H/V spectral ratios obtained from the Nakamura method does not provide reliable ratios for a soil site over a rock site during an earthquake. The variation of the H/V amplitudes were highly influenced by the variation of some of the parameters, such as the impedance (velocity) contrast, Poisson's ratio and source-receiver distances (Lachet and Bard, 1994). This subject was also stressed in the previous chapter. In this respect, only the relative spectral ratios between the two measurement sites were assumed to be significant (Lachet and Bard, 1994; Bour, 1998; Bard, 1999; Duval et al., 2001). Therefore, instead of creating an interpolation map, the graduated symbols were utilized to create a map to assess and compare the maximum spectral ratios of the sites as a discrete location on the map (Figures 84a and 84b).

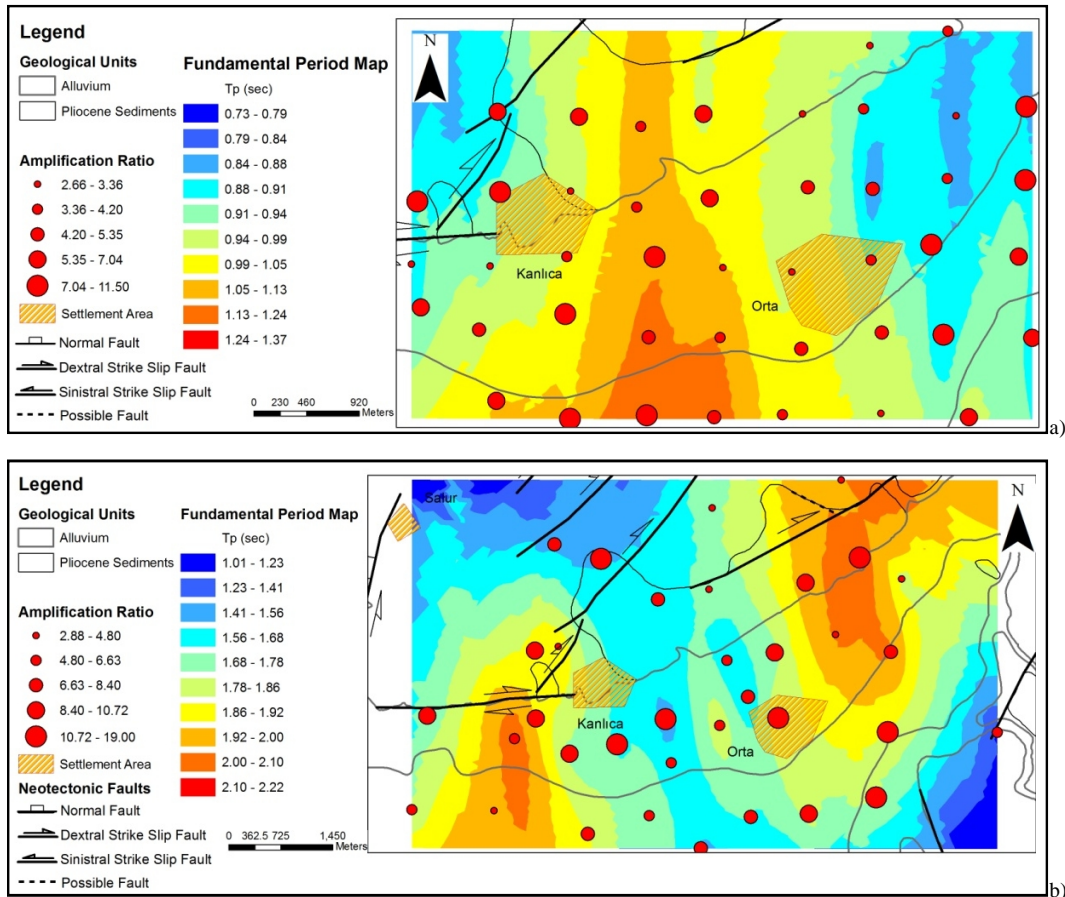


Figure 84. An interpolation map of the fundamental period along with the graduated symbols of amplification values observed at these periods overlying the geological units and the structural geological elements for a) Phase1 and b) Phase2.

When the spatial distributions of the fundamental periods in Figure 84a are compared with the variations in Figure 84b, it can be observed that the region is characterized by totally different behavior of the periods. As can be seen in both figures, a soil corridor zone is determined between Kanlıca village and Orta District. Figure 84a indicates that this region has relatively higher periods when compared with the other sites in the close proximity, however, the fundamental period of this area is classified as a low period zone with respect to the periods of other adjacent sites. Additionally, this type of difference between the period maps can be seen in the NE of the study area where relatively lower period values are assigned to this zone in Figure 84a. On the contrary, the acquired periods have totally opposite behavior at this zone in Figure 84b. Briefly, under these

circumstances, the maps are incompatible with each other. When these figures are examined in order to compare the variations of the H/V spectral amplifications, the same type of discrepancy can be observed. This comparison leads to a conclusion that the result of at least one of the microtremor surveys is not correct. However, a differentiation in regards to which result represents the actual case is not an easy task without performing soil response analyses.

Furthermore, before comparing the experimental results with the outputs of the 1D and 2D soil response analyses, the spectral curves of the individual components were investigated especially for the second phase since the relatively higher fundamental periods were obtained from this phase. Large vertical spectral amplitudes manifest themselves at the majority of the sites. Two of the distinctive samples are given in Figure 85. These sites are situated at the Quaternary units of which the depositional setting is controlled by the river. As can be seen in the figure, the amplitudes of the vertical components are greater than those of both of the horizontal ones at the similar frequency ranges.

The reason for this can be related with the P-wave velocity (V_P) contrast within the same layers which also controls the behavior of the horizontal components (Raptakis et al., 2005). One of the main factors influencing the V_P is the ground water level (GWL). If the soil layers which are located above the GWL are considered, it is observed that they have significantly lower P-wave velocity values when compared with V_P values of the layers below the GWL. As stated in Chapters 4 and herein, the area consists of abundant permanent rivers and based on the geotechnical boring logs and the excavated trial pits, the ground water level is very high in almost the entire study area even within the Pliocene sediments. Therefore, this may be the reason for the observation of the higher fundamental periods in the second phase of the microtremor survey.

In order to clarify which phase of the microtremor survey has more representative outcomes in the determination of the site effects for the Orta pull-apart basin, 1D

and 2D soil response analyses were performed. In the further sections of this chapter, the discussions regarding the results of the response analyses and the evaluation of the site effect studies in the area are given.

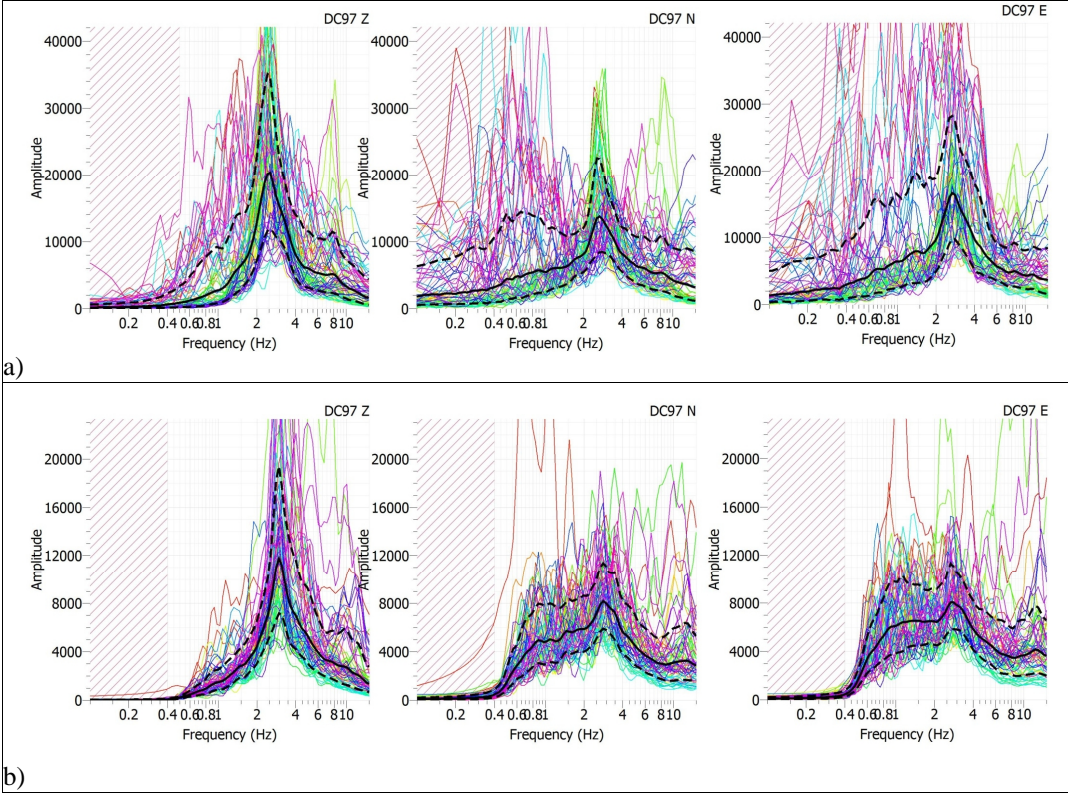


Figure 85. The individual spectral curves of vertical (z), N-S and E-W components of a) Ort-07 (2), b) Ort19 (2).

5.2. Results of 1D and 2D numerical analyses

In order to perform 1D and 2D soil response analyses, two cross sections were constructed with numerous considerations as explained in detailed in Chapter 4. To characterize the sedimentary deposits in the basin properly, the N-S (A-A') and E-W (B-B') trending sections were prepared. The N-S trending section is geographically more or less parallel to the main fault system of the region, NAFS. However, the other one is nearly perpendicular to this fault system. Based on the strike of the Dodurga Fault Zone, the A-A' and B-B' cross sections get parallel and perpendicular relative positions, respectively .

A total of 11 different sites were characterized by 1D shear wave velocity profiles utilized in the generation of these cross sections. Comb05(2), Comb06(2), Comb07(2), Comb04(2) and Comb08(2) are located along the N-S section. The order is given in the direction of north to south. Additionally, The sequence of the quantitatively investigated 1D sites along the E-W section is Comb14(1), Comb09(2), Comb06(1), Comb04(2), Comb01(2), Comb03(2) and Comb12(2) from west to east. These two sections share one common site, Comb04(2). It should be noted that the numbers in parentheses indicate the phase stage during which the geophysical characterization of the sites were performed. A total of 5 sites are located within the Orta basin, namely Comb01(2), Comb04(2), Comb06(1), Comb07(2) and Comb09(2). The sites of Comb12(2) and Comb14(1) that are assigned as the end points of the E-W section are present at the boundary of the Quaternary deposits and Miocene units (Boundary group). Additionally, the Pliocene units were characterized by three sites, namely, Comb03(2), Comb06(2) and Comb08(2). The remaining site, Comb05(2), fell within the boundary of the Miocene sediments.

Before carrying out the ground response analyses, initially 7 earthquakes were specified as the input rock motion based on the described target spectrum in this study. The selection and scaling procedure of these earthquakes are given in

Chapter 4. 1D and 2D soil response analyses were carried out by using the Shake2000 (Ordonez, 2000) and QUAD4M (Hudson et al., 1994) softwares, respectively. As explained in Chapter 4, these two softwares use equivalent linear assumptions and consider non-linear stress-strain behavior of soils under a possible ground motion.

The 1D analyses were executed for each site by utilizing the selected seven earthquakes in order to check the variations of the soil responses regarding the input ground motion records. In other words, it was investigated whether or not the soil responses were statistically stable at each site. A total of 77 runs was performed at 11 sites during the investigation of the 1D ground responses. In the 2D ground response analyses, these seven input rock motion records were used for each seismically and geotechnically characterized sections. 14 runs were performed in the determination of the 2D soil response along two sections.

The amplification and acceleration response spectra of the surface layers were examined in order to check whether the soil responses have stationary behavior or not. It should be noted that all the response spectral accelerations were constructed for a 5% damping ratio. Results of the dimensional seismic response analyses for two sites are given for the sake of comparison of the results obtained by the 1D and 2D numerical analyses. At these sites, the mean of the variations and their deviations of spectral acceleration and the amplification ratio spectra with respect to the utilized input motions can be observed in Figures 86 and 87, respectively. As can be seen in these figures, the responses of the sites do not change with the selection of the input motions. This means that the mean values of the soil responses with respect to the ground motions can be utilized as the 1D and 2D seismic responses of the site. In order to investigate the ground motion variation within the Orta pull-apart basin, the acceleration and amplification ratio spectra are taken into consideration.

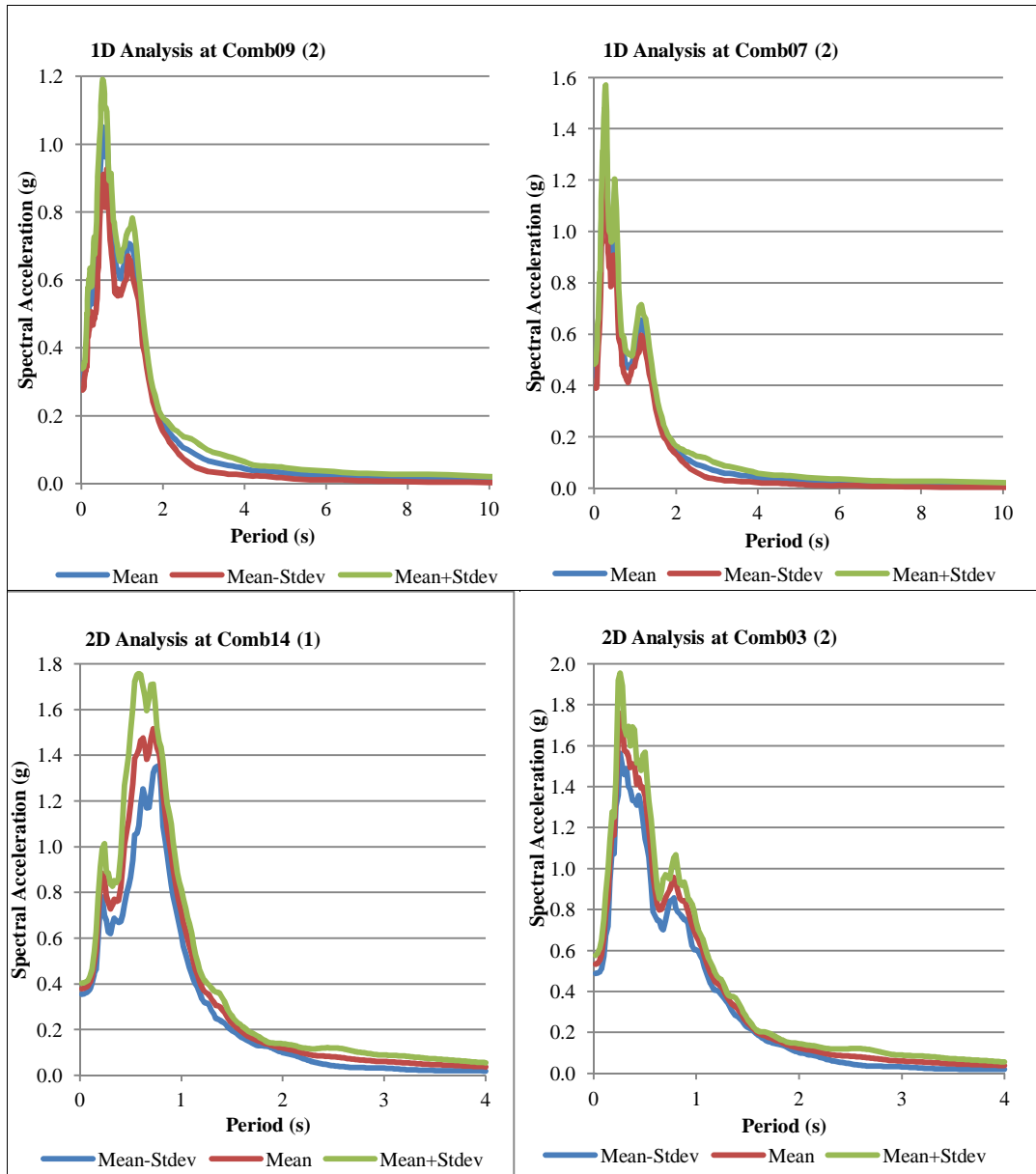


Figure 86. The comparison of the stability of the soil responses by investigating the variations of the acceleration spectra after running 1D and 2D analyses for seven earthquakes.

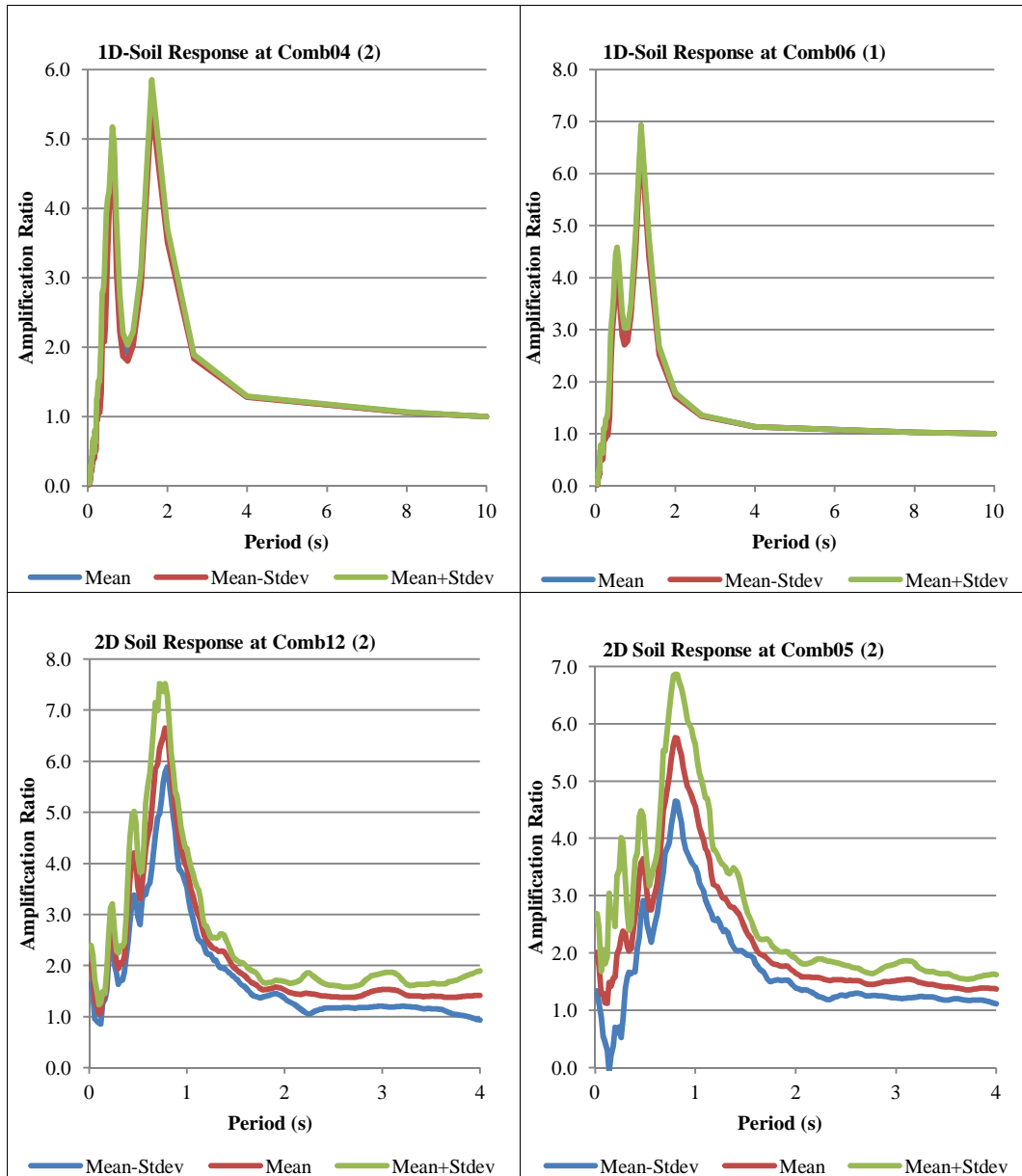


Figure 87. The comparison of the stability of the soil responses by investigating the variations of the amplification ratio spectra after running 1D and 2D analyses for seven earthquakes.

After examining and correlating the behaviors of the spectral acceleration curves, the results of the 1D and 2D numerical analyses were grouped based on the geological units where the utilized sites are present. The sites are divided into 4 groups. A list of the classified sites were given at the beginning of this section. Initially, 1D and 2D seismic responses of the sites were investigated with respect to the variation of the input rock motions obtained by selecting and scaling seven ground motion records by using the time-domain spectral matching technique. As stated in Chapter 4, the spectral matching was performed according to the constructed target spectrum. In this comparison, the mean of the selected suit was considered as given in Figure 88. It can be seen from the figure that, the dominant period of the input motion is 0.18 s with a spectral acceleration value of 0.533g. When the results of both numerical analyses are considered and compared with the input motion, the characteristics of the surface response spectra are described by the higher dominant periods and the higher spectral acceleration values along the entire period range for all of the sites (Figure 88).

Based on the results of the 1D soil response, it can be concluded that the highest spectral acceleration values (S_a) of the Quaternary sites are within the range of 1.05g to 1.4g at corresponding periods between 0.27 s and 0.53 s. The maximum S_a values in the Pliocene group is changing between 1.11g and 1.43g that are observed at periods ranging between 0.27 s and 0.52 s. The 1D numerical analysis of the two sites at the geological boundaries along the E-W section show that the S_a values are 1.07g and 0.72g for the sites located at the west and east ends of the section, respectively. These peaks emerge at the period of 0.62 s and 0.64 s in the above given order. Due to the insufficient population amount, rather than giving a range, only the highest S_a value and its corresponding period is obtained for the Miocene sediments. These values are 1.07g and 0.62 s in the above given order. One of the representative examples from each group can be seen in Figure 88.

As a result of the 2D seismic response analysis, the spectral acceleration peaks are observed in the range of 1.19g to 2.06g for the sites within the Quaternary while

their corresponding periods is changing between 0.24 s and 0.72 s. In the Pliocene sites, the maximum spectral acceleration values are clustered between 1.50g and 1.99g in the period range of 0.24 s to 0.28 s. At sites located at the boundaries of the Quaternary unit, the highest S_a values that are ranging between 1.38g and 1.52g were observed at same period value of 0.72 s. The Miocene site has the peak S_a value of 1.15g at the period value of 0.48 s. The Quaternary group shows more variations in terms of either the peak S_a values or their corresponding periods after the 2D numerical analyses. The comparison between the spectral acceleration graphs obtained by the utilization of 1D and 2D numerical analyses is given in Figure 88 for one representative example from the each group.

When the results of the 2D response analysis are examined individually at the characterized sites, it can be observed that the spectral peaks of the 2D response analyses at all of the sites are greater than that of the 1D analyses (Figures 88 and 89). As can be seen in the comparison of the spectral curves for Comb09 (2), Comb06 (2) and Comb14 (1) in Figure 88, the 1D numerical analyses can estimate the similar behaviors of the spectral curves acquired by the 2D response analyses. However, when the response spectra of the sites [i.e., Comb09 (2) and Comb14 (1)] are examined in Figure 88, there is a considerable difference in the maximum spectral values. In addition, the position of the peaks with respect to the period axis is compatible with each other except the site of Comb06 (2). A shift in the period towards the lower values can be observed in the 2D response spectrum of Comb06 (2) according to the results of the 1D analyses (Figure 88). This response may be related with the topographical rise at this site and its close vicinity as stated by Jibson (1987), Geli et al. (1988), and Rathje and Bray (2001).

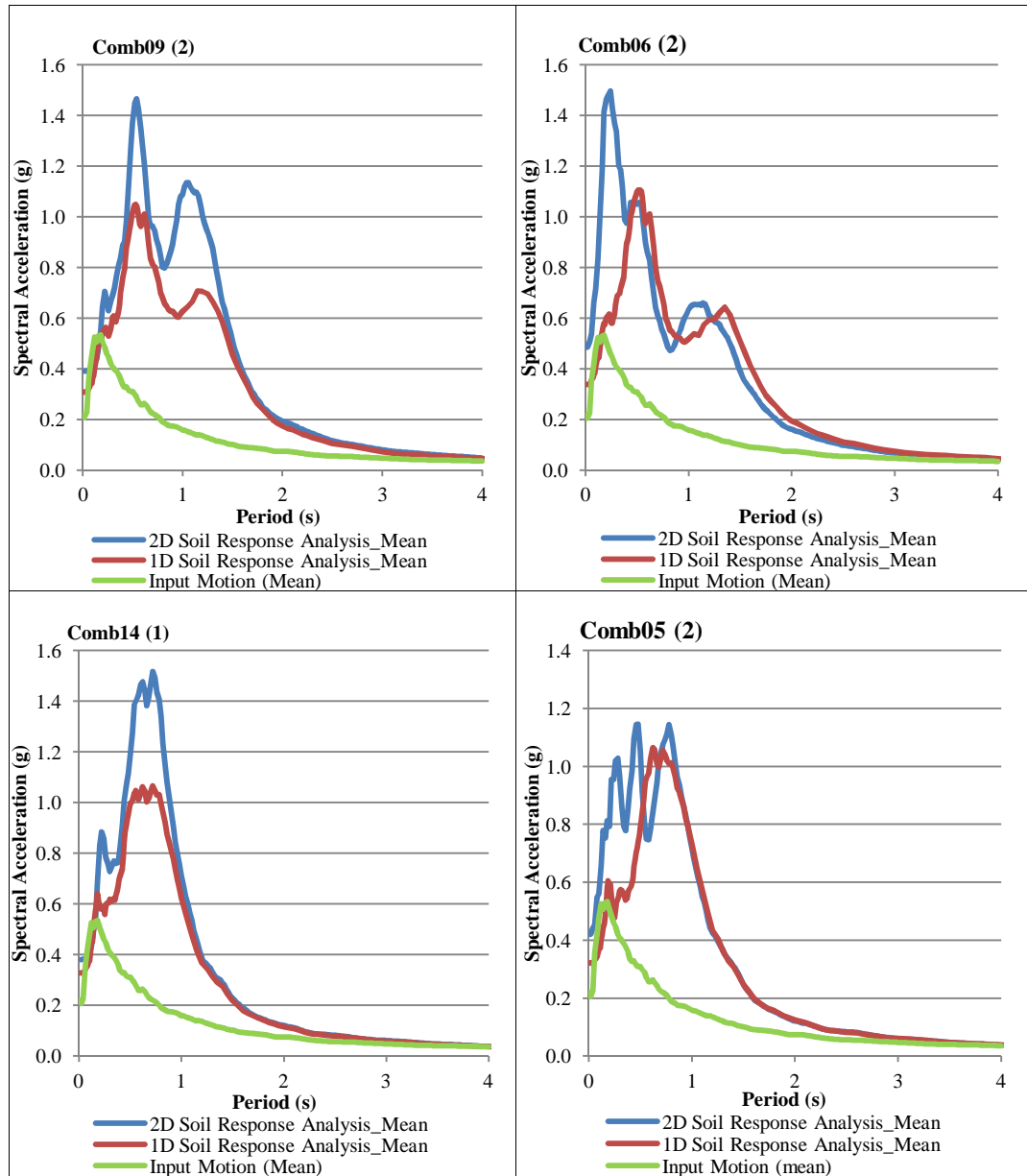


Figure 88. The obtained spectral acceleration curves for one representative site of the geological groups after performing 1D and 2D numerical analyses.

When the 1D and 2D spectral responses in the Miocene group example [i.e., Comb05 (2)] are examined in Figure 88, it can be seen that the behavior of the 1D and 2D peaks are different from each other. While the multiple peaks are revealed at the 2D spectrum, one strong peak takes its position in the 1D spectrum. When the 2D model of the N-S section given in Figure 92 is examined, it can be seen that this site is placed at the northern end of the N-S section. Also it is present within the Miocene unit. Due to the rise of the subsurface topography to the surface, the thicknesses of the sedimentary layers overlying the bedrock gradually decrease towards the north. It is evident that the thinning of these soft layers results in an impedance contrast in the results of the 1D analysis. Therefore, the amplitude of the peak S_a value is nearly similar with that of the 2D peak. However, because of the complexity of the wave field such as the effects of wave diffraction and phase conversion, 2D resonance can be observed at the low frequencies (high periods) in the 2D spectrum in Figure 88. The geometry of the bedrock surface and the boundaries of the geological units are the main factors responsible for this resonance.

In addition to these example sites given above, the 1D and 2D S_a responses of other sites [i.e., Comb01 (2), Comb04 (2), Comb12 (2)] where the 2D site effect phenomenon may make itself evident are given in Figures 89a, 89b and 89c. At Comb01 (2), the period of the maximum spectral acceleration value determined from the 2D analysis slightly shifts towards longer periods and the behavior of the curves are similar with each other (Figure 89a). This case is also observed at Comb04 (2) (Figure 89b). As stated before, Comb04 (2) is the site located approximately in the middle of the basin and the thickness of the sedimentary cover at this site is higher than the other sites characterized in this study. This condition may cause this non-linear behavior along with the effect of the subsurface topography and boundaries of the geological layers. One of the reasons leading to the differences between the results of the 1D and 2D numerical analyses may be that it is not possible to describe the complexity of the wave field regarding the effects of wave diffraction and phase conversion in the 1D numerical

model due to 2D/3D geometries of a valley. As stated above, these effects may lead to the generation of surface waves in different directions and the 2D resonance such as those observed in these sites in this study.

Figure 89c shows the 1D and 2D response spectral accelerations calculated at Comb12 (2) which is located close to the eastern end of the E-W section and the site is in the close proximity to the Miocene volcanics. Based on the constructed 2D model, the upper surface of the bedrock has an inclination beneath this site (Figure 93). Therefore, the influence of the 2D site effects manifests itself highly at this site as stated above. As can be seen in Figure 89c, the results of the 1D and 2D numerical analysis reveal two peaks in the spectral curve. Even though there are significant differences in the amplitudes of the peaks, the trend of the curves are almost similar. A slight shift to the longer periods can be followed in the 2D spectrum due to the 2D site effect. However, the S_a spectrum of the 1D analysis does not show a clear dominant peak, in other words, it has a broader peak. This observation may be related with the influence of soil stratigraphy on the 1D model since layer 3 was not observed at this site according to the results of the characterization studies.

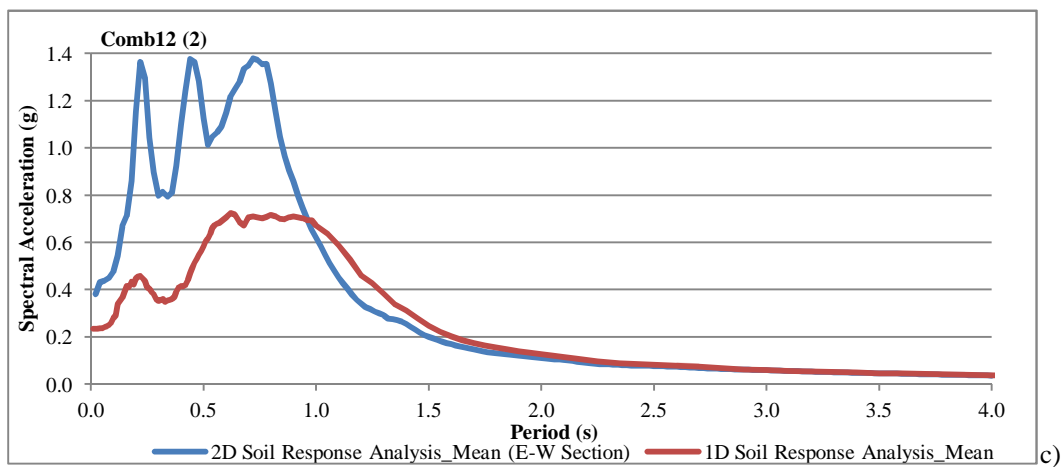
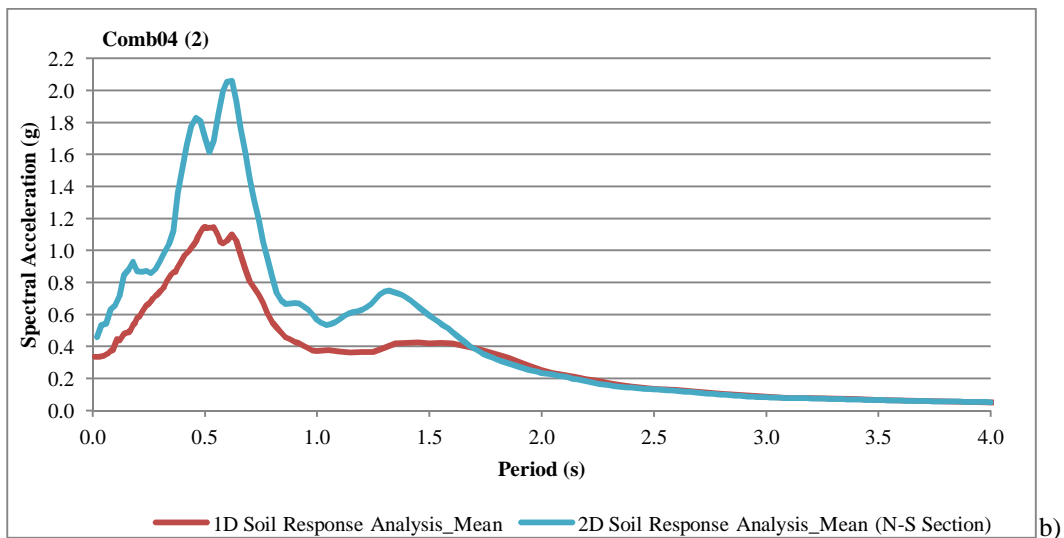
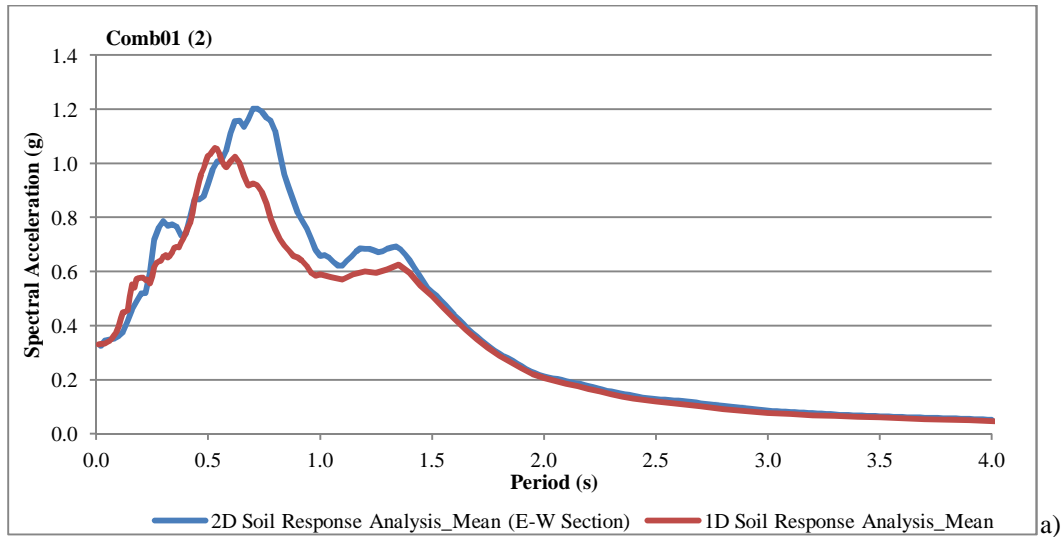


Figure 89. 1D and 2D S_a responses of the sites a) Comb12 (2), b) Comb04 (2) and c) Comb01 (2) where 2D effect phenomenon is observed.

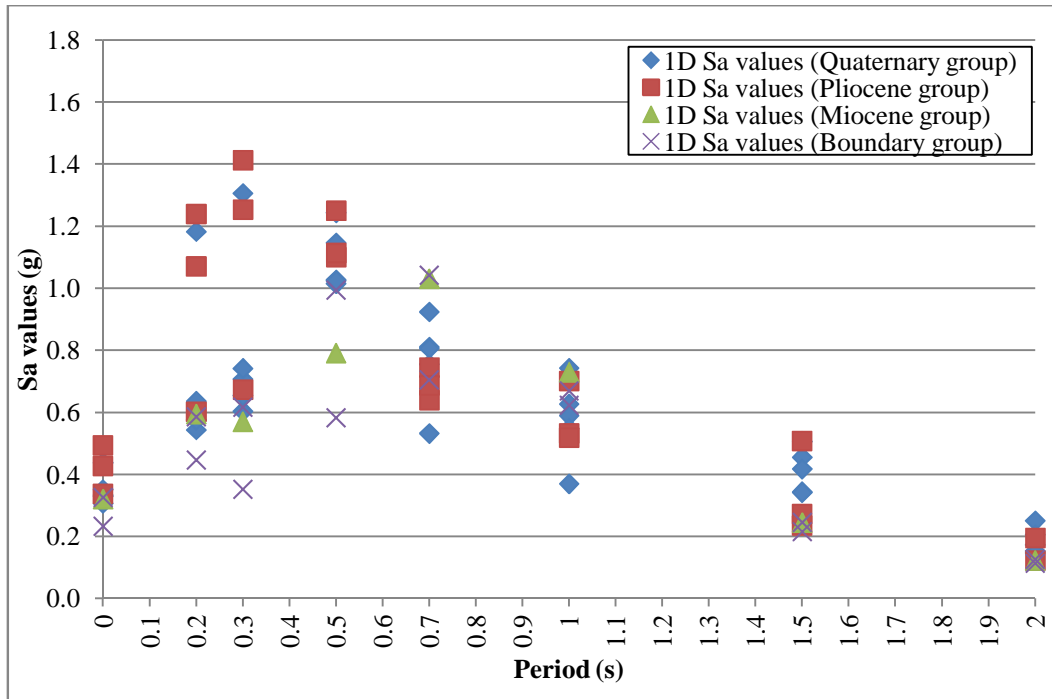
The variation of the peak S_a values with respect to the specified periods are given in Figure 90 in order to compare the performance of both numerical analyses for the seismic responses of the 11 sites. When the results of 1D analysis are examined, Figure 90a shows that the sites within the Quaternary and Pliocene groups show similar behavior at almost all specified periods. This means that the older Pliocene units have the same seismic response characteristics with the younger Quaternary units and the differentiation of these two units is not possible by using their responses. When the responses of the other groups are investigated in Figure 90a, it is observed that their characteristics are different from the above mentioned two groups, particularly at periods in the range of 0 -0.7 s. They have lower S_a values until 0.5 s. However, higher degree of responses emerge at the period of 0.7 s. After 1 s, their responses are determined as the lower bound.

The 2D Analysis results are grouped with respect to the geological units and examined by considering the specific periods (Figure 90b). As traceable from the figure, the Pliocene group shows high seismic response particularly the shorter periods. On the contrary, the Quaternary group behaves as a high dynamic response characteristic material at the period of 0.3 s. Their S_a values represent the upper boundaries of the responses of the other sedimentary units present at the study area. When the pattern of the S_a values of the Miocene is examined, it was observed that the relatively lower results are introduced for the Miocene site. These multiple peaks come out at the periods changing between 0.7 s and 1.0 s. Additionally, although the population number of the Boundary groups is only 2, it is remarkable that this group presents less variation at all specified periods and it gives a strong peak at around 0.7 s. In general, it can be stated that the Pliocene group shows significant peaks at relatively shorter periods when compared with the spectral accelerations of the Quaternary sites according to the results of 2D analysis.

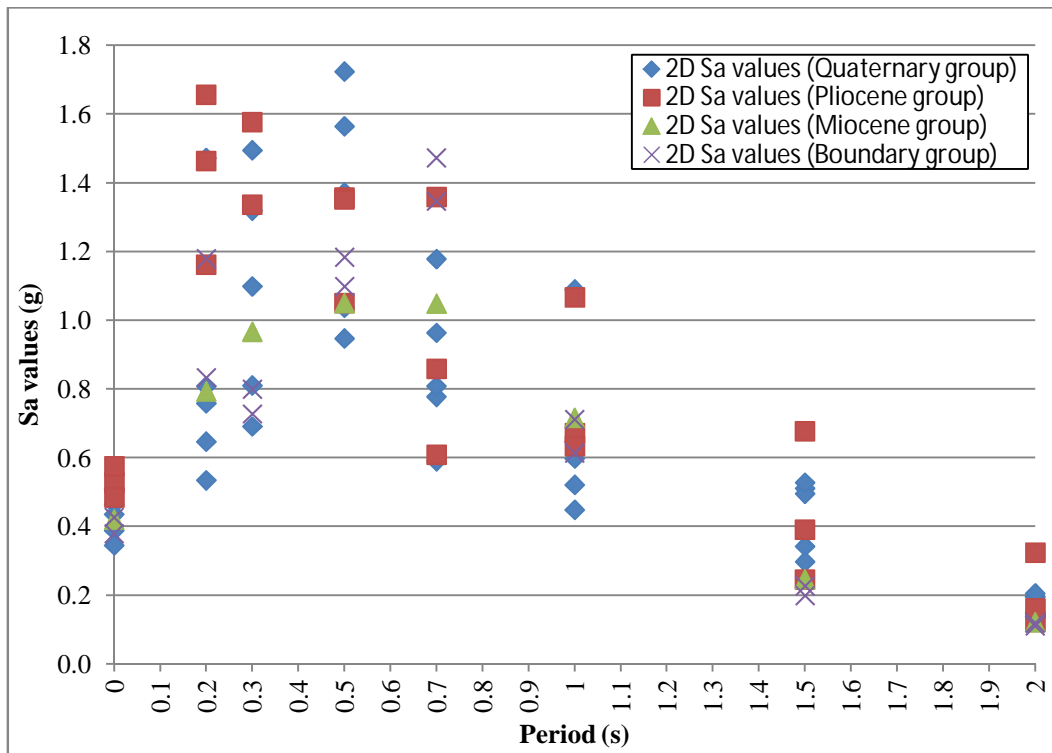
When the spectral acceleration results of the 1D and 2D analyses are compared (Figures 90a and 90b), it is evident that the 2D analysis estimates higher spectral

peaks at the determined periods less than 1 s for all geological groups. In addition to this, the 2D numerical results of the Quaternary sites give higher S_a values at the longer periods, when compared with the results of the 1D analysis. When these two figures are examined, the maximum S_a values obtained by the 2D analysis is compared with the results of the 1D analysis and generally it can be stated that the ratio of the maximum 2D S_a values to the highest 1D S_a peaks ranges between 1 and 1.5. There are only two outlier sites present above the upper boundary (i.e., 1.5) in the data. These sites Comb04 (2) and Comb12 (2) are classified into the Quaternary and Boundary groups.

Moreover, in order to investigate the prediction skills of the models, the maximum horizontal accelerations (MHA) at the surface determined by the 1D and 2D numerical analyses are correlated. The utilized MHAs were calculated by taking an arithmetic average of the 1D and 2D results of the utilized seven input motions for the 11 sites. The data in Figure 91 show that the variations of the mean MHA values are constrained by the upper (1:1.35 line) and lower (1:1 line) bounds. The data shows these variations especially when MHA_{1D} is changing between 0.2g and 0.4g. For the range of the above given MHA_{1D} , the results of 1D analysis are considerably unconservative since the ratio of the MHA_{1D} to the MHA_{2D} is less than 0.75. For the greater MHA_{1D} values, the distribution of the data approaches the line of equality. As can be seen in the figure, the MHA_{1D} and MHA_{2D} values of the majority of the sites are calculated within the range of 0.2g to 0.4g. However, the Quaternary group has significant variations in the MHA_{1D} and MHA_{2D} data when compared with the Pliocene sites. Also, both the higher and lower values of the Pliocene sites are greater than the corresponding upper and lower bounds of the MHA values of the Quaternary sites based on the results of either the 1D. Additionally, the MHA_{1D} and MHA_{2D} values of the Miocene and Boundary sites are substantially lower than the other two groups. This can be observed in Figures 90a and 90b.



a)



b)

Figure 90. Comparison of the results of the a) 1D and b) 2D numerical analyses in terms of the peak spectral acceleration values and their corresponding periods.

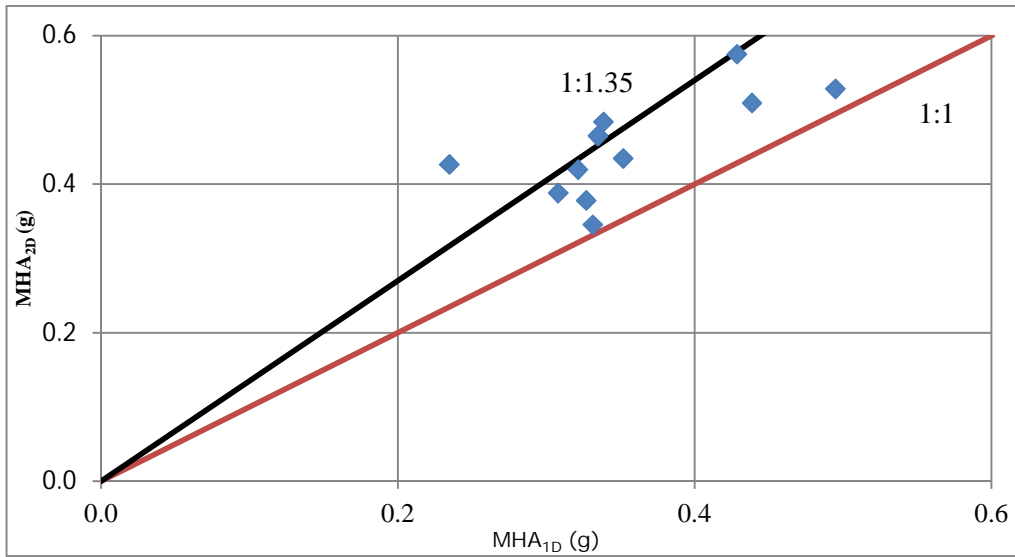


Figure 91. Comparison of the maximum horizontal accelerations obtained by the 1D and 2D numerical analysis.

5.3. Comparison of the results of the site effect studies

In this stage, the characteristic seismic responses of the 11 sites obtained by the experimental and numerical methods were compared and evaluated. As stated in the previous sections of this chapter, the site effects within the Orta pull-apart basin was primarily assessed by the results of the experimental study based on the determination of the fundamental frequencies and H/V amplitudes at the sites. This methodology was based on the microtremor measurements processed by the Nakamura method. Secondly, the numerical seismic response analyses were performed by using 1-D Shake2000 and 2-D QUAD4M programs via the utilization of the data acquired from the studies given in Chapter 3. A comparison and evaluation of the site effects determined by using these different techniques enabled to confirm the results of Nakamura method of which the usage is under discussion for the site effect studies in the literature.

Since the excessive information was already given in Chapter 4, briefly it can be summarized that many studies (e.g., Lermo and Chavez-Garcia, 1993; Nakamura, 1989, 1996 and 2000; Toshinawa et al., 1997; Konno and Ohmachi, 1998) show that the actual site amplification can be estimated by the H/V spectrum obtained by the Nakamura method. Additionally, other studies (e.g., Cid et al., 2001; Satoh et al., 2001; De Luca et al., 2005; Barani et al., 2013) regarding the comparison between experimental and 1D/2D numerical methods show that there is a good correlation between the results of the utilized techniques. However, many theoretical and experimental studies proposed by different researchers (e.g., Lachet and Bard, 1994; Teves-Costa et. al., 1996; Bour, 1998; Bard, 1999; Duval et al., 2001; Nguyen et. al., 2004; Haghshenas et al., 2008; De Ferrari et al., 2010) reveal that the derived spectral ratio by using the Nakamura method is not capable of estimating a reliable amplification value of a ground motion at the surface.

In order to compare the utilized site effect techniques, the amplification ratio spectra of the results of the 1D and 2D analyses at the 11 sites were prepared, according to the outputs of the Nakamura method. However, before examining and comparing the spectral acceleration curves, initially the results of the 1D and 2D analyses covering the entire two cross sections were introduced in order to understand the effect of basin geometry on the dynamic response. In this respect, the spatial variation of the ratio (hereafter termed as A_{MHA}) between the maximum horizontal acceleration (MHA) on the each node along the surface ($A_{MAX,S}$) and the MHA corresponding to the nodes at the bedrock ($A_{MAX,R}$) was investigated. Therefore, the arithmetic average of the A_{MHA} values acquired by the simulation of the seven earthquakes was compared with the geometrical properties of the generated 2D models. The distributions of the 1D and 2D A_{MHA} values along the 2D soil model of N-S (A-A') and E-W (B-B') sections are given in Figures 93 and 94, respectively.

When the A_{MHA} results of 1D and 2D response analysis along the N-S cross section is examined in Figure 92, it is easily seen that 2D analysis results of the

A_{MHA} values are higher than the 1D numerical method. The 2D amplification ratios show variations in the range of 1 to 4. Generally, the A_{MHA} values are clustered between 2 and 3. This means that the PGA values of the input rock motion are amplified by 2 to 3 times at the surface. On the other hand, the 1D A_{MHA} values vary between 1.6 and 2.3. The values are generally gathered around the value of 1.7. As can be observed from the figure, de-amplification phenomenon is not present along this section based on the results of the 1D and 2D analyses. When the figure is examined from north to south, the highest amplification can be seen at the slopes of the subsurface topography [i.e., zone1 between the western end of the section and Com05 (2); zone2 between the sites of Comb07 (2) and Comb04 (2); zone3 between the sites of Comb04 (2) and Comb08 (2)]. These observations are mostly related with the lateral variations of the upper boundary of the bedrock. When the trend of the A_{MHA} values obtained from 2D analysis are compared with the 1D A_{MHA} values (Figure 92), it can be observed that the 2D site effects take place especially at the measurement sites Comb06 (2); Comb04 (2) and Comb08 (2). At Comb04 (2) and its close vicinity, the 2D numerical analysis estimates moderately higher A_{MHA} values. At this area, the thickness of the basin reaches its highest value (Figure 93). Finally, some abrupt changes of A_{MHA} values can be seen along the sections especially at the sites of Comb04 (2) and Comb08 (2) due to the presence of the interlayer boundaries within the 2D model.

As can be seen in Figure 93, the 1D A_{MHA} values show variations in the range of 1.2 to 2.5. The values are generally clustered around 1.7. The prominent deviations from the general trend can be observed at the site of Comb03 (2) and Comb12 (2). Since the sites are present in areas where relatively lower 1D and 2D A_{MHA} values were obtained, making interpretations regarding the comparison of discrete 1D A_{MHA} values with the relatively continuous 2D A_{MHA} outcomes has some difficulties while tracing the trend of the 1D A_{MHA} values along the section especially for the first five sites from the north. However, at the last three sites along the section, 1D analysis is able to capture the pattern of the 2D A_{MHA} values (Figure 93). When the figure is examined, it can generally be said that the

variations of the 1D results can be correlated with the behavior of the MHA amplifications calculated by a 2D analysis. However, it is obvious that the degree of the 2D A_{MHA} is greater than 1D A_{MHA} at every site.

Figure 93 shows the distribution of the A_{MHA} results obtained from the 2D soil response analysis along the E-W section. These amplification ratio values vary in the range of 1.7 to 3.6. As can be seen in Figure 93, the A_{MHA} values do not decrease below the amplification ratio value of 1. This means that de-amplification phenomenon is not observed along the E-W section as present at the other section and the results of the 1D analysis. Along this section, the A_{MHA} values show clustering between 2 and 2.5. The spatial variation of this value along the E-W section is less than what it is observed at the first one. When the figure is followed from east to west, the highest amplification can be observed at the slopes of the subsurface topography. This observation is also given and valid for the N-S section.

On the basis of conservation of energy, along the basin, the ratio of 2D to 1D maximum horizontal accelerations is expected to be higher than 1.0 where basin effects are more pronounced; and smaller than 1.0 where basin effects are less pronounced. However due to lack of closely spaced 1D site response analyses, the regions where 1D analyses are expected to be more critical could not be captured. This is listed as one limitation of current study. However, the number of the zone and the width of these zones where the largest A_{MHA} values are revealed are relatively lower when compared with those along the N-S section as stated above. Three zones are determined; i) zone1 between the western end of the section and Comb14 (2); ii) zone2 at around Comb09 (2) and iii) zone3 between Comb12 (2) and the eastern end of the section.

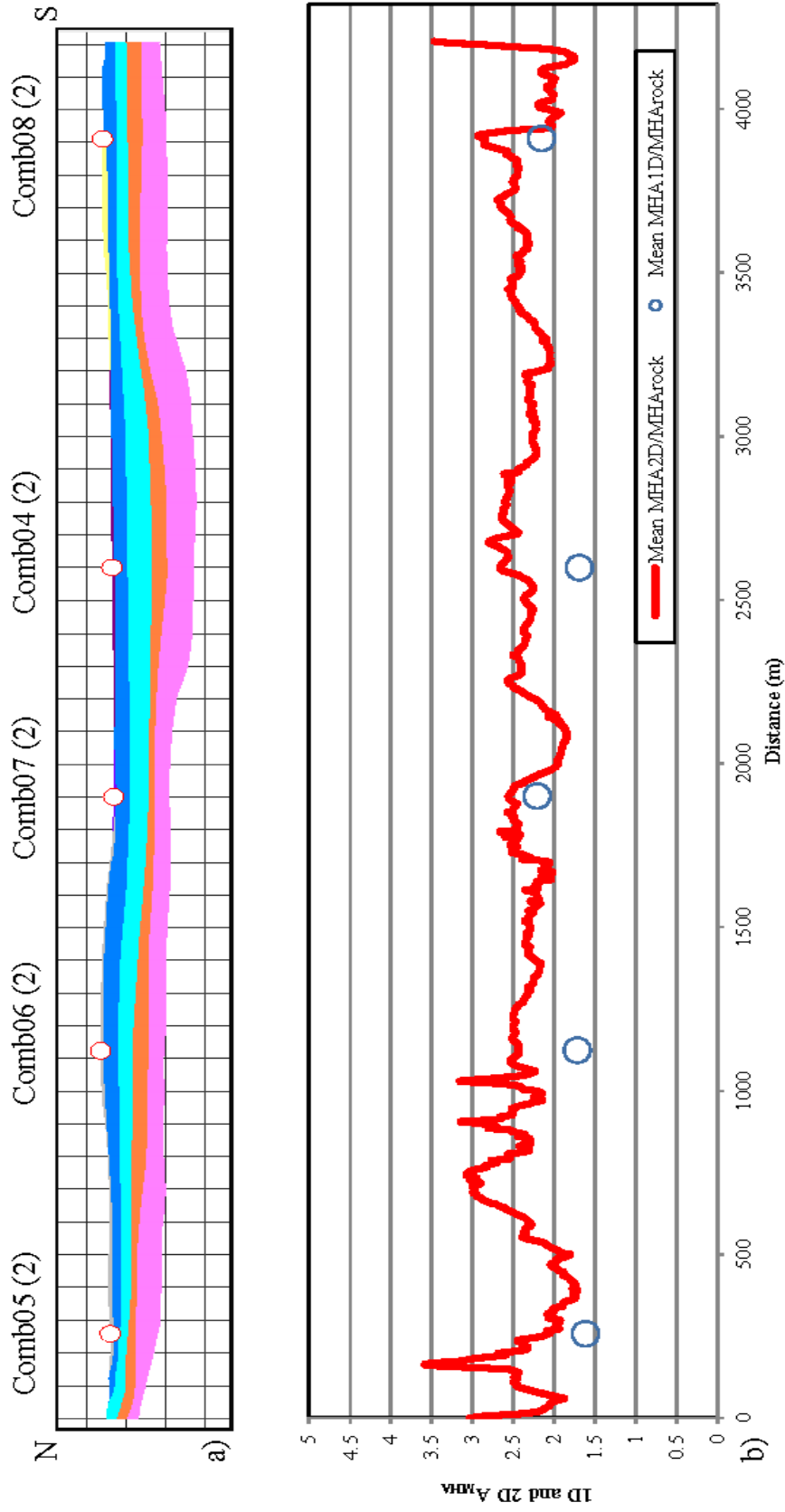


Figure 92. a) The 2D soil model of N-S (A-A) section along with distribution of the b) 1D and 2D A_{mHA} values.

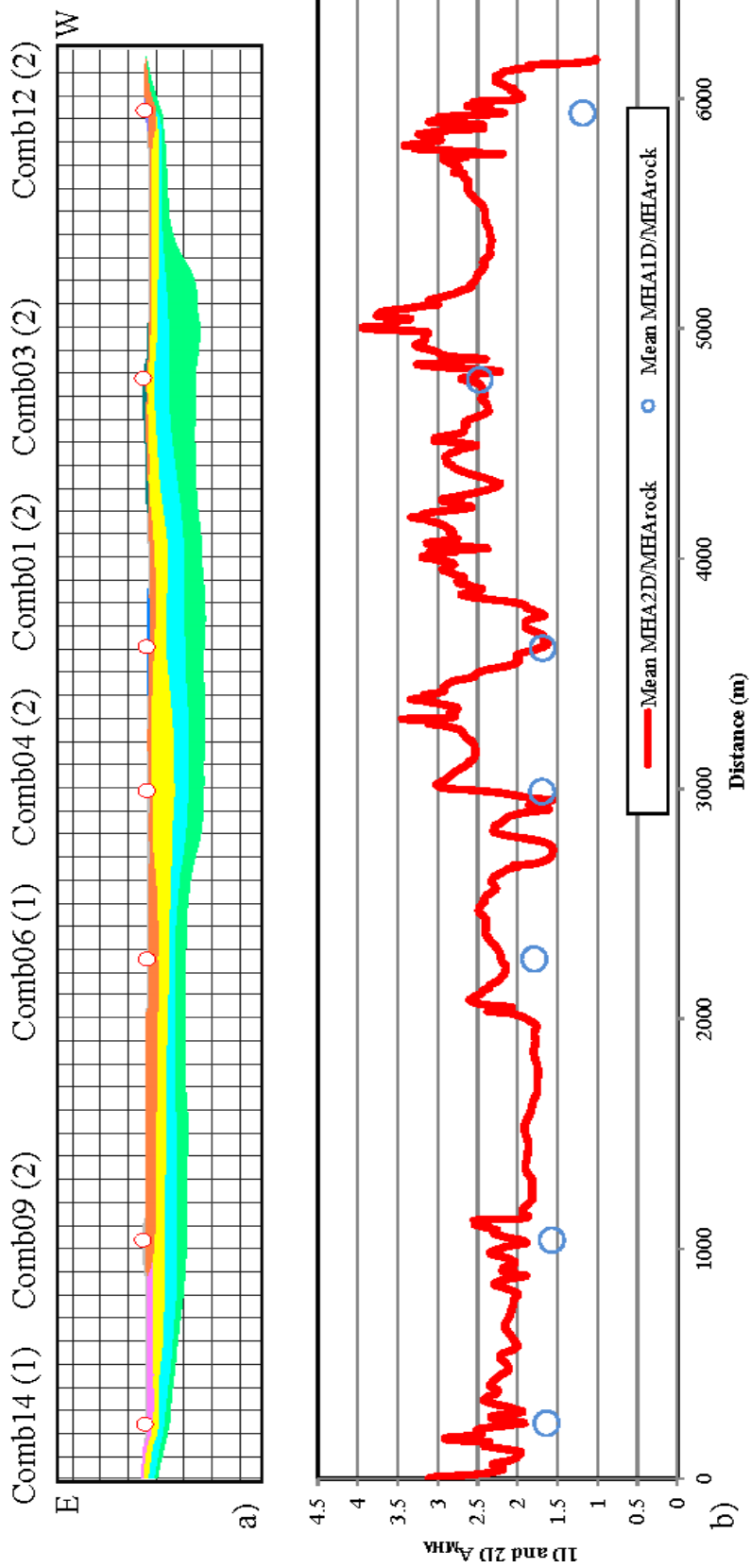


Figure 93. a) The 2D soil model of E-W (B-B') section along with distribution of the b) 1D and 2D A_{MHA} values.

In order to understand the existence and influence of the 2D site effects at a site, the best way is to compare the amplification ratio spectra obtained by both the 1D and 2D numerical analyses. In order to make a comparison between the results of both numerical models, four examples sites were selected (Figure 94). These sites are present mostly at the Quaternary unit where a 2D site effect is observed. Additionally, during the selection of the sites, one of the considerations was the availability of the microtremor survey conducted at both phase 1 and 2 in order to demonstrate the degree of the correlation between the site effect estimation methods. As can be seen in Figure 94, the two peaks are captured by a 2D analysis at these four sites. Also, 1D analysis gives similar amplification ratio spectra at the three sites such as Comb01 (2), Comb04 (2) and Comb06 (2). The thickness of the sediment cover is very high at these sites. As stated before, Comb01 (2) and Comb04 (2) are situated almost in the middle of the basin. As can be seen in the figure, the performance of 1D analysis is highly sufficient to estimate the fundamental period of the sites.

When compared with the results of the 1D analysis, a 2D numerical analysis gives higher amplification ratios especially at the sites along the E-W sections. This was observed due to two important reasons: i) the performed numerical analyses is based on the different theoretical fundamentals. Therefore, the QUAD4M analyses can reveal systematically higher S_a values than the results of the Shake2000 at these sites since it is known that this program generates lower damping ratios for the input motions with higher intensity and frequency, and ii) presence of the 2D site effects in the study area, namely focusing of seismic waves, generation of surface waves at fault controlled edge structures and possible 2-D resonance. Because of these, the 2D model introduces amplification peaks that can be increased to some extent (Lanzo and Pagliaroli, 2012). On the other hand, the 1D model only considers the resonance of vertically propagating shear waves, as explained in the previous chapter. However, a considerable period shift to the longer periods was not observed in the amplification spectra of the given examples due to the 2D site effect. Therefore, the differences between the results of the

numerical methods may also be related with their different assumptions in order to simulate the soil responses along with the 2D resonance.

When the sites present along the N-S sections are taken into consideration, the amplification ratio of the sites [Comb06 (2); Comb07 (2) and Comb08 (2)] obtained by 1D analysis are greater than those calculated by the 2D analysis. The comparison of the 1D and 2D amplification spectra of Comb06 (2) can be seen in Figure 94. Because of the decrease of the thickness of the sedimentary layers overlying the bedrock at these sites (Figure 92), the impedance (velocity) contrast in the results of the 1D analysis makes itself significant and this leads to the estimation of the higher amplification ratio values with respect to the results of 2D analysis (edge to basin effect). By considering all the calculated spectra at each site, it can be concluded that, although there are major differences in the amplification ratios, the behavior of the 1D amplification curves appears to estimate the site effect at many sites [e.g., Comb01 (2), Comb05 (2), Comb06 (2) and Comb08(2)] in the study area.

In general, based on the results of the 1D and 2D analyses at the sites located along the two constructed sections, it can be concluded that different seismic surface responses were calculated at the sites present at different sections. A comparison of the simulated results basically reveals that the basin effect manifests itself especially at the sites along the E-W section. As stated before, the trend of this section is along the same direction with the longer axis of the basin. In other words, it is more or less parallel to the depositional zone of the active river system. Based on the results of the 2D seismic simulation, higher amplification ratios are observed when compared with the results of the 1D analysis at all the sites along this section. At the sites [i.e., Comb06 (2) and Comb07 (2)] located along the N-S section, the basin edge effect is more dominant and higher ratios arise after the 1D analysis. At the common site of these two section [i.e., Comb04 (2)], it is noted that the basin effect governs the site responses.

Figure 94 also contains the H/V spectral curves derived by the processing of the records acquired by both Phase 1 and 2 of the microtremor survey. Four H/V spectra obtained by phase 2 shows peaks at lower frequencies. This is observed at many sites such as Comb01 (2), Comb03 (2), Comb05 (2), Comb06 (1), Comb07 (2), Comb08 (2), Comb09 (2) and Comb14 (1). In other words, the Phase 2 H/V results is compatible with the results of the numerical methods for only three investigated sites, two of them [i.e., Comb04 (2) and Comb06 (2)] are given as an example in Figure 94. These discrepancies are mostly associated with the P-wave velocity (V_p) contrast within the same layer governing the behavior of the horizontal components. This contrast is probably related with high groundwater level in almost the entire area covered with the Plio-Quaternary units. Therefore, in the context of this study, the results of the second phase microtremor survey were proved to be inadequate to estimate the seismic response at the study area. Consequently, its utilization is not suggested at sites with similar geological characteristics.

The results of the Phase 1 study can be compared for 8 sites where numerical analyses were performed. There are no measurements at the Phase 1 study for the remaining 3 sites. According to Figure 94, the pattern of the H/V curves obtained by the first phase microtremor survey is compatible with the results of the 1D and 2D numerical analyses in terms of the fundamental periods. The Phase 1 H/V curves are very promising for the determination of the fundamental periods of the sites such as Comb01 (2), Comb03 (2), Comb04 (2), Comb06 (1); Comb07 (2), Comb08 (2) and Comb09 (2). This means that more than 85% of the sites could be characterized by using the microtremor method. One of the incompatible sites [i.e., Comb06 (2)] is given as an example in Figure 94. However, H/V amplitudes generally represent the lower boundaries when compared with the results of the 1D and 2D amplification spectra. This is valid especially for the sites such as Comb01 (2), Comb04 (2), Comb06 (1) and Comb09 (2). However, when the impedance contrast ratio between the relatively stiff and soft sediments is high, or the upper surface of the bedrock is close to surface, H/V amplitudes give the upper boundary

of amplification values at the site effect studies in this study. The behavior of the H/V results has similarities with the outputs of 1D and 2D analyses when the sites are located at the different sections. It should be noted that the numerical analysis utilizing equivalent linear approach causes over-amplification at soil response spectrum during a large magnitude earthquake due to nature of the method. As mentioned in Chapter 4, 2D QUAD4M (Hudson et al., 1994) and 1D Shake2000 (Ordonez, 2000) programs use equivalent linear assumptions. This means that higher amplification values or higher spectral acceleration values might be obtained by performing these methods. Therefore, the microtremor results might represent actual soil response at the ground surface rather than giving lower bounds. However, there is no available destructive earthquake record at the site, therefore it is not possible to compare the results of the site effect studies with the actual data. Therefore, the usefulness of the spectral H/V ratio of the microtremor method remains a mystery.

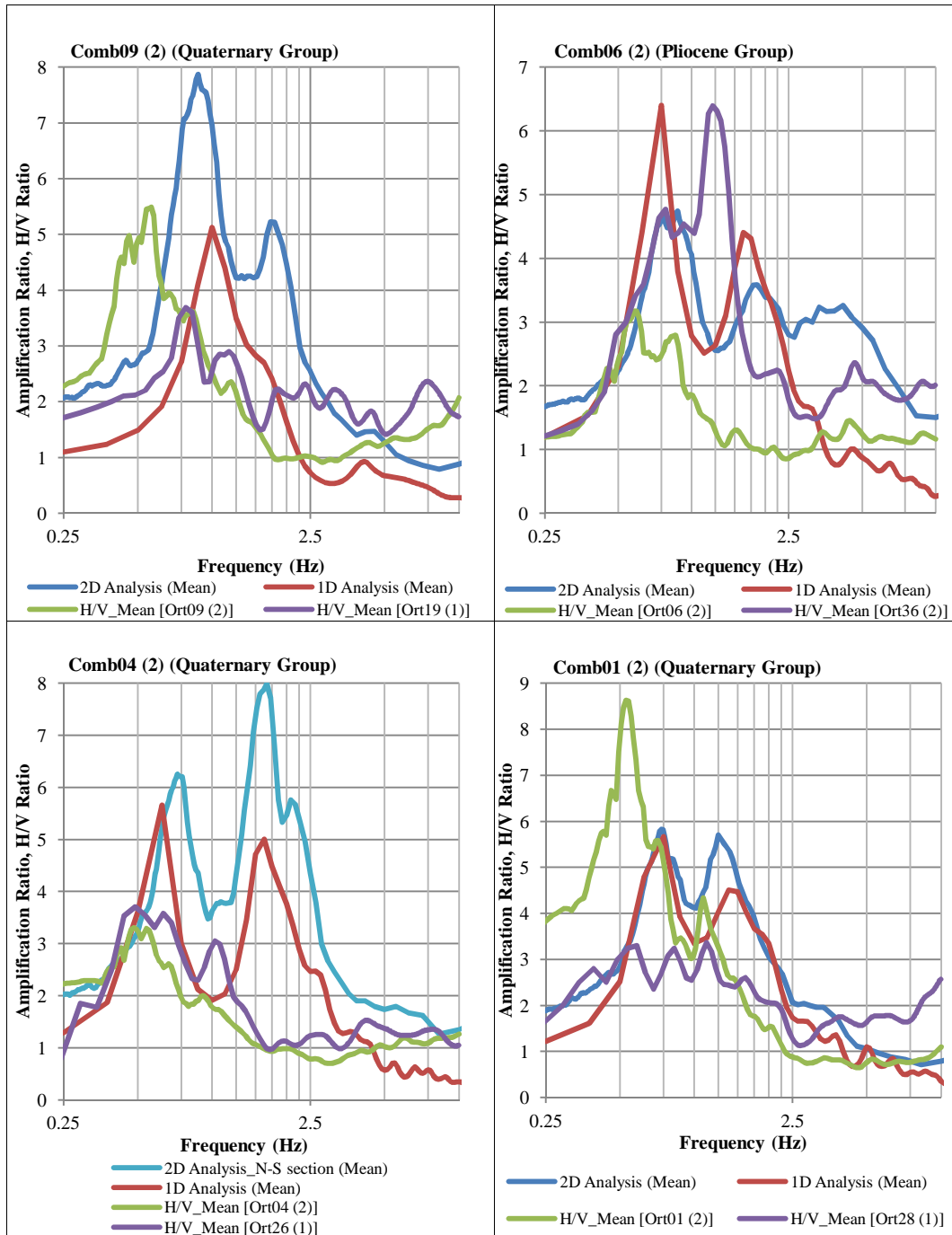


Figure 94. The acquired amplification ratio curves obtained by the site effect studies.

CHAPTER 6

DISCUSSION AND CONCLUSION

This study encompasses an accurate estimation of seismic responses at sites possessing soft and unconsolidated characteristics within the Orta basin by performing 1D and 2D numerical analyses. In accordance with this purpose, 2D QUAD4M (Hudson et al., 1994) and 1D Shake2000 (Ordones, 2000), which are widely used programs in scientific and engineering applications were preferred. As stated in the previous chapters, these programs use equivalent linear approach. Based on the results of these two numerical methods, similarities and differences between the 1D and 2D ground response analyses simulated by considering high intensity levels of the selected and scaled earthquake sets were identified. The earthquake set (suit) was determined based on the seismo-tectonics of the study area.

In the context of this study, to simulate dynamic soil response behavior by using either 1D or 2D analysis techniques stated above, four main tasks were performed: i) constructing target spectrum for the site, ii) selecting and scaling input rock motions, iii) characterization of shear wave velocity profile, and iv) determination of the non-linear soil characteristics. All these items were obtained based on the field studies and analyses conducted within this dissertation. Therefore, this approach of identifying all the input and output parameters in the same research resulted in and was accompanied by the discussions of the many parameters obtained in each sub-study. Additionally, low strain measurements were acquired from the field by using a single and mobile velocimeter in order to compare the results of the 1D and 2D numerical simulation with the H/V curves obtained from

microtremor records. Therefore another research topic investigating the capability of the low strain measurements in the estimation of the site effects observed during a ground motion having a high strain level was addressed.

In order to perform the research subjects described above, the Orta District located to the west of the Çankırı Province was selected as the study area. The reasons for this preference were: i) the district is located at a region close to the North Anatolian Fault System which is one of the most significant active fault systems both in Turkey and in the world with a considerable earthquake potential, ii) the occurrence of the 2000 Orta earthquake along a fault zone (Dodurga Fault Zone, DFZ) which was not identified before in the active faults map of Turkey (Şaroğlu et al., 1992), and the introduction and addition of this fault zone to the literature in the close vicinity of the study area (Emre et al., 2000; Koçyiğit et al., 2001), iii) a possibility of the continuation of the active DFZ to the south until the Çubuk District in Ankara (Koçyiğit, 2008), and iv) the tectonic evolution of the basin where the Orta District is settled.

When the study area was examined geologically on a regional scale, although there are different geological evolution models for NW Central Anatolia in the literature, the general consensus is that, the region has been exposed to a new tectonic period due to the continental collision during the Neogene period. In other words, all the proposed models (Koçyiğit, 1991a, 1991b, 1992 and 1995, Seyitoğlu, 1997 and 2000, Kaymakçı, 2000 and Kaymakçı et al., 2001) refer to a new tectonic period during Late Miocene or Late Pliocene. Since the sedimentary units deposited during the time of neotectonic period show soft and unconsolidated characteristics, this information is a good indicator to designate the geological units where the field studies are focused in order to determine the local soil conditions (Koçkar and Akgün, 2008 and 2012; Eker et al, 2012; Eker et al., 2015). Based on the statement given above, the Pliocene and Quaternary sediments were considered as the most susceptible deposits where this study was mainly concentrated on.

On the other hand, even though these models generally agree on the time of this new tectonic period, they have a major discrepancy about the tectonic setting dominating the region. Based on the results of the performed studies in this dissertation and by synthesizing the information acquired by the excessive literature survey about the geology and seismo-tectonics on a local scale, the new tectonic setting considered in this thesis is considered to be an intra-continental tensional Neotectonic regime with oblique slip normal faulting as stated by Koçyiğit et al. (2001) and Koçyiğit (2003).

Under these geological conditions, it can be stated that the area is a pull-apart basin and its evaluation has been controlled by the oblique slip normal faults. At the study area, there are many local faults having strike slip mechanism with a significant normal component (Koçyiğit et al., 2001). This mechanism led to the formation of a depression at that time and this depression was occupied by both lacustrine and mostly fluvial clastics. The depth of the depression increases due its center line. It is known that the sediment thickness within the basin is more than 145 m (Tokan and Özgen, 1976). Based on the deep borings compiled from the previous MTA studies (Tokan and Özgen, 1976), volcanic products, especially basalts, are inter-fingering with the sedimentary deposits at the western side of the pull-apart basin. It was considered that this intrusion which occurred in Miocene might have a significant lateral extent within the area. This inference is of significant importance to describe the seismic properties of the layers in the construction of the 1D and 2D models utilized in the further analyses.

When the seismo-tectonic properties of the NW Central Anatolia are investigated, it can be observed that the major earthquakes have mostly occurred along the sections of the NAFS. There are five destructive earthquakes ($M > 6$) recorded during the instrumental period in the vicinity of the study area. Based on the spatial distribution of these earthquakes and the relevant fault segments, a characteristic earthquake magnitude was calculated with a deterministic approach. As a result of the studies regarding the description of the seismo-tectonic

properties of the area, the segments of the major fault zones were defined. Based on their closest proximity to the area and their capabilities of creating earthquakes in terms of magnitude, the fault segment of the NAFS belonging to the 1951 Kurşunlu Earthquake fault rupture was determined as the most critical one among the others. According to the equations proposed by Wells and Coppersmith (1994), the characteristic moment magnitude was determined as 7.2. Based on the statistical distributions in the estimation of the earthquake magnitudes along a strike slip fault by using the rupture area (Wells and Coppersmith, 1994), this magnitude is equal to the median value plus about a 1.7 standard deviation. When it is considered that the moment magnitude of the major earthquakes experienced is ranging between 6.0 and 6.8 at the region (EERC-ERD, 2009; DDA, 2015; KOERI, 2015), it can be stated that the calculated moment magnitude (7.2) is sufficient to cover the aleatoric variability. This corresponds to a value having more than 84% probability of non-exceedence.

As stated before, the recent most destructive earthquake occurred in the area is the 2000 Orta event. This event was recorded by six different strong ground motion stations located at a distance ranging between 12.3 km and 276.6 km away from the DFZ. Based on the recorded maximum horizontal acceleration values (MHA), various next generation ground motion prediction equations and previously proposed attenuation relationships were utilized to predict the MHA values of the actual records of this earthquake. It was observed that the prediction capabilities of the GMPEs such as ASK 2014, BSSA 2014, CB 2014 and CY 2014 were considerably better than the others especially for the MHA values recorded at the mid- and far-field stations. Additionally, none of the utilized equations were able to predict the MHA value observed at the Çerkeş Station located at the near distance of the DFZ. Based on the distribution of the estimated MHA values obtained from the four GMPEs with respect to the actual records given above, a logic-tree approach was used in the weighing process of these GMPEs. According to the four weighted GMPEs, a target spectrum was constructed. Additionally, in order to take the epistemic uncertainties related with these equations into

consideration, one standard deviation was added to the weighted median value. It was observed that this is a more conservative approach than multiplying the median values by 1.5 as suggested by ASCE 7 (2010).

After all these processes were completed, the input ground motions were selected in order to perform the deconvolution process in the numerical analyses. Various suits containing seven earthquake records were formed by utilizing PEER NGA West-2 database with the consideration of a set of criteria including: i) only main shocks were taken into account, ii) only one record from any single event was selected for each suit, iii) the moment magnitude of the interested records was constrained between 6.5 to 8, iv) the distance between the strong motion stations and the relevant faults was limited to range between 10 km and 45 km, v) the records of the stations installed at stiff sites were picked and the stiffness was controlled by the V_{S30} value, and finally vi) the records having MHAs greater than 0.05g were utilized in the suits. By implementation of these criteria, 15 earthquake records of nine events were selected. Also in the creation of the suits, these records were scaled with respect to the MHA values of the target spectrum. A database consisting of a total of 30 records were established and the suits were constituted by the selection of seven ground motion records from the this database according to the criteria given above. Each of the suits was scaled with respect to the target spectrum based on the time-domain technique proposed by Lilanand and Tseng (1988). After the trial and error process with respect to the degree of maximum and average misfits of the suits, the most representative suits for the target spectrum were selected in order to perform 1D and 2D seismic response analyses. Depending on the mean of the seven scaled records forming the best fit suit, the dominant period of the mean input motion was calculated as 0.18 s with a spectral acceleration value of 0.533g.

Associated with the main purpose of this study, accurate characterization of the shear wave velocity profile at the sites is a very critical step in order to obtain reliable results from the numerical methods. Therefore, an elaborate database

including the results of the geotechnical field and laboratory tests, and in-situ geophysical tests based on surface wave testing methods was constructed. During the construction stage of this database, the main considerations were to quantitatively characterize the geological characteristics of the area with field tests within soft and unconsolidated sediments where a potential to observe the influences of the local soil condition and topographical effect on the ground motion were present. Therefore, these studies mainly concentrated on the Pliocene and especially Quaternary alluvial sediments deposited at the north of the Orta pull-apart basin where most of the settlement area is located.

In the geotechnical studies, a database was constructed by a compilation of the previous studies conducted in the Orta District. This data encompasses 20 geotechnical borings having a total of 308 m depth drilled at the sites falling within the Quaternary and Pliocene geological units. The database contains the results of the SPT performed at every 1.5 m of the boreholes at each of the 20 sites. Along with this data, total of 122 disturbed and undisturbed soil samples were taken from the borings to determine the soil index parameters (i.e., natural water content, liquid limit, plastic limit, plasticity index, grain size distribution and natural unit weight) via geotechnical laboratory tests. In addition to this data, 9 trial pits were excavated during this study to expand the data for the shallow layers (<2 m). The samples were taken from the pits and the laboratory tests were performed to assign these index parameters to the sites. Also, these pits allowed a geological inspection of the sediments.

According to the geotechnical data, coarse grained soils were present at the uppermost depth of 8.5 m within the Quaternary alluvium deposits. The deeper parts of the Quaternary units (>8.5 m) and the entire Pliocene data were mostly comprised of fine grained particles. Based on the geotechnical boring logs and trial pits, the ground water level has higher variations within the Quaternary unit. The level can be observed at a depth ranging between 0.9 m and 5.4 m, and the data cluster is around 2 m in this unit. Interestingly, the level is also located at the

shallower parts of the soil within the Pliocene unit and it has a range between 0.6 m and 2 m.

Moreover, when the Quaternary and Pliocene data is compared, the variation of the SPT-N value with depth shows a similar trend after a depth of 12 m. However, these two datasets show considerable variations at the shallower parts of the 15 m soil column. When the distributions of the SPT-N values throughout the soil columns of the entire data set was examined, it was figured out that the average SPT-N values increase almost gradually with depth. Characterization of the soils based on the geotechnical data is available up to the depth of 20 m which is the maximum depth of the boreholes drilled in the region. Furthermore, in the database, there are several refusal values belonging to the Quaternary deposits due to the considerable gravel content of the layers. Due to the nature of this field test, artificially higher values can be obtained from coarse cohesionless soil bearing layers. Therefore, utilizing SPT-N results to determine the stiffness of these layers may lead to misinterpretation (Eker et al., 2013 and 2015). In the context of this study, considerably deeper parts of the sediment layers should have been characterized as much as possible along with the accurate identification of the shallower layers in terms of shear wave velocity values. The surface wave measurement technique is one of the most preferred ways due to its advantages regarding time, cost and application when compared with this destructive geotechnical method.

In the scope of this study, two campaigns were organized to acquire active (MASW) and passive (MAM) surface wave measurements in order to determine the seismic properties of soft and unconsolidated Quaternary alluvium deposits and Pliocene sediments within the Orta pull-apart basin. The first survey was performed in September 2009 and the second was executed in June 2014. A total of 58 surface wave measurements were taken at 29 different sites by using linear array configurations. Additionally, a MAM survey was performed by using L-shape and triangular array geometries at 12 and 6 sites, respectively, in the second

phase. These geometric arrays were constructed at the same sites where a linear configuration was already applied. The geometric array measurements were taken only for comparison and validation of the results of the MAM surveys having linear array.

Before implementing further analyses regarding the seismic characterization, initially, the dispersion curves of the MAM results recorded by the anisotropic and isotropic field configurations were compared, and the results revealed that linear array appears to produce compatible results. The difference between the curves was calculated to range between 2% and 7%. When the error margin of the performed non-linear least square inversion technique was taken into account, it can be stated that this is a negligible variation. According to the study proposed by Xia et al. (2002), the upper and lower bounds of the margin are reported as -15% and 15%, respectively. Therefore, the results of the anisotropic (i.e., linear) MAM measurements were utilized to increase the maximum penetration distance due to its longer spread length.

Linear array configurations in either MASW or MAM surveys were constructed by using twelve (12) 4.5 Hz natural frequency vertical geophones. Although the brand of the seismographs and some field configuration parameters (i.e., geophone spacing, spread length) were different at the first and second phases, based on the utilized available equipment during both phases, the seismic arrays were configured with the consideration of penetrating the deeper parts of the sediments as much as possible along with the accurate characterization of the shallower layers.

In order to increase the characterized frequency range and the resolution of the shear wave velocity profile from shallower to deeper layers, the dispersion curves acquired from the MASW and MAM surveys were combined at 29 sites. According to the results of this combination method (CSWM) performed for both phases, the maximum reliable depth that could be characterized changes between

35 m and 85 m. The shear wave velocity values were determined in the range of 500 m/s to 600 m/s at the depth of 85 m.

Based on the results of the CSWM, the shear wave velocity (V_S) variations of Quaternary alluvial deposits show that shallower layers have V_S values ranging between 100 m/s and 270 m/s. Also, the Pliocene sediments have almost the same V_S variations at shallower layers with the Quaternary units. The shear wave velocity value of 270 m/s was assigned as the threshold value to detect the vertical V_S variation of the soft overlying sediment from that of the stiffer underlying layers. Based on this classification, the soft layer thickness of either the Quaternary and Pliocene sites was determined as nearly 20 m. This means that the Quaternary and Pliocene sediments could not be differentiated quantitatively by comparing the vertical and lateral variations of their V_S values. In other words, these two units were deemed to have the same seismic behaviors.

When all the measured sites are considered, it can be mentioned that the characteristics of the Quaternary sediments and shallower parts of the Pliocene and Miocene sediments are almost identical. However, according to the shear wave velocity variations, it can be suggested that sedimentation is under the control of the axial depositional setting within the basin. The existence of the lateral and vertical variation of the cohesionless soils is dependent on the severity degree of the flooding. This means that grain size distribution has a major influence on the V_S data variation rather than density, consolidation and degree of cementation.

Besides examining the variation of the V_S values in the vertical and lateral directions in order to differentiate the Plio-Quaternary sediments from each other, the harmonic average of the V_S values was calculated at the uppermost 30 m as suggested by Borchardt (1994). By using this value at each site, an interpolation map was generated and the spatial and statistical distribution of this value with respect to the geological units over the area was examined. It was observed that this value was also insufficient to distinguish the sedimentary units from each

other. V_{S30} values of all the sites fell within the boundary of D soil class ($180 \text{ m/s} < V_{S30} < 360 \text{ m/s}$) based on IBC 2012. Similar observations regarding the incapability of the V_{S30} values to quantitatively differentiate Plio-Quaternary sediments are stated in other studies (e.g., Eker et al., 2012; Eker et al., 2013; Eker et al., 2015).

The geophysical investigations show that the shallower Pliocene sediments have lower V_S values when compared with the values of Quaternary deposits at some places. Also, the Miocene units are characterized by the lower V_S values. Furthermore, this value changes when the sites are present at the up-thrown or down-thrown blocks of the faults. This behavior was also supported by the spatial distribution of the V_{S30} value. All these are indicators of the effect of the presence of the faults and their deformation zones at the measurement locations. Therefore, it can be concluded that grain size distribution and locations of the faults are significant factors affecting the seismic behavior of the sediments.

The 3D model of the V_S values demonstrate that the layer having a V_S value of greater than 600 m/s has an inclination towards the basin and it continues either from the west to the east or from the north to the south beneath the basin. Therefore, it was considered that this observation might be related with the mechanism of the faults controlling the basin. As stated before, these are strike slip faults with a considerable normal component. Therefore, it should be emphasized that the faults located at the northern side of the basin dip towards the south. The others located at the south of the Orta basin have a northward dip direction. This means that the results of the geological studies were compatible with the outcomes of the geophysical studies.

These interpretations were made according to the V_S profiles inverted by using a blind way technique. In order to confirm the results of this technique, the inverted V_S profiles were compared with the geotechnical boring logs and the variation of the SPT-N values with depth. However, the comparisons could be made for the layers down to a depth of 20 m due to the unavailability of the geotechnical data

for the greater depths. Apart from the slight differences, it can be stated that the independent data were generally consistent with each other. Additionally, Although it was observed that the coarse grain bearing layers resulted in obtaining artificially high or refusal SPT-N values, these layers could be characterized by the V_S value without facing any technical difficulties.

In order to perform 1D and 2D numerical analyses, initially representative data and sections were selected by examining all of the V_S profiles in detail. Two sections covering a total of 11 different measurement sites with one common site were selected. One of the sections is almost in the N-S direction and perpendicular to the strike of the NAFS while the other one is nearly in the E-W direction which is more or less parallel with the trend of the NAFS. In the generation of these sections, the main idea was to properly represent the seismic behavior of the geological units and to reflect the possible 2D site effects at the area.

When the sections were examined, it could be seen that the N-S and E-W sections are 4208 m and 6172 m in length, respectively. In other studies by Rathje and Bray (2001), De Luca et al. (2005), Cılız et al. (2007), De Ferrari et al. (2010), Barani et al. (2013) where 2D seismic response analyses were performed, it can be easily seen that the length of the constructed sections in this study are greater than the 2D models utilized in the cited example studies. Even though these sections were able to provide invaluable information regarding the site effect phenomenon, their construction stage caused some problems related with the description of the layer distributions along the lateral direction. There is no way to avoid misidentifying the layers where the distance between the characterized sites increases due to heterogeneity. These difficulties were attempted to be overcome by generalizing the V_S values along the profiles and taking the distribution of the geological features (i.e., courses of rivers, lithological boundaries, location of the faults, etc.) into consideration.

Depending on the correlation of the results of the seismic survey with that of the geotechnical data and the variation of the V_S values throughout the profile, a new inversion process was performed by using the constructed dispersion curves via utilizing the combination of the active and passive surface wave measurements. In this process, instead of using a blind way technique, the inversion was performed based on a four layered model. This was an important approach to simplify the layers in order to construct 2D V_S sections in a more acceptable manner.

As mentioned before, assigning a V_S value to the bedrock (half space) in the 1D and 2D model is an ambiguous subject in the seismic response studies. Some studies (e.g., Borchardt, 1994, Pitilakis, 2004; Boore, 2006; Havenith et al., 2007; Sitharam and Anbazhagan, 2008) state that a V_S value of 760m/s is sufficient to characterize the half space of the numerical model as a bedrock. On the contrary, other studies (e.g., Bodin et al., 2001; Liu et al., 2004; Nguyen et al., 2004; Parolai et al., 2006; Boaga et al., 2012) show that more of the sediment column should be described in the models. A V_S value of 3500 m/s was assigned to the bedrock for seismic response analysis in some studies (e.g., Andrus et al., 2006; Chapman et al., 2006). It is believed that the variations of the mechanical properties of the deeper layers have a contribution to the ground motion characteristics. However, the results of the conducted shear wave velocity surveys were not sufficient to penetrate the layers lying at a depth of greater than 85 m.

Under these conditions some assumptions had to be made in order to locate the depth of the bedrock depending on the findings from the geological and geophysical data. As stated before, the sediment thickness within the basin is more than 145 m according to the deep borings within the basin (Tokan and Özgen, 1976). The same study indicates that the most probable unit underlying this sediment column is the basalt and/or the andesite layer. The maximum penetrated depth is 85 m and a V_S value of 600 m/s was determined for the layer at that depth. Therefore, this value should be extrapolated down to the bedrock. At this stage, the main assumption is that the volcanic layer has a consistent lateral extent beneath

the Orta basin and its shear wave velocity value is greater than 1500 m/s. This V_s value is classified as hard rock according to IBC 2012. At the extrapolation stage, the results of particularly the first phase of the microtremor surveys were also utilized to derive the bedrock depth from the fundamental periods. Another important assumption during generation of these sections was that this layer possessed homogeneous engineering and seismic properties at every point within the area.

Based on the change of the V_s values, 6 layers including bedrock were described at the sites. The third layer was not observed at Comb12 (2) which was located at the geological boundary between the Quaternary deposits and Miocene volcanics. The plasticity index and unit weight of the shallower layer (i.e., <15 m) were determined based on the geotechnical data. However, the deeper layers were differentiated as clay deposits until the fifth layer based on the geological characterization. Due to the unavailability of the data for these layers (i.e., >15m), the result of the laboratory tests at the last depth were utilized and some revisions were made based on the V_s variations. The fifth layer was considered as the weathered upper part of the basalt layers based on the total core recovery taken from the deep borings (Tokan and Özgen, 1976). The non-linear properties of the layers (the normalized modulus and material damping curves) were determined by using the soil models proposed by Darendeli (2001) for each layer based on the data regarding soil class, soil plasticity and mean effective confining stress values of the soils. The bedrock behavior was characterized by using the G/G_{\max} - γ and D - γ curves proposed by Schnabel (1973) in the 1D analysis.

A total of 77 runs were performed at the 11 sites during the investigation of the 1D ground responses. In the 2D numerical analyses, these seven input rock motion records were utilized for the constructed 2D models. 14 runs were performed in the determination of the 2D soil response along the two sections. The amplification and acceleration response spectra of the surface layers at each site were examined and based on the results, the soil responses are determined to possess stationary

behavior at all sites. Therefore, the arithmetic mean of the calculated amplification and acceleration response spectra were utilized in the further analyses.

After examining and correlating the behaviors of the spectral acceleration curves, the results of the 1D and 2D numerical analyses were classified based on the geological units categorized into 4 classes such as Quaternary, Pliocene, Miocene and Boundary groups. After of the 1D and 2D numerical analysis was performed, the response acceleration spectra of the sites were examined. It should be noted that the numbers in the brackets show the results of the 2D analysis. The results can be summarized as; i) the maximum S_a values at the Quaternary sites are within the range of 1.05g [1.19g] to 1.4g [2.06g] at corresponding periods between 0.27 s [0.24 s] and 0.53 s [0.72 s], ii) the S_a peaks in the Pliocene group is changing between 1.11g [1.50g] and 1.43g [1.99g] that are observed at periods ranging between 0.27 s [0.24 s] and 0.52 s [0.28 s], iii) the maximum S_a values are 1.07g [1.39g] and 0.72g [1.52g] at the periods of 0.62 s [0.72 s] and 0.64 s [0.72 s] for the sites located at the west and east ends of the B-B' section, respectively, iv) the highest S_a value and its corresponding period is 1.07g [1.15g] and 0.62 s [0.48 s], respectively.

When the results of the 2D response analysis are examined individually at the characterized sites, it can be observed that the spectral peaks of the 2D response analyses at all of the sites are greater than those of the 1D analyses. This means that 1D analysis underestimates the site responses. The same conclusion come out when comparing the maximum horizontal accelerations (MHA) at the surface determined by the 1D and 2D numerical analyses. The results of 1D analysis are considerably unconservative since the ratio of the MHA_{1D} to the MHA_{2D} is less than 0.75. This ratio is similar with the output of the study proposed by Rathje and Bray (2001). Additionally, it should be noted that this ratio is more significant especially when MHA_{1D} is changing between 0.2g and 0.4g.

By performing numerical analyses, it can be stated that the seismic surface responses depend on the sites located whether along the A-A' or B-B' sections. A comparison of the simulated results basically reveals that the basin effect manifests itself especially at the sites along the E-W section. Based on the results of the 2D seismic simulation, higher amplification ratios arise when compared with the results of the 1D analysis at all the sites along this section. On the other hand, at the sites located along the N-S section, the basin edge effect is more dominant and higher ratios are observed after a 1D analysis. On the basis of conservation of energy, along the basin, the ratio of 2D to 1D MHAs is expected to be higher than 1.0 where basin effects are more pronounced; and smaller than 1.0 where basin effects are less pronounced. However due to lack of closely spaced 1D site response analyses, the regions where 1D analyses are expected to be more critical could not be captured

Besides performing numerical analysis, the site effects within the Orta pull-apart basin was also assessed by the results of the experimental study based on the determination of the fundamental frequencies and H/V amplitudes at the sites. This methodology was based on the microtremor measurements processed by the Nakamura method (Nakamura, 1989). In order to conduct this survey, two campaigns were organized to take microtremor records for the purpose of investigating the site effect phenomenon experimentally. The first one was conducted in November, 2007 and the second was carried out in June, 2014. Two different velocimeters were utilized to record the microtremors along with the different data acquisition parameters during the field surveys performed in these two phases. Additionally, the data acquisition procedure and processing stage were followed differently in these phases.

In the first phase, 44 ambient noise measurements were taken to estimate the site effects of different lithologies within the Orta pull-apart basin. However, the ambient noise was recorded at 35 sites during the second phase. The data acquisition and signal processing were completed according to the methodology

(e.g., Mirzaoğlu and Dikmen, 2003; Eker et al., 2015). The data of the second phase was recorded and analyzed based on the suggestions stated by SESAME (2004). After processing the signals acquired from these two phases, the H/V curves derived from the two phases were compared with each other. In the great majority of the sites, the compatibility were not observed between the two datasets. Therefore, the reasons for these inconsistencies were investigated.

The spectral curves of the individual components (i.e., N-S, E-W and vertical) were investigated especially for the second phase since the relatively higher fundamental periods were obtained at this phase. It is revealed that the vertical component emerge a significant peak within the frequency ranges when the spectral peaks of the two horizontal components take their position at similar ranges almost at all sites. Therefore, although these peaks appeared at a relatively shorter period, when the horizontal to vertical component noise ratios were derived, the position and amplitude of the vertical component leaded to shift the fundamental period to the longer values. One of the possible reasons of this observation might be related the P-wave velocity contrast within the same layers controlling the response of the horizontal components (Raptakis et al., 2005). The high ground water level determined almost at the entire area can create this contrast. Therefore, utilization of the results of the second phase may lead to an incorrect evaluation of the site effect phenomenon in the area.

Before excluding the data from the general data set, the amplification spectra calculated by the numerical analyses at 11 sites were compared with the H/V ratio curved obtained from two phases. The behavior of the H/V curves acquired by the first phase microtremor survey is compatible with the results of the 1D and 2D numerical analyses in terms of the fundamental periods. But, the H/V amplitude shows variations according to the degree of the impedance contrast ratio at the sites. On the contrary, the pattern of the H/V results obtained by the second phase were incompatible with the amplification ratio spectra calculated by either 1D or 2D analysis at the majority of the 11 sites. Therefore, it was confirmed that the

results of the second phase of the microtremor survey is not sufficient to estimate the seismic response at the study area. Consequently, its utilization is not suggested at sites with similar geological characteristics.

As stated above, the first phase microtremor survey showed same fundamental period characteristics with the results of 1D and 2D analyses. The fundamental periods determined from the microtremor survey is commonly used to estimate the bedrock depth (e.g., Bour, 1998; Duval et al., 1998; Guegen et al., 1998; Delgado et al., 2002; Nguyen et al., 2004; Özalaybey et al., 2011; Koçkar and Akgün, 2012; Eker et al., 2015). Therefore, this can be inferred that the assumptions regarding the position of the bedrock and its mechanical properties may reflect the actual case. Moreover, it should also be noted that the performed numerical analysis utilizing equivalent linear approach causes over-amplification of the soil response spectrum during a large magnitude earthquake due to the nature of the method as stated by Kramer (1996). This means that higher amplification values or higher spectral acceleration values might be obtained by performing these methods. Therefore incompatibility of the amplification ratio of the site effect studies might not be originated due to the insufficiency of the microtremor method. However, this statement could not be verified due to lack of the strong motion record in the area. The discussion about the usefulness of the H/V amplitude preserves its ambiguity in this dissertation.

Finally, it can be proposed that based on the first phase of the survey, the maximum H/V amplitudes were in the period range of 0.73 s to 1.37 s with their amplitude changing between 2.7 and 11.5 within the area. Apart from ascribing a meaning to the distribution of the spectral H/V amplification ratio over the area, making an interpretation regarding only the relative amplifications between the two sites is more meaningful.

REFERENCES

Abrahamson, N. A. 1992. "Non-Stationary Spectral Matching", Seismological Research Letters, 63 (1), 30.

Abrahamson, N. A., Silva, W. J. 1997. "Empirical Response Spectral Attenuation Relations for Shallow Crustal Earthquakes", Seismol. Res. Lett., 68 (1), 94-127.

Abrahamson, N. A., Silva, W. J., Kamai, R. 2014. "Summary of the ASK14 Ground Motion Relation for Active Crustal Regions", Earthquake Spectra, 30(3), 1025-1055.

Açıkgoz, S. 2004. "Yaylakent (Orta Çankırı) Civarının Jeolojisi ve Jeotermal Enerji Olanakları", MTA Report No: 10728 (unpublished).

Aki, K. 1957. "Space and Time Spectra of Stationary Stochastic Wave with Special Reference to Microtremors", Bull. Earthq. Res. Inst., 35, 415-17, Tokyo University.

Aktuğ, B., Doğru, A., Özener, H., Peyret, M. 2015. "Slip Rates and Locking Depth Variation along Central and Easternmost Segments of North Anatolian Fault", Geophysical Journal International, 202 (3), 2133-2149.

Akyürek, B., Bilginer, E., Çatal, E., Dağer, Z., Soysal, Y., Sunu, O. 1980. "Eldivan Şabanözü (Çankırı), Hasayaz-Çandır (Kalecik-Ankara) Dolayının Jeolojisi", MTA Report, No: 6741, Ankara (unpublished).

Akyürek, B., Bilginer, E., Akbas, B., S. Sunu, O., Soysal, Y., Dağer Z., Çatal, E., Sözeri, B., Yıldırım, H. Hakyemez, Y. 1982. "Geology of Ankara-Elmadag-Kalecik Area", MTA Report No: 7298 (unpublished).

Akyürek, B., Bilginer, E., Akbaş, B., Hepsen, N., Pehlivan, S., Sunu, D., Soysal, Y., Dağer, Z., Çatal, E., Süzen, B., Yıldırım, H., Hakyemez, Y. 1984. "Ankara-Elmadag-Kalecik Dolayının Temel Jeoloji Özellikleri", Jeoloji Müh. Dergisi, 20, 21-46.

Akyüz, H. S., Hartleb, R., Barka, A., Altunel, E., Sunal, G., Meyer, B., Armijo, V. R. 2002. "Surface Rupture and Slip Distribution of the 12 November 1999 Düzce Earthquake (M 7.1), North Anatolian Fault, Bolu, Turkey", *Bulletin of the Seismological Society of America*, 92 (1), 61-66.

Alsan, E., Tezuçan, L., Bath, M. 1975. "An Earthquake Catalogue for Turkey for the Interval 1913-1970", Kandilli Observatory, Seismological Department, İstanbul, Turkey, 160 p.

Ambraseys, N. N. 1970. "Some Characteristic Features of the North Anatolian Fault Zone", *Tectonophysics*, 9, 143-165.

Ambraseys, N. N., Finkel, C. F. 1987. "Seismicity of Turkey and Neighbouring Regions, 1899-1915", *Annales Geophysicae*, 87, 701- 725.

Andrade, J. E., Borja, R. I. 2006. "Quantifying Sensitivity of Local Site Response Models to Statistical Variations in Soil Properties", *Acta Geotechnica*, 1 (1), 3-14.

Andrus, R.D., Fairbanks, C. D., Zhang, J., Camp, W. M., Casey, T. J., Cleary, T. J., Wright, W. B. 2006. Shear-Wave Velocity and Seismic Response of Nearsurface Sediments in Charleston, South Carolina", *Bulletin of the Seismological Society of America*, 96 (5), 1897–1914.

Anggraeni, D. 2010. "Modelling the Impact of Topography on Seismic Amplification at Regional Scale", Enschede, UT-ITC, 46.

ASCE 7. 2010. "Minimum Design Loads for Buildings and Other Structures", American Society of Civil Engineers, Reston, VA.

Asten, M. W., Dhu, T., Lam, N. 2004. "Optimised Array Design for Microtremor Array Studies Applied to Site Classification; Comparison of Results with SCPT Logs", Paper 2903 Conference Proceedings of the 13th World Conference of Earthquake Engineering, Vancouver, Aug 1–6.

Asten, M. W., Boore, D. M. 2005. "Blind Comparisons of Shear-Wave Velocities at Closely Spaced Sites in San Jose, California", U.S. Geological Survey Open-File Report-1169

ASTM, 2006. "Standard Practice for Classification of Soils for Engineering Purposes (Unified Soil Classification System)", ASTM Standard D-2487, ASTM International, West Conshohocken, PA.

Augello, A. J., Bray, J. D., Abrahamson, N. A., Seed, R. B. 1998. "Dynamic Properties of Solid Waste Based on Back-Analysis of the OII Landfill", *Journal of Geotechnical Engineering*, 124, 211-222.

Bard, P-Y. 1999. "Microtremor Measurements: A Tool for Site Effect Estimation? In: The effects of Surface Geology on Seismic Motion. Eds: Irikura, Kudo, Okada and Sasatani, Rotterdam, 1251-1279.

Barani, S., Massa, M., Lovati, S., Ferretti, G. 2013. "Topographic Effects in Probabilistic Seismic Hazard Analysis: The Case of Narni, Central Italy", *WCEE proceedings, lisboa, September, 10 p.*

Barka, A. A., Kadinsky-Cade, K. 1988. "Strike-Slip Fault Geometry in Turkey and Its Influence on Earthquake Activity", *Tectonics*, 7 (3), 663-684.

Beroya, M. A. A., Aydin, A., Tiglao, R., Lasala, M. 2009. "Use of Microtremor in Liquefaction Hazard Mapping", *Eng. Geol.*, 107(3), 140–153.

Bingöl, E., Akyürek, B., Korkmazer, B. 1973. "Biga Yarımadası'nın Jeolojisi ve Karakaya Formasyonunun Bazı Özellikleri", *Cumhuriyetin 50. yılı Yerbilimleri Kongresi, Maden Tetkik ve Arama Enstitüsü, Ankara, 70-75.*

Bilginer, E., Pehlivan, Ş., Aksay, A. 2002. "1/100.000 Ölçekli Türkiye Jeoloji Haritaları Bolu-G29 Paftası [1:100,000 scale geological map of Turkey-Bolu G29 section]", Map no. 36, Geological Research Department, MTA (General Directorate of Mineral Research and Exploration), Ankara, Turkey.

Blumental; M. 1945. "Ladik Deprem Hattı (Samsun İli)", *Mineral Research and Exploration Institute of Turkey Publications*, 1 (33), 153-162 [in Turkish].

Boaga, J., Renzi, S., Vignoli, G., Deiana, R., Cassiani, G. 2012. "From Surface Wave Inversion to Seismic Site Response Prediction: Beyond the 1D Approach", *Soil Dynamics and Earthquake Engineering*, 36, 38-51.

Bodin, P., Smith, K., Horton, S., Hwang, H. 2001. "Microtremor Observations of Deep Sediment Resonance in Metropolitan Memphis, Tennessee", *Eng. Geol.*, 62, 159-168.

Bohlen, T., Saenger, E. H. 2006. "Accuracy of Heterogeneous Staggered-Grid Finite-Difference Modeling of Rayleigh Waves", *Geophysics*, 71, 109–115.

Bommer, J., Acevedo, A. 2004. "The Use of Real Earthquake Accelerograms as Input to Dynamic Analysis", *Journal of Earthquake Engineering*, 8 (special issue 1), 43-91.

Boore, D. M. 1972. "A Note on the Effect of Simple Topography on Seismic SH Waves", *Bulletin of the Seismological Society of America*, 62 (1), 275-284.

Boore, D. M., Joyner, W. B., Fumal, T. E. 1993. "Estimation of Response Spectra and Peak Accelerations from Western North American Earthquakes", *An Interim Report, U.S. Geol. Surv. Open-File Rept. 93-509pp.*

Boore, D. M., Brown L. T. 1998. "Comparing Shear-Wave Velocity Profiles from Inversion of Surface-Wave Phase Velocities with Downhole Measurements: Systematic Differences between the CXW Method and Downhole Measurements at Six USC Strong-Motion Sites", *Seism. Res. Lett.*, 69, 222–229.

Boore, D M. 2006. "Determining Subsurface Shear-Wave Velocities: A Review", *Third International Symposium on the Effects of Surface Geology on Seismic Motion Grenoble, France*, 103.

Boore, D. M., Stewart, J. P, Seyhan, E., Atkinson, G. M. 2014. "NGA-West 2 Equations for Predicting PGA, PGV, and 5%-Damped PSA for Shallow Crustal Earthquakes", *Earthquake Spectra*, 30(3), 1057-1085.

Borcherdt, R. D. 1994. "Estimates of Site-Dependent Response Spectra for Design (Methodology and Justification)", *Earthquake Spectra*, 10, 617–653.

Bouckovalas, G. D., Papadimitriou, A. G., Kondis, A., Bakas, G. J. 2006. "Equivalent-Uniform Soil Model for the Seismic Response Analysis of Sites Improved with Inclusions", *Proc., 6th European Conf. on Numerical Methods in Geotechnical Engineering, Taylor & Francis, London*, 801–807.

Bonnefoy-Claudet, S. 2004. "Nature du bruit de fond sismique: Implications pour les études des effets de site", Ph.D. thesis, University Joseph Fourier, Grenoble, France. (In French with English abstract).

Bonnefoy-Claudet, S., Baize, S., Bonilla, L. F., Berge-Thierry, C., Pasten, C., Campos, J., Volant, P., Verdugo, R. 2009. "Site Effect Evaluation in the Basin of Santiago de Chile Using Ambient Noise Measurements", *Geophys. J. Int.*, 176, 925-937.

Bour, M., Fouissac, D., Dominique P., Martin, C. 1998. "On the Use of Microtremor Recordings in Seismic Microzonation", *Soil Dynamics and Earthquake Engineering*, 17, 465-474.

Bowles, J. E. 1998. "Foundation Analysis and Design", 6th ed., McGraw-Hill International press.

Box, G. E. P., Cox, D. R. 1964. "An Analysis of Transformations", *Journal of the Royal Statistical Society, B*, 26, 211-234.

Brennan, A. J., Thusyanthan, N. I., Madabhushi, S. P. J. 2005. "Evaluation of Shear Modulus and Damping in Dynamic Centrifuge Tests", *J Geotech Geoenviron Eng ASCE*, 131 (12), 1488 - 1497.

Brown, L. T., Boore, D. M., Stokoe, K. H. I. 2002. "Comparison of Shear Wave Slowness Profiles at 10 Strong-Motion Sites from Noninvasive SASW Measurements and Measurements Made in Boreholes", *Bull. Seismol. Soc. Am.*, 92 (8), 3116–3133.

Burchfiel, B. C., Zhiliang, C., Hodges, K. V., Yuping, L., Royden, L. H., Changrong, D., Jiene, X. 1992. "The South Tibetan Detachment System, Himalayan Orogen: Extension Contemporaneous with and Parallel to Shortening in a Collisional Mountain Belt", *Spec. Pap. Geol. Soc. Am.*, 269; 48 pp.

Cambazoğlu, S. 2012. "Preparation of a Source Model for the Eastern Marmara Region Along the North Anatolian Fault Segments and Probabilistic Seismic Hazard Assessment of Düzce Province", M.Sc. Thesis, METU, Ankara.

Campbell, K. W., Bozorgnia, Y. 2014. "NGA-West2 Ground Motion Model for the Average Horizontal Components of PGA, PGV, and 5%-Damped Linear Acceleration Response Spectra", *Earthquake Spectra*, 30(3), 1087-1115.

Cara, F., Cultrera, G., Azzara, R., Rubeis, V., Giulio, G., Giammarinaro, M., Tosi, P., Vallone, P., Rovelli, A. 2008. "Microtremor Measurements in the City of Palermo, Italy: Analysis of the Correlation between Local Geology and Damage", *Bull. Seismol. Soc. Am.*, 98(3), 1354–1372.

Cavallaro, A., Ferraro, A., Grasso, S., Maugerib, M. 2008. "Site Response Analysis of the Monte Po Hill in the City of Catania", *Seismic Engineering Conference Commemorating the 1908 Messina and Reggio Calabria Earthquake*, CP1020.

Cavallaro, A., Ferraro, A., Grasso, S., Maugerib, M. 2012. "Topographic Effects on the Monte Po Hill in Catania (Italy)", *Soil Dynamics and Earthquake Engineering* 43, 97–113.

Chaillat S., Bonnet M., Semblat J. F. 2009. "A New Fast Multi-domain BEM to Model Seismic Wave Propagation and Amplification in 3D Geological Structures", *Geophysical Journal International*, 177, 509-531.

Chapman M. C., Martin, J. R., Olgun, C. G., Beale J. N. 2006. "Site Response Models for Charleston, South Carolina and Vicinity Developed from Shallow Geotechnical Investigations", *Bulletin of the Seismological Society of America*, 96, 467-489.

Chavez-Garcia, F. J., Rodriguez M., Stephenson W. R. 2006. "Subsoil Structure Using SPAC Measurements along a Line", *Bull. Seism. Soc. Am.*, 96, 729–736.

Chavez-Garcia, F. J. 2007. "Site effects: From Observation and Modeling to Accounting for Them in Building Codes", *Earthquake Geotechnical Engineering*, 53-72.

Chavez-Garcia, F. J., Dominguez, T., Rodriguez, M., Perez, F. 2007. "Site Effects in a Volcanic Environment: A Comparison between HVSR and Array Techniques at Colima, Mexico", *Bull. Seism. Soc. Am.*, 97, 591-604.

Chiou, B. S.-J., Youngs, R. R. 2014. "Update of The Chiou And Youngs NGA Model for the Average Horizontal Component of Peak Ground Motion and Response Spectra", *Earthquake Spectra*, 30(3), 1117-1153.

Chouinard, L., Rosset, P., De La Puente, A., Madriz, R., Mitchell, D., Adams, J. 2004. "Seismic Hazard Analysis for Montreal", In Proceedings of the 13th World Conference on Earthquake Engineering, Vancouver, Canada, Paper Vol. 7010.

Cılız, S., Özkan, M. Y., Çetin, K. Ö. 2007. "Effect of Basin Edge Slope on the Dynamic Response of Soil Deposits", 4th International Conference on Earthquake Geotechnical Engineering, Thessaloniki.

Cid, J., Susagna, T., Goula, X., Chavarria, L., Figueras, S., Fleta, J., Casas, A., Roca, A. 2001. "Seismic Zonation of Barcelona Based on Numerical Simulation of Site Effects", *Pure Appl. Geoph.*, 158, 2559–2577.

Coduto, D. P. 1994. "Foundation Design Principles and Practices", Prentice Hall, Englewood Cliffs, New Jersey.

Comina, C., Boiero, D., Foti, S., Socco, L. V. 2006. "Noise Blind Test Interpretation Using f–k Analysis and Monte Carlo Inversion", Eds: Bard, P. Y., Chaljub, E., Cornou, C., Cotton, F., Gueguen. Proceedings of the Third International Symposium on the Effects of Surface Geology on Seismic Motion, Grenoble, 2LCPC, France.

Cornell C. A. 1968. "Engineering Seismic Risk Analysis", *Bulletin of the Seismological Society of America*, 58 (5),1583-1606.

Çetin K. Ö., Seed R. B. 2002. "Nonlinear Shear Mass Participation Factor, rd for Cyclic Shear Stress Ratio Evaluation", *J. Soil Dynamics and Earthquake Eng.* 24(2), 103-113.

Çetin K. Ö., Youd T. L., Seed R. B., Bray J. D., Durgunoglu H. T., Lettis W., Yilmaz M. T. 2004. "Liquefaction-Induced Lateral Spreading at Izmit Bay during the 1999 Kocaeli (Izmit) – Turkey Earthquake", *ASCE J. of Geotech. and Geoenviron. Eng.* 130(12), 1300-1313.

D'Amico, V., Picozzi, M., Baliva, F., Albarello, D. 2008. "Ambient Noise Measurements for Preliminary Site-Effects Characterization in the Urban Area of Florence, Italy", *Bull. Seism. Soc. Am.*, 98 (3), 1373-1388.

Darendeli, M. 2001. "Development of a New Family of Normalized Modulus Reduction and Material Damping Curves", Ph.D. Thesis, Dept. of Civil Eng., Univ. of Texas, Austin.

Dawson, E. M.; Roth, W. H.; Nesarajah, S., Davis, C. A. 2001. "A Practice-Oriented Pore-Pressure Generation Model", published at 2nd International FLAC Symposium, Lyon, France, October, 8 p.

De Ferrari R., Ferretti G., Barani S., Spallarossa D. 2010. "Investigating on the 1920 Garfagnana Earthquake (Mw = 6.5): Evidences of Site Effects in Villa Collemandina (Tuscany, Italy)", *Soil Dyn. Earthquake Eng.*, 30, 1417-1429.

De Luca, G., Marcucci, S., Milana, G., Sano, T. 2005. "Evidence of Low Frequency Amplification in the City of l'Aquila, Central Italy, through a Multidisciplinary Approach Including Strong and Weak-Motion Data, Ambient Noise, and Numerical Modeling", *Bull Seism Soc Am.*, 95 (4), 1469 - 1481.

Delgado, J., Alfaro, P., Galindo-Zaldivar, J., Jabaloy, S., Lopez Garrido, A. C., Sanz De Galdeano, C., 2002. "Structure of the Padul- Nigüelas Basin (S Spain) from H/V Ratios of Ambient Noise: Application of the Method to Study Peat and Coarse Sediments", *Pure and Applied Geophysics*, 159 (11–12), 2733–2749.

Del Gaudio, V., Muscillo, S., Wasowski, J. 2014. "What We Can Learn about Slope Response to Earthquakes from Ambient Noise Analysis: An Overview", *Eng. Geol.*, 182, 182–200.

Del Monaco, F., Tallini, M., De Rose, C., Durante, F. 2013. "HVNSR Survey in Historical Downtown L'Aquila (Central Italy): Site Resonance Properties vs. Subsoil Model", *Eng. Geol.*, 158, 34–47.

Delavaud, E., Cupillard, P., Festa, G., Vilotte, J. P. 2006. "3D Spectral Element Method Simulations of the Seismic Response in the Caracas Basin", *InProc. of the Third International Symposium on the Effects of Surface Geology on Seismic Motion*, 1, 512-522.

Demirtaş, R., Iravul, Y., Erkmén, C., Baran, B., Yaman, M., Baykal, M., Kılıç, T. 2000. "Orta (Çankırı) Earthquake of June 6, 2000", *Bull. Geology*, 1–2, 6–15 (in Turkish).

Department of Earthquake Research, General Directorate of Disaster Affairs (DDA). 2015. "Earthquake Catalogue", retrieved September 1, 2015 from <http://www.deprem.gov.tr/en/ddacatalogue>.

Di Giulio, G., Improta, L., Calderoni, G., Rovelli, A. 2008. "A Study of the Seismic Response of the City of Benevento (Southern Italy) through a Combined Analysis Of Seismological And Geological Data", Eng. Geol. 97 (3), 146–170.

Dikmen, U. 2009. "Statistical Correlations of Shear Wave Velocity and Penetration Resistance for Soils", Journal of Geophysics and Engineering, 6, 61–72.

Douglas, J., 2015. "Ground Motion Prediction Equations 1964-2015", <http://www.gmpe.org.uk>.

Duru, M., Aksay A. 2002. "1/100.000 Türkiye Jeoloji Haritaları H29 Paftası", MTA. Geological Research Department, MTA (General Directorate of Mineral Research and Exploration), Ankara, Turkey.

Duval, A. M., Méneroud, J. P., Vidal, S., Singer, A. 1998. "Relation between Curves Obtained from Microtremor and Site Effects Observed after Caracas 1967 Earthquake", Proceedings of the 11th European Conference on Earthquake Engineering, Paris, France, 1998.

Duval, A. M., Méneroud, J. P., Vidal, S., Singer, A., De Santis, F., Ramos, C., Romero, G., Rodriguez, R., Pernia, A., Reyes, A., Griman, C. 2001. "Caracas, Venezuela, Site Effect Determination with Microtremors", Pure and Applied Geophysics, 158, 2513-2523.

Earthquake Engineering Research Center (EERC) METU, Earthquake Research Department (ERD) General Directorate of Disaster Affairs. 2009. " Seismological Features of Re-Compiled Turkish Strong-Motion Database (1976-2007)", TUBITAK Project.

Eker, A. M. 2009. Determination of The Dynamic Characteristics and Local Site Conditions of the Plio-Quaternary Sediments Situated towards the North Of Ankara through Surface Wave Testing Methods. M.Sc. Thesis, METU, 145 p (unpublished).

Eker, A. M., Akgün H., Koçkar M. K. 2010. "A Comparison of Local Site Conditions with Passive and Active Surface Wave Methods", Fifth International Conference on Recent Advances in Geotechnical Earthquake Engineering and Soil Dynamics Symposium in Honor of Professor I. M. Idriss San Diego, CA., May 24-29.

Eker, A. M., Akgün, H., Koçkar, M. K. 2012. "Local Site Characterization and Seismic Zonation Study by Utilizing Active and Passive Surface Wave Methods: A Case Study for the Northern Side of Ankara, Turkey", *Engineering Geology*, 151, 64-81.

Eker, A. M., Akgün, H., Koçkar, M. K. 2013. "A Comprehensive Study to Define Local Site Effects in Northern Ankara, Turkey", SE-50EEE International Conference on Earthquake Engineering - 29 to 31 May, Skopje, R. Macedonia.

Eker, A. M., Koçkar, M. K. and Akgün, H. 2015. "Evaluation of Site Effect within the Tectonic Basin in the Northern Side of Ankara", *Engineering Geology*, 192, 64-81.

Emre, Ö., Duman, T. Y., Dogan, A., Özalp, S. 2000. "6 Haziran 2000 Orta (Çankırı) Depremi Değerlendirme Raporu", MTA Rapor No: 10323, Ankara (in Turkish).

Electrical Power Research Institute (EPRI). 1988. "A Criterion for Determining Exceedance of the Operating Basis Earthquake", Report No. EPRI NP-5930, Palo Alto, California.

Ergin, K., Güçlü, U., Uz, Z. 1967. "Türkiye ve Civarının Deprem Katoloğu (Milattan Sonra 11 Yılından 1964 Sonuna Kadar)", İstanbul Teknik Üniversitesi, Maden Fakültesi, Arz Fiziği Enstitüsü Yayınları, 24, 169 s (in Turkish).

European Committee for Standardization 2004. "Eurocode 8, prEN 1998-1: Design of Structures for Earthquake Resistance, Part 1: General rules, Seismic Actions and Rules for Buildings", Final Draft, December 2003.

Faccioli, E., Maggio, F., Quarteroni, A., Tagliani, A. 1996. "Spectral Domain Decomposition Methods for the Solution of Acoustic and Elastic Wave Equations", *Geophysics*, 61, 1160-1174.

Fäh, D., Rüttener, E, Noack, T, Kruspan, P. 1997. "Microzonation of the City of Basel", *Journal of Seismology*, 1, 87-102.

Fäh, D., Kind, F., Giardini, D. 2003. "Inversion of Local S-Wave Velocity Structures from Average H/V Ratios, and Their Use for the Estimation of Site-Effects", *J. Seismol.*, 7(4), 449-467.

Field, E. H., Jacob, K. 1993. "The Theoretical Response of Sedimentary Layers to Ambient Seismic Noise", *Geophysical Res. Lett.*, 20-24, 2925-2928.

Fossen, H. 2000. "Extensional Tectonics in the Caledonides: Synorogenic or Postorogenic?", *Tectonics*, 19(2), 213-224.

Finn, W. D. 1991. "Geotechnical Engineering Aspects of Seismic Microzonation", In: *Proceedings of the Fourth International Conference on Seismic Zonation*, August 25-29, Stanford, California, E.E.R.I. (ed), Oakland CA, I, 199-250.

Foti, S. 2005. "Surface Wave Testing for Geotechnical Characterization", 47–71. *Surface Waves in Geomechanics-Direct and Inverse Modeling for Soil and Rocks*. Eds: Lai, Wilmski, CISM Lecture Notes. Springer-Verlag, Wien-Newyork,.

Fumal, T. E., Tinsley, J. C. 1985. "Mapping Shear Wave Velocities of Near Surface Geological Materials", 127–150. *Predicting Areal Limits of Earthquake Induced Landsliding; In Evaluation of Earthquake Hazards in the Los Angeles Region – An Earth Science Perspective*. Eds: Ziony, T. I. USGS Paper, Vol., 1360.

Gasparini, D. A., Vanmarcke, E. H. 1976. "SIMQKE: Simulated Earthquake Motions Compatible with Prescribed Response Spectra", Massachusetts Institute of Technology-, Cambridge, Massachusetts.

Gelagoti, F., Kourkoulis, R., Anastasopoulos, I., Tazoh, T., Gazetas, G. 2010. "Seismic Wave Propagation in a Very Soft Alluvial Valley: Sensitivity to Ground-Motion Details and Soil Nonlinearity, and Generation of a Parasitic Vertical Component", *Bulletin of the Seismological Society of America*, 100 (6), 3035-3054.

Geli, L., Bard, P-Y., Jullien, B. 1988. "The Effect of Topography on Earthquake Ground Motion: A Review and New Results", *Bulletin of the Seismological Society of America*, 78 (1), 42-63.

General Directorate of Mineral Research and Exploration (MTA). 2008. "1/25000 scaled digitized geological map archive".

Geometrics Inc. 2006. "SeisImager/SW Software Manual-Windows Software for analysis of Surface Waves", Geometrics Inc., California-USA, 281p.

Geovision, 2009. Retrieved June 12, 2015 from <http://www.geovision.com/seismic.html>

Gosar, A. 2007. "Microtremor HVSR Study for Assessing Site Effects in the Bovec Basin (NW Slovenia) related to 1998 Mw 5.6 and 2004 Mw 5.2 Earthquakes", *Eng. Geol.*, 91(2), 178–193.

Gosar, A., Stopar, R., Roser, J. 2008. "Comparative Test of Active and Passive Multichannel Analysis of Surface Waves (MASW) Methods and Microtremor HVSR Method", *RMZ - Materials and Geoenvironment*, 55(1), 41-66.

Gueguen, P., Chatelain, J. L., Guillier, B., Yepes, H., Egred, J. 1998. "Site Effect and Damage Distribution in Pujili (Ecuador) after the 28 March 1996 Earthquake", *Soil Dyn. and Earthq Eng.*, 17 (5), 329-334.

Guillier, B., Atakan, K., Chatelain, J. L., Havskov, J., Ohrnberger, M., Cara, F., Duval, A. M., Zacharopoulos, S., Teves-Costa, P., Accera, C., Alguacil, G., Azzara, R., Bard, P.-Y., Blarel, F., Borges, A., Grandison, M., Rao, S., Theodulidis, N., Tvedt, E., Utheim, T., Vidal, S., Vollmer, D. 2008. "Influence of Instruments on the H/V Spectral Ratios of Ambient Vibrations", *Bull. Earthq. Eng.*, 6, 3–31.

Haghshenas, E., Bard, P.-Y., Theodulidis, N. 2008. "Empirical Evaluation of Microtremor H/V Spectral Ratio", *Bulletin of Earthquake Engineering*, 6, 75-108.

Havenith, H. B., Fäh, D., Polonu, U., Roullé, A. 2007. "S-Wave Velocity Measurements Applied to the Seismic Microzonation of Basel, Upper Rhine Graben", *Geophys. J. Int.*, 170, 346–358.

Hakyemez, Y. Barkurt, M. Y., Bilginer, E., Pehlivan, Ş., Can, B., Dağcı, Z., Sözeri, B. 1986. "Yapraklı-Ilgaz-Çankırı-Çandır Dolayının Jeolojisi", MTA Report, No: 7966, Ankara (unpublished).

Hancock, J., Watson-Lamprey, J., Abrahamson, N., Bommer, J., Markatis, A., McCoy, E., Mendis, R. 2006. "An Improved Method of Matching Response Spectra of Recorded Earthquake Ground Motion Using Wavelets, *J. Earthquake Eng.*, 10, 67–89.

Hayashi, K. 2008. "Development of Surface-Wave Methods and Its Application to Site Investigations", Ph.D. Thesis, Kyoto University, 278 p.

Hestholm, S. 1999. "Three-Dimensional Finite Difference Viscoelastic Wave Modelling Including Surface Topography", *Geophysical Journal International*, 139 (3), 852-878.

Hestholm, S., Moran, M., Ketcham, S., Anderson, T., Dillen, M., McMechan, G. 2006. "Effects of Free-Surface Topography on Moving-Seismic-Source Modeling", *Geophysics*, 71 (6), 159-166.

Hudson, M., Idriss, I. M., Beikae, M., 1994. "QUAD4M – A Computer Program to Evaluate the Seismic Response of Soil Structures Using Finite Element Procedures and Incorporating a Compliant Base Center for Geotechnical Modeling", Department of Civil and Environmental Engineering, University of California, Davis, CA.

Hunter, J. A, Benjumea, B., Haris, J., Miller, R., Pullan, S., Burns, R. A. 2002. "Surface and Down-Hole Shear Wave Seismic Methods for Thick Soil Site Investigations", *Soil Dynamics and Earthquake Engineering*, 22(9-12), 931–941.

Idriss, I. M., Seed, H. B. 1967. "Response of Earthbanks during Earthquakes", *J. Soil Mech. Found. Div., ASCE*, 93 (SM3), 61-82.

Idriss, I. M. 1991. "Earthquake Ground Motions at Soft Soil Sites", Proceedings of the Second International Conference on Recent Advances in Geotechnical Earthquake Engineering and Soil Dynamics, March 11-15, St. Louis, MO. Ed: Prakesh, S. University of Missouri-Rolla.

Inazaki, T. 2006. "Relationship between S-Wave Velocities and Geotechnical Properties of Alluvial Sediments", 19th EEGS Symposium on the Application of Geophysics to Engineering and Environmental Problems.

International Code Council, (ICC). 2012. "International Building Code, Structural and Fire and Life-Safety Provisions (Seismic, Wind, Accessibility, Egress, Occupancy and Roof Codes)", Whittier, CA.

Jibson, R. 1987. "Summary of Research on the Effects Topographic Amplification of Earthquake Shaking of Slope Stability" U.S. Geological Survey, Open-File Report 87-268, Manlo Park, California, USA.

Jin, X., Luke, B., Louie, J. 2006. "Comparison of Rayleigh Wave Dispersion Relations from Three Surface Wave Measurements in a Complex-Layered System", Proc., ASCE Geocongress (Atlanta), ASCE Press, New York.

Kalkan, E., Gülkan, P. 2005. "Erratum: Site-Dependent Spectra Derived from Ground Motion Records in Turkey", *Earthquake Spectra*, 21(1), 283.

Kanai, K., Tanaka, T. 1961. "Measurement of the Microtremor 1", *Bulletin of the Earthquake Research Institute, University of Tokyo*, 32, 200-208.

Kanai, K. 1966. "Conf. on Cone Penetrometer", The Ministry of Public Works and Settlement (Ankara, Turkey) (presented by Y Sakai, 1968).

Kandilli Observatory and Earthquake Research Institute (KOERI). 2015. "Earthquake Records", retrieved September 1, 2015 from <http://www.koeri.boun.edu.tr/sismo/map/tr/index.html>.

Kaplan, T. 2004. "Neotectonics and Seismicity of the Ankara Region: A Case Study of the Uruş Area", Master Thesis, METU, Ankara, 98 p.

Kasapoğlu, K. E., Ulusay, R., Gökçeoğlu, C., Köse, O. 2000. "6 Haziran 2000 Orta (Çankırı) Depreminin Saha İnceleme Raporu", Hacettepe Üniversitesi, Jeoloji Müh.Böl., Uygulamalı Jeoloji Anabilim Dalı, Ankara.

Kayabalı, K. 1996. "Soil Liquefaction Evaluation Using Shear Wave Velocity", *Engineering Geology*, 44 (1), 121-127.

Kaymakçı, N. 2000. "Tectono-Stratigraphical Evolution of the Çankırı Basin (Central Anatolia, Turkey)", Ph.D. thesis, Utrecht University, *Geologica Ultraiectina*, 190, 247 pp.

Kaymakçı, N., Özçelik, Y., White, H. S., Van Dijk, P. M. 2001. "Neogene Tectonic Development of the Çankırı Basin", *Turkish Association of Petroleum Geologist Bulletin*, 13(1), 27-56.

Keller, J., Jung, D., Eckhardt, F. J., Kreuzer, H. 1992. "Radiometric Ages and Chemical Characterization of the Galatean Andesitic Massif, Pontus, Turkey", *Acta Volcanologica*, 2, 267-276.

Ketin, İ. 1969. "Über die Nordanatolische Horizontalverschiebung", Mineral Research and Exploration Institute of Turkey Bulletin, 72, 1-28.

Kramer, S. L. 1996. "Geotechnical Earthquake Engineering", Prentice-Hall, Upper Saddle River.

Koçkar M. K., Akgün H. 2008. "Development of a Geotechnical and Geophysical Database for Seismic Zonation of the Ankara Basin Turkey", Environmental Geology, 55, 165–176.

Koçkar M.K., Akgün H., Eker, A. M. and Cambazoğlu, S. 2011. "Engineering Geological and Geotechnical Characteristics of Ankara Clay", European Clay Conference, 156 p (Abstract only).

Koçkar, M. K., Akgün, H. 2012. "Evaluation of the Site Effects of the Ankara basin, Turkey", Journal of Applied Geophysics, 83, 120-134.

Koçyiğit, A. 1991a. "An Example of an Accretionary Forearc Basin from Northern Central Anatolia and Its Implications for the History of Subduction of Neo-Tethys In Turkey", Geological Society of America Bulletin, 103, 22-36.

Koçyiğit, A. 1991b. "Changing Stress Orientation in Progressive Intracontinental Deformation as Indicated by the Neotectonics of the Ankara Region (NW Central Anatolia)", Turkish Association of Petroleum Geologist Bulletin, 3(1), 43-55.

Koçyiğit, A. 1992. "Southward-Vergent Imbricate Thrust Zone in Yuvaköy: A Record of the Latest Compressional Event Related to the Collisional Tectonic Regime in Ankara-Erzincan Suture Zone", Turkish Association of Petroleum Geologist Bulletin, 4(1), 111-118.

Koçyiğit, A., Türkmenoğlu, A., Beyhan, A., Kaymakçı, N., Akyol, E. 1995. "Post-Collisional Tectonics of Eskişehir-Ankara-Çankırı Segment of İzmir-Ankara-Erzincan Suture Zone (IAESZ): Ankara Orogenic Phase", Turkish Association of Petroleum Geologist Bulletin, 6(1), 69-86.

Koçyiğit, A., Rojay, B., Cihan, M., Özacar, A. 2001. "The June 6, 2000 Orta (Çankırı, Turkey) Earthquake: Sourced from a New Antithetic Sinistral Strike-Slip Structure of the North Anatolian Fault System, the Dodurga Fault Zone", Turkish Journal of Earth Sciences, 10, 69-82.

Koçyiğit, A. 2003. "General Neotectonic Characteristics and Seismicity of Central Anatolia", TPJ. Spec. Publ., 5, 1–26 (in Turkish with English Abstract).

Koçyiğit, A. 2008. "Ankara ve Çevresinin Deprem Kaynakları", Ankara'nın Deprem Tehlikesi ve Riski Çalıştayı, Bildiriler Kitabı. Gazi Üniversitesi, Ankara, pp. 4–53 (in Turkish).

Komatitsch, D., Vilotte, J. P. 1998. "The Spectral Element Method: an Efficient Tool to Simulate the Seismic Response of 2D and 3D Geological Structures", Bulletin of the seismological society of America, 88 (2), 368-392.

Konno, K., Ohmachi, T. 1998. "Ground-Motion Characteristics Estimated from Spectral Ratio between Horizontal and Vertical Components of Microtremor", Bull. Seism. Soc. Am. 88 (1), 228- 241.

Kottke, A., Rathje, E. M. 2009. "Technical Manual for Strata", Rep. No. 2008/10, Pacific Earthquake Engineering Research Center, Berkeley, Calif.

Krinitzsky, E. L., Chang, F. K. 1975. "State-of-the-Art for Assessing Earthquake Hazards in the United States Earthquake Intensity and the Selection of Ground Motions for Seismic Design Miscellaneous", Paper S-73-1, Army Engineer Waterways Experiment Station CE Vicksburg Mississippi.

Kudo, K., Kanno, T., Okada, H., Özel, O., Erdik, M., Sasatani, T., Higashi, S., Takahashi, M., Yoshida, K. 2002. "Site-Specific Issues for Strong Ground Motions during the Kocaeli, Turkey, Earthquake of 17 August 1999, As Inferred From Array Observations of Microtremors and Aftershocks", Bull. Seismol. Soc. Am., 92(1), 448–465.

Kuhlemeyer R.L., Lysmer, J. 1973. "Finite Element Method Accuracy for Wave Propagation Problems", J. Soil Mech. & Foundations, Div. ASCE 99 (SM5), 421-427.

Kuşçu, İ., Okamura, M., Matsuoka, H., Yamamori, K., Awata, Y., Özalp, S. 2009. "Recognition of Active Faults and Stepped Geometry in Gemlik Bay, Sea of Marmara, NW Turkey", Marine Geology, 260 (1), 90-101.

Lacave, C., Bard, P.-Y., Koller, M. G. 1999. "Microzonation: Techniques and Examples. In: Block 15: Naturgefahren Erdbebenrisiko, 23 p. Available from: <<http://www.ndk.ethz.ch/pages/publ/Koller.pdf>> (electronic book on the Internet).

Lachet, C., Bard, P. Y. 1994. "Numerical and Theoretical Investigations on the Possibilities and Limitations of Nakamura's technique", *J. Phys. Earth*, 42, 377-397.

Lanzo, G., Silvestri, F., Costanzo A., d'Onofrio A., Martelli, L., Pagliaroli, A., Sica, S., Simonelli, A. 2011. "Site Response Studies and Seismic Microzoning in the Middle Aterno Valley (L'Aquila, Central Italy)", *Bull. Earthquake Eng.*, 9, 1417-1442.

Lanzo, G., Pagliaroli, A. 2012. "Seismic Site Effects at Near-Fault Strong-Motion Stations along the Aterno River Valley during the Mw = 6.3 2009 L'Aquila Earthquake", *Soil Dyn. Earthq. Eng.*, 40, 1 - 14.

Lebrun, B., Hatzfeld, D., Bard, P. Y. 1999. "Experimental Study of Ground Motion on a Large Scale Topography", *J. of Seismology*, 3(1), 1-15.

Lee, S. J., Chen, H. W., Liu, Q., Komatitsch, D., Huang, B. S., Tromp, J. 2008. "Three-Dimensional Simulations of Seismic-Wave Propagation in the Taipei Basin with Realistic Topography Based upon the Spectral-Element Method", *Bulletin of the Seismological Society of America*, 98 (1), 253-264.

Lee, S. J., Chan, Y. C., Komatitsch, D., Huang, B. S., Tromp, J. 2009. "Effects of Realistic Surface Topography on Seismic Ground Motion in the Yangminshan Region of Taiwan based upon the Spectral-Element Method and LiDAR DTM", *Bulletin of the Seismological Society of America*, 99 (2A), 681-693.

Lermo, J., Chavez-Garcia, F. J. 1993. "Site Effect Evaluation Using Spectral Ratios with Only One Station", *Bull. Seism. Soc. Am.*, 83, 1574-1594.

Lermo, J., Chavez-Garcia, F. J. 1994. "Are Microtremors Useful in Site Response Evaluation?", *Bull. Seism. Soc. Am.*, 84, 1350-1364.

Lilhanand, K., Tseng, W. S. 1988. "Development and Application of Realistic Earthquake Time Histories Compatible with Multiple-Damping Design Spectra", *Proceedings of the 9th World Conference on Earthquake Engineering, Tokyo Japan, II*, 819-824.

Liao, S., Whitman, R. V. 1986. "Overburden Correction Factors for SPT in Sand", *J. Geotech. Engineering, ASCE*.

Louie, J. N. 2001. "Faster, Better: Shear-Wave Velocity to 100 Meters Depth from Refraction Microtremor Arrays", *Bulletin of the Seismological Society of America*, 91 (2), 347–364.

Louie, J. N., Abbott, R. E., Pullammanappallil, S. 2002. "Refraction Microtremor and Optimization Methods as Alternatives to Boreholes for Site Strength and Earthquake Hazard Assessments", *Proceedings 15th Annual Symposium on the Application of Geophysics to Environmental and Engineering Problems (SAGEEP '02)*, February 11-13, Las Vegas, Nevada.

Magnifesta, M. 2015. "User's Guide Visual-Q4M", Italy, 122 p.

Margaris, B., Papazachos, C., Papaioannou, C., Theodulidis, N., Kalogeras, I., Skarlatoudis, A. 2002. "Ground Motion Attenuation Relations for Shallow Earthquakes in Greece", In: *Proceedings of the XXVIII General Assembly of the European Seismological Commission (ESC)*.

Martin, A. J., Diehl, J. G. 2004. "Practical Experience Using a Simplified Procedure to Measure Average Shear-Wave Velocity to a Depth of 30 meters (VS30)", in *13th World Conf. on Earthquake Engineering*, Vancouver, B.C., Canada, 1–6 August.

Matasovic N., Ordonez G., 2012. "D-MOD2000 – A Computer Program for Seismic Site Response Analysis of Horizontally Layered Soil Deposits, Earthfill Dams and Solid Waste Landfills", Geomotions, LLC; Lacey, Washington, USA.

Mayne, P. W., Kulhawy, F. H. 1982. "Ko -OCR Relationships in Soil", *Journal of the Geotechnical Engineering Division, ASCE*, 108 (GT6), 851-872.

Midorikawa, S. 1987. "Prediction of Iseismic Map in Kanto Plain due to Hypothetical Earthquake", *Journal of Structural Dynamics*, 33B, 43-48.

Miller, R. D., Xia, J., Park, C. B., Ivanov, J. M. 1999. "Multichannel Analysis of Surface Waves to Map Bedrock", *Kansas Geological Survey, The Leading Edge* 1392–1396 (December).

Ministry of Public Works and Settlement Government of Republic of Turkey. 1998. "Turkish Seismic Code, Specification for Structures to Be Built in Disaster Areas", Ankara, Turkey.

Mirzaoğlu, M., Dikmen, Ü. 2003. "Application of Microtremors to Seismic Microzoning Procedure", *Balkan Geophysical Society*, 6(3), 143–156.

Moczo, P., Kristek, J., Vavrycuk, V., Archuleta, R. J., Halada, L. 2002. "3D Heterogeneous Staggered-Grid Finite-Difference Modeling of Seismic Motion with Volume Harmonic and Arithmetic Averaging of Elastic Moduli and Densities", *Bulletin of the Seismological Society of America*, 92 (8), 3042-3066.

Moix, P., Beccaletto, L., Kozur, H. W., Hochard, C., Rosselet, F., Stampfli, G. M. 2008. "A New Classification of the Turkish Terranes and Sutures and Its Implication for the Paleotectonic History of the Region", *Tectonophysics*, 451(1), 7-39.

Moss, R. E. S. 2008. "Quantifying Measurement Uncertainty of 30-meter Shear-Wave Velocity, *Bull. Seismol. Soc. Am.*, 98, 1399–1411.

Motoki, K. 2002. "MicPlot Version 1.1, A UNIX Code to Analyze Ambient Noise Records", Tokyo Institute of Technology, Japan.

Murthy, V. N. S. 2002. "Geotechnical Engineering: Principles and Practices of Soil Mechanics and Foundation Engineering", CRC Press.

Nakamura, Y. 1989. "A Method for Dynamic Characteristics Estimation of Subsurface Using Microtremor on the Ground Surface", *Quarterly Report of Railway Technical Research Institute (RTRI)*, 30 (1), 273-281.

Nakamura, Y. 1996. "Real Time Information Systems for Seismic Hazards Mitigation UrEDAS, HERAS and PIC", *Quarterly Report of RTRI*, 37 (3), 112-127.

Nakamura, Y. 2000. "Clear Identification of Fundamental Idea of Nakamura's Technique and Its Applications", *Proc. 12th World Conf. on Earthq. Engng. (CD-ROM)*, Paper ID 2656, 8 s.

Natale, M., Nunziata, C., Panza, G. F. 2004. "FTAN Method for the Detailed Definition of Vs in Urban Areas", *Proc. 13th World Conference on Earthquake Engineering*, Vancouver, B.C., Canada, August 1-6, 11 p.

Nazarian, S. 1984. "In Situ Determination of Elastic Moduli of Soil Deposits and Pavement Systems by Spectral-Analysis-of-Surface-Waves Method", Ph.D. Dissertation, Univ. of Texas, Austin.

Nguyen, F., Van Rompaey, G., Teerlynck, H., Van Camp, M., Jongmans, D., Camelbeeck, T. 2004. "Use of Microtremor Measurement for Assessing Site Effects in Northern Belgium — Interpretation of the Observed Intensity During the Ms=5.0 June 11 1938 Earthquake", *Journal of Seismology*, 8 (1), 41-56.

Nixon, I. K., 1982 "Standard Penetration Test: State-of-the-Art Report", *Proceedings of the 2nd European Symposium on Penetration Testing*, Amsterdam, Netherlands, 3-21.

Nogoshi, M., Igarashi, T. 1971. "On the Amplitude Characteristics of Microtremor (Part 2)", *Jour. Seis. Soc. Japan*, 24, 26-40.

Nunziata, C. 2007. "A Physically Sound Way of Using Noise Measurements in Seismic Microzonation, Applied to the Urban Area of Napoli", *Eng. Geol.*, 93(1), 17–30.

Oliveira, C. S. 2004. "The Influence of Scale on Microzonation and Impact Studies", 3-26. *Recent Advances in Earthquake Geotechnical Engineering and Microzonation*. Ed: Ansal, A. Kluwer Academic Publishers,.

Ohta, Y., Goto, N., Kagami, H., Shiono, K. 1978. "Shear Wave Velocity Measurement During a Standard Penetration Test", *Earthquake Engineering and Structural Dynamics*, 6, 43–50.

Okada, H. 2003. "The Microtremor Survey Method", *Geophysical Monograph Series*, 12. Published by Society of Exploration Geophysicists (SEG), Tulsa.

Okay, A. I., Tüysüz, O. 1999. "Tethyan Sutures of Northern Turkey", *Geological Society, London, Special Publications*, 156(1), 475-515.

Ordonez, G. A. 2000. "SHAKE 2000: A Computer Model for the I-D Analysis of Geotechnical Earthquake Engineering Problems".

Ordóñez, I. M. 2009. "Influence of the Boundary Conditions on the Seismic Response Predictions of a Rockfill Dam by Finite Element Method", Mater Thesis, Università degli Studi di Pavia, 67 p.

Özalaybey, S., Zor, E., Ergintav, S., Tapırdamaz, M. C. 2011. "Investigation of 3-D Basin Structures in the İzmit Bay Area (Turkey) by Single-Station Microtremor and Gravimetric Methods", *Geophys. J. Int.*, 186, 883–894.

Öztürk, A. 1968. "Çerkeş-Eskipazar-Gerede Bölgesinin Jeolojisi", Ph.D. Thesis, Ankara University (unpublished, in Turkish).

Pagliaroli, A., Lanzo, G., D'Elia, B. 2011. "Numerical Evaluation of Topographic Effects at the Nicastro Ridge in Southern Italy", *J Earthq Eng*, 15 (3), 404–432.

Panca, A., Anderson, J. G., Louie, J. N. 2007. "Characterization of Near-Surface Geology at Strong-Motion Stations in the Vicinity of Reno, Nevada", *Bull. Seism. Soc. Am.*, 97, 2096-2117.

Panzerà, F., Lombardo, G., Muzetta, I. 2013. "Evaluation of Buildings Dynamical Properties through In-Situ Experimental Techniques and 1D Modelling: The Example of Catania, Italy", *J. Phys. Chem. Earth*, 63, 136–146.

Panzerà, F., Pischiutta, M., Lombardo, G., Monaco, C., Rovelli, A. 2014. "Wavefield Polarization in Fault Zones of the Western Flank of Mt. Etna: Observations and Fracture Orientation Modelling", *Pure Appl. Geophys*, 171(11), 3083–3097.

Parolai, S., Richwalski, S. M. and Milkereit, C. 2006, "S-Wave Velocity Profiles for Earthquake Engineering Purposes for the Cologne Area (Germany)", *Bulletin of Earthquake Engineering*, 4, 65–94.

Park, C. B., Miller, R. D., Xia, J. 1999. "Multi-Channel Analysis of Surface Waves", *Geophysics*, 64 (3), 800–808.

Park, C. B., Miller, R. D., Xia, J. 2001. "Offset and Resolution of Dispersion Curve in Multichannel Analysis of Surface Waves (MASW)", *Proceedings of the SAGEEP 2001*, Denver, Colorado, SSM-4.

Park, C. B., Miller, R. D., Miura, H. 2002. "Optimum Field Parameters of a MASW Survey", [Exp. Abs.]. SEG-J, Tokyo (May 22–23).

Park, C. B., Miller, R. D., Xia, J., Ivanov, J. 2007. "Multichannel Analysis of Surface Waves Active and Passive Methods", the Leading Edge, January- (MASW).

Pınar, N. 1953. "13 Ağustos 1951 Kurşunlu Depreminin Jeolojik ve Makrosismik Etüdü", İstanbul Üniversitesi Fen Fakültesi Dergisi, Seri A XVIII, 131-141 [in Turkish].

Pitarka, A. 1999. "3D Elastic Finite-Difference Modeling of Seismic Motion Using Staggered Grids with Nonuniform Spacing", "Bulletin of the Seismological Society of America", 89 (1), 54-68.

Pitilakis, K. D., Anastasiadis, A., Raptakis, D. 1992. "Field and Laboratory Determination of Dynamic Properties of Natural Soil Deposits", Proceedings of 10th World Conf. Earthquake Engineering, Rotherdam, 1275–1280.

Pitilakis, K. 2004. "Site Effects", 139–193. Recent Advances in Earthquake Geotechnical Engineering and Microzonation. Ed: Ansal, A. Kluwer Academic Publishers, Dordrecht, the Nederland.

Pruska, M. J. 1973. "Effect of Initial Stress on the Stress-Strain Relation", Proceedings of the 8th International Conference on Soil Mechanics and Foundation Engineering, Moscow, 4, 26-28.

Pullammanappallil, S., Honjas, W., Louie, J. N. 2003. "Determination of 1-D Shear Wave Velocities Using the Refraction Microtremor Method", Proceedings of the Third International Conference on the Application of Geophysical Methodologies and NDT to Transportation and Infrastructure, Orlando, Florida.

Raptakis, D., Manakou, M. V., Chavez-Garcia, F. J., Makra, K., Pitilakis, K. 2005. "3D Configuration of Mygdonian Basin and Preliminary Estimate of Its Site Response", Soil Dynamics and Earthquake Engineering 25 (11), 871 - 887.

Rathje, E. M., Bray, J. D. 2001. "One- and Two-Dimensional Seismic Analysis of Solid-Waste Landfills", Can. Geotech. J., 38, 850–862.

Rathje, E. M., Kottke, R. K., Trent, W. L. 2010. "Influence of Input Motion and Site Property Variabilities on Seismic Site Response Analysis", *J. Geotech. Geoenviron. Eng.*, 136, 607-619.

Reiter, L. 1990. "Earthquake Hazard Analysis", Columbia University Press, New York, 254 s.

Riggs, C. O. 1986. "North American Standard Penetration Test Practice: An Essay, in Use of in Situ Tests in Geotechnical Engineering", ASCE Geotechnical Special Publication, 6.

Rix, G. J., Hebler, G. L., Orozco, M. C. 2002. "Near Surface vs. Profiling in the New Madrid Seismic Zone Using Surface-Wave Methods", *Seismological Research Letters*, 73 (3), 380–392.

Rix, G. J. 2005. "Near-Surface Site Characterization Using Surface Waves". *Surface Waves in Geomechanics – Direct and Inverse Modeling for Soil and Rocks*. Eds: Lai, Wilmanski. CISM Lecture Notes, Springer-Verlag, Wien-Newyork.

Rodriguez-Marek, A., Eeri, M., Bray, J., Abrahamson, N. 2001. "An Empirical Geotechnical Seismic Site Response Procedure", *Earthquake Spectra*, 17 (1), 65-87.

Rodriguez, V. H. S., Midorikawa, S. 2002. "Applicability of the H/V Spectral Ratio of Microtremors in Assessing Site Effects on Seismic Motion", *Earthq. Eng. Struct. Dyn.*, 31, 261-279.

Rucker, M.L. 2003. "Applying the Refraction Microtremor (ReMi) Shear Wave Technique to Geotechnical Characterization", *Proceedings of the Third International Conference on the Application of Geophysical Methodologies and NDT to Transportation Infrastructure*, Dec. 8-12, Orlando, Florida, USA.

Sadigh, K., Chang, C. Y., Egan, J. A., Makdisi, F., Youngs, R. R. 1997. "Attenuation Relationships for Shallow Crustal Earthquakes based on California Strong Motion Data", *Seismological Research Letters*, 68(1), 180–189.

Sağlamer, A. 1979. "Standart Penetrasyon Deneyi Nedir - Ne Değildir", *Zemin Mekaniği ve Temel Mühendisliği Türk Milli Komitesi Bülteni*, 1(4), 267-271.

Satoh, T., Kawase, H., Matsushima, S. 2001. "Differences Between Site Characteristics Obtained from Microtremors, S-waves, P-waves, and Codas", Bull. Seismol. Soc. Am., 91, 313-334.

Schmertmann, J. H., 1978. "Guidelines for Cone Penetration Test: Performance and Design", U.S. Dept. of Transportation, Washington.

Schnabel, P. B. 1973. "Effects of Local Geology and Distance from Source on Earthquake Ground Motions", Ph.D. Thesis, University of Calif., Berkeley.

Seed, H. B., Tokimatsu, K., Harder, L. F., Chung, R. M. 1985. "Influence of SPT Procedures in soil liquefaction resistance evaluations", Journal of Geotechnical Engineering, ASCE, 111(12), 1425-1445.

Seed, H. B., Wong, R. T., Idriss, I. M., Tokimatsu, K. 1986. "Moduli and Damping Factors for Dynamic Analysis of Cohesionless Soils", J. of the Geotechnical Engineering Division, ASCE, 112 (11), 1016-1032.

SESAME 2004. "Guidelines for the Implementation of the H/V Spectral Ratio Technique on Ambient Vibrations. Measurements, Processing and Interpretation", European Commission – Research General Directorate Project No. EVG1-CT-2000–00026 SESAME, report D23.12, <http://SESAME-FP5.obs.ujf-grenoble.fr>.

Sevin, M., Uğuz, M. F. 2011. "1/100.000 Ölçekli Türkiye Jeoloji Haritaları, Çankırı G30 Paftası", MTA Yayınları, Pafta No: 146. Geological Research Department, MTA (General Directorate of Mineral Research and Exploration), Ankara, Turkey.

Seyitoğlu, G. and Scott, B. C. 1992. "Late Cenozoic Volcanic Evolution of the Northeastern Aegean Region", Journal of Volcanology and Geothermal Research, 54, 157-176.

Seyitoğlu, G., Kazancı, N., Karakuş, K., Fodor, L., Araz, H., Karadenizli, L. 1997. "Does Continuous Compressive Tectonic Regime Exist during Late Paleogene to late Neogene in NW Central Anatolia, Turkey? Preliminary Observations", Turkish Journal of Earth Sciences, 6, 77-83.

Seyitoğlu, G., Kazancı, N., Karadenizli, L., Şen, Ş., Varol, B., Karabıyıkdoğan, T. 2000. "Rockfall Avalanche Deposits Associated with Normal Faulting in the NW

of Çankırı Basin: Implications for the Postcollisional Tectonic Evolution of the Neo-Tethyan Suture Zone", *Terra Nova*, 12, 245-251.

Silva, W., Lee, K. 1987. "WES RASCAL Code for Synthesizing Earthquake Ground Motions, State-of-the-Art for Assessing Earthquake Hazards in the United States", Report 24, Miscellaneous Paper S-73-1, US Army Corps of Engineers, Vicksburg, Mississippi.

Silva, W. J. 1991. "Global Characteristics and Site Geometry." Chapter 6 in *Proceedings: NSF/EPRI Workshop on Dynamic Soil Properties and Site Characterization*. Palo Alto, Calif.: Electric Power Research Institute, NP-7337.

Site Investigation Steering Group. 1993. "Specification for Ground Investigation", No. 3, Thomas Telford.

Sitharam, T. G., Anbazhagan, P., 2008, "Seismic Microzonation: Principles, Practices and Experiments", *EJGE Bouget08*.

Siyako, F. 1987. "Şabanözü-Çankırı-Çandır Çevresinin Jeolojisi ve Kömür Olanakları", MTA Report, No: 8149, Ankara (unpublished).

Skempton, A. W. 1986. "Standard Penetration Test Procedures and the Effects in Sands of Overburden Pressure, Relative Density, Particle Size, Aging and Overconsolidation", *Geotechnique*, 36(3), 425-447.

Stephenson, W. J., Williams, R. A., Odum, J. K., Worley, D. M. 2005. "Comparison of ReMi, and MASW Shear-Wave Velocity Techniques with the CCOC Borehole to 100 m, Santa Clara Valley", In *Blind Comparisons of Shear-Wave Velocities at Closely-Spaced Sites in San Jose, California*. Eds: Asten M. W., Boore D. M. U.S. Geol. Surv. Open-File Rept. 1169, part 2, 15 s.

Stokoe II, K. H., Wright, S. G., Bay, J. A., Roesset, J. M. 1994. "Characterization of Geotechnical Sites by SASW Method", In *Geophysical Characterization of Sites*. Ed: Woods, R. D. ISSMFE Technical Committee #10. Oxford Publishers, New Delhi.

Şengör, A. M. C.; Tüysüz, O., İmren, C., Sakıncı, M., Eyidoğan, H., Görür, N., X. Le Pichon, Rangin, C. 2005. "The North Anatolian Fault: A New Look. Annual Review of Earth and Planetary Sciences", 33, 37-112.

Taşkın B, Özdemir P, Özel N M. 2003. "06 Haziran 2000, Orta Çankırı Depreminin Değerlendirilmesi (Evaluation of Orta-Çankırı June 06, 2000 earthquake)", 5th National Conference on Earthquake Engineering, Istanbul - Turkey.

Taşman, C. E. 1944. "Gerede-Bolu Depremi", Mineral Research and Exploration Institute of Turkey Bulletin, 1 (31), Ankara [in Turkish].

Taymaz, T., Wright, T. J., Yolsal, S., Tan, O., Fielding, E., Seyitoğlu, G. 2007. "Source Characteristics of the 6 June 2000 Orta-Çankırı (Central Turkey) Earthquake: A Synthesis of Seismological, Geological and Geodetic (InSAR) Observations, and Internal Deformation of the Anatolian plate", Geological Society, London, Special Publications, 291 (1), 259-290.

Tevez-Costa, P., Matias L., Bard P. Y., 1996. "Seismic Behaviour Estimation of Thin Alluvium Layers Using Microtremor Recordings", Soil Dynamics and Earthquake Engineering 15 (3), 201–209.

Teves-Costa, P., Almeida, I. M., Silva, P. L., 2001. "Microzonation of the Lisbon Town: 1D Theoretical Approach", Pageoph, 158, 2579-2596.

The subcommittee for geotechnical survey of the Ashigara Valley blind prediction test 1992. "The Japanese Working Group on the Effects of Surface Geology on Seismic Motion (prepared by Y. Sawada)", Geotechnical data, in Proc. of International Symposium on Effects of Surface Geology on Seismic Motion, 29-42.

Tokay, M., Öztürk, A., Koçyiğit, A. 1973. "Arkotdağ Formasyonunun Litolojisi, Kökeni ve Kuzey Anadolu Fay Zonu ile Muhtemel Bağlantısı", Scientific and Technical Research Council of Turkey Project, No. TBAG 43, 53 s (unpublished, in Turkish).

Tokan, A., Özgen, S. 1976. "Çankırı Orta Linyit Sahası Raporu", MTA Report, No: 6127, Ankara (unpublished).

Tokimatsu, K. 1997. "Geotechnical Site Characterization Using Surface Waves", Earthquake Geotechnical Engineering. Ed: Isihara. Balkema Rotterdam.

Tokimatsu, K., Arai, H., Yamazaki, M. 2004. "Multi-Dimensional Vs-Profiling with Microtremor H/V and Array Techniques", Paper 1348 Conference

Proceedings of the 13th World Conference of Earthquake Engineering, Vancouver, Aug 1–6.

Toshinawa, T., Taber, J. J., Berrill, J. J. 1997. "Distribution of Ground Motion Intensity Inferred from Questionnaire Survey, Earthquake Recordings, and Microtremor Measurements – A Case Study in Christchurch, New Zealand, during the 1994 Arthurs Pass Earthquake", Bull. Seism. Soc. Am. 87 (2), 356-369.

TS 1900-1-2. 2006. "İnşaat Mühendisliğinde Zemin Laboratuar Deneyleri - Bölüm 1: Fiziksel özelliklerin tayini".

Türkecan, A., Hepşen, N., Papak, İ. 1991. Seben-Gerede (BOLU), Güdül-Bey pazarı (ANKARA) ve Çerkeş-Orta-Kurşunlu Yörelere nin Jeolojisi ve Volkanik Kayaçların Petrolojisi", MTA Report, No: 9193, Ankara (unpublished).

Türkmenoğlu, A., Akıman, O., Aker, S., Tankut, A. 1991."Orta (Çankırı) Yöresi Kil Yataklarının Jeolojisi ve Oluşumu", MTA Dergisi, 113, 127-132.

Vucetic, M., Dobry, R. 1991. "Effect of Soil Plasticity on Cyclic Response", J. of the Geotechnical Engineering Division, ASCE, 111 (1), 89-107.

Wallace, R. M., ROLLINS K.M. 1996. "Amplification of Earthquake Motions in Great Salt Lake Valley due to Deep Basin Shape and Shallow Soil Stratigraphy", Procs. 11th World Conf. on Earthquake Engineering, Acapulco, Mexico, Elsevier, Paper No. 897

Walling, M. Y., Mohanty, W. K., Nath, S. K., Mitra, S., John, A. 2009. "Microtremor Survey in Talchir, India to Ascertain Its Basin Characteristics in Terms of Predominant Frequency by Nakamura's Ratio Technique" Eng. Geol. 106(3), 123–132.

Wells, D. L.; Coppersmith, K. J. 1994. "New Empirical Relationships among Magnitude, Rupture Length, Rupture Width, Rupture Area, and Surface Displacement", Bulletin of the Seismological Society of America, 84, 974-1002.

WESDOT. 2013. "Project Management–Delivering the Capital Construction Programs at the Project Level", Washington State Department of Transportation, Olympia, Washington, USA.

Wills, C. J., Petersen, M., Bryant, W. A., Reichle, M., Saucedo, G. J., Tan, S., Taylor, G., Treiman, J. 2000. "A Site-Conditions Map for California Based on Geology and Shear Wave Velocity", *Bull. Seism. Soc. Am.*, 90 (6B), 187-208.

Wills, C. J., Clahan, K. B. 2006. "Developing a Map of Geologically Defined Site Condition Categories for California", *Bulletin of the Seismological Society of America*, 96 (4A), 1483–1501.

Xia, J., Miller, R. D., Park, C. B. 1999. "Estimation of Near-Surface Shear-Wave Velocity by Inversion of Rayleigh Wave", *Geophysics*, 64 (3), 691-700.

Xia, J., Miller, R. D., Park, C. B., Hunter J. A., Harris J. B., Ivanov J. 2002. "Comparing Shear-Wave Velocity Profiles Inverted from Multichannel Surface Wave with Borehole Measurements", *Soil Dynamics and Earthquake Engineering*, 22 (3), 181-190.

Xia, J., Miller, R. D., Park, C. B., Ivanov, J., Tian, G., Chen, C. 2004. "Utilization of High Frequency Rayleigh Waves in Near Surface Geophysics", *The Leading Edge*, 23 (8), 753–759.

Xu, Y., Xia, J., Miller, R. D. 2006. "Quantitative Estimation of Minimum Offset for Multichannel Surface-Wave Survey with Actively Exciting Source", *Journal of Applied Geophysics*, 59, 117-125.

Yokoi, T., Margaryan, S. 2007. "Interpretation of SPAC Method Based on Seismic Interferometry - Theory and Observation", 50th Anniversary Earthquake Conference Commemorating the 1957 Gobi-Altay Earthquake.

Yoon, S., Rix, G. J. 2005. "Active and Passive Surface Wave Measurements at the William Street Park Site, using F-K methods", In *Blind Comparisons of Shear-Wave Velocities at Closely-Spaced Sites in San Jose, California*. Eds: Asten, M. W., Boore, D.M. U.S. Geol. Surv. Open-File Rept. 2005–1169, part 2.

Yousefi-Bavil, K., Akgün, H., Eker, A. M., Camabzoğlu, S., Koçkar, M. K. 2015. "Integration of Surface Wave Seismic Survey Testing Results and Segmented Seismic Source Model of NAFS for PSHA of the Gölyaka-Düzce Tectonic Basin, Turkey", 6ICEGE (6th International Conference on Earthquake Geotechnical Engineering), 1-4 November, Paper No 402, Christchurch, New Zealand, 8 p.

Yüçemen M. S., 2008, "Deprem Tehlikesinin Tahmininde Olasılıksal Yöntemler", 14. Bölüm, Binalar için Deprem Mühendisliği Temel İlkeleri (In Turkish). Ed: E. Canbay, Bizim Büro Basımevi, Ankara.

C URRICULUM VITAE

PERSONAL INFORMATION

Surname, Name: Eker, Arif Mert
Nationality: Turkish (TC)
Date and Place of Birth: 18 July 1983, Ankara
Marital Status: Married
Phone: +90 312 442 03 14
Fax: +90 312 442 03 16
email: merteker@gmail.com

EDUCATION

Degree	Institution	Year of Graduation
MS METU	Geological Engineering	2009
BS METU	Geological Engineering	2006
High School	Ayrancı Foreign Language (English) Intensive High School, Ankara	2001

WORK EXPERIENCE

Year	Place	Enrollment
2013-Present	SDS Energy, Inc.	Site Supervisor
2007-2013	METU Department of Geological Engineering	Research Assistant

FOREIGN LANGUAGES

Advanced English, Beginer Level German

PUBLICATIONS

1. Eker, A. M., Koçkar, M.K. and Akgün, H. "Evaluation of Site Effect within the Tectonic Basin in the Northern Side of Ankara", Engineering Geology, 192, 64-81 (2015).
2. Hou, Z., Şen, O, Gou, Yang; Eker, A.M., Li, M., Yal, G. P., Cambazoğlu, S. and Were, P. " Preliminary Geological, Geochemical and Numerical Study on the First

EGS Project in Turkey", *Environmental Earth Sciences*, 73(11), 6747-6767 (2015).

3. Yousefi-Bavil, K., Akgün, H., Eker, A.M., Camabzoğlu, S. and Koçkar, M.K., "Integration of Surface Wave Seismic Survey Testing Results and Segmented Seismic Source Model of NAFS for PSHA of the Gölyaka-Düzce Tectonic Basin, Turkey", 6ICEGE (6th International Conference on Earthquake Geotechnical Engineering), 1-4 November, Paper No 402, Christchurch, New Zealand, 8 p (2015).

4. Arslan, A., Kelam, M.A., Eker, A.M., Akgün, H. and Koçkar, M.K. "Optical Fiber Technology to Monitor Slope Movement", In *Engineering Geology for Society and Territory*, 2: 425-1429 (2015), Springer International Publishing.

5. Yousefi-Bavil, Eker, A.M., Camabzoğlu, S., Koçkar, M.K., Akgün,H. "Yüzey Dalgası Etüt sonuçlarının Entegrasyonu ile Gölyaka-Düzce Tektonik Baseninin Olasılıksal Sismik Tehlike Değerlendirmesi", 3.TDMSK (3. Türkiye Deprem Mühendisliği ve Sismoloji Konferansı), 14-16 Ekim, No: 224, DEU, Izmir, Turkey, 8 p (2015).

6. Arslan, A., Akgün, H., Koçkar, M.K., Eker, A.M., and Kelam, M. A. "Slope Movement Monitoring with Optical Fiber Technology", In *ISRM Regional Symposium-EUROCK 2015*. International Society for Rock Mechanics (2015).

7. Eker, A.M., Dikmen, M., Cambazoğlu, S., Düzgün, Ş.H.and Akgün, H. "Evaluation and comparison of landslide susceptibility mapping methods: a case study for the Ulus district, Bartın, northern Turkey", *International Journal of Geographical Information Science*, 29(1), 132-158 (2014).

8. Yal, G. P., Cambazoğlu, S., Eker, A. M., Şen, O. Koçkar, M. K. and Akgün, H. "Thermal Anomaly and Alteration Mineral Mapping at İzmir-Dikili Region by Using Aster and Investigation of Geothermal Potential of the Region", 3rd. Turkey National Geological Remote Sensing Symposium (JEOUZAL-3), 81-84 (2014), (Abstract only).

9. Dikmen, M., Eker, A. M., Cambazoğlu, S. Akgün H. "Effect of Spatial Resolution on Landslide Susceptibility Mapping", 3rd. Turkey National Geological Remote Sensing Symposium (JEOUZAL-3), 49-52 (2014), (Abstract only).

10. Eker, A.M., Koçkar, M.K. and Akgün H. "Zemin Sınıflamasında Kullanılan Parametrelerin Yeterliliği", 2. Türkiye Deprem Mühendisliği ve Sismoloji Konferansı- 25 - 27 Eylül 2013, Mustafa Kemal Üniversitesi, Hatay, 1-10 (2013).

11. Cambazoğlu S., Akgün H., Eker A.M. and Koçkar, M.K. "Probabilistic Seismic Hazard Assessment with the Integration of Local Site Characterization

Studies for Düzce Province, Turkey", SE-50EEE International Conference on Earthquake Engineering - 29 to 31 May 2013 Skopje, R. Macedonia, 1-8 (2013).

12. Eker, A.M., Akgün H. and Koçkar M.K. "A Comprehensive Study to Define Local Site Effects in Northern Ankara, Turkey", SE-50EEE International Conference on Earthquake Engineering - 29 to 31 May, Skopje, R. Macedonia, 1-7 (2013).

13. Kelam, A. M., Eker, A.M., Akgün, H., Arslan, A. and Koçkar, M.K. "Heyelan ve Şev Duraylılığının İzlenmesinde Yeni Bir Yöntem: Fiber Optik Teknolojisi", 66. Türkiye Jeoloji Kurultayı, ODTÜ Kültür ve Kongre Merkezi, Ankara, 312-313 (2013), (Abstract only).

14. Eker A.M., Akgün H. and Koçkar M.K., "Sismik Saha Karakterizasyonlarında Birleştirilmiş Yüzey Dalgası Yöntemlerinin Kullanılması", 2. Türkiye Deprem Mühendisliği ve Sismoloji Konferansı, 25 - 27 Eylül 2013, Mustafa Kemal Üniversitesi, Hatay, 1-10 (2013).

15. Cambazoğlu S., Eker A.M., Koçkar M.K. and Akgün H. "Kilis ve Civarı için Sismik Kaynak Modeli Oluşturulması ve Şahinbey İlçesi için Örnek Bir Sismik Tehlike Analizi", 2. Türkiye Deprem Mühendisliği ve Sismoloji Konferansı- 25 - 27 Eylül 2013, Mustafa Kemal Üniversitesi, Hatay, 1-11 (2013).

16. Eker, A. M., Akgün H. and Koçkar M.K. "Local Site Characterization and Seismic Zonation Study by Utilizing Active and Passive Surface Wave Methods: A Case Study for the Northern Side of Ankara, Turkey". Engineering Geology, 151; 64-81 (2012).

17. Eker, A. M., Dikmen, M., Cambazoğlu, S., Düzgün., Ş. and Akgün H. "Application of Artificial Neural Network and Logistic Regression Methods to Landslide Susceptibility Mapping and Comparison of the Results for the Ulus District, Bartın", Journal of the Faculty of Engineering and Architecture of Gazi University (in Turkish), 27(1), 163-173 , (2012).

18. Koçkar M.K., Akgün H., Eker, A. M. and Cambazoğlu, S. "Engineering Geological and Geotechnical Characteristics of Ankara Clay", European Clay Conference, June-July, 156, (2011), (Abstract only).

19. Eker, A. M., Dikmen, M., Cambazoğlu, S., Düzgün., Ş. and Akgün H. "Preperation and Analysis of Data Sets in Landslide Susceptibility Mapping", 64th Geology Congress of Turkey, April, 347-348 (2011), (Abstract only).

20. Eker, A. M., Akgün H. and Koçkar M.K. "A Comparison of Local Site Conditions with Passive and Active Surface Wave Methods", Fifth International Conference on Recent Advances in Geotechnical Earthquake Engineering and Soil

Dynamics Symposium in Honor of Professor I. M. Idriss San Diego, CA., May 24-29 (2010).

21. Akgün H., Eker, A. M. and Koçkar M.K. "A Comparison of Local Site Conditions of the Plio-Quaternary Sediments Situated towards the North of Ankara with Microtremor Measurements", Sakarya International Symposium of Earthquake Engineering, the Learning Outcomes of Marmara Earthquake in the First Decade, 1-2 October, 620-629 (2009).

22. Koçkar, M.K., Akgün, H., and Eker, A. M. "Earthquake Risk in Low and Medium Seismicity Regions: A Case Study for Ankara", International Earthquake Symposium Kocaeli, 17-19 August 2009, 93-94 (2009), (Abstract only).

23. Eker, A. M. "Determination of the Dynamic Characteristic and Local Site Conditions of the Plio-Quaternary Sediments Situated towards the North of Ankara Through Surface Wave Testing Methods", M.Sc. Thesis, METU, p 145, 2009.

24. Akgün H., Koçkar M.K and Eker, A. M. "Determination of the Dynamic Characteristic and Local Site Conditions of the Plio-Quaternary Sediments Situated towards the North of Ankara (The Capital City of Turkey) Through Surface Wave Testing Methods", 61st International Geology Congress of Turkey, March, 83-84 (2008), (Abstract only).

HOBBIES

Etymology, Politics, Movies, Sports, Video Games